3

BNWL-2100 PT3
UC-11

Pacific Northwest Laboratory Annual Report for 1976 to the ERDA Assistant Administrator for Environment and Safety

Part 3 Atmospheric Sciences

August 1977

Prepared for the Energy Research and Development Administration under Contract EY-76-C-06-1830

Battelle
Pacific Northwest Laboratories

BNWL-2100 PT3

NOTICE

This report was prepared as an account of work sponsored by the United States Government. Neither the United States nor the Energy Research and Development Administration, nor any of their employees, nor any of their contractors, subcontractors, or their employees, makes any warranty, express or implied, or assumes any legal liability or responsibility for the accuracy, completeness or usefulness of any information, apparatus, product or process disclosed, or represents that its use would not infringe privately owned rights.

The views, opinions and conclusions contained in this report are those of the contractor and do not necessarily represent those of the United States Government or the United States Energy Research and Development Administration.

PACIFIC NORTHWEST LABORATORY
operated by
BATTELLE
for the
ENERGY RESEARCH AND DEVELOPMENT ADMINISTRATION
Under Contract EY-76-C-06-1830

Printed in the United States of America
Available from
National Technical Information Service
U.S. Department of Commerce
5285 Port Royal Road
Springfield, Virginia 22151
Price: Printed Copy $_____*; Microfiche $3.00

*Pages	NTIS Selling Price
001-025	$4.50
026-050	$5.00
051-075	$5.50
076-100	$6.00
101-125	$6.50
126-150	$7.00
151-175	$7.75
176-200	$8.50
201-225	$8.75
226-250	$9.00
251-275	$10.00
276-300	$10.25

ERDA-RL RICHLAND, WA

3 3679 00062 6855

BNWL-2100 PT3
UC-11

Pacific Northwest Laboratory Annual Report for 1976 to the ERDA Assistant Administrator for Environment and Safety

Part 3 Atmospheric Sciences

by
J. M. Hales and Staff Members
of Pacific Northwest Laboratory

August 1977

Battelle
Pacific Northwest Laboratories
Richland, Washington 99352

PREFACE

Pacific Northwest Laboratory's 1976 Annual Report to the ERDA Assistant Administrator for Environment and Safety is organized by major program categories into five Volumes, or Parts. Parts 1-4 are oriented to particular segments of the program supported by the Division of Biomedical and Environmental Research. Part 5 includes reports on projects supported by the Division of Safety, Standards and Compliance; Division of Technology Overview; Division of Environmental Control Technology; and the Office of Environmental Policy Analysis. Each Part consists of project reports authored by scientists from several PNL research departments, reflecting the interdisciplinary nature of the research effort. The Parts of the 1976 Annual Report are:

Part 1	Biomedical Sciences Program Manager - W. R. Wiley	R. C. Thompson, Report Coordinator D. L. Felton, Editor
Part 2	Ecological Sciences Program Manager - B. E. Vaughan	B. E. Vaughan, Report Coordinator J. L. Helbling, Editor
Part 3	Atmospheric Sciences Program Manager - C. L. Simpson	J. M. Hales, Report Coordinator E. L. Owzarski, Editor
Part 4	Physical and Technological Programs Program Manager - J. M. Nielsen	J. M. Nielsen, Report Coordinator G. M. Garnant, Editor
Part 5	Control Technology, Overview, Safety, and Policy Analysis Program Managers - N. E. Carter D. B. Cearlock J. C. Fox D. L. Hessel H. V. Larson	W. J. Bair, Report Coordinator L. C. Counts/R. W. Baalman, Editors

Activities of the Environmental and Safety Research Program at PNL are broader in scope than the articles in this report indicate. PNL staff members participate throughout the year in many projects not funded through specific 189s. These efforts include overall program planning, response to requests for information from the ERDA Assistant Administrator for Environment and Safety and other officials, participation on national and international standard-setting committees, and public education. During 1976, staff of PNL's Environmental and Safety Research Program:

- prepared two volumes (Fission and Fusion) of ERDA's Balanced Program Plan for Biomedical and Environmental Research;
- contributed to a number of environmental assessments and impact statements, including the Generic Environmental Statement for Mixed Oxide Fuels and the Clinch River Breeder Reactor Statement, and participated in hearings on nuclear issues;
- sat on National Academy of Sciences/National Research Council Committees, the National Council on Radiation Protection and Measurements, and the International Commission on Radiological Protection;
- compiled and prepared the final reports for two of these committee efforts; and
- provided, in response to requests from the Assistant Administrator for Environment and Safety, interpretations of research results to clarify information given to the public on a number of issues. These included the Hanford Mortality Study findings, faulty published interpretations of data on mortality in plutonium workers, and several other issues concerned with nuclear power.

W. J. Bair, Manager
S. Marks, Associate Manager
Environmental and Safety Prsearch Program

Previous Reports in this Series:

Annual Report for

1951	HW-25021, HW-25709
1952	HW-27814, HW-28636
1953	HW-30437, HW-30464
1954	HW-30306, HW-33128, HW-35905, HW-35917
1955	HW-39558, HW-41315, HW-41500
1956	HW-47500
1957	HW-53500
1958	HW-59500
1959	HW-63824, HW-65500
1960	HW-69500, HW-70050
1961	HW-72500, HW-73337
1962	HW-76000, HW-77609
1963	HW-80500, HW-81746
1964	BNWL-122
1965	BNWL-280, BNWL-235, Vol. 1-4
1966	BNWL-480, Vol. 1, BNWL-481, Vol. 2, Pt. 1-4
1967	BNWL-714, Vol. 1, BNWL-715, Vol. 2, Pt. 1-4
1968	BNWL-1050, Vol. 1, Pt. 1-2, BNWL-1051, Vol. 2, Pt. 1-3
1969	BNWL-1306, Vol. 1, Pt. 1-2, BNWL-1307, Vol. 2, Pt. 1-3
1970	BNWL-1550, Vol. 1, Pt. 1-2, BNWL-1551, Vol. 2, Pt. 1-2
1971	BNWL-1650, Vol. 1, Pt. 1-2, BNWL-1651, Vol. 2, Pt. 1-2
1972	BNWL-1750, Vol. 1, Pt. 1-2, BNWL-1751, Vol. 2, Pt. 1-2
1973	BNWL-1850, Pt. 1-4
1974	BNWL-1950, Pt. 1-4
1975	BNWL-2000, Pt. 1-4

FOREWORD

Tools needed to describe the nature and fate of pollution in the atmosphere are the goal of atmospheric transport and transformation research at the Pacific Northwest Laboratory (PNL). Pollutants being investigated are those resulting from development and use of two energy resources: coal and nuclear power. We plan future investigations of atmospheric problems caused by oil shale technology development.

Coal Combustion

The behavior of air pollution resulting from coal-fired power plants, particularly the physical and chemical transformations that occur during transport and the removal of pollutants by wet and dry scavenging processes, is being defined. The release of large quantities of sulfur dioxide to the atmosphere, its transformation to sulfates, and its removal and ultimate delivery to biological systems where serious health and environmental consequences can result are serious problems in coal utilization. The greatest emphasis in atmospheric transport studies will be placed, in the future, on fossil fuel pollutant transformation and removal. This expanded non-nuclear research is being conducted in the Multi-State Atmospheric Power Production Pollution Studies (MAP3S).

Nuclear Energy

Concern about long-lived particulates (i.e., plutonium and other radionuclides) released to the environment from LMFBRs dictates that deposition and resuspension of these substances be studied. The primary hazard from plutonium is inhalation; therefore, its residence in the atmosphere must be defined clearly. Removal of particulates from the atmosphere by deposition (which limits initial exposure) and any future resuspension from the surface (which continues the potential for inhalation) are being evaluated.

Oil Shale

In the future, significant atmospheric processes connected with shale oil production will be investigated. Air flow and dispersion in complex terrain will be studied in connection with oil shale developments in Colorado, Utah and Wyoming. The mountainous oil shale region represents a particularly difficult air pollution problem; air is trapped in valleys for extended periods under certain meterological conditions, and thus especially stringent siting requirements must be fulfilled to meet State and Federal air quality standards. Adequate models and field measurements for the complex air flow and dispersion conditions of the area are not available; they must be developed to assure acceptable siting. Recent efforts to accelerate the development of synthetic fuels have increased the need for an interdisciplinary evaluation of the health and environmental problems associated with oil shale mining and retorting. PNL plans to undertake these evaluations.

Atmospheric transport and transformation research is being conducted in the following areas:

- Atmospheric Surveys and Weather Modification
- Air Flow and Dispersion
- Deposition and Resuspension
- Pollutant Scavenging
- Pollutant Transformations and Interactions
- Composite Models for Atmospheric Processes

Atmospheric models which provide the means to estimate atmospheric and terrestrial impact, given the nature and distribution of pollutant sources, are a major product of this research. Models are important for evaluating pollutant impacts directly affecting air quality, precipitation quality and surficial response, and indirectly contributing to weather and climate modification.

This report describes progress in 1976 for each of these areas. A divider page summarizes the goals of each area; project 189 titles which fund research in the area are listed as bulleted items.

CONTENTS

(Listing in parenthesis denotes the sponsoring programs under which the research was done.)

PREFACE ii

FOREWORD iv

ATMOSPHERIC SURVEYS AND WEATHER MODIFICATION 1

Elemental Concentrations of Northern Hemispheric Air at Quillayute, Washington - J. D. Ludwick, T. D. Fox and S. R. Garcia (Hemispheric Pollution Behavior Studies of Chemical and Radiation Substances) . . . 3

Atmospheric Fallout During 1976 at Richland, Washington and Point Barrow, Alaska - C. W. Thomas (Fallout Rates and Mechanisms) 5

Radioactive Fallout from the Chinese Nuclear Weapons Tests of January 23, 1976, September 26, 1976, and November 17, 1976 - C. W. Thomas, J. K. Soldat, W. B. Silker and R. W. Perkins (Fallout Rates and Mechanisms) 7

Trace Element and Sulfate Concentrations Downwind of Milwaukee - J. A. Young (Urban Pollutant Characterization, Transport and Deposition . 9

Characterization of Substances in Products, Effluents and Wastes from Solvent Refining Coal Plant - M. R. Petersen, J. C. Laul and P. W. Ryan (Coal Conversion Pollutant Chemistry) 13

Hanford Turbidity During 1976 - N. S. Laulainen (Aerosol and Trace Gas Transformations) 18

Characterization of Prefrontal Precipitation During Winter in Eastern Washington - J. M. Thorp (Precipitation Scavenging in MAP3S) 22

Catch and Storage Characteristics of Three Types of Nonrecording Precipitation Gauges - J. M. Thorp (ALE Administration) 25

Microclimate and Ecosystem Modification by Solar Energy Farms - J. G. Droppo, N. S. Laulainen and D. S. Renne (ERDA/RL Special Studies) . 28

AIR FLOW AND DISPERSION 31

Preparation of a Data Volume Summarizing Hanford Field Diffusion Experiments, 1967-1974 - P. W. Nickola (Atmospheric Boundary Layer Studies) 33

Specification of Errors in Estimating the Mean Plume from Simulated Aircraft Traverses of the Real Plume - P. W. Nickola (Atmospheric Boundary Layer Studies) 37

Planetary Boundary Layer Aircraft Profile Studies Under Inversion Conditions - J. G. Droppo (Atmospheric Boundary Layer Studies) . . . 40

DEPOSITION AND RESUSPENSION 43

Summary of Field Data on Dry Removal Rates of Gases and Particles from the Atmosphere - J. G. Droppo (Atmospheric Boundary Layer Studies) . . 45

Proof Test of a System to Measure the Dry Deposition of Sulfur Aerosols in the Plume from a Northwest Fossil Fuel Power Plant - J. G. Droppo (Atmospheric Boundary Layer Studies) 50

Limitations on the Determination of Deposition Velocities - J. C. Doran (Atmospheric Boundary Layer Studies) 55

Reduction in Annual Average Air Concentrations Due to the Deposition-Resuspension Process - T. W. Horst (Atmospheric Boundary Layer Studies) . 59

Improved Particle Deposition Model - G. A. Sehmel and W. H. Hodgson (Radioisotopes as Particles and Volatiles) 61

Airborne Plutonium Transport of Nonrespirable Particles - G. A. Sehmel (Particle Resuspension and Translocation) 65

Wind-Caused Particle Resuspension Rates - G. A. Sehmel and F. D. Lloyd (Particle Resuspension and Translocation) 74

Application of Soil Erosion Data to Particle Wind Resuspension - M. M. Orgill (Particle Resuspension and Translocation) 79

Weathering of Surfaces as Measured by Airborne Radioactive Particle Concentrations on the Hanford Reservation - G. A. Sehmel (Particle Resuspension and Translocation) 85

Radioactivity in Forest Fire Smoke Plumes - G. A. Sehmel and M. M. Orgill (Particle Resuspension and Translocation) 88

The Crosswind Distribution of Contamination Resuspended from a Surface Area Source - T. W. Horst (Particle Resuspension and Translocation) . . 91

POLLUTANT SCAVENGING 95

Precipitation Scavenging Program Design for FY 1977 - B. C. Scott (Precipitation Scavenging in MAP3S) 97

The MAP3S Precipitation Chemistry Network - M. T. Dana, D. R. Drewes, D. W. Glover, J. M. Hales and J. E. Rothert (Precipitation Scavenging in MAP3S) 101

An Algorithm for Processing and Analyzing Data from the MAP3S Precipitation Network - D. R. Drewes (Aerosol and Trace Gas Transformations) 103

Application of a Mesoscale Model for Determining Transport and Scavenging in Lake-Effect Snowstorms - B. C. Scott and W. J. Eadie (Precipitation Scavenging in MAP3S) 104

Results of Flare Release of AgI and In into a Super Cooled Cloud - W. E. Davis and J. M. Thorp (Precipitation Scavenging in MAP3S) . . . 108

In-Flight Aircraft Exhaust and Tracer Size Distribution Measurements - B. C. Scott and N. S. Laulainen (Precipitation Scavenging in MAP3S) . . 114

A Microphysical Model of Scavenging by Ice Particles - B. C. Scott (Precipitation Scavenging in MAP3S) 120

Precipitation Scavenging of Tritiated Water Vapor: A Controlled-Release Field Experiment - M. T. Dana, M. A. Wolf, N. A. Wogman (Precipitation Scavenging in MAP3S) 123

Submicron Aerosol Washout Experiment: Progress Summary - N. S. Laulainen (Precipitation Scavenging in MAP3S) 126

POLLUTANT TRANSFORMATIONS AND INTERACTIONS 133

Estimation of Transformation Rate of SO_2 to SO_4 from Atmospheric Concentration Data - A. J. Alkezweeny and D. C. Powell (Aerosol and Trace Gas Transformations) 135

SO_2 to Sulfate Conversion in an Urban Plume - A. J. Alkezweeny (Aerosol and Trace Gas Transformations) 141

Airborne Measurements of Pollutants Over Urban and Rural Sites - A. J. Alkezweeny and D. R. Drewes (Aerosol and Trace Gas Transformations) 144

Review of SO_2 Oxidation Rates in Plumes - A. J. Alkezweeny (Aerosol and Trace Gas Transformations) 146

The Design of the Lake Michigan Experiment - A. J. Alkezweeny (Aerosol and Trace Gas Transformations) 151

Airborne Measurements of Hydrocarbons in the St. Louis Plume - A. J. Alkezweeny and R. N. Lee (Aerosol and Trace Gas Transformations) . 154

GC System for the On-Site Analysis of Hydrocarbons at Ambient Concentrations - R. N. Lee (Aerosol and Trace Gas Transformations) . . 157

Estimating Aerosol Optical Properties from Size Distributions Measured by Optical Particle Counters - N. S. Laulainen (Aerosol and Trace Gas Transformations) 159

Airborne Measurements of Particle Size Distribution, Light Scattering and Turbidity at Different Altitudes - A. J. Alkezweeny and N. S. Laulainen (Aerosol and Trace Gas Transformations) 165

Some Aspects of the "Stationary State" Approximation and Its Use in Modeling Kinetic Phenomena - J. M. Hales (Aerosol and Trace Gas Transformations) 168

Numerical Modeling in Support of the Long Range Plume Transformation Study - J. M. Hales (Aerosol and Trace Gas Transformations) 174

An Algorithm for Analyzing and Displaying Aerosol Data - D. R. Drewes and N. S. Laulainen (Aerosol and Trace Gas Transformations) 177

An Algorithm for Processing and Analyzing Data from the BNW DC-3 Research Aircraft - D. R. Drewes and A. J. Alkezweeny (Aerosol and Trace Gas Transformations) 178

A Very Low Frequency Navigation System as a Research Tool - R. F. Edwards, F. O. Gladfelder and J. R. Lugar (Research Aircraft Operations) . . . 180

COMPOSITE MODELS FOR ATMOSPHERIC PROCESSES 183

A Formulation of Time-Varying Depths of Daytime Mixed Layer and Nighttime Stable Layer for Use in Air Pollution Assessment Models - D. C. Powell (Atmospheric Boundary Layer Studies) 185

Computational Economy Measures Applied to the Gaussian Plume Model with Restricted Vertical Mixing - D. C. Powell (Atmospheric Boundary Layer Studies) 189

Precipitation Data Base Manipulation for Use in Regional Transport and Removal Models - T. D. Fox and L. L. Wendell (MAP3S Modeling Studies) . . 191

Some Effects of Isentropic Vertical Motion Simulation in a Regional Scale Quasi Lagrangian Air Quality Model - W. E. Davis and L. L. Wendell (MAP3S Modeling Studies) 193

Comparison of Two Constant Level Trajectory Models - W. E. Davis and L. L. Wendell (Precipitation Scavenging in MAP3S) 198

An Improved Computer Code for Reactive Plume Trajectory Calculations - J. M. Hales (MAP3S Modeling Studies) 202

Air Quality Sector of the Energy-Related Northwest Regional Assessment Program - D. S. Renné and D. L. Elliott (Pacific Northwest Regional Assessment Program) 205

A Multi-Source Comparison of the Effects of Real Time Versus Time Averaged Precipitation Data on SO_2 and Sulfate Particulate Removal in the Regional Assessment Model - L. L. Wendell and D. C. Powell (Precipitation Scavening in MAP3S) 207

PUBLICATIONS AND PRESENTATIONS 213

ORGANIZATION CHART 219

DISTRIBUTION 223

ATMOSPHERIC SURVEYS AND WEATHER MODIFICATION

To identify the most pressing air pollution problems and establish priorities for more detailed investigations, we are continuing surveys of effluents released to the atmosphere. Measurements are taken within the source areas, areas covering several states, and on hemispheric scales.

Fallout measurements and evaluations identify worldwide nuclear test debris, effluents from nuclear power generation and the transfer of this material to the surface. Ambient distributions of pollutants from fossil fuel and coal facilities are also being measured. Atmospheric pollution from urban complexes is being measured to study the physical and chemical changes which occur as the pollutant plume is transported large distances. Measurements have begun of air pollution and energy production effects which might inadvertently modify weather or climate.

- RADIOACTIVE FALLOUT RATES AND MECHANISMS
- COAL CONVERSION POLLUTANT CHEMISTRY
- ARID LANDS ECOLOGY PROGRAM

ELEMENTAL CONCENTRATIONS OF NORTHERN HEMISPHERIC AIR AT QUILLAYUTE, WASHINGTON

J. D. Ludwick, T. D. Fox and S. R. Garcia

Incoming air at Quillayute, Washington, which is representative of hemispheric aerosol levels, is analyzed for stable elements. Results indicate that natural mixing and cleansing processes have significantly reduced anthropogenic and natural aerosols introduced by distant sources. The levels measured are similar to those observed in very remote areas of both the northern and southern hemispheres.

Chemical and meteorological information is being gathered, interpreted and documented to describe source regions and their respective contributions to air masses influencing the continental United States. We have accumulated considerable stable element data from our Air Reference Station at Quillayute, Washington.

The data indicate that clean air days whose 3-day back trajectories do not intercept land occur at a rate of 40 to 50/yr, or 12% of the time. This means that representative sampling of hemispheric values of airborne material is possible from a land-based station. The 3-day criterion is tantamount to being on an island 1500 miles from any other land. The low frequency of such clean days, however, makes long-term sampling necessary. A problem with the clean days is that they tend to come in groups; this does not guarantee accurate representative sampling all year round. The averages can, therefore, be severly influenced by air from cleaner or more polluted regions of the northern hemisphere.

Interpretation of part of the data shows that the ocean itself contributes stable elements to the air. Comparison of x-ray fluorescence analysis for two sampling periods shows increased oceanic components during the winter, probably because more storms occur then. A decrease in crustal and pollutant materials is shown in Table 1. In early data, zinc concentrations appeared anomalous and from an unknown source. Table 1 shows zinc following the ocean component; it may well result from zinc concentrations in the ocean surface film. Iron values have dropped to those observed in mid-ocean. Overall, the indication is that seasonal variations in source regions occur, or different source regions predominate in the winter. Seasonal changes in the incoming air masses may be deduced from the most recent data; these are illustrated in Figure 1.

Another interesting comparison can be made using the stable element data on clean days. Normalizing the concentrations of crustal material to that of iron will reveal the materials from other than crustal sources. Table 2 indicates results of this process.

To summarize our conclusions thus far:

- Unusually high lead values have been attributed to anthropogenic smelting and combustion effluent entering the atmosphere.
- Zinc may be from the ocean surface concentration; arsenic may or may not accompany zinc.

TABLE 1. Ocean Trajectory Trace Element Comparisons for Two Seasonal Sampling Periods

	4/1/74 - 11/30/74	12/1/74 - 6/1/75	TREND
	ng/m^3	ng/m^3	
Cl	701.4 ± 508.3	2045 ± 913	↑
K	35.7 ± 16.6	56.6 ± 17.5	
Ca	43.9 ± 36.3	65.3 ± 36.5	
Br	5.58 ± 307	13.4 ± 5.7	
Zn	4.24 ± 2.32	11.3 ± 10.2	
Ti	1.58 ± 1.45	0.85 ± 0.89	↓
Cr	0.0	0.01 ± 0.17	-
Mn	0.66 ± 0.71	0.83 ± 0.77	↑
Fe	25.3 ± 17.0	13.1 ± 9.7	↓
Ni	0.13 ± 0.09	0.14 ± 0.07	-
Cu	0.97 ± 0.54	0.61 ± 0.52	↓
As	0.12 ± 0.22	0.0	-
Pb	1.93 ± 1.02	1.78 ± 1.19	↓

Neg 770842-2

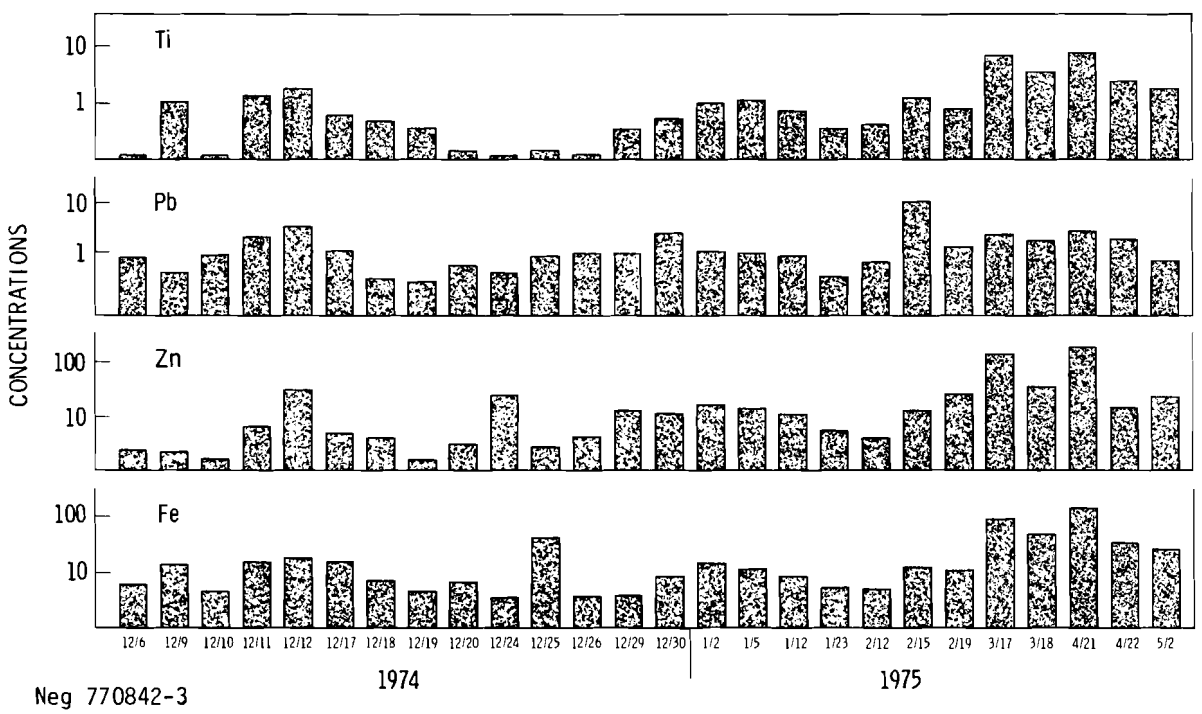

Neg 770842-3

FIGURE 1. Seasonal Hemispheric Air Concentration Variations at Quillayute from Measurements of Individual Clean Days (ng/m^3)

TABLE 2. Stable Element Concentrations Normalized to that of Iron Found in Crustal Materials

METAL	ENRICHMENT over	CRUSTAL FRACTION COMPARED TO Fe*
Pb (1.9 ng/m^3)	300	2.6×10^{-4} (6.6×10^{-3} ng)
As (0.12 ng/m^3)	130	3.6×10^{-5} (9.1×10^{-4} ng)
Zn (4.24 ng)	120	1.4×10^{-3} (3.5×10^{-2} ng)
Cu (0.97 ng/m^3)	35	1.1×10^{-3} (2.8×10^{-2} ng)
V (<1 ng/m^3)	<15	2.7×10^{-3} ($< 6.8 \times 10^{-2}$ ng)
Ni (0.13 ng/m^3)	3.5	1.5×10^{-3} (3.8×10^{-2} ng)
Mn (0.66 ng/m^3)	1.3	1.9×10^{-2} (4.8×10^{-1} ng)
Fe (25.3 ng/m^3)	1.0	
Ti (1.58 ng/m^3)	0.7	8.8×10^{-2} (2.2 ng)

*SEA IS NOT IMPORTANT SOURCE UNLESS SURFACE CONCENTRATION IS IMPORTANT

Neg 770842-1

- High copper values may result from volcanic emission.
- Vanadium and nickel are probably caused by oceanic vehicle combustion of crude oil products.
- Values of manganese and tetanium are well within those expected from crustal sources alone.

ATMOSPHERIC FALLOUT DURING 1976 AT RICHLAND, WASHINGTON AND POINT BARROW, ALASKA

C. W. Thomas

Radionuclide concentrations in surface air are monitored continuously at Richland, Washington, and Point Barrow, Alaska. The concentrations were at their lowest since measurement began in 1953; three Chinese tests and one Russian detonation contributed radionuclides to the atmosphere, which will be evident in 1977.

The concentrations of radionuclides in surface air are measured continously at Richland, Washington and Point Barrow, Alaska, by filtering large volumes of air through IPC filters at a rate of 2400 linear feet per minute. The concentrations of most radionuclides are determined directly by gamma ray spectrometric analyses, though for

certain radionuclides, a chemical separation is necessary before either beta or alpha counting to determine the concentrations. The isotopes routinely measured include radionuclides in terrestrial material, radionuclides produced by cosmogenic spallation reaction, fission and activation products, and fissile material from weapons testing.

Atmospheric weapons tested in the northern hemisphere during 1976 were a 20 kiloton device detonated in January, a 200 kiloton device tested in September, and a large 4200 kiloton device detonated in November, all by the People's Republic of China. In addition, measurements made in late 1975 and early 1976 showed that the large USSR underground test (6.7 on the Richter scale) in October 1975 vented to some degree and contributed to the radionuclide concentrations in northern hemispheric surface air.

During 1976, the concentrations of radionuclides of stratospheric origin associated with weapons testing decreased to the lowest level recorded since measurements began in 1953. Figure 1 shows the ^{137}Cs concentration in surface air at Richland, Washington since 1953. These data are a combination of measurements made at Richland from 1960 to the present and measurements made at Harwell, England from 1953 to 1966 and normalized to Richland. Also shown is the total amount of debris inserted into the northern stratosphere since 1952, along with the yearly stratospheric inventory. Debris inserted into the lower stratosphere during one year will be mainly observed in surface air the following year. The resident half-life was about 1 year for stratospheric debris measured from 1963 through 1967, 1971 through 1973, and 1974 through 1976.

The stratospheric reservoir during 1977 will be composed of the 4.2 megaton detonated in November and a residual 0.7 megaton from the 1976 inventory, but it is possible that due to the very late injection time (November 17, 1976) of the 4.2 megaton the contribution from this debris will be minor during the spring maxima of 1977.

Low yield devices tested during January and September contributed a much larger

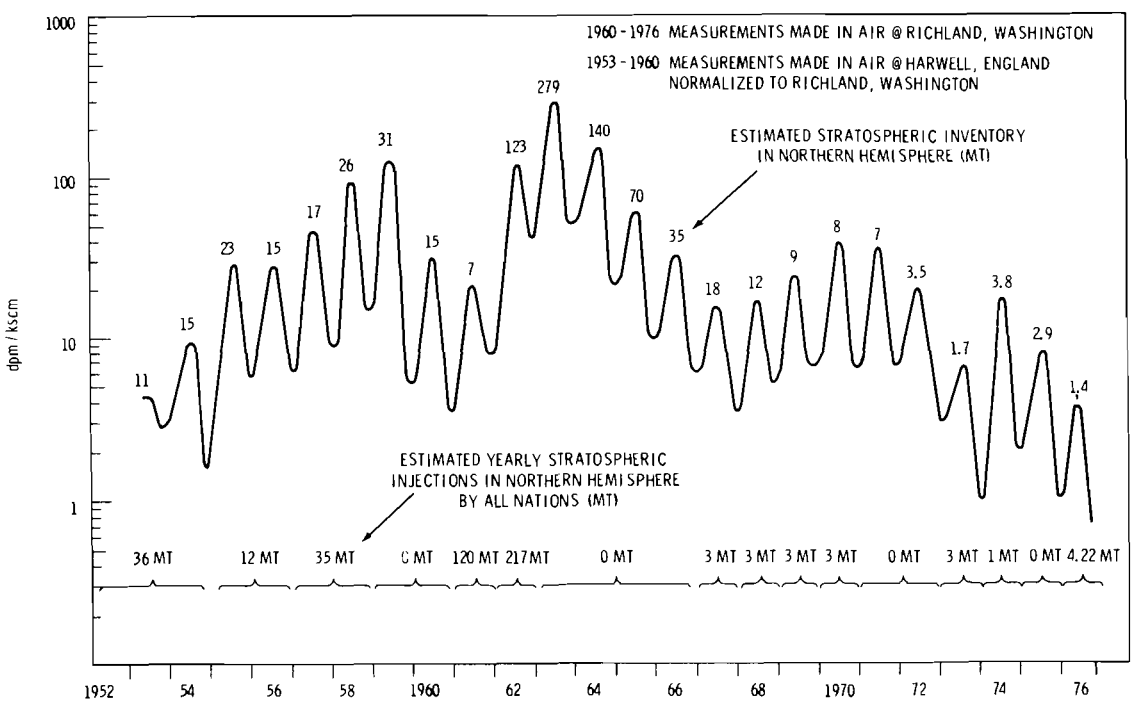

FIGURE 1. ^{137}Cs Concentration in Air at Richland, WA

initial concentration in surface air than the higher yield device of the November test. This is because higher yield devices produce sufficient energy to inject most of the debris into the stratosphere; it then descends rather slowly into the troposphere over a period of years. On the other hand, a low yield device places most of the debris within the troposphere. The trajectory of the debris from the January 1976 low yield test carried most of the debris north of the USA. The concentrations of medium lived radionuclides such as ^{95}Zr, ^{103}Ru, ^{141}Ce, (half lives of 65, 40, 32 days) were 5 times higher at Point Barrow, Alaska than at Richland, Washington. Trajectory analysis of the leading edge of the radioactive debris from the September 200 kiloton test indicated that it moved across the northern United States and southern Canada and that the most southern part of the debris cloud turned southward, entering a low pressure area which carried it to the Gulf States and subsequently along the eastern seaboard. This movement of the debris cloud, together with heavy precipitation along the eastern seaboard, resulted in significant deposition, particularly in eastern Pennsylvania, Connecticut, Massachusetts, and New Jersey.

The atmospheric concentration for ^{131}I measured in Richland, Washington, which was on the southern edge of the debris cloud, reached a maximum value of 140 dpm/10^3M^3 during the first circumnavigation of the earth (October 10, 1976), but due to the horizontal and vertical diffusion attained a higher concentration (200 dpm/10^3M^3) during the second circumnavigation of the earth (October 21, 1976).

RADIOACTIVE FALLOUT FROM THE CHINESE NUCLEAR WEAPONS TESTS OF JANUARY 23, 1976, SEPTEMBER 26, 1976, AND NOVEMBER 17, 1976

C. W. Thomas, J. K. Soldat, W. B. Silker and R. W. Perkins

Concentrations of ^{131}I were measured at Richland, Washington, and estimated for the rest of the United States, for three above-ground nuclear tests in 1976. These concentrations are much greater than those estimated to result from nuclear reactors.

Three above-ground nuclear weapons tests were carried out during 1976 by the People's Republic of China. The first test was a 20 kiloton atmospheric burst on January 23, 1976. The trajectory of the cloud carrying this debris was mainly north of the lower 48 states. Peak concentration of ^{131}I from this debris measured at Richland, Washington was 0.57 dpm/10^3M^3.

On September 26, 1976, a 200 kiloton weapon was detonated in the atmosphere. Again the leading edge of the radioactive debris moved across the northern United States and Southern Canada but entered a low pressure area near the Great Lakes which carried it to the Gulf States and eastern seaboard. There was significant deposition of short-lived radionuclides over much of the U.S. However, because of the trajectory taken by the debris and the occurrence of precipitation along the eastern seaboard states, the deposition was 1000 times greater in regions of precipitation along the eastern seaboard than in other regions of the U.S.

The particle size distribution with which the radionuclides were associated at our Richland, Washington monitoring site became progressively smaller with time following the second detonation. The concentrations of radionuclides with refractory precursors which would therefore be expected to be present on large particles decreased by a factor of up to two relative to ^{103}Ru (which has a noble gas precursor and would be expected to be present more on small

particles) during one circumnavigation of the earth, indicating a deposition loss of at least 50% from gravitational settling. From 30 to 50% of the ^{131}I was gaseous; this gaseous fraction was distributed in roughly comparable amounts between inorganic and organic fractions. The ^{131}I concentration in surface air at Richland reached a maximum of 200 dpm/10^3/M^3 during the second circumnavigation (October 21, 1976).

A 4200 kiloton weapon was tested on November 17, 1976. Tropospheric debris from this test was minor compared to that from the September test. Most of the debris was inserted into the stratosphere from which it will descend rather slowly over many years. Although residual ^{131}I from the September test was still present in surface air in late November, it is estimated that the ^{131}I concentration in air from this November test was about 3 dpm/10^3M^3. Also present at concentrations of 3 dpm/10^3M^3 was ^{237}U, a radionuclide which results from neutron reaction with ^{238}U in the device; its concentration depends on the type of device.

The potential radiation doses to the population of the eastern U.S. seaboard states were estimated from measurements of ^{131}I concentrations in grass samples using reasonably conservative assumptions. The maximum thyroid dose to an infant consuming one liter per day of milk was estimated to be about 1 rem. The integrated population thyroid dose from inhalation and consumption of leafy vegetables and milk was estimated to be 2.4 x 10^6 man-thyroid-rem received by a population of 78 x 10^6 people. The population thyroid doses received in the midwestern and western U.S. were much less than those on the eastern seaboard.

The estimated population thyroid dose from nuclear reactors now operating is approximately 10^4 man-thyroid-rem. Thus, the recent Chinese nuclear test produced a potential population thyroid dose of about 200 times that currently received each year from operating nuclear power reactors.

By comparison, the potential per capita thyroid dose due to ^{131}I received from nuclear power reactors operating in the year 2000, assuming they comply with existing Appendix I guidelines of WASH 1258, would not be over 20 mrem/yr from all pathways of exposure at the boundary of a nuclear reactor site, and would be only 0.2 mrem/yr for the average population. Assuming a per capita dose of 0.2 mrem/yr to the thyroid and a population of 250 x 10^6 in the year 2000, the integrated population dose is not likely to exceed 5 x 10^4 man-thyroid-rem/yr. At this rate, it would take 50 years of such reactor operations to yield the population thyroid dose of 2.4 x 10^6 man-thyroid-rem that the eastern U.S. population may have received from this Chinese nuclear test.

It must be emphasized that the actual dose which is received either from past nuclear tests or from nuclear power reactor operation depends on whether cows are actually on pasture and their milk is actually being consumed; also on whether leafy vegetables are being produced and consumed. We believe, however, that the comparison between the potential exposure to ^{131}I from nuclear power reactors and from this past Chinese nuclear test is certainly valid since they both employ the same assumption on ^{131}I pathways.

TRACE ELEMENT AND SULFATE CONCENTRATIONS DOWNWIND OF MILWAUKEE

J. A. Young

Pollutant concentrations were measured over Lake Michigan as functions of distance downwind of Milwaukee. A relationship will be developed for rate of decrease in concentrations; this will be used to determine the effect of pollutant sources downwind of St. Louis on concentrations further away.

INTRODUCTION

An urban area releases a wide spectrum of pollutants, many of them toxic, into the atmosphere. These pollutants affect not only the urban area itself, but also regions far downwind. The effect of urban pollutants upon downwind areas depends on the rates of atmospheric mixing, wet and dry deposition on the earth's surface, and chemical reactions which cause the pollutant concentrations to decrease downwind of the urban area. Concentrations of certain pollutants even increase downwind of a city as a result of chemical reactions.

From measurements of pollutant concentrations by PNL downwind of St. Louis in previous years, pollutants emitted by St. Louis are easily detected in rural areas over one hundred miles downwind. However, determination of rates at which atmospheric mixing, wet and dry deposition, and chemical reactions changed the pollutant concentrations downwind of St. Louis was complicated by the possibility that pollutant sources downwind of St. Louis significantly increased the pollutant concentrations. Therefore, a Lagrangian experiment was designed in which pollutant concentrations were to be measured over Lake Michigan as a function of distance downwind of Milwaukee, where there are no pollutant sources to complicate the calculations. However, during the experimental period from August 19 through August 30, 1976 there were only two days in which the wind was primarily from the west so that the concentrations of Milwaukee pollutants could be measured as a function of distance over Lake Michigan. On three other days the wind had an easterly component, and pollutant concentrations were measured as a function of downwind distance over land surfaces. On another day the wind was primarily from the south and concentrations were measured at two distances downwind of Chicago over Lake Michigan.

EXPERIMENTAL PROCEDURE

Most pollutant concentrations measurements were made aboard the Battelle DC-3, which was operated out of Muskegon, Michigan.

On each sampling day measurements of particle concentrations and lapse rate were used to determine the depth of the mixed layer. Then pollutant concentrations were at two or more altitudes in the mixed layer approximately 10 miles downwind of Milwaukee while the DC-3 flew horizontally perpendicular to the wind from one side of the Milwaukee plume to the other. During sampling the Global Navigation System aboard the DC-3 was used to calculate the wind speed and direction. The DC-3 then moved downwind the distance necessary to sample the same air, and again made sampling traverses across the plume at two or more altitudes. This procedure was repeated until either the air passed over a major pollutant source or the DC-3 ran short of fuel after 7 to 8 hours. On two occasions sampling was continued after re-fueling the DC-3. The lowest altitude sampled was about 500 feet. Samples were collected up to 120 miles downwind of Milwaukee.

One sample of air was collected in evacuated cylinders during each traverse of the plume to allow later analysis for the conservative gases, carbon monoxide and the

chlorfluoromethame CCl_3F. A flow meter allowed the air to bleed into the evacuated cylinder at a relatively constant rate during each traverse. The rate of decrease of the concentrations of these conservative gases downwind of Milwaukee will be used to calculate the rate of dilution of the Milwaukee plume by atmospheric mixing.

One high volume air sample was collected on IPC-1478 filter paper during each traverse of the plume, to be analyzed later for trace elements and sulfates to determine the emission rates of these pollutants by Milwaukee. On two days of higher wind speeds and therefore lower pollutant concentrations, only one air filter sample was collected during the two or more traverses of the plume at a given distance downwind of Milwaukee. Air filter samples were also collected aboard the Battelle Cessna-411 above the mixed layer and upwind of Milwaukee in the mixed layer. The rate of decrease of the flux of the trace elements downwind of Milwaukee will be used to calculate the deposition velocity of particulates on the earth's surface. The increase in the sulfate to trace element ratio will indicate the rate of conversion of SO_2 to sulfates in the atmosphere. Since certain trace metals are believed to catalyze the conversion of SO_2 to sulfates the concentrations of these metals are being measured along with the conversion rates.

One air sample was collected at each distance (integrated over all altitudes) downwind of Milwaukee using an air filter system supplied to us by Dr. Lenny Newman of Brookhaven National Laboratories. This filter pack contains a filter to remove particulates and then a chemically treated filter which removes SO_2. These filters have been sent to Dr. Newman for sulfate and SO_2 analysis; his results will be compared with those measured by Battelle.

An air sample integrated over all at altitudes was also collected at each distance downwind of Milwaukee on fluoropore filter paper. Some of these samples have been sent to the Argonne National Laboratory to be analyzed by the infrared spectroscopy, and others were sent to the Lawrence Livermore Laboratory to be analyzed by the technique of Electron Spectroscopy for Chemical Analysis (ESCA).

Concentrations of the trace gases SO_2, NO_X, and ozone were measured in real time to determine the rates of the chemical reactions of these gases. The measured concentrations of the conservative gases CO and CCl_3F will be used to correct for dilution due to atmospheric mixing in determining reaction rates. Particulate concentrations were also measured in real time and will be used to determine the fraction of the time the DC-3 was actually in the urban plume during the collection of the integrated samples, and will indicate the variation in concentration across the plume of the contaminants that are in particulate form. On some flights the particle size spectrum was determined using Whidby and Royco analyzers. If trace metals play a significant role in catalyzing the conversion of SO_2 to sulfates, then the rate of conversion of SO_2 will be affected by the size spectrum and therefore the surface area of the particles containing the catalyzing metals.

Air samples were also collected at ground level for CO, CCl_3F, SO_2, sulfate and trace element analysis. Lundgren impactors were operated to obtain particle size distributions of particulates. When the wind was from the west, samples were collected around a chartered fishing boat on traverses across the plume perpendicular to the wind approximately ten miles downwind of Milaukee on the same track as that taken by the DC-3. On one day a sample was also collected 20 miles downwind. Samples were also collected on the east shore of Lake Michigan at the location where the Milwaukee plume crossed the shore.

RESULTS

This article discusses the results of analyzing the high volume air filters by X-ray fluorescence for sulfates and a few trace elements. In the future at least some of these filters will be analyzed by neutron activation to obtain a wider spectrum of trace elements. Analysis of the whole air samples for CO and CCl_3F has not been completed. The results of the analysis for SO_2, NO_X, O_3, and particle concentrations will be discussed by other investigators.

The vertical profiles of particulate material concentrations downwind of Milwaukee differed distinctly over land and over the lake. When the wind was from the east, so the plume traveled over land, the concentrations were fairly uniform throughout the mixed layer, decreasing slightly with altitude (Figure 1). On August 27 the wind was from the west, carrying the plume out over the lake. The concentrations generally showed only a slight decrease with altitude ten miles downwind of Milwaukee (Figure 2), but by the time the plume reached the east shore of Lake Michigan 80 miles downwind the

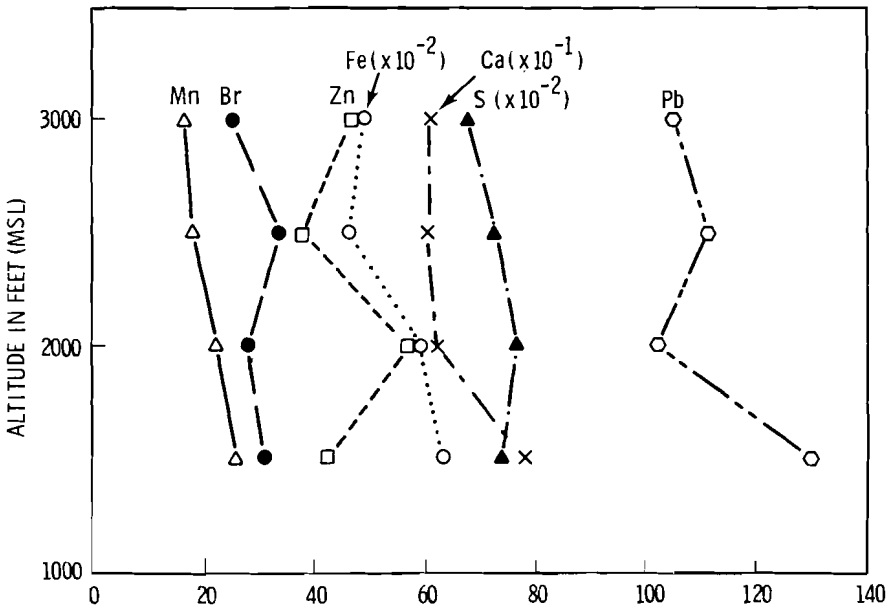

Neg 7611854-1

FIGURE 1. Concentration in 10^{-9} g M^{-3} West of Milwaukee on August 23 and 24, 1976

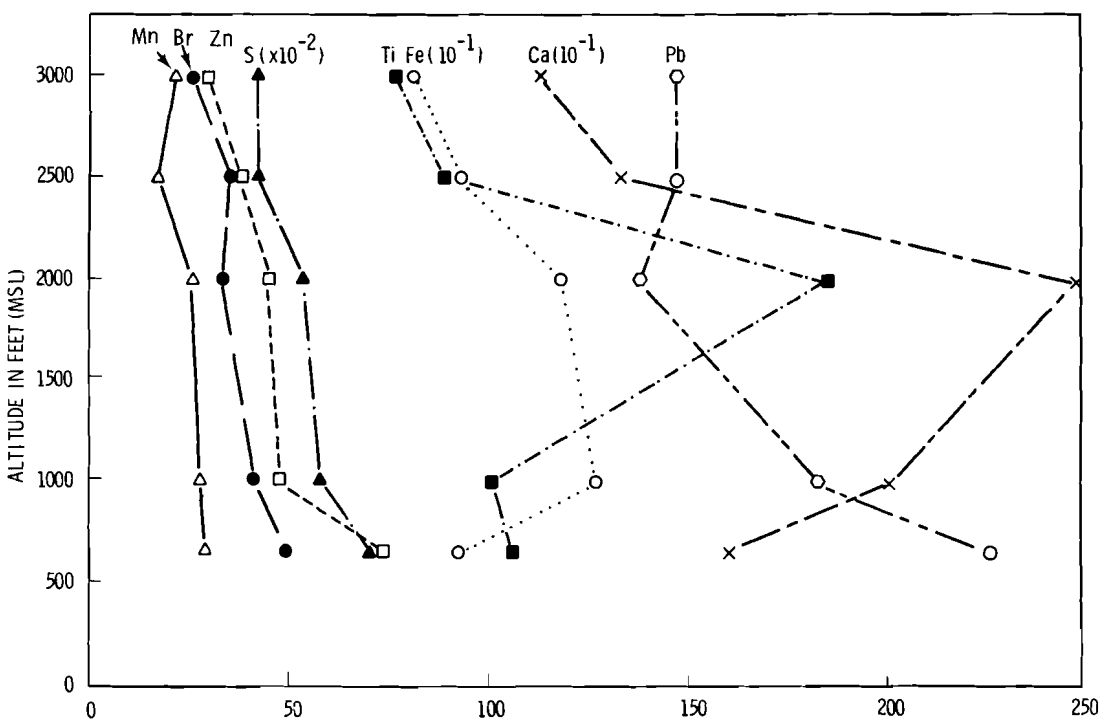

Neg 7611854-2

FIGURE 2. Concentration in 10^{-9} g M^{-3} 10 Miles East of Milwaukee

concentrations had developed a large decrease with altitude in the mixed layer (Figure 3). In addition, the concentrations of Tl and Ca on August 27 showed large maxima at 2000 ft MSL 10 miles downwind of Milwaukee which were still quite evident 80 miles downwind. These results indicate that vertical mixing was considerably less over the lake than over the land. This is expected since land surfaces are warmer than the air during the afternoon, which promotes convection, while water surfaces are colder than the air, inhibiting convection.

The fluxes of sulfur (sulfates), calcium, manganese, iron, zinc, lead and bromine in the mixed layer downwind of Milwaukee have been calculated for the layer between ground level and the highest level sampled. This layer generally included most of the mixed layer. Data on mixed layer depth and particulate concentrations in the mixed layer will later be extrapolated to the top of the mixed layer to obtain mixed layer total fluxes. When analysis of upwind samples is completed the elemental fluxes upwind of Milwaukee will be subtracted from the downwind fluxes to obtain the net fluxes due to Milwaukee.

The calculated trace element fluxes downwind of Milwaukee varied by as much as an order of magnitude on different days. The fluxes of iron, calcium, and manganese, which are generally considered to be of crustal origin, were much higher on days of higher wind speed (9-14 M sec^{-1}), presumably because the higher winds picked up more crustal material. Calcium has also been shown to be introduced into the atmosphere by the concrete of a city, especially at higher wind speeds. Fluxes of sulfates, zinc, lead, and bromine, which are primarily of anthropogenic anthropogenic origin, did not appear to be correlated with the wind speed. Zinc, lead, and bromine fluxes were roughly the same on all days, except one in which the fluxes were much higher. The higher downwind fluxes on this day probably resulted from higher concentrations in the air upwind of Milwaukee. When the air samples collected upwind of Milwaukee have been analyzed, the upwind fluxes of these elements will be subtracted from the downwind fluxes to obtain their net rate of

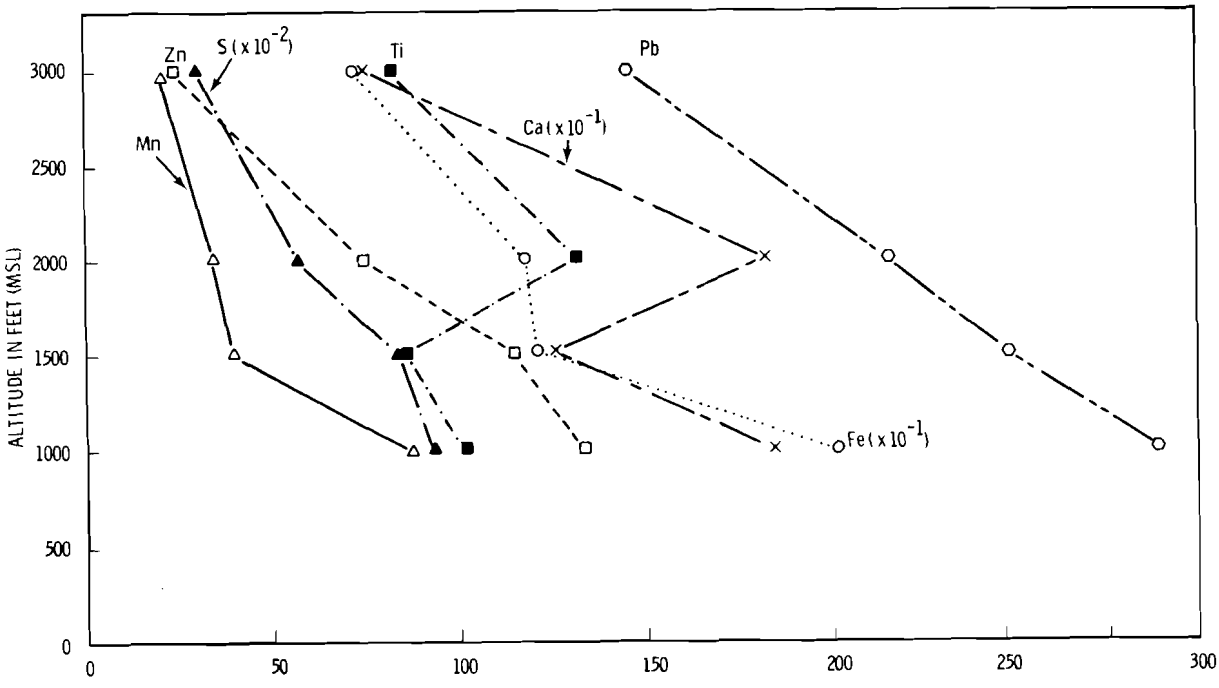

Neg 7611854-3

FIGURE 3. Concentrations in 10^{-9} g M^{-3} 82 Miles East of Milwaukee

emission by Milwaukee; any evidence for variations in the emission rate from day to day will also be determined.

The ratio of the sulfate flux to those of other elements generally increased with distance downwind of Milwaukee, indicating that SO_2 was being converted to sulfate in the atmosphere. The flux of the sulfate produced by SO_2 conversion downwind of Milwaukee was calculated as a function of distance for each day. It was found that up to 2/3 of the sulfate measured downwind was due to SO_2 conversion downwind of Milwaukee. The amount of sulfate resulting from downwind SO_2 conversion also varied by as much as an order of magnitude from day to day, with low conversion amounts being measured on days of low trace element concentrations. This would be expected if days of low downwind concentrations resulted from low emissions from Milwaukee. However, if the Milwaukee SO_2 emissions remained fairly constant, then these results would indicate that the rate of conversion of SO_2 to sulfates was slower on days of low trace element concentrations.

CHARACTERIZATION OF SUBSTANCES IN PRODUCTS, EFFLUENTS AND WASTES FROM SOLVENT REFINING COAL PLANT

M. R. Petersen, J. C. Laul and P. W. Ryan

PNL is conducting a program to characterize products, effluents and wastes from coal conversion processes being tested on a laboratory scale and in pilot plants. The characterization program involves a comprehensive analysis of inorganic constituents including chemical species determination and analysis of organic materials. So far, we have identified about 125 different organic and inorganic compounds in products, byproducts and effluents from the solvent refined coal (SRC) process.

Samples were collected from the SRC plant at Fort Lewis, WA during May, 1976; they included the feed coal, SRC product, mineral residue, retention pond sediment, byproduct sulfur, process water at various treatment stages, process solvent, wash solvent, byproduct light oil, off-gas samples, and aerosol material collected over the cooling product. These samples were to be analyzed to determine their components. Since the SRC plant is a pilot operation, operating conditions and materials are changed frequently for experimental purposes. Therefore, analytical results based on individual samples may vary substantially between plant runs.

The water samples were preserved with hydrochloric acid or methylene chloride for inorganic and organic analysis, respectively. The sediment samples were frozen immediately with dry ice; the organic liquids were kept under refrigeration. The separation scheme which permitted quantitative analysis of the samples for some components consisted of dissolving the sample in isooctane and obtaining the basic, acidic, neutral, and polynuclear aromatic (PNA) fractions. This was done by extracting with 1N HCl, 1N NaOH and finally treating the neutral fraction with dimethylsulfoxide to remove the PNA hydrocarbons. These four fractions (basic, acidic, neutral, and PNA) were then analyzed by gas chromatography and by gas chromatography-mass spectrometry (GC/MS).

The samples of light oil, wash solvent, and process solvent are a set of progressively higher boiling cuts, which are

distilled just before recovery of the dissolved solvent refined coal. The distribution of organic compounds in these samples reflects this boiling range. Substituted benzenes and indans predominate in the light oil; naphthalene and methylnaphthalenes are the most abundant (at least 3% each) in the wash solvent; phenanthrene/anthracene are the major compounds in the process solvent. A total of about 65 aromatic, 25 aliphatic, 15 phenolic, and 15 heterocyclic compounds have been identified in these samples. Polycyclic aromatic compounds up through alkyl-substituted benzopyrenes have been identified.

The untreated process water contains several percent of organic matter, and the preliminary analyses indicate that phenols are the predominant species present. Other hydrocarbons, such as PNA's, are present at the ppm level. The mineral residue and product contain many PNA's in 100 ppm ranges. The aerosol material arising during cooling of the product is composed of many high molecular-weight PNA's with a distribution of compounds similar to that of SRC product. The concentrations are very high since the particulate samples were collected directly over the molten product as it cooled. Quantitative data are given in Table 1 for some of the samples from the May 1976 collection. These data have not been corrected for losses of the low molecular weight compounds, of less than 150 amu. The organic liquids contain considerable tar material; e.g., the process solvent is at least 60% asphaltene. This material precipitates during the partitioning procedure and a satisfactory analysis of the tar has not been obtained.

Analytical procedures are being improved to determine the organics remaining in the treated water. The compounds are present in ppm concentrations and tend to be water soluble. Some additional work is necessary to permit quantitative analysis of the trace organic components in the treated water.

An important part of the research program at the SRC plant is the defining of the distribution and chemical species of the trace elements. Samples of products, effluents, and wastes have been collected and analyses of approximately 30 trace elements are being carried out. Measurements of these elemental concentrations in the coal, mineral residue, and the solvent refined coal product are presented in Table 2. The variability in the composition of coal is illustrated in this table. On comparing the composition of feed coal and the NBS standard coal mixture (columns 2 and 6), one finds up to six-fold differences in concentration. This variability of coal leads us to expect similar variability in the absolute trace element content of products and effluents from a given coal liquefaction process. However, in the SRC process, the most significant observation is that most of the bromine is carried from the coal into the product. Also, a substantial fraction of the zinc, tantalum, and chromium are carried into the product. In general, it appears that the refractory and alkaline metals remain almost entirely with the mineral residue.

A clue as to the mineralogy involved and its contribution to elemental distributions can be obtained by comparing the rare earth spectra in the coal feed, the product and the mineral residue as shown in Figure 1. Here the rare earth concentrations are normalized to that which is believed to be the composition of the primordial earth. The coal feed and mineral residue have similar rare earth distributions, and these are typical of those found in major terrestrial minerals. The rare earth distribution in the solvent refined coal product is substantially different and is actually similar to the accessory mineral hornblende, which crystallizes late in magmatic differentiation processes. Thus, we believe that the mineral phases in coal may provide a clue to the potential for release of toxic trace elements to the product or the gaseous effluent. Analyses are also being performed on process solvent naphtha and liquid effluents from the SRC plant. Chemical speciation measurements are being made of such trace elements as arsenic and mercury. We thus expect to have information on the movement of the various trace elements through the process and the resulting chemical forms.

TABLE 1. Analyses of Samples Collected at Solvent-Refined Coal Plant, Concentration (ppm)

PNA Fraction	Light Oil	Wash Solvent	Process Solvent	Raw Process Water	Mineral Residue	Solvent-Refined Coal	Particulate Filter (concentration μg/m³)
xylene		1300					
o-ethylbenzene	9800	1700					
m/p-ethylbenzene		700					
C_3-benzene	3900	1500					
C_4-benzene		500					
indane	4300	13000			85		
methylindane	510	2500		15	25		
methylindane	180	1400					
methylindane	240	2300			55		
dimethylindane	< 5	40			25		
tetralin	330	4100		< 0.1	110		
dimethyltetralin	< 5	1500		0.5	35		
6-methyltetralin	110	3200			50		
naphthalene	1630	32000	100	5	1500	1	3
2-methylnaphthalene	690	32000	3800	2	740	8	16
1-methylnaphthalene	110	12000	930		180	5	4
dimethylnaphthalene	80	13000	11200	0.3	260	6	170
dimethylnaphthalene	70	700	1700		60	3	20
dimethylnaphthalene		4000	4200		150		
dimethylnaphthalene	10	160	650	2	< 2		10
2-isopropylnaphthalene		40	50	0.7	< 1		< 0.5
1-isopropylnaphthalene		210	1400	2	15		20
C_4-naphthalene		5	50		< 1		4
cyclohexylbenzene		410			5		
biphenyl	80	10000	5900	0.2	270	2	75
acenaphthylene	2	500	3400	< 0.1	45	8	60
dimethylbiphenyl	15	35	2100	0.5	30	9	130
dimethylbiphenyl	21	30	560	0.2	20	7	40
dibenzofuran	8	400	5800	0.6	60	9	160
xanthene	10	30	840	0.1	20	5	40
dibenzothiophene	3	50	4200	1.5	70	30	180
methyldibenzothiophene		15	320	< 0.1	8	4	60
dimethyldibenzothiophene	5	15	1200	< 0.05	20	13	130
thioxanthene		2	3300	0.1	5	3	120
fluorene	15	250	6600	0.3	80	27	200
9-methylfluorene	15	110	3100	0.3	40	11	150
1-methylfluorene	10	10	3000	0.2	50	18	100
anthracene/phenanthrene	25	130	23000	1.1	500	300	1500
methylphenanthrene	6	15	6200	0.3	100	50	400
1-methylphenanthrene	6		3900	0.2	50	30	300
C_2-anthracene	6	25	500	< 0.05	10	1	30
fluoranthene	15	35	10500	0.4	200	180	700
dihydropyrene	6	25	1200	< 0.05	10	1	30
pyrene	20	40	11200	0.6	200	280	900
NEUTRAL FRACTION (n-alkanes)							
n-octane	16000	900		2.3			
n-nonane	8700	2700					
n-decane	9800	5000					
n-undecane	3900	8300	50	0.3	90	4	
n-dodecane	1400	21000	80	0.3	550	10	
n-tridecane	470	14000	30	0.4	9100	8	4
n-tetradecane	170	11000	340	0.3	210	7	12
n-pentadecane	60	4000	1000	0.2	80	12	18
n-hexadecane	10	400	2000	0.2	50	8	50
n-heptadecane	10	120	3100	0.02	20	3	35
n-octadecane		40	920		10	3	18
n-nonadecane		500	800		16	22	30
n-eicosane			930		14		20
n-heneicosane			600		14		35
n-docosane			670		16		55
n-tricosane			980		14		35
n-tetracosane			900		14		45
n-pentacosane			740		10		43
n-hexacosane			450		8	5	40
n-heptacosane			300		6	2	25
n-octacosane			150		5	2	28
n-nonacosane			90		4	1	18
n-triacontane			60		2	1	22
n-hentriacontane			40		1	1	15
n-dotriacontane			10		< 1		11
n-tritriacontane			5				7

Neg 769775-7

TABLE 2. Elemental Contents of Feed Coal, Solvent Refined Coal and Mineral Residue from Ft. Lewis, WA (ppm except as noted)

Element[a]	Feed Coal	Solvent Refined Coal (SRC)	Mineral Residue	Coal/SRC	NBS Coal[b]
Na	180	8.8	3150	20	420
(%) K	0.19	0.003	1.10	70	0.28
(%) Fe	2.29	0.027	13.3	85	0.81
Cr	18.4	7.5	150	2.5	19
Co	5.2	0.26	32	20	5.2
Ni	21	<6	120	4	20
Sc	2.6	0.45	14.7	5.8	3.4
Ba	65	--	260	--	390
Sr	76	<5	360	20	170
La	9.5	0.13	56	73	10.5
Ce	17	0.5	102	40	--
Nd	<10	--	<50	--	--
Sm	1.85	0.18	9.92	10	1.7
Eu	0.36	0.025	1.90	14	0.28
Tb	0.30	0.026	1.3	11	0.23
Yb	0.65	0.080	3.2	8.1	--
Lu	0.090	0.02	0.48	3.3	--
Hf	0.44	0.054	2.3	8.1	0.97
Ta	0.14	0.043	0.62	3.3	0.46
Th	1.9	0.19	10	10	3.4
Rb	13	--	77	--	19
Cs	0.95	0.012	5.8	80	1.4
As	19	2.1	77	9.0	5.7
Sb	1.4	0.066	7.4	21	3.7
Zn	26	8.1	124	3.2	37
Br	3.6	4.7	4.9	0.80	17
Se	3.6	0.17	20.4	21	3.3
Hg	0.16	0.02	<0.005	8.0	0.10

a. Determined by instrumental neutron activation analysis. Estimated errors based on counting statistics are ∿1-3% for Na, La, Co, Fe, Sc, Br, Zn, Sb, Sm, Yb and As; ∿5% for Cr, Ce, Th, Lu, Ta, K, Ba, Eu, Hf and Rb; and ∿10% for Tb, Hg, Cs, Ni, Se and Sr.

b. Abel and Rancitelli (1975).

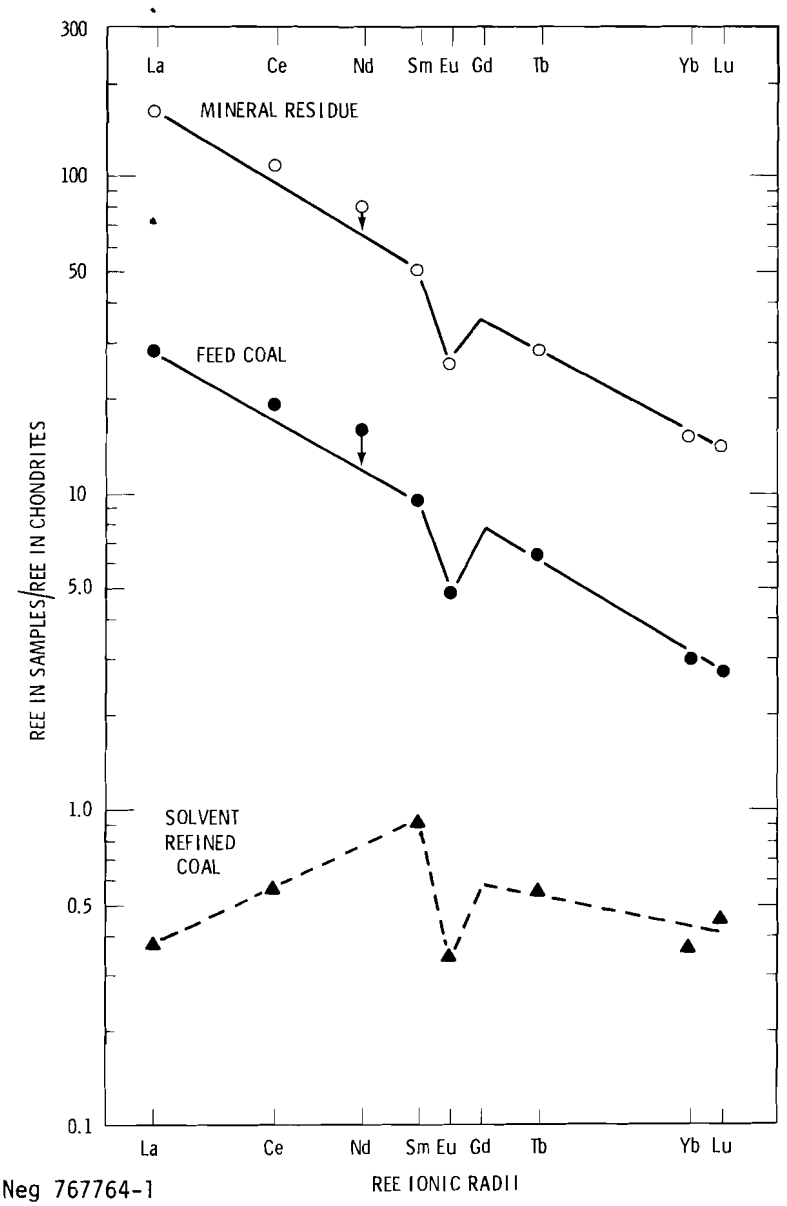

Neg 767764-1

FIGURE 1. Comparison of the Distribution of Rare Earth Elements in Mineral Residue, Feed Coal and Solvent Refined Product

HANFORD TURBIDITY DURING 1976

N. S. Laulainen

Solar radiation measurements were continued at Hanford during 1976 using a multiwavelength sunphotometer. Seasonal variations in aerosol loading are apparent in the data.

INTRODUCTION

The presence of aerosol in the atmosphere significantly affects the incident solar radiation. High aerosol loading severely reduces insolation at the surface; this clearly is important in using solar energy. The climatic effects of aerosol on global and regional scales, through changes of the apparent albedo of the earth, are not yet fully appreciated because the critical aerosol optical properties are difficult to measure. Consequently, too few reliable data on these properties are now available. Aerosol optical depth measurements, combined with other simultaneous optical measurements will be useful in assessing aerosol effects on insolation and albedo.

Multiwavelength aerosol optical depth (turbidity) measurements using sunphotometry were initiated at the Hanford Meteorological Station (HMS) in July 1974. Frequent observations were continued during 1975 and 1976. Results obtained during the last half of 1974 and during 1975 were summarized in earlier reports.[1,2] Here we summarize turbidity data collected over the Hanford area on 83 days during 1976.

The aerosol optical depth is derived from the extinction equation

$$J_\lambda = J_{\lambda 0} \exp(-\tau_\lambda m)/F, \qquad (1)$$

where

- J_λ is the actual photometer reading for wavelength band λ,
- $J_{\lambda 0}$ is the outside-the-atmosphere photometer reading or calibration constant for wavelength band λ,
- F is a correction factor depending on solar distance,
- τ_λ is the total atmospheric optical depth through the zenith at wavelength band λ, and
- m is the relative airmass thickness in units of the atmospheric thickness through the zenith.

The total optical depth, τ_λ, is the sum of attenuation contributions due to molecular (Rayleigh) scattering, molecular (usually ozone) absorption and aerosol scattering and absorption; explicitly it is

$$\tau_\lambda = \tau_{Rayleigh} + \tau_{ozone} + \tau_{aerosol}. \qquad (2)$$

The Rayleigh contribution is relatively constant and predictable. The ozone contribution is mainly from stratospheric ozone and varies with time of year and latitude by as much as 30%. Both these contributions are assumed to be the standard atmosphere values tabulated by Elterman[3] and are subtracted from the total optical depth. Simultaneous and independent measurements of ozone are recommended to determine aerosol extinction accurately.

RESULTS AND DISCUSSION

Daily average total optical depths were determined for six colors from solar radiation measurements on 83 days during 1976, using Equation (1) and the calibration constants $J_{\lambda 0}$ for each wavelength band (calibration of the sunphotometer is discussed elsewhere).[4]

These optical depths are plotted in Figure 1 as a function of time of year for four colors--namely 448.2, 500.0, 557.8 and 598.4 nm, respectively. To better assess any time trends or seasonal variations, these data were further analyzed by a weighted mean regression technique, where the observations are fit to an equation of the form

$$y(t) = \Sigma_i\, a_i\, \chi_i(t) \qquad (3)$$

by a generalized least-square matrix solution. The χ's are the regression variables as a

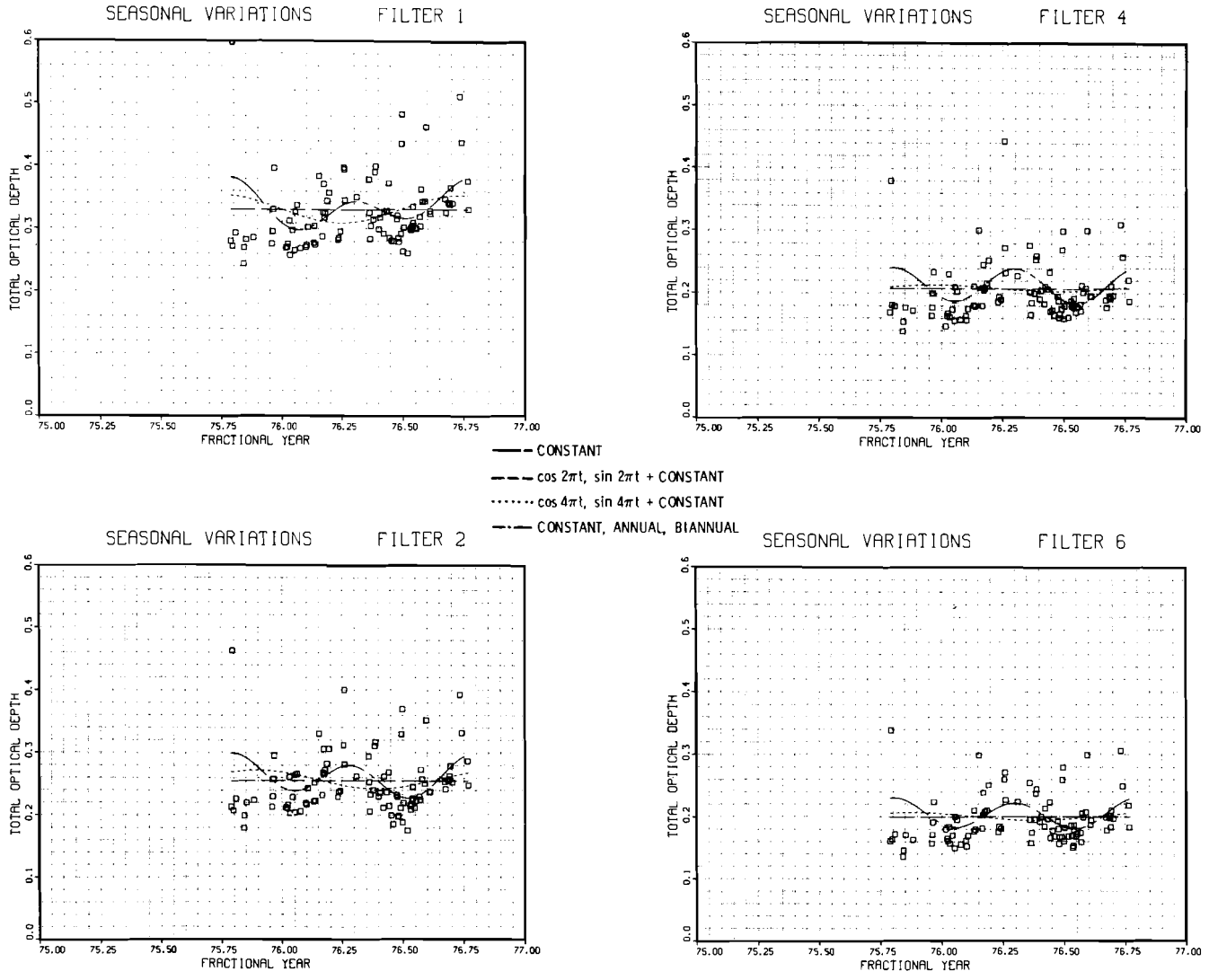

FIGURE 1. Seasonal Variation in Total Atmospheric Optical Depth at Hanford During 1976 Including the Last Quarter of 1975. Weighted mean regression curves fit to the data are also shown (explained in the text).

function of the parameter t and the a's are the regression coefficients. In this study, the observations are fit to the equation

$$\tau(t) = a_0 + a_1 t + a_2 \cos(2\pi t) + a_3 \sin(2\pi t) + a_4 \cos(4\pi t) + a_5 \sin(4\pi t), \qquad (4)$$

where t is time as a fraction of a year, in order to detect annual [$\cos(2\pi t)$, $\sin(2\pi t)$], biannual [$\cos(4\pi t)$, $\sin(4\pi t)$], or linear [t] variations of total optical depth.

Curves for various combinations of regression variables are shown in Figure 1; the regression coefficients are summarized in Table 1, including the average. No significant time trend was found over the observation period. This result is expected, since a minimum of 5-10 years is required to reliably estimate time trends. For the other cases, a fit to an annual variation is less significant than either a biannual (or annual and biannual together) variation. Based on the regression correlation coefficient, which approaches unity for a perfect fit, none of the fits are particularly good.

On the other hand, whenever the uncertainty in a regression coefficient is less than the coefficient itself, i.e. $\Delta a_i \gtrsim a_i$, then that coefficient is of some significance and needs to be examined further. For other than the constant term, one such test is to compare the magnitude of the coefficient to the uncertainty in the constant term. For example, from Table 1 (filter 1) one finds, $|a_4| \sim 3\ \Delta a_0$; hence there is a reasonable basis to conclude that the a_4 term represents a real variation from the mean.

The coefficients given in Table 1 may be interpreted as follows:

1) a_0 gives a mean yearly optical depth due to Rayleigh scattering, ozone absorption and particle extinction (mean values of Rayleigh plus ozone are also listed in Table 1 for each color).

2) a_1 gives a time trend which is essentially zero.

TABLE 1. Regression Coefficients of a Least Squares Fit of Optical Depth Data During 1976 at Hanford to Equation 4

Filter	Case	Rayleigh & Ozone Optical Depths	Regression Coefficients*						Regression Correlation Coefficient
			a_0	a_1	a_2	a_3	a_4	a_5	
	Average		0.331(8)	-	-	-	-	-	0
1	Const. & Annual	0.223	0.332(8)	-	0.000(11)	-0.022(12)	-	-	0.034
(448.2 nm)	Const. & Biannual		0.335(8)	-	-	-	-0.023(11)	-0.014(12)	0.056
	All		0.336(8)	-	-0.004(11)	-0.021(12)	-0.023(11)	-0.014(12)	0.089
	Average		0.255(8)	-	-	-	-	-	0
2	Const. & Annual	0.153	0.257(8)	-	0. 012(10)	-0.009(12)	-	-	0.019
(500.0 nm)	Const. & Biannual		0.260(8)	-	-	-	-0.027(10)	-0.011(11)	0.078
	All		0.262(8)	-	0.008(10)	-0.008(11)	-0.025(11)	-0.012(11)	0.087
	Average		0.208(7)	-	-	-	-	-	0
4	Const. & Annual	0.125	0.208(7)	-	0.005(10)	-0.001(11)	-	-	0.003
(557.8 nm)	Const. & Biannual		0.212(7)	-	-	-	-0.023(10)	-0.016(10)	0.076
	All		0.213(7)	-	0.003(10)	0.000(11)	-0.022(10)	-0.017(11)	0.077
	Average		0.200(7)	-	-	-	-	-	0
6	Const. & Annual	0.110	0.201(7)	-	0.005(9)	-0.004(10)	-	-	0.005
(598.4 nm)	Const. & Biannual		0.204(7)	-	-	-	-0.019(9)	-0.013(9)	0.060
	All		0.204(7)	-	0.003(9)	-0.004(10)	-0.018(9)	-0.013(10)	0.062

*A shorthand convention for expressing standard deviations is used, e.g. 0.331(8) = 0.331 ± 0.008.

3) a_2, a_3 and a_4, a_5 give the magnitudes of annual and biannual variations in *particle* extinction, respectively.

In spite of the apparent poor fit, the qualitative interpretations of the 1975 data[2] are essentially substantiated on a quantitative basis in the 1976 data. Those observations were:

1) Spring and fall show the largest optical depths while the winter and early summer months show minimum values, suggesting a biannual variation. The summer minimum is somewhat larger than in winter, suggesting a biannual variation superimposed on an annual variation.

2) All colors exhibit similar day-to-day optical depth variations, with the magnitudes of the variations roughly comparable in each color.

3) Even during the seasonal maxima, occasional low values ("clean" air) in turbidity are observed. It is also apparent that day-to-day variations can be rather large (much larger than the coefficients for the periodic terms).

This latter observation points out one of the severe problems encountered in interpreting optical depth data, as has been attested to elsewhere.[5,6]

A number of other tests to the data obtained since 1974 at Hanford, as well as other locations, have yet to be completed. These include diurnal and weekly variations, as well as assessment of prevailing meteorological conditions and agricultural activity (which contributes significantly to the smoke and dust burden of the region). These tests will be summarized in a later report.

References

1. N. S. Laulainen, "Atmospheric Turbidity over Hanford," Pacific Northwest Laboratories Annual Report to the USAEC Div. of Biomedical and Environmental Research, Part 3, Atmospheric Sciences, BNWL-1950 PT 3, Battelle-Northwest, Richland, Washington, April 1975, pp. 269-272.

2. N. S. Laulainen, "Atmospheric Turbidity over Hanford During 1975," Pacific Northwest Laboratories Annual Report to the USAEC Div. of Biomedical and Environmental Research, Part 3, Atmospheric Sciences, BNWL-2000, PT 3, Battelle-Northwest, Richland, Washington, March 1976, pp. 265-268.

3. L. Elterman, Vertical Attenuation Model with Eight Surface Meteorological Ranges 2 to 13 Kilometers, Environmental Research Paper No. 318, AFCRL-70-0200, 1970.

4. N. S. Laulainen and E. W. Kleckner, "Calibration of Sunphotometers," Pacific Northwest Laboratories Annual Report to the USAEC Div. of Biomedical and Environmental Research, Part 3, Atmospheric Sciences, BNWL-2000, PT 3, Battelle-Northwest, Richland, Washington, March 1976, pp. 261-264.

5. B. J. Taylor, P. B. Lucke and N. S. Laulainen, "Analysis of Atmospheric Extinction Data Obtained by Astronomers, 1. A Time-Trand Analysis of Data with Internal Accidental Errors Obtained at Four Observatories," Atmos. Environ., 11, 1977, pp. 1-20.

6. N. S. Laulainen, B. J. Taylor and P. W. Hodge, "Analysis of Atmospheric Extinction Data Obtained by Astonomers, 2. Seasonal Variations in Atmospheric Extinction," Atmos. Environ., 11, 1977, pp. 21-27.

CHARACTERIZATION OF PREFRONTAL PRECIPITATION DURING WINTER IN EASTERN WASHINGTON

J. M. Thorp

Precipitation scavenging experiments which monitor changes of the ambient aerosol concentration are necessarily performed in stagnant or stationary air masses. To determine a location in eastern Washington which experiences frequent stagnant air masses in winter coupled with sufficient precipitation for experimental purposes, precipitation records for six eastern Washington stations have been examined.

Confident assessment of precipitation scavenging experiments which examine changes of ambient aerosol concentrations, requires that the air mass through which the precipitation falls not change during the experiment. The Columbia Basin in eastern Washington has the topography conducive to the formation of persistent or stagnant mesoscale air masses, but only in winter is there sufficient precipitation to permit experiments to measure scavenging of the aerosol.

Prefrontal rain of several hours duration, accompanied by stagnant air, occurs with some regularity in eastern Washington from November through February.

Precipitation records for the Hanford Meteorology Station (HMS) 40 km northwest of Richland, Walla Walla (ALW), and Yakima (YKM), have been examined for November to February of 1974-75 and 1975-76. A plot of precipitation amount versus duration for 40 storms during the eight months of data shows a degree of linearity (Figure 1), but there is considerable scatter at all three sites. The best correlation between amount and duration occurs at Hanford (r=0.90), followed by r=0.87 at Walla Walla and r=0.76 at Yakima. The mean precipitation amount per storm is 0.14 in. at both Hanford and Yakima; the average storm duration at these sites is 5 to 6 hr. Walla Walla receives nearly twice as much precipitation (0.29 in.), but the average storm lasts more than 9 hr. The average rate of precipitation is about the same at all three sites (0.02 in./hr to 0.03 in./hr).

For the 1975-76 winter (November-February) the records for Spokane, Wenatchee and Pullman were similarly regressed (Figure 2). With a sample size of only 16, it is wise to withhold conclusions about these data. The correlation coefficient between amount and duration did equal 0.90 for Wenatchee, but was much less at the other two sites. Storm duration averaged ∿10.5 hr at Spokane and Pullman, both situated just windward of the Idaho mountains, and ∿7 hr at Wenatchee, leeward of the Cascades. Average storms total are 0.24 in. for Wenatchee, 0.34 in. for Spokane and 0.42 in. for Pullman during the 1975-76 winter.

Air mass stability categories were based on HMS temperature profiles to 400 ft, and on the 00Z and 12Z radiosonde data from Spokane. Precipitation periods when temperature lapse rates were less than -1°F/1000-ft were rejected from the study.

To check for possible preferential timing of precipitation onset and occurrence at Hanford, Walla Walla and Yakima, the day was divided into four 6-hr periods beginning at midnight. The data was segmented into these periods for the two winters of study. Hanford shows a majority of precipitation events occurring from 0600-1200 PST; Walla Walla and Yakima slightly favor the 0000-0600 PST period. Records from all three stations indicate that most precipitation events in the stable air mass begin in the 0000-0600 PST period. Based on only two winter's data, it is unlikely that these findings are conclusive.

However, precipitation falling through a stagnant air mass in eastern Washington occurs frequently enough, and with sufficient amount and duration to provide a satisfactory base for aerosol scavenging experiments.

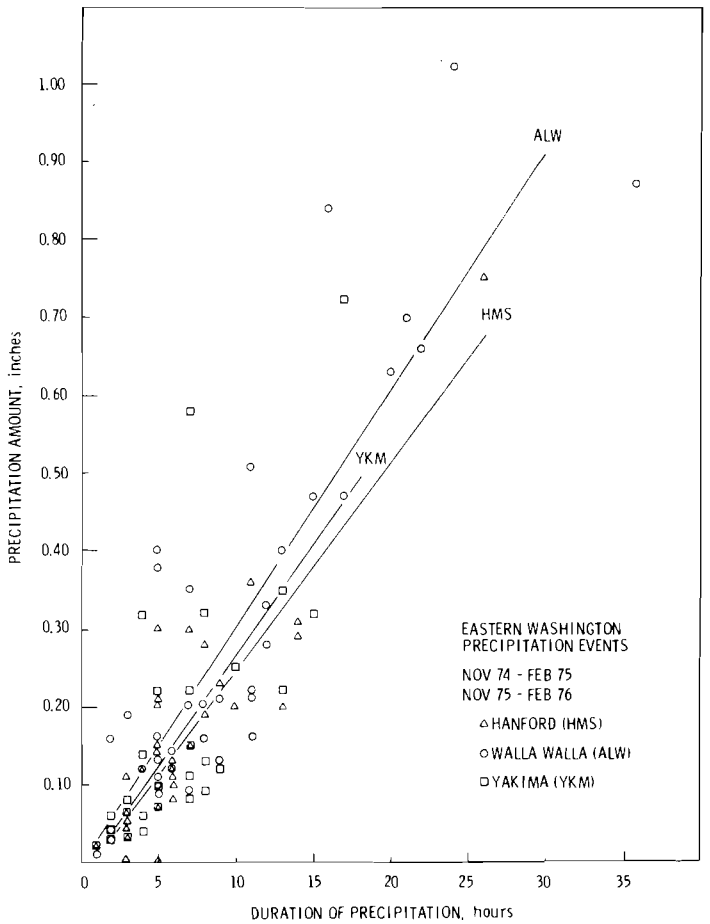

FIGURE 1. Precipitation Amount Versus Duration at Hanford, Walla Walla and Yakima, WA for the Winters 1974-75 and 1975-76

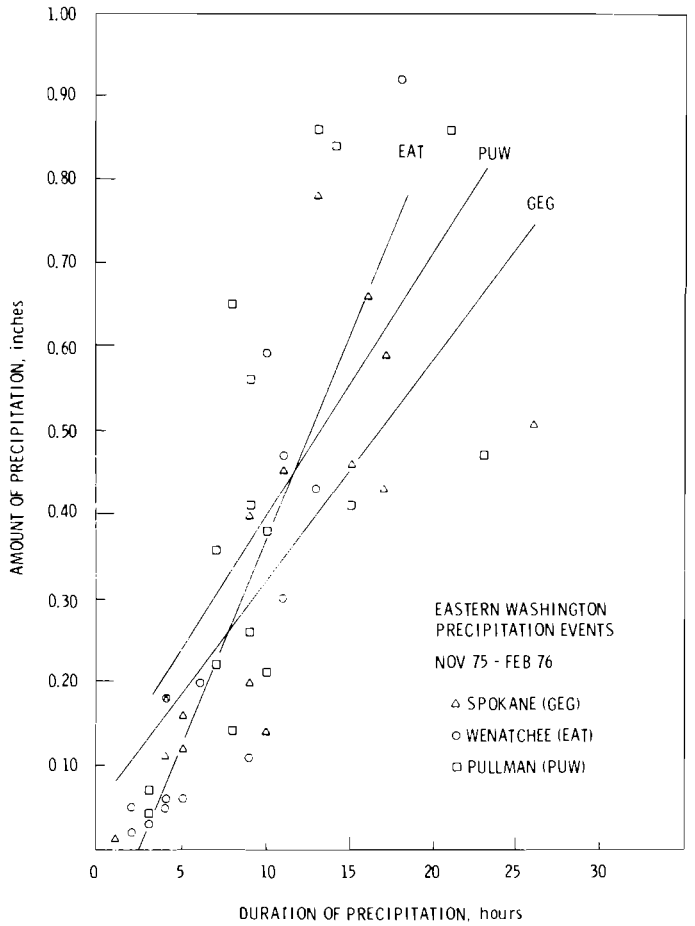

FIGURE 2. Precipitation Amount Versus Duration at Spokane, Wenatchee and Pullman, WA for the Winter 1975-76

CATCH AND STORAGE CHARACTERISTICS OF THREE TYPES OF NONRECORDING PRECIPITATION GAUGES

J. M. Thorp

Precipitation measurements on the Arid Lands Ecology Reserve are made monthly at 26 sites. Despite an oil film evaporation suppressant on the water column in the gauges, monthly losses have been apparent, especially during summer. An experimental test plot of 16 gauges was set up near the 8-in. standard precipitation gauge at the Hanford Meteorology Station to test collection and storage characteristics of three types of nonrecording rain gauges.

In 1968, a network of 26 microclimatological stations was established on a 75,000 acre study area of the Hanford Reservation known as the Arid Lands Ecology (ALE) Reserve.

Our primary task with the microclimatological network was defining patterns of temperature and precipitation that occur over the varied terrain and vegetation of the ALE Reserve. Budget limitations, and inaccessibility of some sites during periods of mud or drifted snow forced a monthly schedule of taking measurements. To meet our needs, precipitation gauges able to collect and hold a month's precipitation, or record precipitation as it falls, have been essential.

Initially, 2-in. diameter plastic gauges were installed at all sites; 8-in. diameter standard Weather Service type gauges provided a backup system at four sites and propane-heated tipping bucket gauges were put at two sites. The tipping bucket gauges consistently recorded less precipitation than the 8-in. gauges and are not considered in this study. A 5 to 8 mm oil film capped the water column in all the storage gauges to inhibit evaporation.

On our scheduled observations during the summer, we often found less water in the 2-in. gauges than had been observed a month earlier; sometimes this was true even when we had observed precipitation falling in that region and when the 8-in. gauge measurement confirmed our observation.

Comparing several types of storage gauges and improving our microclimatological measurement program with better gauges where practical was necessary. An array of 16 rain gauges in a 4 x 4 matrix (Figure 1) was prepared on a plot with a ready accessibility. Each row contained one 2-in. (funnel diameter) plastic gauge buried with the rim 5 cm above the ground, one 2-in. plastic gauge mounted above ground, a similarly mounted 4-in. plastic gauge with inner collector, and a standard 8-in. metal precipitation gauge. The rims of the latter three types were 81 cm above ground. The order of gauge types was different in each row and column. Also, rows 1 and 3 had the 2-in. and 4-in. gauges in full sunlight; rows 2 and 4 provided midday shade for the 2-in. and 4-in. gauges.

To compare catch efficiencies, measurements were made as soon as possible after precipitation occurred, but the gauges were not emptied. Between preciptiation events, measurements were made at intervals of one to several days to check for evaporation loss.

The 8-in. standard National Weather Service type gauge at the Hanford Meteorological Station (about 60 m from the experimental site) was used as the base reference for catch efficiency comparisons. This gauge is emptied every 24 hours if precipitation has occurred. Any amount less than 1/100-inch is logged as a "trace" of precipitation. An accumulation of such "traces" could cause slightly more precipitation to

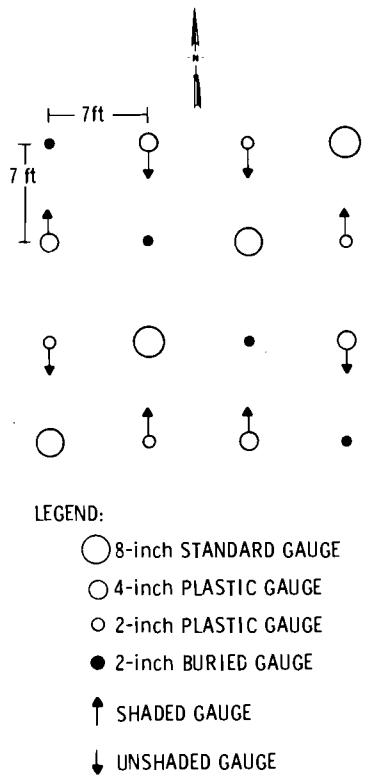

FIGURE 1. Precipitation Gauge Study Plot

be recorded in the test gauges since they were not emptied during the period of the experiment.

Seventy-one precipitation events were measured from October 28, 1974 to July 8, 1976. Replicate gauge samples were averaged, then regressed 1) on the HMS standard and 2) on each other (Table 1). Correlation coefficients are >0.98 for all comparisons except for the buried 2-in. gauge against the standard, and even that has $r > 0.97$. Correlation between test gauges is also uniformly high, though again the 2-in. buried gauge seems to be the least desirable installation for accurate catch measurements. Precipitation consisting of all snow was excluded from these comparisons; the 2-in. gauges bridge over when snow falls at temperatures <32°F, and the amount captured is reduced.

Water lost from the test gauges during extended periods of storage is shown in Table 2. Three sets of measurements were made. Twenty-seven observations, spanning 148 summer (June-September) days in 1975 and 1976 are summed in the first column and then an average loss per month (30 days) is calculated. Similar measurements were made in winter (October-May) with 28 observations over 168 days. Loss during the winter is

TABLE 1. Comparison of Precipitation Catch by Three Types of Nonrecording Gauges

Gauge Type Regressed on Gauge Type Y	X	Intercept	Slope	Correlation Coefficient r
2 in. Buried	HMS 8 in.	0.0001	1.02	0.9717
2 in. Unshaded	"	-0.0072	0.98	0.9821
2 in. Shaded	"	-0.0068	0.99	0.9831
4 in. Unshaded	"	-0.0022	0.99	0.9901
4 in. Shaded	"	0.0005	1.00	0.9873
8 in. Bare Metal	"	0.0038	0.99	0.9896
8 in. Painted Metal	"	0.0052	0.98	0.9886
8 in. Bare Metal	8 in. Painted Metal	-0.0009	1.00	0.9968
4 in. Unshaded	4 in. Shaded	-0.0016	0.98	0.9950
2 in. Unshaded	2 in. Shaded	0.0003	0.98	0.9934
2 in. Buried	2 in. Shaded	0.0079	1.02	0.9827

TABLE 2. Storage Characteristics of Three Types of Nonrecording PCPN Gauges

Gauge Type	Water Loss, Inches					
	Summer (148 Days)		Winter (168 Days)		Summer (63 Days) No Oil	
	Total	Amt/30 Days	Total	Amt/30 Days	Total	Amt/30 Days
2 in. Buried	0.2830	0.06	0.080	0.01	1.43	0.68
2 in. Unshaded	0.5100	0.10	0.160	0.03	2.59	1.23
2 in. Shaded	0.4300	0.09	0.140	0.02	2.59	1.23
4 in. Unshaded	0.1650	0.03	0.037	<0.01	0.52	0.245
4 in. Shaded	0.1450	0.03	0.052	<0.01	0.52	0.245
8 in. Bare Metal	0.2200	0.04	0.045	<0.01	0.55	0.26
8 in. Painted Metal	0.1900	0.04	0.045	<0.01	0.55	0.26

less than 1/3 of that during the summer for all gauges. The 2-in. gauge exposed to the sun shows the maximum loss for all seasons. A short experiment (19 observations over 63 days) in the summer of 1976 with no oil film on the water gave results shown in the last two columns of Table 2. Again the 2-in. gauge shows the greatest loss. These final values represent the average of the shaded and unshaded 2-in. and 4-in. gauges, and the bare and painted 8-in. gauges.

For storage purposes, the 4-in. plastic gauge with inner collecting tube performs as well or slightly better than the standard 8-in. gauge at roughly 1/5 the cost.

CONCLUSION

Catch and storage measurements were made on: 1) 2-in. plastic rain gauges partially buried, shaded and unshaded; 2) 4-in. plastic rain gauges shaded and unshaded; and 3) 8-in. metal rain gauges painted silver and unpainted.

All gauges collected liquid precipitation satisfactorily regardless of exposure, though the partially buried gauges showed the lowest correlation with the standard ($r < 0.98$). The 2-in. gauges are susceptible to under-measurement of frozen precipitation.

Storage characteristics vary between gauge types; the unshaded 2-in. gauge shows the greatest evaporative losses through the suppressing oil film during the summer. As much as 0.10-in./ month may be lost during hot weather from this gauge. Losses during the winter in our semiarid region, which experiences much cloudiness, 70%-80% average relative humidity and a winter maximum precipitation regime[1] were, in general, insignificant (0.02-in./month or less).

The 4-in. plastic gauge and the 8-in. standard metal gauge gave the most accurate collection information and experienced the least loss from evaporation. The 4-in. gauge at 1/5 the cost of the 8-in. gauge is especially useful where multiple installations are needed.

References

1. W. A. Stone, D. E. Jenne and J. M. Thorp, Climatography of the Hanford Area, BNWL-1605, UC-53, Battelle, Pacific Northwest Laboratories, Richland, WA, June 1972.

MICROCLIMATE AND ECOSYSTEM MODIFICATION BY SOLAR ENERGY FARMS

J. G. Droppo, N. S. Laulainen and D. S. Renné

Large scale solar thermal power facilities will cause a large reduction in the direct solar and diffuse sky radiation reaching the surface beneath the collector array, but will be compensated by a large reduction in the net outgoing longwave flux. The magnitude of any effect will depend on many environmental as well as design parameters, most of which are poorly known at present. In general, the collector array should produce a more moderate, but less photosynthetically active, environment at the surface below the collectors.

INTRODUCTION

Many of the engineering designs for utilizing solar radiation to produce electrical energy involve installing solar panels above the ground to collect and redistribute the sun's rays. Large scale solar thermal power installations may cover 10 to 20 km^2 of land surface with such panels. Besides producing obvious changes in the thermal and radiant balance above the panels, these installations can also produce substantial microclimatic changes below the panels that, in certain locations, could benefit agricultural productivity and ecosystem diversity.

As now planned, most large solar energy installations are likely to be located in semi-arid or desert regions such as the southwestern United States. This will take advantage of the many clear, sunny days offered by such areas during the year. In desert and semi-arid regions, the natural ecosystem base is quite narrow and consequently any moderation of the microclimate may allow diversification of the ecosystem base.

The microclimate of a given area is altered essentially by changes in the local energy and water balance. Large solar farms could affect energy and water balance by changing the effective surface albedo or surface reflectivity of solar radiation, by increased shading of the surface by the numerous panels, by reduced surface winds and by introduction of additional water from collector maintenance. Energy is also lost from the farm not only through the usual advection and convection of air heated by the installation, but also because a significant fraction of the incident energy is converted to other energy forms such as electricity and transported to some other location.

Here we examine qualitatively what types of changes can be expected from large solar farms and indicate how these changes can be addressed in a quantitative manner.

ENERGY BALANCE CONSIDERATIONS

The net radiant energy balance, R_N, at the earth's surface can be defined in simple terms as[1]

$$R_N = (S + s)(1 - \alpha) + \Delta L, \qquad (1)$$

where $(S + s)$ = incident direct solar (S) and diffuse sky (s) radiation,

α = albedo (reflectivity) of the earth's surface

ΔL = net longwave (incoming sky minus outgoing terrestrial) radiation.

During nighttime, Equation (1) simplifies to

$$R_N = \Delta L, \qquad (2)$$

where ΔL is usually negative--particularly in desert regions, since a clear sky contributes very little downward longwave radiation and does little to inhibit that radiation leaving the surface.

Whenever the value of R_N is nonzero, the excess or deficit of radiant heat must be dissipated or supplied by other heat transfer mechanisms--namely by sensible heat transfer to or from the air through conduction, convection, and advection (H), by transfer of latent heat to or from the air through evaporation or condensation of water (E), and by transfer of sensible heat to or from the ground (B). Since this is merely a statement of the law of energy convervation, the net radiative energy from either Equation (1) or Equation (2) can be equated to the sum of each contribution

$$R_N = H + E + B. \qquad (3)$$

Since the solar installations convert a significant fraction of the total radiation reaching the surface to other energy forms, such as electricity, which is dispatched elsewhere, an additional term C (for conversion) should be added to the right side of Equation (3).

In summary, the factors influencing the energy budget of a solar farm are:

- Albedo. A decrease results in increased (surface) heating which must be transported away by longwave radiation and convection.
- Sensible heat. An increase leads to a heat island effect (since sensible heat determines buoyancy and convection of air above the farm).
- Latent heat. A decrease tends to increase sensible heat and longwave transport, (since evaporation competes for the available energy).
- Soil heat flux: Usually a small term in the energy budget, but may be significant as far as the local ecology is concerned.
- Plant efficiency. As the overall collection/conversion efficiency approaches unity, less net energy needs to be transported away from the farm by convection, longwave radiation, etc.

EFFECTS OF SOLAR ENERGY FARMS

With an expression for the net energy balance, it is now possible to estimate qualitatively the change in the heat balance terms caused by a large array of solar panels above the ground. First, the panels would drastically reduce the direct solar (S) as well as some of the diffuse sky (s) radiation at the ground. This would reduce substantially the total net radiation, R_N, during daytime, thus reducing also the requirements for the heat dissipation mechanisms described in the preceding section--namely H, E, and B. In desert regions, where there is abundant sunshine and little moisture, a reduction in total net radiation primarily reduces the sensible heat transfer term H. This in turn will reduce the potential evapotranspiration of the area, increasing the water use efficiency of the region. Although the isolation available for photosynthesis is greatly reduced, the heat stress on vegetation beneath the panels is decreased also such that photosynthesis efficiency is not greatly impaired. These factors combined can benefit some agricultural products and harm others.

The net longwave radiation, ΔL, will also be affected by the installation of solar energy collectors. During the daytime, with a net reduction of insolation at the ground, the surface temperature will be reduced thereby decreasing the upward flux of longwave energy. At the same time, the downward flux will increase, since the panels will radiate longwave energy at a higher temperature than the effective sky temperature--this is particularly relevant in desert climates. These processes will make the term ΔL less negative, which will somewhat offset the decreased insolation during the daytime hours. In desert climates, then, it is estimated that the net effect of solar energy installations on the earth's surface is decreased net radiant and heat balance.

During nighttime the ΔL term is also likely to be less negative near a solar energy plant. The panels will reradiate heat back toward the ground at a temperature much warmer than the effective sky temperature. The panels will also impede the loss of longwave radiation from the ground to space. Thus, at night the term R_N will increase, perhaps even from a negative to a positive value, depending on the thermal characteristics of the panels and meteorological conditions. In a desert climate, these factors will reduce the formation of dew [a negative E term in Equation (3)] and maintain a warmer surface temperature. Again, these changes could affect agricultural productivity positively for some crops and negatively for others.

Nonarid sites can expect different changes than those just mentioned for arid sites simply because more water for latent heat transfer will be available.

Air flow over the solar farm may also be modified. Horizontal, flat, elevated collectors, with a significant air space underneath, can be compared to a vegetation canopy,

where relatively lower winds and diffusion rates than in exposed sites prevail. On the other hand, if the collectors are tilted, highly turbulent air motions are possible. Favored design configurations[2] for the panels suggest that the structures will be between these two extremes, i.e., the region underneath the panels should have reduced circulation and turbulence. For calm weather conditions, a low level temperature inversion layer at the height of the panels could be expected much of the day and an inversion from the ground upward at night. The inversion features should be of little consequence under moderate to high winds, where turbulence induced by the collectors mixes the air to the ground surfaces.

Significant perturbations in heat balance might also be expected above the collector panels. A solar farm area of about 20 km^2 is similar in size to a small city. Weather modification on this scale is now only incompletely understood. However, heat island effects over cities have been documented many times and it is plausible that a solar farm could also produce such an effect because of the greater heat input. This heat island should be most pronounced in naturally moist regions. Although considerable energy is removed from the system by the collectors, the change in microclimate of the surface and the change in the energy budget can be expected to result in more net heat in the atmosphere. Since the collectors will be generally dry with respect to ambient air, no evaporation occurs (which would be present at the surface with a soil or vegetation cover) and the upward transfer of energy to the atmosphere from the collectors will be in the form of sensible heat. If the surface beneath the panels is covered with asphalt or concrete, atmospheric heating will be enhanced. Hence, in such a situation, increased convection (heat island effect) would result. On the other hand, if the sub-collector area has a vegetative cover with significant moisture retention, the energy budget might not result in a net increase of sensible heat.

Conversion efficiency of a solar power installation should also be considered, since some fraction of the total radiant energy intercepted by the collectors is transferred somewhere else. Efficiencies of various collector/conversion systems are not yet well defined. The potential for microclimate modification needs to be tied to the overall conversion efficiency per land area. That is, if the collector array only intercepts half of the total insolation available, the appropriate land area efficiency factor would be about half of the collector/converter efficiency. Overall efficiencies of solar farms are estimated at 5 to 40%.[2]

In summary, large solar thermal power facilities will cause large reduction in direct solar and diffuse sky radiation at the surface, but will be compensated by a large reduction in the net outgoing longwave radiation flux. Design configurations, including landscaping the underlying surface and overall conversion efficiency, will have an important bearing on the magnitude of energy balance changes and could be chosen perhaps to minimize some of the adverse effects (such as increased convection). Known quantitative values of many environmental parameters are needed to fully evaluate whether an increase or decrease in net heat balance will occur and how different heat dissipation mechanisms will be affected. In general, solar panels should produce a more moderate, but less photosynthetically active, environment at the surface.

RECOMMENDATIONS FOR ON-SITE MONITORING

The advisability of monitoring the types of changes predicted in this discussion cannot be over-emphasized. This monitoring should include measurement of incoming solar and diffuse sky radiations at a representative location beneath the panels; reflected shortwave radiation to determine the albedo; soil temperature and moisture at several levels; the vertical gradient of temperature and humidity in the lower atmospheric boundary layer; and horizontal wind speed. All measurements at a similar site some distance from the installation.

References

1. W. D. Sellers, Physical Climatology, University of Chicago Press, Chicago, 1965.
2. K. Drumheller, private communication, 1976.

AIR FLOW AND DISPERSION

Many models have been developed to estimate the dispersion of industrial wastes to the atmosphere. Early emphasis in modeling and associated field experiments was on relatively near-source locations and relatively simple meteorological situations. Although reasonable confidence has been displayed in the estimates generated from these near-source models, there is a shortage of good quality field data for model verification. The following articles describe improvements and experiments associated with air flow and dispersion.

A data volume of Hanford field diffusion experiments currently being compiled should add a measurable increment to the bank of quality measurements available for model "tuning" and evaluation.

One study reported specifies the number of aircraft traverses of a plume which are necessary to obtain a selected statistical significance; this should enable more profitable plume sampling flights.

The final contribution in this section outlines a series of cooperative experiments with Argonne National Laboratory. These experiments, entailing aircraft and ground measurements of the atmosphere, provide input data for development of models dealing with regional pollution.

- ATMOSPHERIC BOUNDARY LAYER STUDIES

PREPARATION OF A DATA VOLUME SUMMARIZING HANFORD FIELD DIFFUSION EXPERIMENTS, 1967-1974

P. W. Nickola

A volume listing Hanford field diffusion experimental data is in preparation. The data result from 103 releases of atmospheric tracers during 54 experiments. Tracers were sampled simultaneously on as many as 10 arcs at distances of up to 12.8 km from the tracer release point. Vertical profiles were monitored on towers during 28 experiments involving 43 tracer releases.

An extensive diffusion field grid was first laid out at Hanford prior to the Green Glow field experimental series conducted in the summer of 1959. The Green Glow series was followed by the so-called "30 Series" field tracer releases conducted from 1960 to 1962. Of the total of 67 tracer releases made during these two test series, 21 were considered failures due to equipment malfunction or off-grid wind directions. The successful experiments were examined in a journal article by Fuquay, Simpson and Hinds[1] in 1964. The more pertinent diffusion and meteorological parameters (such as plume centerline exposure, crosswind plume variance, wind speed, wind direction variances and atmospheric stability) were tabled in that publication.

Since 1962, many more "successful" field tracer releases have been made at Hanford--most on a field grid more intensively instrumented for tracer sampling than the Green Glow grid. All tracer releases during the Green Glow/30 Series were from ground level; many of the subsequent releases were made aloft from the 122 m Hanford meteorological tower. Most of the experiments after 1962 involve simultaneous release and sampling of more than one tracer. Particulate tracers employed were fluorescein, rhodamine B, and fluorescent zinc sulfide. The inert gas tracer ^{85}Kr was employed in nine releases.

Data resulting from the post-Green Glow/30 Series tests have been analyzed and various facets have been reported in all volumes since 1962 of this series of annual reports to ERDA (AEC). Results and/or data have also been presented in journals and other media.[2-11] However, the analyses and data presented were a more or less "skimming of the cream" for the particular area being studied at each specific time. The data have not been compiled and published in a form suitable for easy general use by either Hanford or other researchers. That assembly and publishing task is currently being undertaken for the bulk of these field experiments, which will be referred to as the "67 Series."

Tracer sampling was done on a series of arc segments concentric (or nearly concentric) about the release location. Table 1 indicates the number of tracer releases from each elevation and the number of times specific sampling arcs were employed in monitoring these releases. The table reveals that the same group of sampling arcs was not always activated for all field experiments.

TABLE 1. Frequency of Tracer Release and Sampling

RELEASE		NO. TIMES GROUND-LEVEL SAMPLING ON ARC AT RADIAL DISTANCE (METERS) OF													
HT.	NO.	200	300	400	500	600	700	800	1200	1600	2200	3200	5000	7000	12800
2M	28	15	1	10	1	3	3	26	14	22	11	22	11	11	8
26M	46	19	1	35	1	3	3	46	40	46	29	40	24	24	17
56M	20	-	-	20	-	-	-	20	13	20	11	20	19	19	14
111M	9	-	-	9	-	-	-	9	-	9	-	9	9	9	9
TOTAL	103	34	2	74	2	6	6	103	57	97	51	91	63	63	48
*CONTAINED-		56%	100%	62%	0%	50%	67%	71%	78%	70%	78%	75%	56%	51%	54%
*TO PEAK-		94%	100%	84%	100%	100%	100%	91%	100%	96%	96%	98%	90%	98%	85%
*FAILURE-		6%	0%	16%	0%	0%	0%	9%	0%	4%	4%	2%	10%	2%	15%

*CONTAINED - ENTIRE TRACER DISTRIBUTION WITHIN SAMPLING ARC
*TO PEAK - CONTAINED, OR TRUNCATED ONLY ON "TAIL" OF DISTRIBUTION
*FAILURE - TRUNCATION EXCLUDED PEAK CONCENTRATION, OR NO TRACER OBSERVED, OR SAMPLER/ASSAY FAILURE

The spacing of samplers along an arc varied with distance from the source, and the number of samplers generally increased with distance from source. In all but five of the experiments, more than 300 ground-level samplers were exposed. In some instances vertical profiles of tracer were measured on a series of 20 towers located between 200 m and 3200 m from the source. Activation of these towers provided an additional 345 concentration measurements. The number of times the tower sampling arcs were activated and the fraction of the time the towers were intercepted by tracer are listed in Table 2.

TABLE 2. Frequency of Tower Sampling

RELEASE HEIGHT	NO. OF RELEASES	NO. TIMES VERTICAL SAMPLING ON ARC AT RADIAL DISTANCE OF 200M	800M	1600M	3200M	
2M	28	14	14	8	8	BASED ON NUMBER OF ARCS ACTIVATED FOR SAMPLING
26M	46	13	18	14	14	
56M	20	-	-	-	5	
111M	9	-	-	-	6	
TOTAL	103	32	32	22	33	
*CONTAINED-		2%	3%	12%	9%	BASED ON NUMBER OF TOWERS ACTIVATED FOR SAMPLING
*TO PEAK-		80%	69%	66%	63%	
*FAILURE-		20%	31%	34%	37%	

*CONTAINED - ENTIRE TRACER DISTRIBUTION WITHIN SAMPLING HEIGHT
*TO PEAK - CONTAINED, OR TRUNCATED ONLY ON "TAIL" OF DISTRIBUTION
*FAILURE - TRUNCATION EXCLUDED PEAK CONCENTRATION, OR NO TRACER OBSERVED, OR SAMPLER/ASSAY FAILURE

The forthcoming data volume is being prepared in a user-oriented format. The volume will describe the field grid, field and assay techniques, and the meteorology observed during field tracer releases. The bulk of the volume will be composed of computer listings of the field diffusion measurements. Tables 3 and 4 are examples of the format to be employed in the diffusion data presentation. Table 3 is a sample listing exposures and normalized exposures for only two of the seven sampling arcs employed during fluorescein tracer release U58. Table 4 displays the summary of diffusion data for all arcs operated during that same release.

TABLE 3. Above Background Exposures Observed on Two Sampling Arcs Following Fluorescein Tracer Release U58

TEST U58 AUGUST 24, 1967 0415 TO 0445 PST
FLUORESCEIN RELEASE FROM ELEVATION OF 26M
1600M ARC SAMPLER HT 1.5M U= 5.6 M/SEC AT 26M

AZIMUTH DEGREES	EXPOSURE GM-SEC/CU.M X10E+6	E/Q SEC/CU.M	EU/Q 1/SQ.M	DISTANCE METERS
E 80.0	0	0.	0.	1600
82.0	20	5.234E-08	2.931E-07	1600
E 84.0	149	3.855E-07	2.159E-06	1600
86.0	379	9.744E-07	5.457E-06	1600
88.0	568	1.463E-06	8.191E-06	1600
90.0	1252	3.220E-06	1.803E-05	1600
92.0	2240	5.759E-06	3.225E-05	1600
94.0	2164	5.563E-06	3.115E-05	1600
96.0	1898	4.880E-06	2.733E-05	1600
98.0	1214	3.122E-06	1.749E-05	1600
100.0	1366	3.513E-06	1.967E-05	1600
102.0	1290	3.318E-06	1.858E-05	1600
104.0	222	5.715E-07	3.200E-06	1600
106.0	37	9.573E-08	5.361E-07	1600
108.0	1	4.138E-09	2.317E-08	1600
110.0	0	6.974E-10	3.905E-09	1600

CROSSWIND INTEGRATED= 1.839E-03 SEC/SQ.M 1.030E-02 1/M

TEST U58 AUGUST 24, 1967 0415 TO 0445 PST
FLUORESCEIN RELEASE FROM ELEVATION OF 26M
3200M ARC SAMPLER HT 1.5M U= 5.6 M/SEC AT 26M

AZIMUTH DEGREES	EXPOSURE GM-SEC/CU.M X10E+6	E/Q SEC/CU.M	EU/Q 1/SQ.M	DISTANCE METERS
82.0	0	0.	0.	3200
E 84.0	2	7.221E-09	4.044E-08	3200
86.0	24	6.341E-08	3.551E-07	3200
88.0	81	2.083E-07	1.167E-06	3200
90.0	361	9.288E-07	5.201E-06	3200
92.0	315	8.104E-07	4.538E-06	3200
94.0	749	1.926E-06	1.079E-05	3200
4 96.0	611	1.571E-06	8.799E-06	3200
98.0	413	1.064E-06	5.958E-06	3200
100.0	519	1.334E-06	7.473E-06	3200
102.0	571	1.470E-06	8.231E-06	3200
104.0	246	6.350E-07	3.556E-06	3200
106.0	29	7.629E-08	4.272E-07	3200
108.0	2	7.221E-09	4.044E-08	3200

CROSSWIND INTEGRATED= 1.128E-03 SEC/SQ.M 6.319E-03 1/M

TABLE 4. Diffusion Data Summary for Fluorescein Release U58

TEST U58 AUGUST 24, 1967 0415 TO 0445 PST
FLUORESCEIN RELEASE FROM ELEVATION OF 26M
SAMPLER HT 1.5M U= 5.6M/SEC AT 26M

DISTANCE FROM SOURCE	CROSSWIND DISTRIBUTION MEAN	STAND DEV	COEFFICIENT SKEW	KURT	THREE MAXIMUM EXPOSURES AZIMUTH	E/Q	EU/Q	CROSSWIND INTEGRATED VALUES CI(E/Q)	CI(EU/Q)
METERS	DEG	DEG			DEG	SEC/CU.M	1/SQ.M	SEC/SQ.M	1/M
400	94.4	5.75	-.059	2.598	94.0	8.05E-06	4.51E-05	8.78E-04	4.91E-03
					90.0	7.70E-06	4.31E-05		
					98.0	5.95E-06	3.33E-05		
600	95.0	4.67	.200	2.266	94.0	1.10E-05	6.17E-05	1.35E-03	7.54E-03
					90.0	7.70E-06	4.31E-05		
					102.0	5.95E-06	3.33E-05		
700	94.8	4.81	.205	2.606	92.0	1.26E-05	7.06E-05	1.86E-03	1.04E-02
					96.0	9.97E-06	5.59E-05		
					100.0	6.65E-06	3.72E-05		
800	94.9	5.54	-.322	2.580	94.0	9.62E-06	5.39E-05	2.07E-03	1.16E-02
					91.0	9.27E-06	5.19E-05		
					100.0	9.27E-06	5.19E-05		
1200	94.9	5.03	-.173	2.606	92.0	7.03E-06	3.94E-05	1.65E-03	9.27E-03
					90.0	5.95E-06	3.33E-05		
					94.0	5.56E-06	3.12E-05		
1600	95.0	4.56	-.027	2.464	92.0	5.76E-06	3.22E-05	1.84E-03	1.03E-02
					94.0	5.56E-06	3.12E-05		
					96.0	4.88E-06	2.73E-05		
3200	96.7	4.42	-.056	2.173	94.0	1.93E-06	1.08E-05	1.13E-03	6.32E-03
					96.0	1.57E-06	8.80E-06		
					102.0	1.47E-06	8.23E-06		

? INDICATES UNCERTAINTIES IN DATA.

X INDICATES INVALID OR INCOMPLETE DATA.

References

1. J. J. Fuquay, C. L. Simpson and W. T. Hinds, "Prediction of Environmental Exposures from Sources Near the Ground Based on Hanford Experimental Data," J. of Applied Meteor., Vol. 3, No. 6, pp. 761-770, December 1964.

2. P. W. Nickola, Field Testing of a Fluorescein-Zinc Sulfide Dual Atmospheric Tracer Technique, BNWL-103, Battelle, Pacific Northwest Laboratories, Richland, WA, August 1965.

3. J. D. Ludwick, "Atmospheric Diffusion Studies with Fluorescein and Zinc Sulfide Particles as Dual Tracers," J. Geophys. Res., Vol. 71, pp. 1553-1558, March 1966.

4. W. T. Hinds, "Peak-to-Mean Concentration Ratios from Ground-Level Sources in Building Wakes," Atmos. Environ., Vol. 3, No. 2, pp. 145-156, March 1969.

5. P. W. Nickola, J. V. Ramsdell, Jr. and J. D. Ludwick, Detailed Time-Histories of Concentrations Resulting from Puff and Short-Period Releases of an Inert Radioactive Gas: A Volume of Atmospheric Diffusion Data, BNWL-1272, Battelle, Pacific Northwest Laboratories, Richland, WA, February 1970.

6. J. V. Ramsdell, Jr. and W. T. Hinds, "Concentration Fluctuations and Peak-to-Mean Concentration Ratios in Plumes from a Ground-Level Continuous Point Source," Atmos. Environ., Vol. 5, pp. 483-495, 1971.

7. P. W. Nickola, "Measurement of the Movement, Concentrations and Dimensions of Clouds Resulting from Instantaneous Point Sources," J. Applied. Meteor., Vol. 10, No. 5, October 1971.

8. P. W. Nickola, J. D. Ludwick and J. V. Ramsdell, Jr., "An Atmospheric Tracer Technique Employing ^{85}Kr and Use of This Technique in Defining Puff Dimensions and Transport Speed," Isotopes and Rad Tech., Vol. 9, No. 1, November 1971.

9. P. W. Nickola and G. H. Clark, "Field Measurements of Particulate Plume Depletion by Comparison with an Inert Gas Plume," in Proceedings of Atmosphere-Surface Exchange of Particulate and Gaseous Pollutants (1974), Richland, WA, September 4-6, 1974, pp. 74-86, CONF-740921, NTIS, Springfield, VA, 1976.

10. C. E. Elderkin, D. C. Powell and P. W. Nickola, "Diffusion-Deposition Measurements and Modeling," in Preprints Volume, Symposium on Atmospheric Diffusion and Air Pollution, Santa Barbara, CA, September 9-13, 1974, pp. 296-302, American Meteor. Soc., Boston, MA, 1974.

11. P. W. Nickola, "Measured Differences in Real and Apparent Plume Paramters," in Preprints, Third Symposium on Atmospheric Turbulence, Diffusion and Air Quality, Raleigh, NC, October 19-22, 1976, pp. 283-287, American Meteor. Soc., Boston, MA, 1976.

SPECIFICATION OF ERRORS IN ESTIMATING THE MEAN PLUME FROM SIMULATED AIRCRAFT TRAVERSES OF THE REAL PLUME

P. W. Nickola

Data from real time monitoring of tracer plumes with fixed samplers are used to develop a prototype predictor relating meteorology and the number of aircraft traverses through a plume to the expected error in the estimate of mean plume concentration. An improved data base will be used in developing an improved predictor.

Use of an aircraft to measure concentrations of pollutant plumes raises the question of how well the essentially instantaneous sample tranverses across a real plume can be translated into estimates of the mean plume. Nickola and Clark[1] discussed this problem and presented examples of the standard error of measurement of two parameters of interest (crosswind integrated concentration and plume centerline concentration) as a function of the number of crosswind traverses through the plume. The example measurements were derived from a field experimental release of ^{85}Kr tracer. Tracer concentrations were simultaneously monitored as a function of time at more than 100 field locations at distances up to 1600 m from the release point.

The data base for the Nickola and Clark note was a single field experiment; the data was largely reduced by hand. Since that time a computer program has been developed to generate plume parameters of

interest, and seven more field experiments will soon be readied for analysis. Further consideration has been given to the statistics applicable in the plume sampling procedure, and to possible simple meteorological measurements that might be applicable to forecasting, at the time of sampling, the number of aircraft traverses necessary to achieve a desired confidence in measurement.

Perhaps the best way to demonstrate the planned technical approach for the ongoing work in this area is to use some relatively crude data already on hand.

Although the case to be examined in the following three paragraphs deals with variations in plume crosswind summed concentration, the same rationale applies to other plume parameters.

If more than one traverse is made through a plume, a mean crosswind summed concentration ($\overline{cws}$) and a variance of the individual traverses about that mean (S^2_{cws}) can be computed. Although the computed $\overline{cws}$ is an unbiased estimate of the long period mean crosswind summed concentration ($\overline{CWS}$), an estimate is needed of the precision of $\overline{cws}$ as an approximation to $\overline{CWS}$. Intuitively and statistically, the greater the number of traverses (N) through the plume, the closer $\overline{cws}$ can be expected to fall to $\overline{CWS}$.

If a series of N traverses through the plume is repeated a great number of times, then the computed $\overline{cws}$ variance ($S^2_{\overline{cws}}$) can be related to the true variance (σ^2_{CWS}) of all the plume elements contributing to the time integrated concentration. This relationship is estimated by

$$S^2_{\overline{cws}} = \sigma^2_{CWS}/N. \qquad (1)$$

Since each traverse through a plume can be expensive in terms of experimental time and money, one of the important questions to be answered is how many crosswind plume traverses are necessary to achieve a given confidence that a measured $\overline{cws}$ is within specified limits of $\overline{CWS}$. If σ^2_{CWS} were known, then the number of traverses, N, could be selected to bring $S^2_{\overline{cws}}$ within whatever practical bounds desired. But σ^2_{CWS} is not known. One is placed in the paradoxical position of knowing how many traverses to make to be able to describe a plume if he already has a complete description of the plume.

The purpose of the study is to suggest a reasonable number of traverses on the basis of statistical theory and past field experience. The procedure boils down to estimating the value of N to employ in Equation (1) on the basis of values of σ^2 previously observed under various meteorological conditions. Figures 1 and 2 present the guidance.

The ordinate in Figure 1 is the standard error of the mean of a series of samples of a variable x. The abscissa is the number of traverses comprising one sample. The family of curves permits selection of the curve with the population standard deviation, σ_x, appropriate for the variable x. This σ_x value is derived from field experience. The family of curves on Figure 1 presents a purely statistical relationship.

Figure 2 gives the value $\sigma_x/\bar{x}$ as a function of an example empirical relationship; the ratio of wind speed range to mean wind speed at the 15 m elevation. In Figure 2, x is crosswind summed concentration, the points are current tentative values from eight experiments and the curve is a least squares fit to the data points.

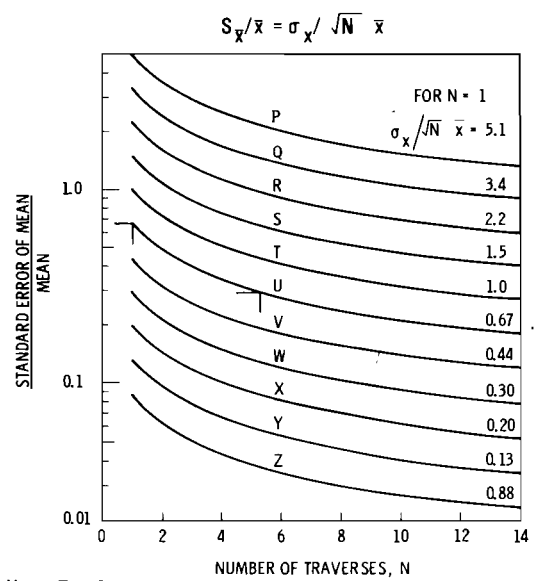

Neg 753125-5

FIGURE 1. Curves Relating the Normalized Standard Error of the Mean of Samples of the Variable x to the Number of Traverses, N, Comprising One Sample

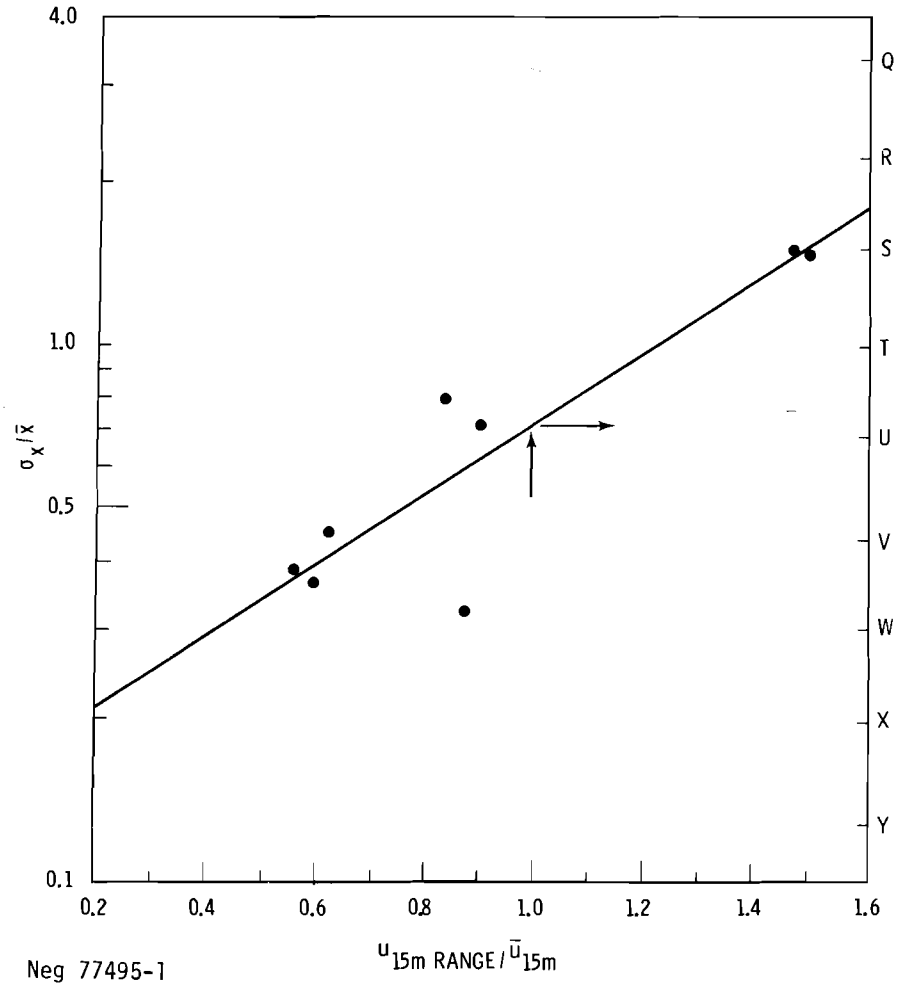

FIGURE 2. Normalized True Standard Deviation of Crosswind Summed Concentration Versus an Empirical Wind Speed Relationship

For example, if the abscissa speed range/mean speed ratio for the 15-min period preceding sampling were 1.0, $\sigma_x/\bar{x}$ = 0.7 (left ordinate) or "U curve" (right ordinate) is predicted by Figure 2. Reference to the curve U on Figure 1 reveals, for instance, that under the existing meteorological conditions, six plume traverses would be required to bring the expected standard error of $\overline{cws}$ down to a value of 30% of $\overline{cws}$. One traverse would have left the standard error/mean relationship at 67%.

Current plans are to incorporate the real time concentration data from eight field tracer releases and the accompanying meteorological measurements into a series of empirical predictive graphs similar to Figure 2. The empirical predictors will be derived from relatively easily observable parameters such as wind speed, wind speed range, wind direction, wind direction range, and vertical temperature profiles. The predicted variables will include crosswind integrated concentration, real plume centerline concentrations and mean plume centerline concentration.

Reference

1. P. W. Nickola and G. H. Clark, "Estimation of Mean Crosswind Concentration Profiles from 'Instantaneous' Crosswind Traverses," Pacific Northwest Laboratory Annual Report for 1973 to the USAEC Division of Biomedical and Environmental Research Part 3, Atmospheric Sciences, BNWL-1850 Pt 3, Battelle, Pacific Northwest Laboratories, Richland, WA, April 1974.

PLANETARY BOUNDARY LAYER AIRCRAFT PROFILE STUDIES UNDER INVERSION CONDITIONS

J. G. Droppo

The PNL Cessna 411 aircraft was used in a study of multiple inversion layers within the Planetary Boundary Layer. This was a cooperative effort with Argonne National Laboratory in the 1976 Sagamon Experiment over farmland in Illinois. Vertical profiles of ozone, condensation nuclei, temperature, relative humidity, dew point, and pertinent air speed and location variables were obtained.

INTRODUCTION

The objective of the Sagamon Experiments is to provide input data for numerical models of regional scale pollution from power production. This is a cooperative experiment with Argonne National Laboratory. The PNL Cessna 411 is used with their ground based effort including tetroon, radiosonde, and acoustic soundings. The 1976 field experiments examined several poorly understood aspects of physical mechanisms related to inversion formation in the Planetary Boundary Layer (PBL).

EXPERIMENTS

PNL provided an airborne platform for determining pollutant and meteorological profiles from near surface (20 m) to the top of the inversion layer in the Sagamon Experiments by deploying the Cessna 411 aircraft. Profiles of ozone, condensation nuclei, temperature, relative humidity, dew point temperature, height, and station locations were recorded on digital tape at a rate of about one complete set every 5 m vertical height. These data were also visually monitored during the flights.

The interest in the 1976 Sagamon Experiment was for the development of inversion layer during evening hours. Six evening runs of 1 to 4 hr duration were made in conjunction with the ground based Argonne effort. In addition, two extra flights were made just after dawn to characterize the morning profile conditions. Morning conditions were the topic of the 1975 Sagamon Experiments in which aircraft transects were not made.

The vertical aircraft profiles were coordinated with the Argonne tetroon and radiosonde flights to provide common data points for comparison of results. The data acquisition technique used was spiraling in a reasonably tight circle over the site. Multiple passes were made through inversion layers when they were detected. The communication via radio with the Argonne ground crew was particularly useful in location of the layering in the Planetary Boundary Layer.

One set of evening experiments were in conjunction with an EPA air pollution monitoring helicopter.

DISCUSSION

Based on preliminary inspection, data obtained demonstrate several effects of interest:

- Development of multiple inversion layers,
- Effects of vertical source-sink distribution on pollutants and their vertical dispersion rate,
- Strong correlations between pollutant and meteorological profiles.
- Consistent temporal definition of vertical structure.

The data is currently being processed and analyzed. The interpretation will be in conjunction with the concurrent Argonne data on the same layers.

DEPOSITION AND RESUSPENSION

Deposition of airborne particles and gases is an important natural air cleaning mechanism, one that must be considered when evaluating the impact on man and the environment of toxic materials released from nuclear power plants and fossil fuel systems. Once such particles are deposited on soil surfaces, wind stress may be sufficient to resuspend particles of soil and the deposited material. Our principle objectives are to identify the controlling parameters in deposition and resuspension, and develop theoretical models which describe these processes. The models will then be justified with laboratory and field experiments, and sensitivity analyses will be made to determine the relative importance of the variables. These studies will be vital in environmental impact assessment of many sources of contamination.

The experimental and theoretical work accomplished in 1976 improved our understanding of deposition and resuspension. These studies are contributing much to the understanding of deposition and resuspension, yet much remains to be learned about the physical processes governing these mechanisms.

Deposition velocity data obtained in field experiments for gas and particles (especially those containing sulfur) are reviewed and summarized. The accuracy of such measurements was evaluated. We found that deposition velocities are of limited use when measured too near the source.

Wind tunnel data on deposition of particles to coarse gravels improved predictive correlations for surface mass transfer resistance. Wind erosion data were reviewed for possible application to contamination resuspension.

Resuspension experiments were directed toward studies of Rocky Flats plutonium resuspension on large particles, the resuspension of a tracer particle in a controlled field plot, and the resuspension of fallout isotopes in forest fires. Other investigations included observations on the depletion of a resuspension source due to weathering. Availability of particles for release continues for much longer periods than others have reported.

- ATMOSPHERIC BOUNDARY LAYER STUDIES
- RADIOISOTOPES AS PARTICLES AND VOLATILES
- PARTICLE RESUSPENSION AND TRANSLOCATION

SUMMARY OF FIELD DATA ON DRY REMOVAL RATES OF GASES AND PARTICLES FROM THE ATMOSPHERE

J. G. Droppo

This report cites literature values for dry removal rates of various gases and particles. Included are both radioactive and non-radioactive materials; iodine, SO_2, O_3, NO_x, NO, particles. This summary incorporates recent PNL SO_2 and sulfur aerosol results.

INTRODUCTION

Obtaining values for the actual rates of dry removal of fossil fuel pollutants is a topic of current concern. These values are needed to model the fate of pollutants on a regional scale and in efforts aimed at defining receptor pollutant loading levels.

As part of the Boundary Layer Program, which considers directly measuring dry deposition of these pollutants, literature values of dry removal rates have been summarized. These summaries are given here; they include a variety of substances to illustrate the variations in removal rates both between pollutants and for the same pollutant.

DEPOSITION VELOCITY

The deposition velocity concept is widely used. This relationship for dry removal rate of deposition (G) is assumed to be directly proportional to the ambient air concentration (χ) at a defined height over the surface (z). The constant of proportionality is the "deposition velocity" (V_d)[1]. The equation is:

$$G = v_d/\chi_z \qquad (1)$$

with the height traditionally assumed to be 1 m.

The deposition velocity has been a framework for much of the research and most of the applications in dry deposition and will be used in this summary.

GASES

Table 1 summarizes dry deposition velocity data for various gases on different surfaces. Iodine, SO_2, O_3, NO_2 and HF all have reasonably high deposition velocity values. The limited data on NO indicate a much lower value. The high and low relative deposition rates of NO_2 and NO are supported by the intermediate value for NO_x. These studies of deposition demonstrate that various processes may be limiting under differing conditions and that a range of deposition velocities result.

The effect of vegetative canopies on deposition is not clearly defined. For example, increased surface roughness and area are expected to cause high deposition rates. Although this is generally true for SO_2, the rougher surface (pine forest) has a lower deposition velocity than other canopies and surfaces, suggesting that other factors limit deposition. The effect of atmospheric delivery is obvious in the data that include groupings by atmospheric stability.

Several studies have considered the penetration of materials into canopies. Markee[2]

TABLE 1. Summary of Deposition Velocities for Various Gases

Substance	Deposition Velocity (cm/sec)	Type of Surface/ Number of Experiments ( )	Methodology and Reference
Iodine[a]	Range: 1.1 - 3.7 Mean: 2.1	Grass (7)	Field experiments[1,4]
Iodine	Range: 0.3 - 1.3 Mean: 0.75	Clover leaves (4)	
Iodine	Range: 0.6 - 2.0 Mean: 1.3	Paper leaves (4)	
Iodine	Range: 0.3 - 0.9 Mean: 0.62	Filter paper (5)	
Iodine	Range: 0.09 - 2.43 Mean: 0.87	Grass (19)	Field experiments[5,6]
Iodine	Range: 0.6 - 0.7 Mean: 6.5	Carbon (12)	[7,2,8]
SO_2	2.8	Alfalfa canopy in chambers	Windspeed: 1.8 to 2.2 m/s,[3]
SO_2	Range: 1.0 - 2.06 Mean: 1.3	Grass (14)	Surface flux determination for SO_2,[9]
$^{35}SO_2$	Range: 0.5 - 2.6 Mean: 1.3	Grass (3)	Radioactivity labeled SO_2 release used as tracer in field experiments.[10]
$^{35}SO_2$	0.5	Water (1)	Radioactivity labeled SO_2 release used as tracer in field experiments.[10]
SO_2	Range: 0.27 - 1.5 Mean: 0.76	Grass (5)	[11]
SO_2	1.3	Grass (1)	Surface flux determination for SO_2,[12]
SO_2	1.8	Short grass	Surface flux (radioactive tracer).[13]
SO_2	(0.84) 1.3	Medium grass	
SO_2	0.91	Bare calcareous soil	
SO_2	2.2	Fresh water (pH = 8)	
SO_2	<0.50	Forest pine	
SO_2	2.4 2.6 0.5	Lapse Neutral Stable	Over grass[14]
	1.6 0.52 0.05	Lapse Neutral Stable	Snow
	4.0 2.2 0.16	Lapse Neutral Stable	Water
NO	0	All surfaces	Not a field result,[15,16]
NO	0.1	Alfalfa canopy	In special chambers,[3]
NO_x	0.5	Alfalfa and oats	Derived from data in[17,18]
NO_2	2.0	Alfalfa canopy	Special chamber,[3]
HF	1.6	Alfalfa	Fumigation with constant concentrations,[19]
	3.1	Field crops	Fumigation with constant concentrations
O_3	Range: 0.7 - 1.7 Mean: 1.13	Several	Review of research by several authors.[20,21,22,23,24,25]
O_3	0.6 - 1.8	Soil, peat, grass	Wind tunnel experiments,[13]
O_3	1.4 - 6.3	Several	Decay rate experiment in box,[13]
O_3	1.7	Alfalfa canopy	Special chambers,[3]

considered the dry deposition of iodine as a function of leaf surface area for low canopies. He found that deposition increased with increasing leaf area. The absorption of gaseous air pollutants by alfalfa canopies and resultant profiles were studied in an environmental growth chamber[3]. Hydrogen fluoride, SO_2 and NO_2 profiles suggested efficient removal by both the upper and intermediate surface vegetation. Profiles of NO indicated a much less efficient removal rate. Although not strictly a field result the deposition velocities derived from this study are included in Table 1.

PARTICLES

Dry deposition of particles depends on the delivery rate in the atmosphere and on surface interactions. (Large particles that deposit by gravitational forces are not considered here.) Transport in the atmosphere is a function of the atmospheric turbulence. At the surfaces the principle processes are impaction and molecular diffusion. Electrical forces may also be important, depending on the mobility and charges of the particles and the electrical field. In addition, concurrent mass and heat fluxes may influence the dry deposition rate when molecular processes are important.

The wide range of field data values for dry deposition of various particles is summarized in Table 2. Included are results from the literature as well as results of current experiments at PNL.

TABLE 2. Dry Deposition of Various Particles

Substance	Deposition Velocity (cm/sec)	Type of Surface/ Number of Experiments	Methodology and Reference
Fission Products	0.07	Gummed Paper	Surface activity measurements particles are formed by an electric core[26]
^{137}Cs	0.9	Water (5)	Field release test measurements[27]
	0.04	Soil (15)	
	0.2	Grass (21)	
	0.2	Sticky paper (117)	
^{103}Ru	2.3	Water (9)	
	0.4	Soil (16)	
	0.6	Grass (20)	
	0.4	Sticky paper (8)	
^{93}Zr, ^{95}Nb	5.7	Water (6)	
	2.9	Soil (6)	
	1.4	Sticky paper (10)	
^{141}Ca	0.7	Sticky paper	
^{127}Te, ^{129}Te	0.7	Sticky paper (8)	
Pb	0.13	Dilute HCl Solution	Plastic pluviometer[28]
Industrial-derived Trace Elements	0.4 to 0.3	Deposition plates	Field Data,[29]
Soil-derived Trace Elements	0.3 to 1.0	Deposition plates	
Zinc Sulfide (2.5 μm diameter)	0.5	Sagebrush	Stable atmospheric conditions[30]
Particles of 0.1 μm	0.2 to 9.2	Desert	[31]
Natural Particulate Material	0.8 to 7.6 (7)	Great Lakes (water)	[32]
Fallout	0.2 to 3.4	Fallout Collectors	Monthly values[33]
Fallout	0.51 and .75	Fallout Collectors	Annual Values
Total Sulfur Aerosol	0.1 to 0.3	Sagebrush (3)	Surface flux technique[34]

SOURCES OF VARIABILITY

Application of these results requires input on the source of the variability in dry deposition velocities. The wide range of values may have two origins. First, large variations are expected from situation to situation as different processes discussed above become variously limiting. Secondly, variations can be partially the result of experimental uncertainties, which are generally relatively large in dry removal rate experiments.

In current dry deposition efforts, there is an attempt to separate these two factors by estimating experimental accuracy for each data value obtained. Initial estimates show that the experimental accuracy of values varies widely from case to case reflecting the relative reliance that may be placed on each case.

References

1. A. C. Chamberlain and R. C. Chadwick, "Deposition of Airborne Radioiodine Vapor," Nucleonics, 11 (8), 22-25, 1953.

2. E. H. Markee, Jr., Studies of the Transfer of Radioiodine Gas to and from Natural Surfaces, ERL-ARL-29, Environmental Research Laboratories, Air Resources Laboratories, Silver Spring, MD, 1971.

3. A. C. Hill, "Vegetation: A Sink for Atmospheric Pollutants," J. Air Pollution Control Assoc., 21 (6), 341-346, 1971.

4. A. C. Chamberlain, "Transport of Gases to and from Grass-Like Surfaces," Proc. Royal Society (A), London, 290, 236-265, 1966.

5. D. F. Bunch, Controlled Environmental Radioiodine Tests (CERT), Progress Report No. 2, IDO-12053, AEC Operations Office, Idaho Falls, ID, 1966.

6. D. F. Bunch, Controlled Environmental Radioiodine Tests (CERT), Progress Report No. 3, IDO-12063, AEC Operations Office, Idaho Falls, ID, 1968.

7. C. A. Hawley, Controlled Environmental Radioiodine Tests (CERT) at NRTS. 1965 Progress Report IDO-12047, AEC Operations Office, Idaho Falls, ID, 1966.

8. J. D. Zimbrick and P. G. Voilleque, "Controlled Environmental Radioiodine Tests (CERT) at HRTS. Progress Report No. 4, IDO-12065, AEC Operations Office, Idaho Falls, ID, 1969.

9. J. A. Garland, D. H. F. Atkins, C. J. Readings, and S. J. Cauhey, "Technical Note: Deposition of Gaseous Sulphur Dioxide to the Ground," Atmos. Environ., 8, 75-79, 1974.

10. M. J. Owers and A. W. Powell, "Deposition Velocity of Sulfur Dioxide on Land and Water Surfaces Using a 35C Tracer Method," Atmos. Environ., 8, 63-67, 1974.

11. J. C. Shepard, "Measurements of the Direct Deposition of Sulphur Dioxide into Grass and Water by the Profile Method," Atmos. Environ., 8, 69-74, 1974.

12. J. G. Droppo, D. W. Glover, O. B. Abbey, C. W. Spicer and J. Cooper, Measurement of Dry Deposition of Fossil Fuel Pollutants, Draft final report under EPA Contract 68-02-1747, Battelle, Pacific Northwest Laboratories, Richland, WA, 1976.

13. J. A. Garland, "Dry Deposition of SO_2 and Other Gases," Proc. Atmosphere-Surface Exchange of Particulate and Gaseous Pollutants, CONF-740 921, ERDA Symposium Series 38, 1974.

14. D. M. Whelpdale and R. W. Shaw, "Sulphur Dioxide Removal by Turbulent Transfer over Grass, Snow and Water Surfaces," Tellus, 26, 196-205, 1974.

15. E. Robinson and R. C. Robbins, Sources, Abundance and Fate of Gaseous Atmospheric Pollutants. Final Report, SRI Project PR-6755, 1968.

16. E. Robinson and R. C. Robbins, "Gaseous Nitrogen Compound Pollutants from Urban and Natural Sources," J. Air Pollution Control Assoc., 20, 303-306, 1970.

17. D. T. Tingey, Foliar Absorption of Nitrogen Dioxide. M.A. Thesis, Dept. of Botany, University of Utah, 1968.

18. K. H. Rasmussen, M. Taheri and R. L. Kabel, Sources and Natural Removal

Processes for Some Atmospheric Pollutants. Report EPA-650/4-74-032, Center for Air Environmental Studies, Pennsylvania State University, 1974.

19. G. W. Israel, "Deposition Velocity of Gaseous Fluorides on Alfalfa," Atmos. Environ., 8, 1329-1330, 1974.

20. I. Galbally, "Ozone Profiles and Ozone Fluxes in the Atmospheric Surface Layer," Quarterly J. Royal Meteorological Society, 97, 18-29, 1971.

21. I. Galbally, "Ozone Variation and Destruction in the Atmospheric Surface Layer," Nature, 218, 456-457, 1968.

22. I. Galbally, "Evaluation of the Ehmert Technique for Measuring Ozone Profiles in the Atmospheric Surface Layer," J. Geophysical Research, 74, 6869-6872, 1968.

23. L. Aldaz, "Flux Measurements of Atmospheric Ozone Near Land and Water," J. Geophysical Research, 74, 6939-6946, 1969.

24. V. H. Regener and L. Aldaz, "Turbulent Transport Near the Ground as Determined from Measurements of the Ozone Flux and the Ozone Gradient," J. Geophysical Research, 74, 6935-6942, 1969.

25. J. J. Kelly, Jr. and J. D. McTaggart Cowan, "Vertical Gradient of Net Oxidant Near the Ground Surface at Barrow, Alaska," J. Geophysical Research, 73, 3328-3330, 1968.

26. W. J. Megaw and R. C. Chadwick, Some Field Experiments on the Release and Deposition of Fission Products and Thoria. AERE-HP-M-114, available from NTIS, Springfield, VA, 1956.

27. D. H. Slade, Meteorology and Atomic Energy 1968. TID-24190, available from NTIS, Springfield, VA, 1968.

28. J. Servant, "Deposition of Atmospheric Lead Particles to Natural Surfaces in Field Experiments," Proc. Atmosphere-Surface Exchange of Particulate and Gaseous Pollutants, CONF-740 921, ERDA Symposium Series 38, 1974.

29. P. A. Cawse and D. H. Peirson, An Analytical Study of Trace Elements in the Atmospheric Environment. AERE-R-7.34, available from NTIS, Springfield, VA, 1972.

30. C. L. Simpson, Some Measurements of the Deposition of Matter and Its Relation to Diffusion from a Continuous Point Source in a Stable Atmosphere. HW-69292, available from NTIS, Springfield, VA, 1961.

31. N. F. Islitzer and R. K. Dumbauld, "Atmospheric Diffusion-Deposition Studies Over Flat Terrain," International J. of Air and Water Pollution, 7 (11-12), 999-1022, 1963.

32. D. M. Whelpdale, "Dry Deposition over the Great Lakes," Proc. Atmosphere-Surface Exchange of Particulate and Gaseous Pollutants, CONF-740 921, ERDA Symposium Series 38, 1974.

33. S. H. Small, "Wet and Dry Deposition of Fallout Materials at Kjeller," Tellus, 12, 308-314, 1960.

34. J. G. Droppo, "Dry Removal of Air Pollutants by Vegetative Canopies," Preprint Volume, Fourth National Conference on Fire and Forest Meteorology, St. Louis, MO, November 16-18, 1976.

PROOF TEST OF A SYSTEM TO MEASURE THE DRY DEPOSITION OF SULFUR AEROSOLS IN THE PLUME FROM A NORTHWEST FOSSIL FUEL POWER PLANT

J. G. Droppo

An instrumentation system designed to provide "in situ" determinations of sulfur aerosol dry deposition removal rates is tested in six experiments on the Hanford Reservation. The results indicate that the technique is workable. Removal rates are obtained corresponding to deposition velocities on the order of a few tenths of a centimeter per second. These are consistent with projected wind tunnel-based measurements of similar sized aerosols.

INTRODUCTION

Evaluation of actual and potential impacts of use of fossil fuels is the impetus for current efforts at definition of regional scale pollutant budgets. Data are needed on the dry removal rate of sulfur and other aerosols. This report presents results of proof tests of a system designed to measure "in situ" dry deposition of aerosols.

DRY REMOVAL DETERMINATION MODEL

The model uses combined eddy flux-gradient methodology. Since the basis of the model has been previously documented,[1-5] only the elements of method are presented here.

From micrometeorological and pollutant measurements in the surface layer the deposition velocity, V_{da} for a given pollutant, a, with air concentration χ_a is given by

$$V_{da} = \frac{K_{az}}{\Delta z} \frac{\Delta \chi a}{\chi_a} \qquad (1)$$

where K_{az} is the eddy diffusivity for the pollutant at height z and $\Delta\chi_a$ is the change in pollutant concentration over the vertical distance Δz, geometrically centered at height z.

EXPERIMENTAL ACCURACY

By referring to Equation (1), the restraints on the accuracy may be better realized. The experimental accuracy of the deposition velocity depends primarily on the accuracy of eddy diffusivities and pollutant profiles. Battelle studies indicate that either or both of these experimental accuracies may limit the accuracy of the results[1]. Equation (1) clearly shows that the pollutant profile accuracy depends on the accuracy of the fractional change in concentration. The relative accuracy between pollutant concentration values controls the accuracy of the deposition velocity rather than the absolute concentration accuracy.

For materials which deposit at a relatively slow rate, the vertical changes in concentration will be correspondingly smaller. Based on anticipated aerosol dry deposition rates, the experimental definition of the aerosol concentration profile was deemed necessary within a ±1% profile accuracy.

The relative accuracy in the aerosol profile is a function of the sampling procedure, the analysis accuracy, and the flow rate determination.

The design of the sampling procedure reflects the aim of obtaining the best relative

values. Flow rates were great enough ($\sim 2 \times 10^{-3}$ m^3/s) to insure isokinetic sampling for particles in the size range of combustion-derived sulfur particles. In addition, consistent sampling errors will often not appear as relative errors if the sampling procedures are identical. Hence, identical filter holders, sample lines, air pumps, calibrated orifices, and flow meters were used for each of the sample heights.

A technique to maximize the relative analysis accuracy of concentrations of material collected on nucleopore filters was developed in previous studies[1]. These tests indicated that the required ±1% was obtained in the analysis of relative concentrations on the filters.

The earlier studies indicated the limiting factor was the accuracy of the flow rate determination. The emphasis in these proof tests was to demonstrate that the necessary profile accuracy could be obtained, primarily by upgrading the relative flow rate determinations.

PROOF TESTS

Six tests were made near 622R, PNL's Atmospheric Sciences Laboratory, at Hanford. The field system consisted of a 17 m tower instrumented at three heights with gill anemometers, thermometers, and nuclepore filter sample intake lines.

The ground cover for these tests is a relatively low dry cover with occasional sagebrush. The aerosol concentrations were expected to be near background, particularly for sulfur.

Table 1 summarizes the conditions during the six tests. All tests occurred during winter with unstable atmospheric conditions. Tests 1 and 3 are under conditions that most closely met the criteria for application of this methodology. Test 2 lasted longer than the ideal time, and had several periods of bad fetch (not shown in Table 1). Test 4 was for a very low wind. Test periods 5 and 6 exhibited significant changes in conditions, making application of the methodology doubtful.

Although our analysis indicates that the required level of accuracy was obtained in each stage of the sulfur aerosol profile determination, the real proof of the accuracy is the vertical consistency of the profiles and the prediction of reasonable and consistent dry removal rates.

TABLE 1. Summary of Tests

DATE	TEST NO.	START TIME	DURATION (MIN)	$\bar{u}$(17m) (m/s)	$\bar{T}$(17m) (^{0}C)	RI
12-5-75	1	1216	109	1.13	2.95	-1.15
12-12-75	2	0857	23	3.50	2.29	-0.425
12-17-75	3	0915	269	1.28	-0.03	-0.364
12-18-75	4	1046	59	0.72	-1.28	-6.32
12-18-75	5	1155	60	2.03	0.26	-0.291
12-18-75	6	1307	60	1.17	1.22	-1.033

Figures 1-4 contain semi-log plots of the wind speed, temperature, and pollutant concentration profiles for the first four tests. Since the profile accuracy is not known, the error bars are plotted to indicate ±1% concentration profile relative accuracy for inspection of the vertical consistency of the profiles. The middle temperature aspiration system was faulty and this data point is not included. The profile expected for the wind speed and (by the analogy processes) the pollutant profiles of transport are a very near linear fit of the data points to an exponential profile. A slight concavity downward is anticipated to reflect the effect of the unstable conditions during these tests.

Tests 1 and 3 show the best fit and consistency between wind speed and pollutant concentrations. The requirement for ±1% concentration profiles appears to be met by these tests. These produce deposition velocity values of 0.10 and 0.27 cm/s respectively based on a momentum eddy diffusivity analogy.

Tests 2 and 4, although not meeting the criteria for application of the methodology, are interesting tests. Test 2 contains bad fetch periods which include the influences of nearby buildings and parking lots. The similar deviation of wind speed and concentration values from an exponential profile reflects the inter-relationship of profiles. Test 4 was made during very low winds. The Gill anemometer data can be in serious error under such conditions. The aerosol concentration profile was very near vertical--well within a ±1% fit. A real zero vertical change indicates zero flux. Using the profile accuracy value of ±1% alone with the computed momentum eddy diffusivity a range of about ±.05 cm/s is obtained for test 4. Inclusion of the error in the eddy diffusivity can easily increase this range by a factor of 2 or 3. Hence, the occurence of a "zero" profile does not necessarily indicate an insignificant flux rate.

The two tests (1 and 3) that best met the criteria for application of the methodology are also the two tests that indicate the methodology works. The excellent fit of the

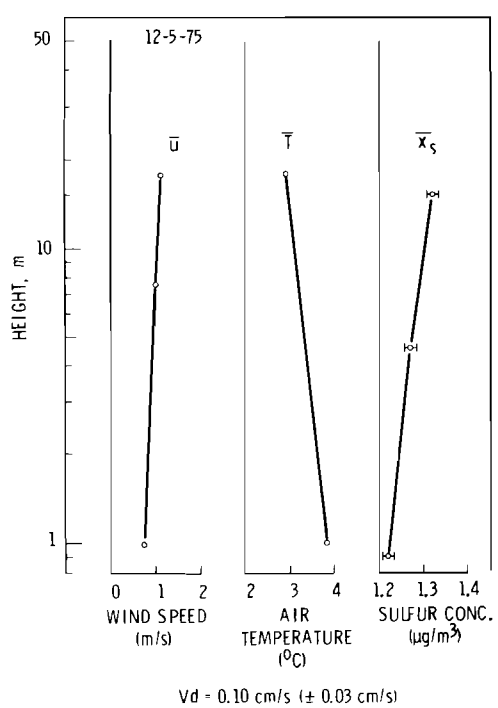

FIGURE 1. Semi-Log Plot of Wind Speed, Temperature, and Pollutant Concentration Profiles for Test 1, December 5, 1975

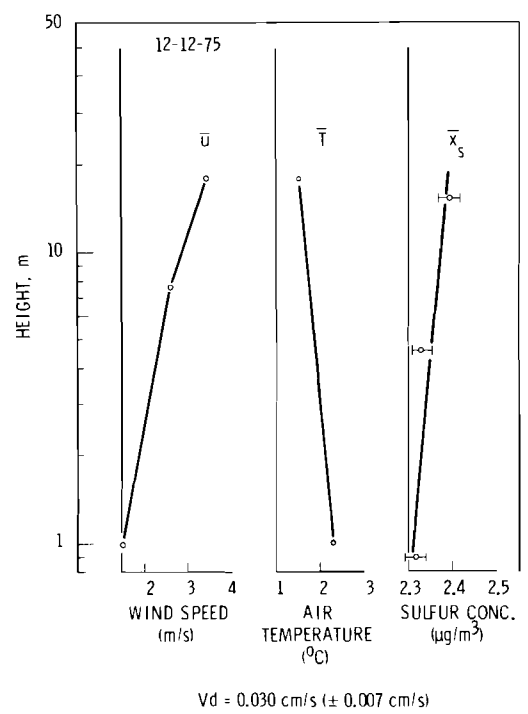

FIGURE 2. Semi-Log Plot of Wind Speed, Temperature, and Pollutant Concentration Profiles for Test 2, December 12, 1975

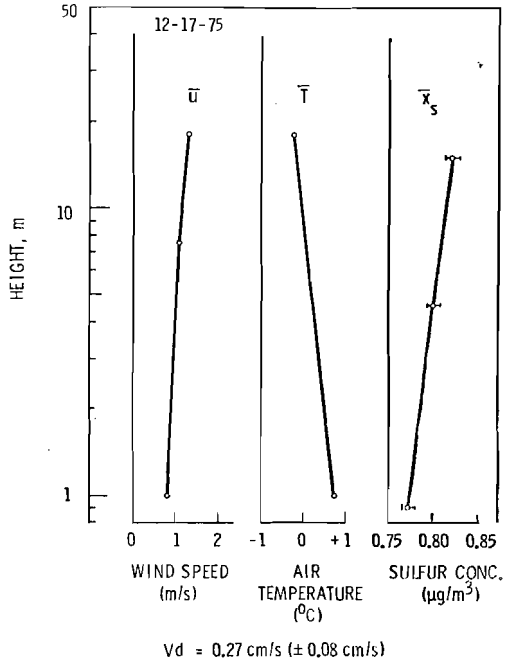

FIGURE 3. Semi-Log Plot of Wind Speed, Temperature, and Pollutant Concentration Profiles for Test 3, December 17, 1975

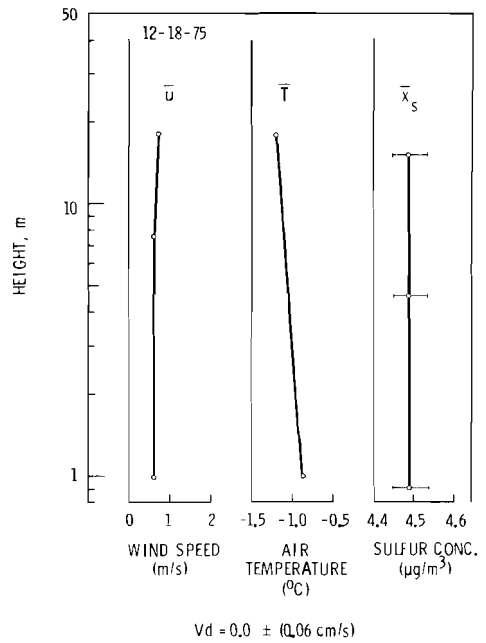

FIGURE 4. Semi-Log Plot of Wind Speed, Temperature, and Pollutant Concentration Profiles for Test 4, December 18, 1975

sulfur aerosol concentration profiles in Figures 1 and 3 and the reasonable dry deposition velocities computed for these cases are very encouraging.

RESISTANCE VALUES

Table 2 contains preliminary results for tests 1 and 3 in terms of the resistance values as discussed in previous reports[3]. R_T is the inverse of the deposition velocity, R_a is the atmospheric resistance (computed as equal to the momentum resistance), and R_s is the effective surface resistance computed as the difference between the total and surface resistances. The last column is the mean wind speed at 17 m.

As far as we are aware, these preliminary data provide the first values that directly assess sulfur containing particle removal rates in the field within reasonable accuracy. The range of values is encouraging. These are positive results in the first stages of this developing methodology.

TABLE 2. Summary of Results for Dry Deposition of Sulfur Aerosols

Test	V_d (cm/s)	R_T (s/cm)	R_a (s/cm)	R_s (s/cm)	$\bar{u}$(17m) (m/s)
1	0.10	10.0	2.3	7.7	1.13
3	0.27	3.7	0.44	3.3	1.28

ADDITIONAL PROFILES

Based on the above encouraging results, additional aerosol profile field data have been obtained and are presently under analysis for sulfur and additional species. These include six sets of profiles over a corn canopy in Illinois during a cooperative effort with Argonne National Laboratory during July 1977 and several sets of additional profiles this fall from the prototype system being tested at Hanford for experiments in the plumes from fossil fuel plants.

FUTURE PLANS

The prototype system at Hanford being used for two purposes. First, systems are being tested for studies in the plume from fossil fuel facilities. Second, a data base for dry removal of pollutants as a function of a range of ambient conditions at near background concentrations is being compiled.

An open question with the current pollutant profile method is the applicabilities of momentum and heat eddy diffusivities to pollutant fluxes. Studies are underway to determine pollutant eddy diffusivities directly by simultaneous eddy flux and profile determinations.

A series of experiments are planned to attempt to determine the flux of particles in discrete size ranges directly by eddy flux compulation based on laser measurements. This is a cooperative effort with G. Sehmel.

A field study is planned for early spring downwind of a coal-fired fossil fuel plant at Centralia, Washington. The dry deposition of gases (SO_2, O_3, NO_x, NO) and additional aerosol species will be studied.

References

1. J. G. Droppo, D. W. Glover, O. B. Abbey, C. W. Spicer and J. Cooper, Measurement of Dry Deposition of Fossil Fuel Pollutants. Draft Final Report under EPA Contract 68-02-1747, Battelle, Pacific Northwest Laboratories, Richland, WA, 1976.

2. R. K. Hadlock, J. G. Droppo and R. K. Woodruff, "Dry Deposition of Sulfur Particles from Northwest Fossil Fuel Plants," Pacific Northwest Laboratory Annual Report for 1973 to AEC, BNWL-1850 PT 3, available from NTIS, Springfield, VA, 1974.

3. J. G. Droppo, "Dry Deposition Processes on Vegetation Canopies," Proc. Atmosphere-Surface Exchange of Particulate and Gaseous Pollutants, CONF-740 921, ERDA Symposium Series 38, 1974.

4. J. G. Droppo and J. M. Hales, "Profile Methods of Dry Deposition Measurement," Proc. Atmospheric-Surface Exchange of Particulate and Gaseous Pollutants, CONF-740 921, ERDA Symposium Series 38, 1974.

5. J. G. Droppo, "Dry Removal of Air Pollutants by Vegetative Canopies," Preprint Volume, Fourth National Conference on Fire and Forest Meteorology, St. Louis, MO, November 16-18, 1976.

LIMITATIONS ON THE DETERMINATION OF DEPOSITION VELOCITIES

J. C. Doran

The constant flux condition necessary for the proper measurement of deposition velocities, v_d, may not be realized close to localized sources. Measurements in this area may lead to erroneous values of v_d, as is evident from an examination of solutions to a simple advection-diffusion model.

The proper specification of boundary conditions is important in modeling the transport and diffusion of a depositing substance. While mechanisms of removal at the surface are varied and complex, their effect may often be described in terms of a deposition velocity v_d,[1] where

$$v_d(z) = F/C \qquad (1)$$

Here, F is the vertical flux of the pollutant at some height, z, and C is the concentration of the pollutant at that same height. At small distances above the surface, v_d depends upon the properties of the viscous sublayer and does not change rapidly with height, although it may also depend strongly on factors such as moisture, particle size, surface composition, etc. At somewhat larger distances, e.g., $\gtrsim$10 cm, the deposition velocity is affected by the turbulent eddy structure of the atmosphere which is, in turn, a function of height. If $v_d(z_L)$ is some known "intrinsic" value which is approached as $z \rightarrow a_L$, then $v_d(z)$ may also be calculated as a function of height.[2]

In this approach, the assumption is made that the flux is constant over the vertical region of interest. While v_d may always be defined as in Equation (1), the quantity so derived can not be uniquely related to $v_d(z_L)$ unless this criterion is met. The following discussion shows that the required condition may not be trivially satisfied, and that the results of certain experiments designed to measure v_d must be regarded with caution.

A two-dimensional diffusion equation of the form

$$\frac{\partial C}{\partial t} + u(z)\,\frac{\partial C}{\partial x} = \frac{\partial}{\partial z}\left[K(z)\,\frac{\partial C}{\partial z} + S\right] \qquad (2)$$

was assumed, where C is the concentration per unit area, u is the velocity in the x-direction, S is a continuously emitting line source, and diffusion along the downwind direction has been neglected. While the use of a gradient description of the diffusion process is associated with a number of difficulties in principle,[3] in practice it has been shown capable of yielding surprisingly satisfactory results by Lamb, et al.[4] Their K(z) profile for a slightly unstable case was adopted, and joined to that described by Businger, et al.[5] below approximately 10 m. (The latter profile was adjusted slightly to produce a smoother match where they joined.)

Equation (2) was solved numerically using a modified approach of Runca and Sardei[6]. A logarithmically varying grid spacing was used for approximately the first 60 m above the ground, with constant intervals thereafter. The smallest increment was $\approx$0.02 m. An inversion lid was assumed near 500 m.

Solutions were obtained for two separate velocity profiles, one in which u(z) was uniform with height, and another in which u(z) was a fourth order polynomial in z

between 13 and 150 meters,[4] constant above 150 m and matched to the velocity profile from Monin and Yaglom[7] below 13 m. This second case was approximated in the numerical solution by a step function with 7 discrete values.[6]

The lower boundary condition for diffusion was given by

$$v_d(z_L)\left\{\frac{C(0) + C(z_1)}{2}\right\} = \frac{K(z_1)}{2}\left\{\frac{C(z_1) - C(0)}{z_1}\right\} \qquad (3)$$

where $z_1 \approx 0.02$ m, and $z_L = z_1/2$. Equation (3) is the finite difference approximation to

$$V_d(z_L)\, C(z_L) = K\,(z_L)\, \frac{\partial C}{\partial z}\Big|_{z=z_L} \qquad (4)$$

when $K(z=0) = 0$.

After completion of the desired number of advection and diffusion steps, the deposition velocity at the jth vertical grid point was determined from

$$v_d(z_j) = \frac{C(z_{j+1}) - C(z_{j-1})}{z_{j+1} - z_{j-1}} \cdot \frac{K(z_j)}{C(z_j)} \qquad (5)$$

Figure 1 shows the variation of $v_d(z = 1\text{ m})$ with time after release of the pollutant for the uniform wind profile, with $v_d(z_L) = 0.01$ m/s and a release height of 10 m. At $t \to \infty$, $v_d(z)$ approaches an asymptotic value of 0.007 m/s, which agrees well with that calculated by Sehmel and Horst,[2] but at smaller times the departures from this result can be significant. If an equilibrium time t_{95} is defined by the time required for $v_d(z)$ to reach 95% of its asymptotic value, then t_{95} may be plotted as a function of $v_d(z_L)$; the results are shown in Figure 2 for z_{ref} = 1 and 10 m. Clearly a finite time is required to establish a constant flux condition, and this time increases with increasing height over which

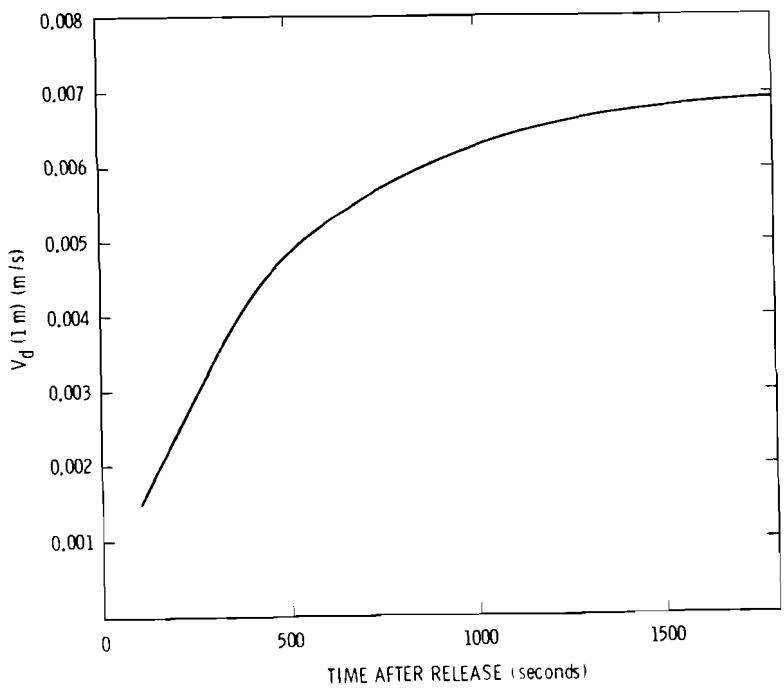

FIGURE 1. Deposition Velocity at z = 1 m as a Function of Time After Release. Source height = 10 m; $v_d(z_L) = 0.01$ m/s.

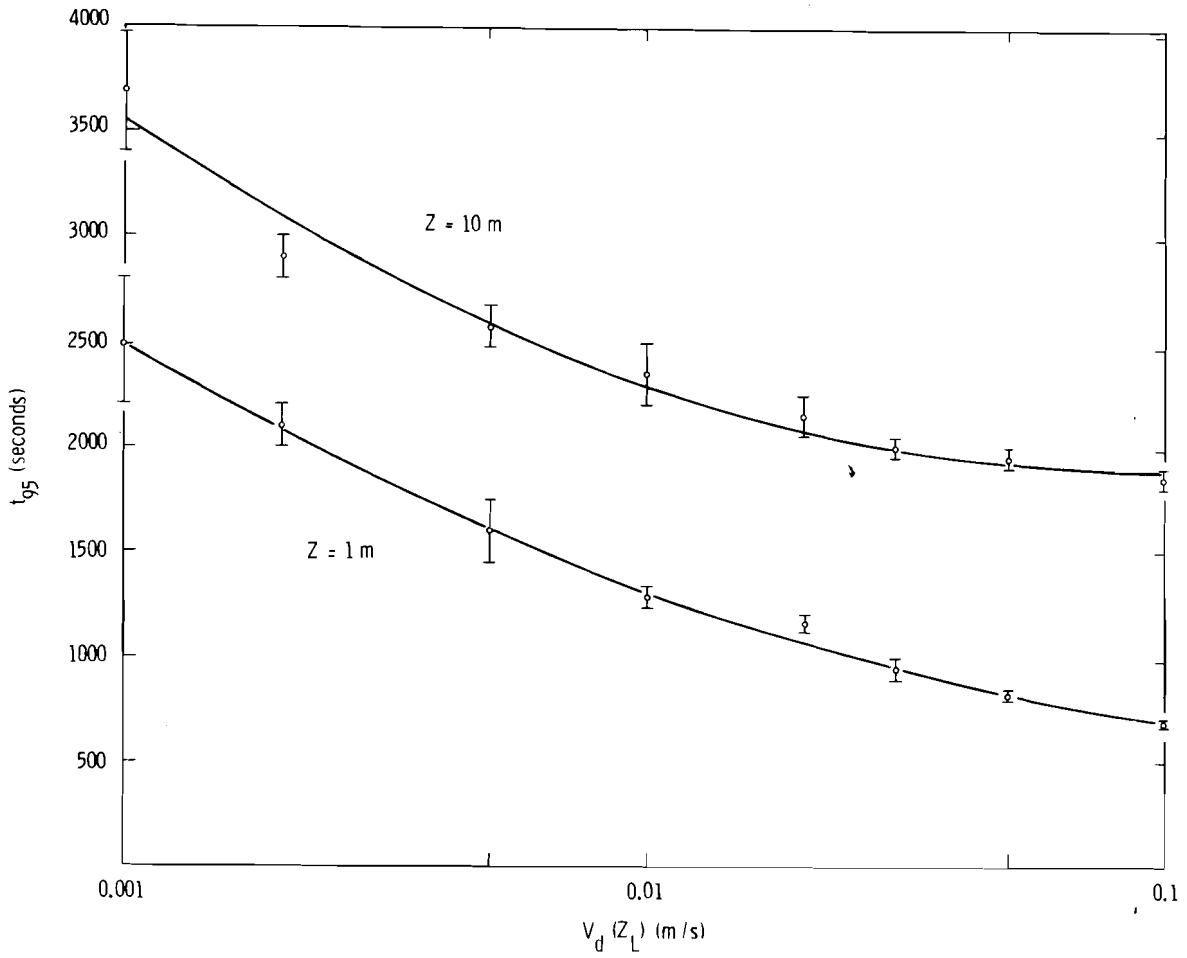

FIGURE 2. t_{95} as a Function of $v_d(z_L)$ for a Source Height of 10 m. The upper curve corresponds to $z \cong 10$ m; the lower curve is for $z = 1$ m. The lines are least square quadratic fits to the points shown, while the error bars for t_{95} are due to uncertainties arising from the numerical integration of Equation 2.

the flux is presumed constant. Measurements before this time, or measurements made too close to the source, may introduce errors.

For the wind profile which is variable in the vertical, $v_d(z)$ may be plotted as a function of downwind distance, after sufficient time has elapsed for steady state conditions to be established. This has been done in Figure 3, which shows that $v_d(z = 1\ \text{m})$ only reaches 95% of its asymptotic value at $\approx$14 km downwind from the release point.

It is important to distinguish between experimental measurements and numerical or theoretical modeling in assessing the implications of these results. In the latter case, the concept of deposition velocity is still valid, provided that it is applied at sufficiently small distances from the surface. This is true regardless of whether a constant flux layer has been established up to some arbitrary reference height. In the former case, however, care must be exercised in the interpretation of results. A gradient method of determining v_d could give erroneous results if the source of the measured pollutant is too close to the measuring apparatus. Similarly, a $v_d(z)$ obtained from direct flux measurements might not be readily extrapolated to $z = z_L$, unless some assurances can be provided that the deposition flux is indeed constant through some layer.

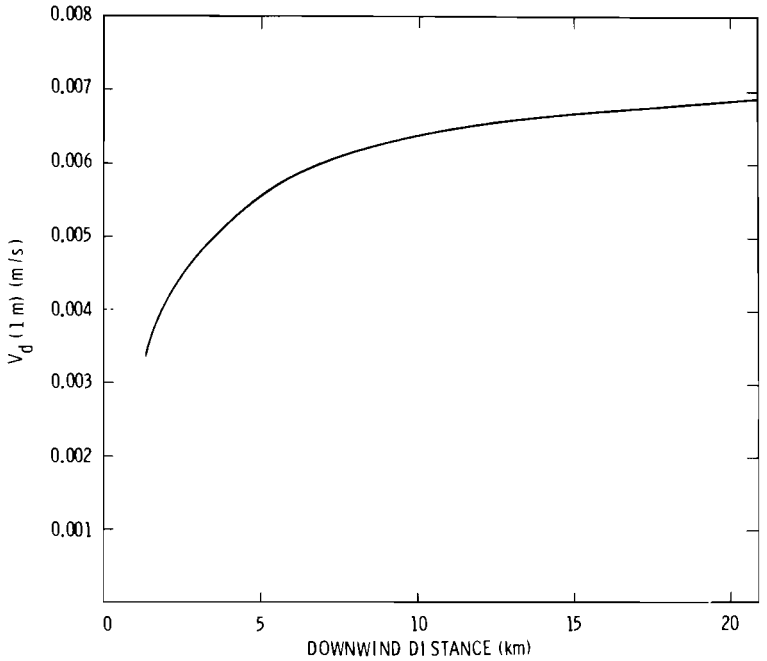

FIGURE 3. Deposition Velocity at z = 1 m as a Function of Downwind Distance, for the Case of a Nonuniform Velocity Profile in the Vertical. Source height = 10 m; $v_d(z_L)$ = 0.01 m/s.

References

1. D. Slade. Meteorology and Atomic Energy, U.S. Atomic Energy Commission, Washington, DC, 1968.

2. G. A. Sehmel and T. W. Horst. "Deposition Velocities as a Function of Particle Concentration Reference Height and Atmospheric Stability," Pacific Northwest Laboratory Annual Report for 1971 to the USAEC Division of Biology and Medicine, Volume II: Physical Sciences, Part 1, Atmospheric Sciences, BNWL-1651 PT 1, Battelle, Pacific Northwest Laboratories, Richland, WA, December 1972.

3. S. Corrsin. "Limitations of Gradient Transport Models in Random Walks and in Turbulence," Advances in Geophysics, 18A, Academic Press, New York, NY, 1974.

4. R. G. Lamb, W. H. Chen and J. H. Seinfeld. "Numerico-Empirical Analyses of Atmospheric Diffusion Theories," J. Atmos. Sci., 9, 1794-1807, 1975.

5. J. A. Businger, J. C. Wyngaard, Y. Isumi and E. F. Bradley. "Flux-Profile Relationships in the Atmospheric Surface Layer," J. Atmos. Sci., 28, 181-189, 1971.

6. E. Runca and F. Sardei. "Numerical Treatment of Time Dependent Advection and Diffusion of Air Pollutants," in the Proc. of the Symposium on Atmospheric Diffusion and Air Pollution, Santa Barbara, CA, September 9-13, 1974, pp. 345-351, American Meteorological Society, Boston, MA, 1974.

7. A. S. Monin and A. M. Yoglom. Statistical Fluid Mechanics, Vol. 1, MIT Press, Cambridge, MA, 1971.

REDUCTION IN ANNUAL AVERAGE AIR CONCENTRATIONS DUE TO THE DEPOSITION-RESUSPENSION PROCESS

T. W. Horst

Simulation of the diffusion-deposition-resuspension process with a numerical model has shown that the net effect of the deposition-resuspension sequence is a reduction in the annual average surface air concentration. This is because deposition occurs predominantly during periods of low atmospheric dispersion and high air concentrations and the subsequent resuspension occurs during periods of high wind and consequent high dispersion.

The estimation of the impact of plutonium and other actinides in the environment is complicated by their very long radioactive half-lives. Since these materials are continually available for uptake by man, an assessment of the resulting airborne contamination must consider not only their atmospheric diffusion and deposition, but also their possible subsequent resuspension and continued atmospheric dispersal.

Calculation of the exposure due to resuspension is a complicated procedure due to the horizontal distribution of the deposited contamination. Further, the resuspension rates which determine the effective source strength are known very poorly. Hence, it is desirable to somehow relate the exposure caused by resuspension to the exposure caused by the original depositing plume, because the latter can be characterized with more ease and confidence.

Horst[1,2] has compared the surface air concentrations of the resuspended plume C_r to those of the original depositing plume C_d. Assuming a steady state situation during constant atmospheric conditions (i.e., wind speed, wind direction and atmospheric stability) and also assuming that all deposited material is available for resuspension, it is readily apparent[1] that the total air concentration $C_d + C_r$ is equal to C_o, that which would be calculated with neither deposition nor resuspension. The surface contamination due to deposition increases until the resuspension flux exactly balances the deposition flux. At this time steady-state is achieved and $C_d + C_r = C_o$ because the net vertical flux at the surface is zero.

Horst[2] has also calculated the annual average value of C_d, C_r and C_o subject to the climatological distribution of wind speed, wind direction and atmospheric stability for a typical year of data from the Hanford Meteorological Tower. The results may be seen in Figure 1, which again includes the assumption that all deposited material is available for resuspension. By comparing the resuspended air concentration C_r with the reduction due to deposition, $C_o - C_d$, it may be seen that surprisingly, $C_d + C_r < C_o$: the net effect of the deposition-resuspension process is a reduction in the annual average surface air concentration. Thus a conservative estimate of the total air concentration may be made by ignoring deposition and resuspension altogether.

Research during the past year has led to an understanding of the reason for this unexpected result. Calculations of C_d, C_r and C_o have been made for a variety of cases with a single wind speed and atmospheric stability and with a uniform wind rose, i.e., the wind is equally likely to blow from any direction. Within the accuracy of the computations the result is identical to that for a single wind direction, $C_d + C_r = C_o$: the resuspension balances the loss due to deposition. The reduction in the annual average surface air concentration which follows from the deposition-resuspension sequence, then, is due primarily to the mix of wind speeds and atmospheric stabilities

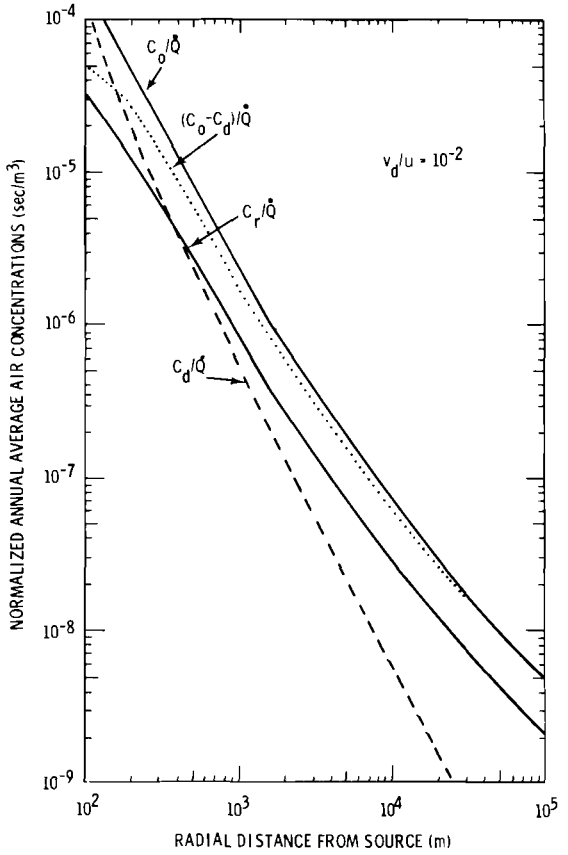

Neg. 77A006-A

FIGURE 1. Annual Average Air Concentrations Due to Deposition and Resuspension

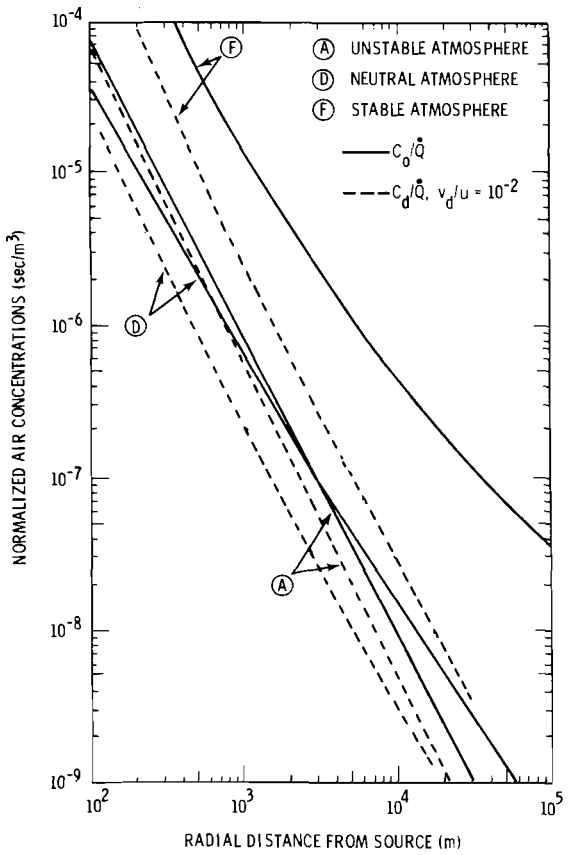

Neg. 77A006-2

FIGURE 2. Typical Air Concentrations During Specified Atmospheric Conditions

found in a climatological average and is not a consequence of the varying wind direction.

The annual average value of C_o is found as the sum of the air concentrations for each combination of atmospheric stability, wind speed and direction with each contribution weighted by its probability of occurrence. For most climatologies this sum will be dominated by the contributions during stable atmospheric conditions because of the associated high air concentrations, as shown in Figure 2. These high air concentrations are due to the minimal turbulent mixing during stable conditions and also due to the low wind speeds which are a prerequisite for stable conditions. Correspondingly, the reduction of the annual average surface air concentration due to deposition, $C_o - C_d$, is also dominated by the large contribution during stable conditions.

Resuspension, on the other hand, occurs predominantly during periods of high winds which produce neutral atmospheric stability. Consequently the contaminant, which has been deposited predominantly during a time of high surface air concentration, is resuspended during a time when the dispersive capability of the atmosphere is considerably greater. If instead the resuspension is independent of wind speed, the contaminant is resuspended during a climatological mix of stabilities, which on the average also produces lower air concentrations than those during which the bulk of the deposition occurred. Only if the material deposited during each combination of wind speed and stability were resuspended during identical atmospheric conditions would the increase in surface air concentration due to resuspension C_r make up for the decrease due to deposition $C_o - C_d$.

References

1. T. W. Horst, "The Resuspension Ratio for a Gaussian Plume," Pacific Northwest Laboratory Annual Report for 1974 to the USAEC Division of Biomedical and Environmental Research, Part 3, Atmospheric Sciences, BNWL-1950, PT 3, Battelle-Northwest, Richland, WA, February 1975.

2. T. W. Horst, The Resuspension of Material Dispersed by Atmospheric Diffusion from a Point Source, BNWL-1964, Battelle-Northwest, Richland, WA, December 1975.

IMPROVED PARTICLE DEPOSITION MODEL

G. A. Sehmel and W. H. Hodgson

Recent experimental deposition velocities from wind tunnel experiments were incorporated with previously used data to improve surface mass transfer resistance correlations. The new data were all deposition velocities measured for 3.8 to 5.1 cm gravel. Prediction from the correlations show deviations from previous models. Predicted minimum deposition velocities for rough surfaces are less than predicted from previous models.

INTRODUCTION

Particle deposition velocities are a function of many variables including surface, particle, and meteorological parameters. Limited deposition velocity measurements in the field have never been correlated into any predictive model. Possibly no field-based predictive model exists because experimental conditions in the field cannot be controlled. Indeed, even deposition velocity measured in wind tunnels have been somewhat difficult to correlate[1-4]. However, deposition velocities measured in controlled experiments in wind tunnels do show the greatest promise for developing predictive mass transfer or deposition velocity correlations.

In this on-going study, particle deposition velocities have been determined in wind tunnel experiments for the range of variables shown in Table 1. In these experiments, the deposition velocity, K_1, is defined as the deposition flux divided by the air concentration 1 cm above the deposition surface. Thus, K_1 is an index of the surface mass transfer resistance. All deposition data with the exception of the gravel data were incorporated into prediction models earlier[1].

The present objective was to incorporate the deposition velocity data acquired in 1975-76 for 3.8 to 5.1 cm "diameter" gravel into predictive correlations[1] for surface mass transfer resistance. This gravel had the largest aerodynamic surface roughness of any surface extensively studied to date. Dimensionless correlations including these more recent data should more adequately predict deposition velocities for even more complex deposition surfaces.

The form of the predictive equations will be the usual steady state approximation of the atmospheric deposition boundary conditions. However, once atmospheric transport equations start to approximate nonequilibrium conditions, the predictive correlations are developed to still describe surface mass transfer resistance immediately adjacent to the deposition surface.

TABLE 1. Experimental Range of Variables Used in Developing Integral Resistance Correlation

Deposition Surface		Range of Variables Used in Developing INT Correlation		
Type	Dimensions, cm	Particle Diameter, μm	Friction Velocity, u_*, cm/sec	Roughness Height, z_o, cm
Brass shim stock	"smooth"	0.03 to 28	11 to 73	0.004
Artificial grass	0.7 height	0.03 to 28	19 to 144	0.12 to 0.40
Gravel	0.5 to 1.6 "diameter"	0.03 to 26	22 to 133	0.13 to 0.18
Water	Wave Height to 2.5 cm	0.03 to 29	11 to 122	0.001 to 0.002
Gravel	3.8 to 5.1 "diameter"	0.03 to 28	15 to 107	0.3 to 0.6

MODEL

Relating measured deposition velocities to surface mass transfer resistance requires equations relating the different variables. The particle deposition velocity in terms of an airborne concentration at any height (rather than 1 cm) is described by the equation,

$$K = \frac{v_t}{1 - (1/\alpha)} \qquad (1)$$

This equation indicates the lower limit of deposition velocities to be the gravity settling velocity. However, as the terminal settling velocity decreases, mass transfer is assisted by Brownian and eddy diffusion. Ultimately as particle diameter approaches molecular size, mass transfer is controlled by Brownian diffusion. The term α is a model-derived expression containing a grouping of mass transfer resistance:

$$\alpha = \exp(-v_t \, \mathrm{Int}/u_*), \qquad (2)$$

Int is an integral mass transfer resistance term. Obviously, Int is related to a simple electrical analog resistance R by,

$$R = \frac{1}{K} = \frac{1 - \exp\left(\frac{v_t}{u_*} \mathrm{Int}\right)}{v_t}. \qquad (3)$$

Two dimensionless modeling approaches were used to correlate Int calculated from Equation (3) and measured deposition velocities K_1. One of these is identified as the model A correlation,[2,3] the other, as the model B correlation.[1] In both cases, correlations were developed for constant particle density of 1.5 g/cm^3, air viscosity of 1.78×10^{-4} g/(cm·sec), and air density of 1.2×10^{-3} g/cm^3. Both correlations were recalculated to include the range of variables shown in Table 1, which includes the more recent gravel data.

The model A(1976) correlation is:

$$\mathrm{Int}_{A\text{-}1976} = -\exp\left\{-28.625 + 6.198 \ln \frac{d}{z_o} - 0.04691 \left(\ln \frac{d}{z_o}\right)^2 + 1.1823 \ln \frac{u_*}{v_t} + 0.03170 \left(\ln \frac{u_*}{v_t}\right)^2 - 2.707 \ln \frac{D}{u_* z_o} - 4.446 \ln \frac{\rho_p u_* d^2}{18 \mu z_o}\right\} \qquad (4)$$

Each term is dimensionless. Similarly, the 1976 model B correlation is

$$\mathrm{Int}_{B\text{-}1976} = \exp\left\{-208.153 + \ln \mathrm{Sc}\left[17.41 - 0.41195 \ln \mathrm{Sc} - 0.03327 \ln\left(\frac{d}{z_o}\right)\right] + \ln \tau^+\left[-13.065 - 0.3126 \ln \tau^+ + 0.3383 \ln\left(\frac{d}{z_o}\right) - 0.3711 \ln\left(\frac{D}{z_o u_*}\right)\right]\right\} \qquad (5)$$

In both correlations all terms are statistically significant at the 99% level and the multiple correlation coefficients are 0.92. There appears to be no statistically significant difference between fitting the data with either Equation (4) or (5).

PREDICTED DEPOSITION VELOCITIES

Deposition velocities were predicted using the mass transfer resistances from both correlations combined with the meteorological mass transfer resistances from 1 cm to 1 m heights. These deposition velocities, K_{1-M}, are referenced to the airborne concentration 1 m above the surface. Deposition velocities were predicted as a function of particle diameter, friction velocity, surface roughness, and particle density. Particle density changes affect v_t, but Int in equations (2) through (5) is assumed independent of particle density (i.e., use 1.5 g/cm^3).

Predicted K_{1-M} from the two models are shown in Figures 1, 2, 3, and 4 for a friction velocity of 30 cm/sec, aerodynamic roughness heights from 0.001 to 10 cm, and particle densities of 1, 4, and 11.5 g/cm^3. Predictions in Figure 1 and 2 are from model A (1974) and model B (1975), whereas predictions from the 1976 version of the two models are shown in Figures 3 and 4. For all predictions, deposition velocities are greater than the terminal settling velocity v_t. The main differences between predictions are values of the minimum deposition velocities for each roughness height.

Minimum deposition velocities are less sensitive to surface roughness for model A in the 1976 version. Model A(1976) predictions compared to model A(1974) predictions indicate: (1) comparable values for a z_0 of 0.1 cm, (2) lower values for z_0 of 3 and 10 cm, and (3) higher values for a z_0 of 0.001 cm. In contrast, model B(1976) predictions show a nearly uniform decrease in the minimum deposition velocity.

When comparing models, model A(1976) and model B(1976) predict nearly the same deposition velocities for a surface roughness of 0.1 cm. Model predictions show greater deviations for other surface roughness.

CONCLUSIONS

Correlations to predict surface resistance for particle deposition velocities were previously developed using least squares techniques and dimensional analysis. The data base for the correlations was expanded by including our deposition velocity data for 3.8 to 5.1 diameter crushed gravel. This surface had the largest aerodynamic surface roughness studied to date in controlled wind tunnel experiments. Since the data base was significantly increased, correlations were developed to include the recent data.

Attempts to include additional relationships between nondimensional model terms indicated the published models (A and B) included all statistically significant terms. Only the correlation constants were changed by including the crushed gravel data.

Deposition velocity predictions show closer agreement between model A(1976) and model B(1976) than agreement between the original models, A(1974) and B(1975), However, both models (1976) are equally valid from a statistical sense. Future model improvements may be based upon physical rather than dimensional analyses.

NOMENCLATURE

a = particle radius, cm

d = particle diameter, cm

D = Brownian diffusion coefficient cm^2/sec, see Eq. 6

Int = Integral mass transfer resistance next to surface, dimensionless

k = Boltzmann's constant, 1.32×10^{-16} erg/(molecule °K)

p = pressure, cm of mercury, (76.0 cm used)

Sc = Schmidt number, ν/D

T = temperature, °K,(296°K used)

u_* = friction velocity, cm/sec

v_t = monodispersed particle gravity settling velocity, cm/sec

z_0 = aerodynamic surface roughness, cm

μ = air viscosity, g/(cm·sec),[1.78×10^{-4} g/(cm·sec) used]

ν = kinematic viscosity, μ/ρ

ρ = air density, g/cm^3,(1.2×10^{-3}g/cm^3 used)

ρ_p = particle density, g/cm^3 (1.5 g/cm^3 **used)**

$\tau+$ = dimensionless relaxation time, $\frac{\rho_p d^2}{18\mu} \frac{u_*^2}{\nu}$

where Brownian diffusivity was calculated[5] from

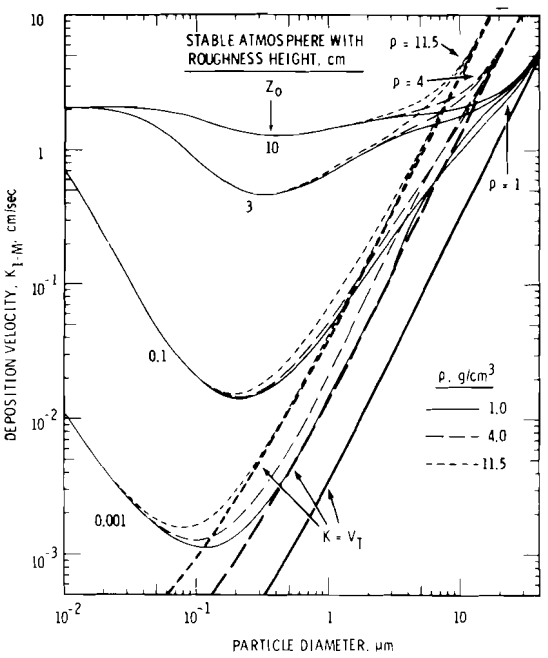

Neg. 760188-11

FIGURE 1. Model A(1974) Predicted Deposition Velocities at 1 m for u_* = 30 cm/sec and Particle Densities of 1, 4 and 11.5 g/cm³

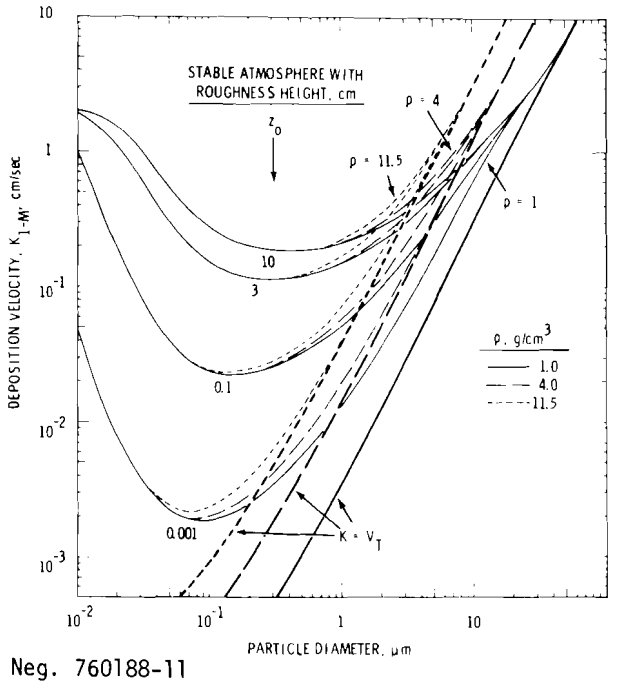

Neg. 760188-11

FIGURE 2. Model B(1975) Predicted Deposition Velocities at 1 m for u_* = 30 cm/sec and Particle Densities of 1, 4 and 11.5 g/cm³

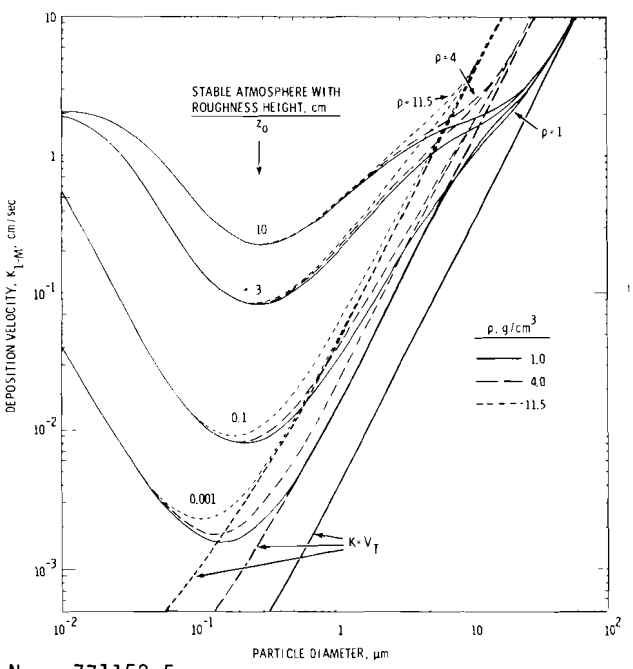

Neg. 771152-5

FIGURE 3. Model A(1976) Predicted Deposition Velocities at 1 m for u_* = 30 cm/sec and Particle Densities of 1, 4 and 11.5 g/cm³

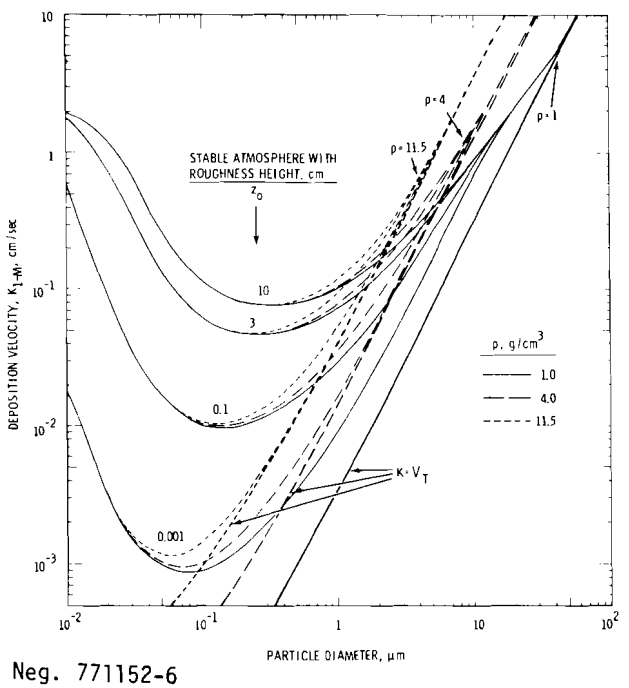

Neg. 771152-6

FIGURE 4. Model B(1976) Predicted Deposition Velocities at 1 m for u_* = 30 cm/sec and Particle Densities of 1, 4 and 11.5 g/cm³

$$D = \frac{kT}{6\pi\mu a}\left\{1 + \frac{10^{-4}}{pa}\left[6.32 + 2.01\exp(-2190pa)\right]\right\} \qquad (6)$$

References

1. G. A. Sehmel, "Comparison of Deposition Velocities Predicted from Dimensionless Analysis Correlation," Pacific Northwest Laboratory Annual Report for 1975 to the USAEC Division of Biomedical and Environmental Research, Part 3, Atmospheric Sciences, BNWL-2000 PT 3, Battelle-Northwest, Richland, WA, pp. 83-86, 1976.

2. G. A. Sehmel and W. H. Hodgson, "Predicted Dry Deposition Velocities," Proc. of the Atmosphere-Surface Exchange of Particulate and Gaseous Pollutants - 1975 Symposium, Richland, WA, September 4-6, 1974. Energy Research and Development Administration Symposium Series CONF-740921, National Technical Information Service, U.S. Dept. of Commerce, Springfield, VA, pp. 399-422, 1976.

3. G. A. Sehmel and W. H. Hodgson, "Particle and Gaseous Removal in the Atmosphere by Dry Deposition," in the Proc. of the Symposium on Atmospheric Diffusion and Air Pollution, Santa Barbara, CA, September 9-13, 1974, pp. 253-260, American Meteorological Society, Boston, MA, 1974.

4. G. A. Sehmel and W. H. Hodgson, "Particle Dry Deposition Velocities," Pacific Northwest Laboratory Annual Report for 1974 to the USAEC Division of Biomedical and Environmental Research, Part 3, Atmospheric Sciences, BNWL-1950 PT 3, Battelle-Northwest, Richland, WA, pp. 175-180, 1975.

5. C. N. Davies, Aerosol Science, Academic Press, N.Y., p. 408, 1966.

AIRBORNE PLUTONIUM TRANSPORT OF NONRESPIRABLE PARTICLES

G. A. Sehmel

Airborne nonrespirable particles were collected with rotating cowl systems near U-Pond on the Hanford Reservation, and east of the Rocky Flats, Colorado, plant. Both ^{238}Pu and ^{239}Pu were transported on nonrespirable particles. Airborne fluxes for ^{238}Pu ranged from 10^{-8} to 10^{-5} $\mu Ci/m^2/day$ and ^{239}Pu fluxes ranged from 10^{-8} to 10^{-4} $\mu Ci/m^2/day$. These are the first reported values for airborne plutonium fluxes on nonrespirable particles. Airborne plutonium concentrations ranged from about 10^{-9} up to 10^{-4} $\mu Ci/g$ of airborne nonrespirable solids. The airborne solids at Rocky Flats were sized into 12 increments from 10 to 230 μm. Plutonium was found on all size increments.

INTRODUCTION

Wind will resuspend plutonium attached to host soil particles from surfaces contaminated with plutonium. In most previous resuspension research reported by other workers as well as in air monitoring activities, airborne concentrations of particles

have been measured without regard for particle sizes present. However, only respirable or near-respirable size particles are frequently measured since the usual air sampling techniques do not collect larger, nonrespirable particles.

In this research, airborne particles were separated in the sampling process into two main fractions. One of these contained particles collected by gravity settling in the inlet section of the sampler. The second fraction contained those particles passing through the inlet section and collecting on the stages of a high volume cascade impactor.

The smallest particles collected in the inlet section were about 10 μm in diameter; the fraction collected in the inlet section is termed "nonrespirable." This fraction was assayed for ^{238}Pu and ^{239}Pu. In some cases, particles in this fraction were further separated into smaller size fraction and these fractions also assayed for ^{238}Pu and ^{239}Pu.

SAMPLER DESCRIPTION

Nonrespirable airborne particles were collected using the rotating cowl system shown in Figure 1. This device collected nonrespirable particles by gravity settling within the cowl body. Since the cowl was always directed into the wind by the wind vane, a reasonably accurate sample of airborne nonrespirable particles was obtained. There was no particle sampling directional error. The following flux calculations assume that nonrespirable particles are so large that they continue in a straight trajectory while approaching the inlet, and their motion is not influenced by the presence of the cowl. From the cross sectional area of the cowl inlet, total sampling time, and the total plutonium collected within the cowl, the airborne plutonium flux can be calculated for nonrespirable particles. If the total weight of particles collected is determined, the plutonium per gram of airborne soil can be calculated.

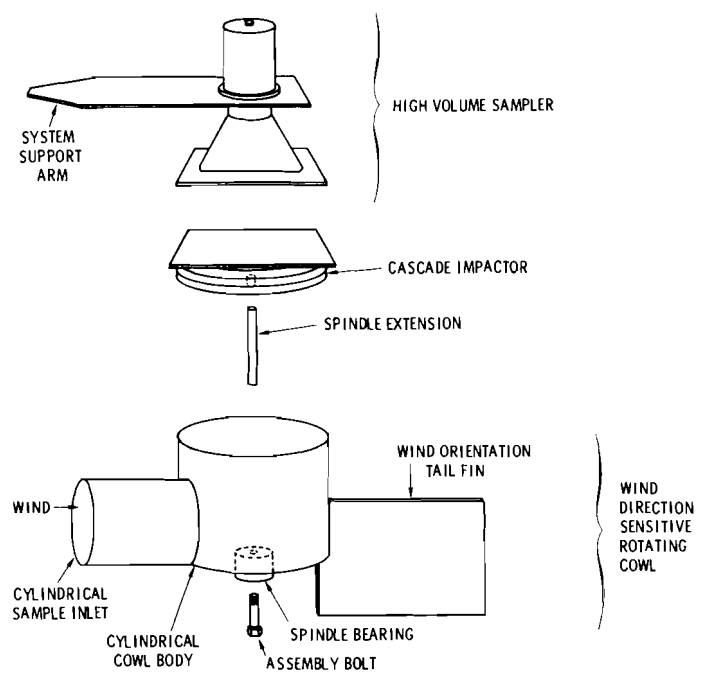

Neg. 744581-12

FIGURE 1. Rotating Cowl and Impactor

SITES INVESTIGATED

Plutonium associated with airborne nonrespirable particles was collected at Rocky Flats, Colorado, and on the Hanford Reservation. At Rocky Flats, airborne samples had been collected in July 1973 and analyzed[1] for respirable particles; however, the original experiment did not analyze nonrespirable particles for plutonium.

Samples were obtained at three Rocky Flats sites. Site A was along the eastern security fence, site B was along the cattle fence, and site AB was between sites A and B. At these sites, nonrespirable particles were collected at several heights. In the original experiment, some of the samples had been separated into different size fractions while other samples were not so separated because of the small quantities of particles collected. Those samples retained from the original experiment were analyzed for ^{238}Pu and ^{239}Pu.

The Hanford site was near U-pond within 200-West area of the Hanford Reservation. Airborne nonrespirable particles were collected west of U-pond as well as east of U-pond from February to November, 1975. The distance between sampling sites was 480 m. Prevailing winds were from west to east.

All samples were analyzed for plutonium by a procedure which involved total dissolution, radiochemical separation, electroplating, counting using a Frisch[(a)] grid and pulse height analysis.

AIRBORNE PLUTONIUM FLUXES

Nonrespirable airborne plutonium fluxes were calculated for both ^{238}Pu and ^{239}Pu. The Rocky Flats data are shown in Figures 2 and 3. In Figure 2, horizontal airborne nonrespirable ^{239}Pu fluxes are shown as a function of distance from site A. Airborne nonrespirable fluxes were greatest near the original oil storage area (source of contaminated leakage) and near ground level. Fluxes ranged from 10^{-7} up to 10^{-3} $\mu Ci/m^2/day$. In contrast, fluxes of ^{238}Pu ranged from 10^{-8} to 10^{-5} $\mu Ci/m^2/day$, as is shown in Figure 3.

Nonrespirable airborne plutonium fluxes around U-pond on the Hanford Reservation are shown in Figure 4. The ^{238}Pu flux was less than the ^{239}Pu flux. This decrease is similar to the Rocky Flats data. However, the U-pond data show the nonrespirable plutonium flux extends at least up to 30 m above ground level. Also, there was a greater airborne plutonium flux east of U-pond than west of U-pond. This is to be expected since prevailing winds are from the west.

At U-pond, the airborne ^{238}Pu flux ranged from 10^{-8} to 10^{-7} $\mu Ci/m^2/day$, which is within the midrange of 10^{-9} to about 10^{-5} $\mu Ci/m^2/day$ measured at Rocky Flats. Similarly, the ^{239}Pu flux at U-pond ranged from about 10^{-6} to 10^{-5} $\mu Ci/m^2/day$, which is within the 10^{-7} to 10^{-3} $\mu Ci/m^2/day$ measured at Rocky Flats. The bracketing of the airborne nonrespirable particle flux near U-pond and at Rocky Flats even within two to three orders of magnitude is considered entirely coincidental since surface sources and other factors are peculiar to each site.

PLUTONIUM CONCENTRATION PER GRAM OF AIRBORNE SOIL

Nonrespirable soils collected at 0.3 m above ground level at Rocky Flats were sized into 12 size increments. Each size increment was analyzed for ^{238}Pu and ^{239}Pu. Plutonium concentrations were normalized ($\mu Ci/g$) to the grams of soil collected within each size increment. Results are shown in Figure 5 for ^{238}Pu as a function of particle size at sites A and AB. Plutonium-238 was associated with all particle sizes. The maximum concentration was about 10^{-5} $\mu Ci/g$ for particle sizes between 10 and 20 μm. For particle diameters up to 230 μm, concentrations tended to decrease with increasing particle diameter. Concentrations at Site A were greater than at site AB. This was expected since site A was closer to the original oil storage area at which leakage of plutonium occurred.

Similarly, airborne ^{239}Pu concentrations are shown in Figure 6 for nonrespirable as well as respirable particle diameters. The data for respirable particles have been reported previously.[1,2] Plutonium-239 concentrations were larger at site A than at site AB. Concentrations were again found on all particle sizes analyzed. Plutonium-239 concentrations ranged from 10^{-8} to about 10^{-4} $\mu Ci/g$.

Plutonium concentrations on nonrespirable particles collected near U-pond were analyzed for total plutonium within each collected sample rather than as a function of sample

(a) LFE Environmental Laboratories, Richmond, California

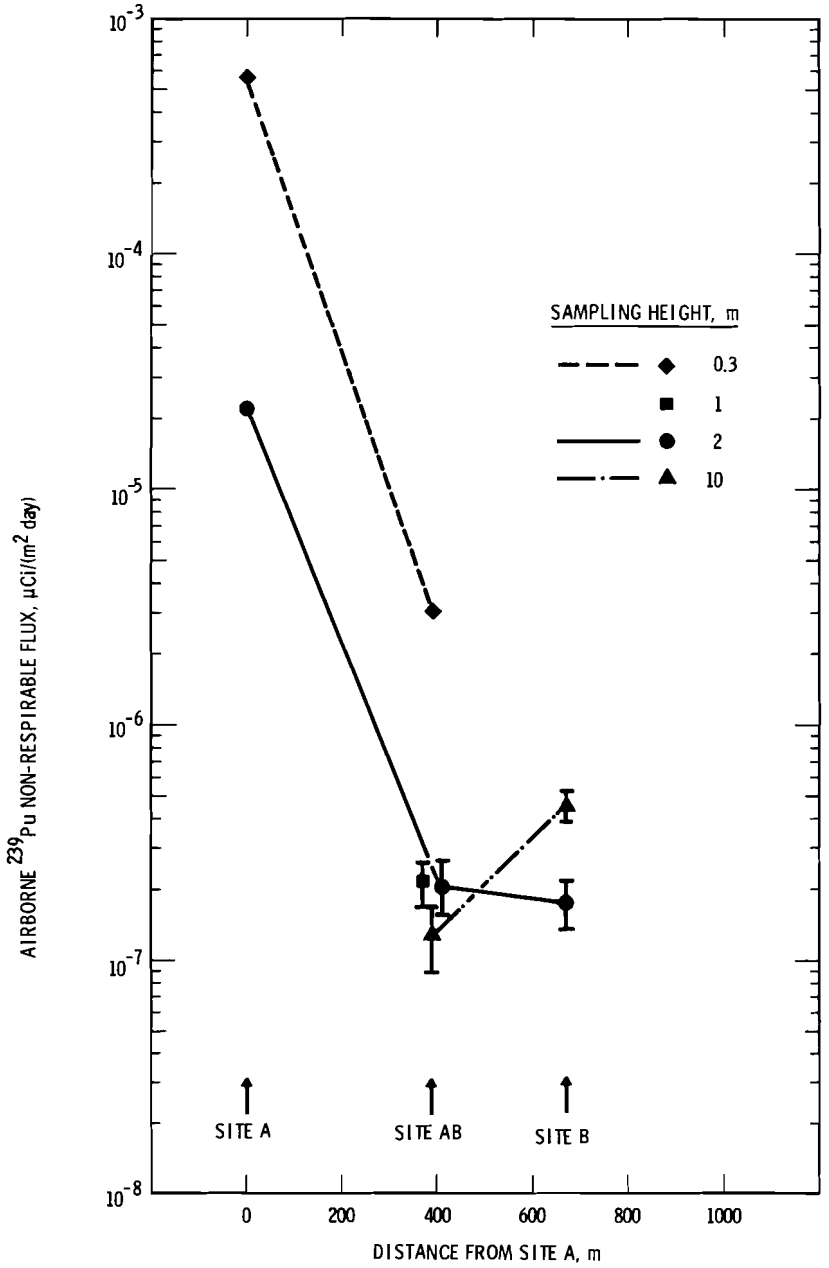

Neg. 767208-4

FIGURE 2. Decrease with Distance of Total ^{239}Pu Flux on Nonrespirable Particles at Rocky Flats

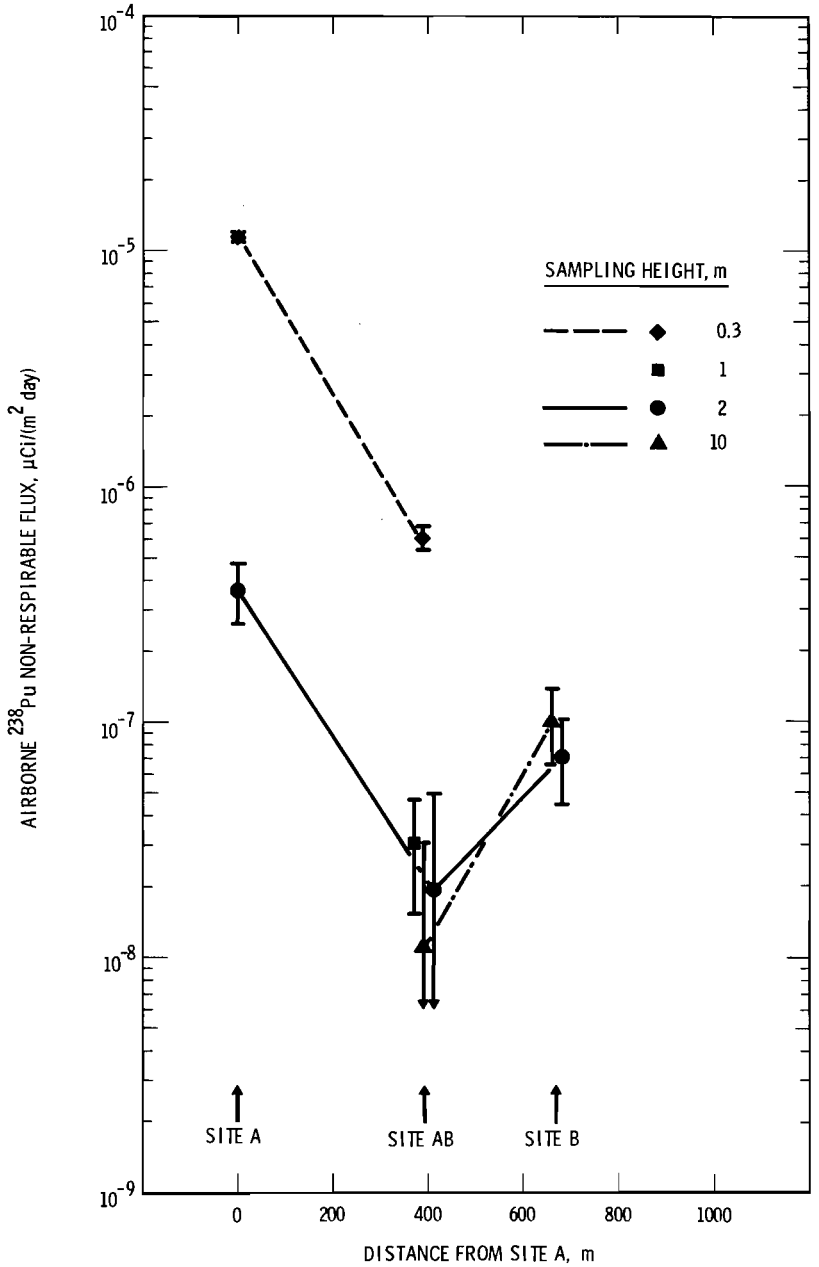

Neg. 767208-6

FIGURE 3. Decrease with Distance of Total ^{238}Pu Flux on Nonrespirable Particles at Rocky Flats

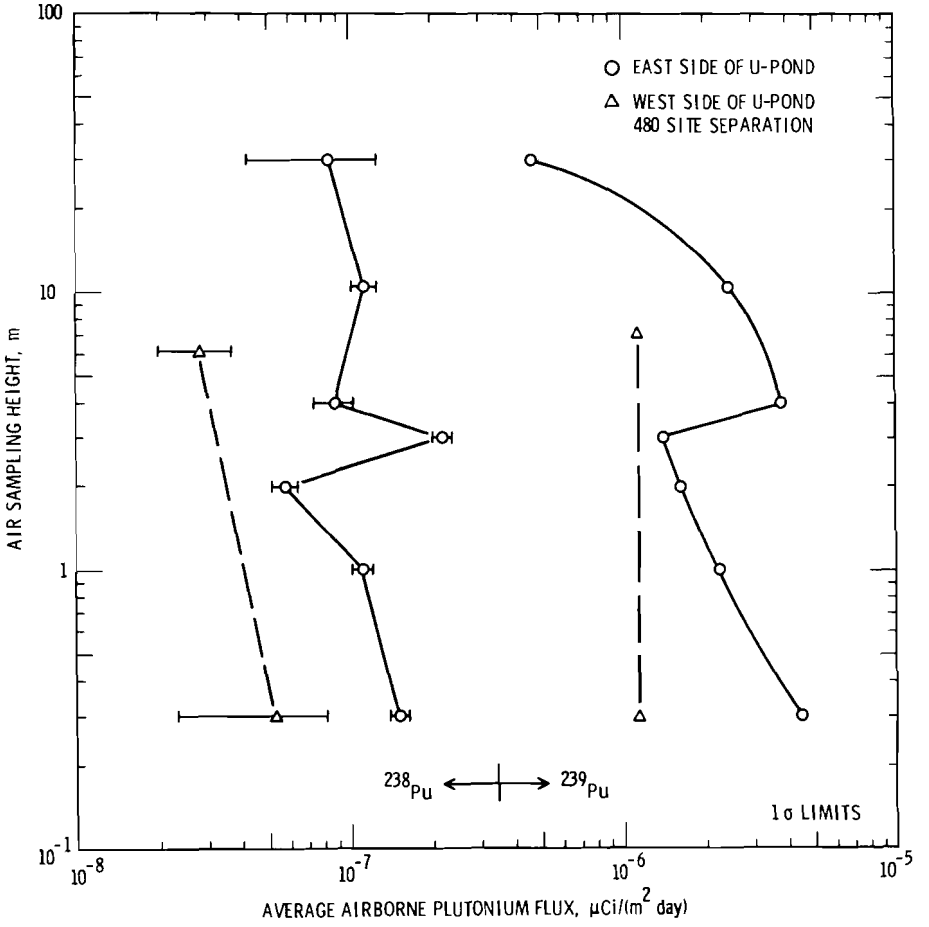

FIGURE 4. ^{238}Pu and ^{239}Pu Airborne Fluxes on Nonrespirable Particles at U-Pond During February 27-November 10, 1975 (Particles Collected in Cowls)

particle size increments. Normalized results are shown in Figure 7. Concentrations of ^{238}Pu ranged from about 10^{-9} to 10^{-7} μCi/g. These results are in the same range reported in Figure 5 for ^{238}Pu at Rocky Flats. Similarly ^{239}Pu concentrations ranged from about 10^{-7} to 10^{-5} μCi/g. Again, ^{239}Pu concentrations are in the same range reported in Figure 6 for Rocky Flats. The comparable magnitude of the fluxes is entirely coincidental.

CONCLUSIONS

Wind stresses can resuspend plutonium from contaminated surfaces. Resuspended plutonium is attached to nonrespirable as well as respirable particles. Hence, large soil particles may contribute significantly to downwind concentrations of plutonium and represent one mechanism for transporting plutonium to surrounding land.

The data reported are the first results to quantify the range of nonrespirable airborne plutonium fluxes. A spread from 10^{-9} to 10^{-5} μCi/m^2/day brackets the range of fluxes at Rocky Flats and U-pond. It is coincidental that the fluxes are even this similar. Ground contamination on nonrespirable particles at both sites is poorly defined,[2] hence, the data can at present not be analyzed to reflect resuspension rates or a resuspension factor.

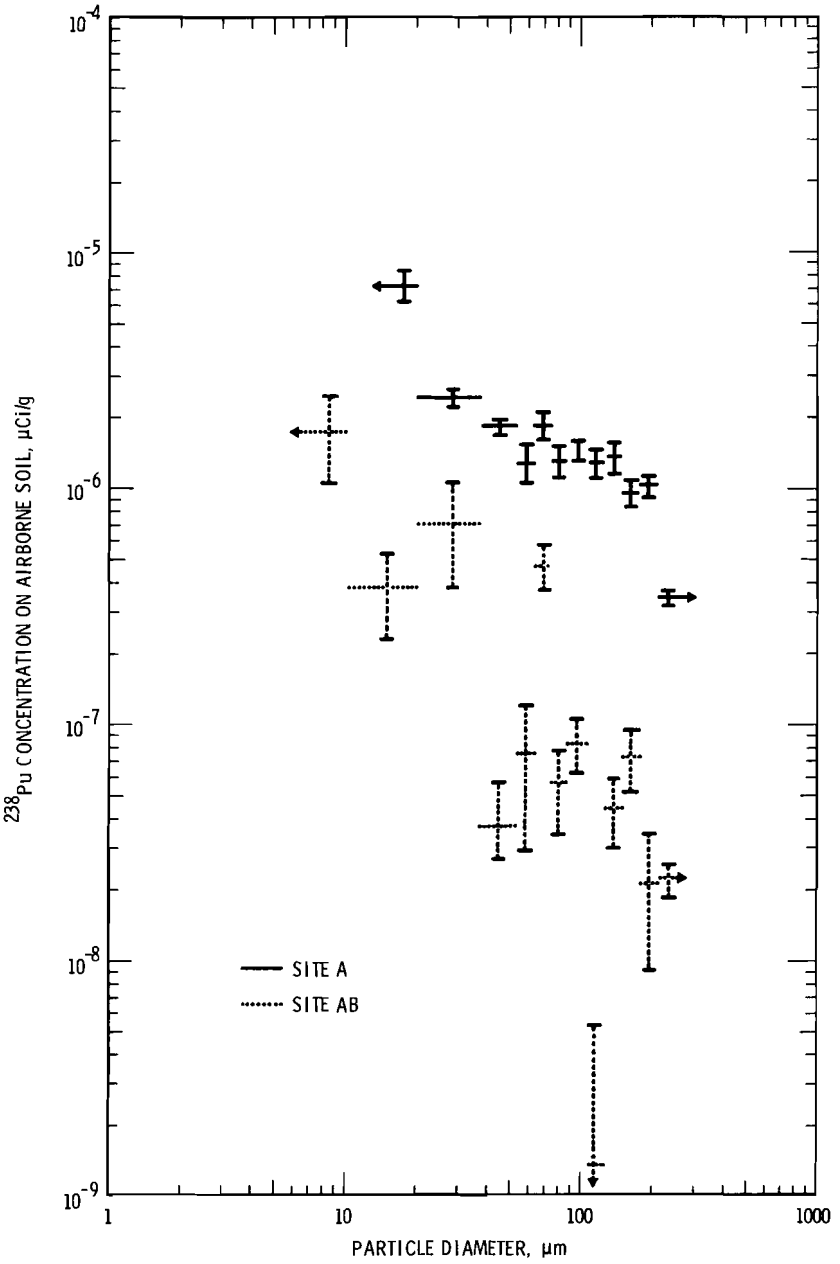

Neg. 767208-5

FIGURE 5. Decrease in ^{238}Pu Concentration on Airborne Soil as a Function of Particle Diameter

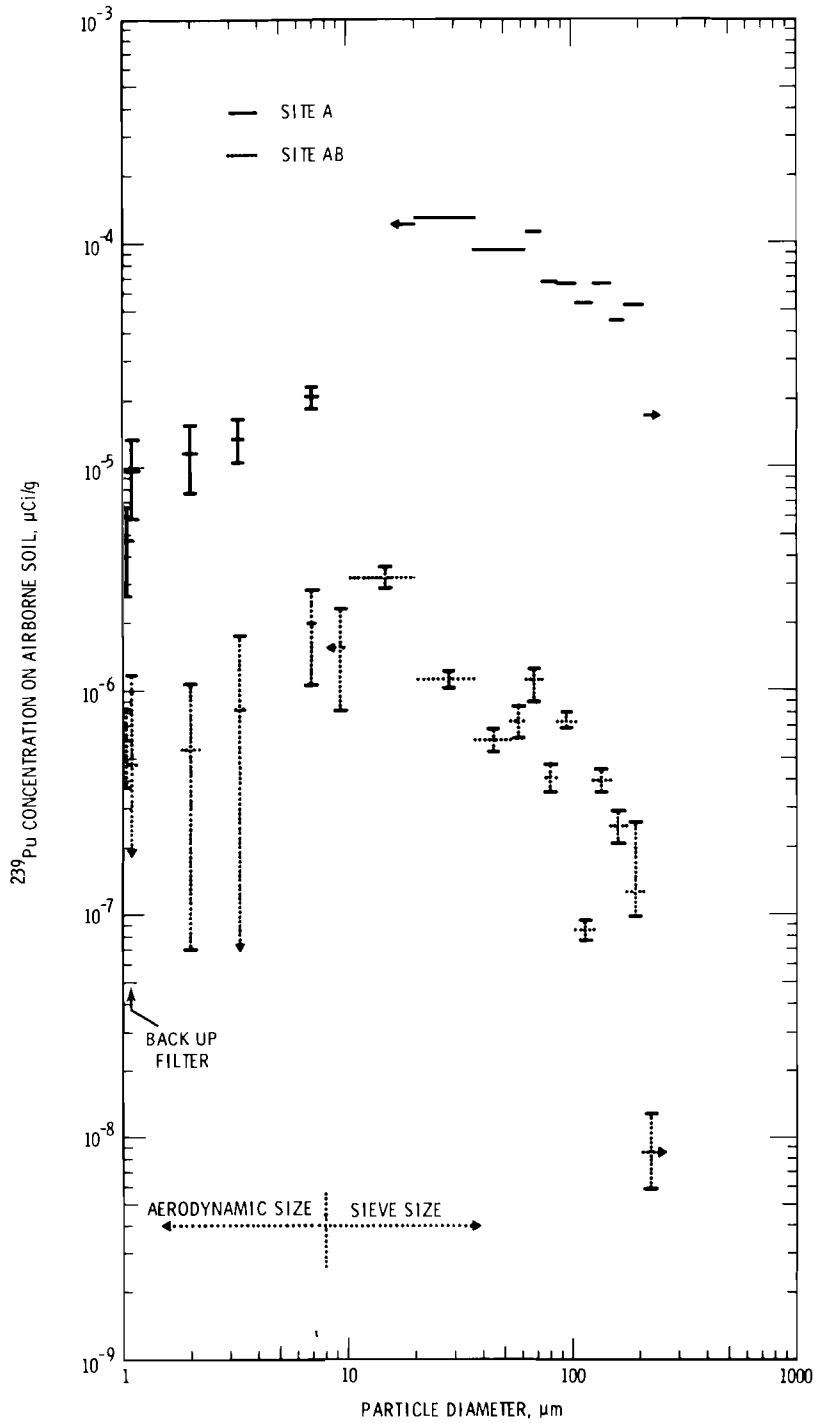

Neg. 767208-1

FIGURE 6. Decrease in ^{239}Pu Concentration on Airborne Soil as a Function of Particle Diameter

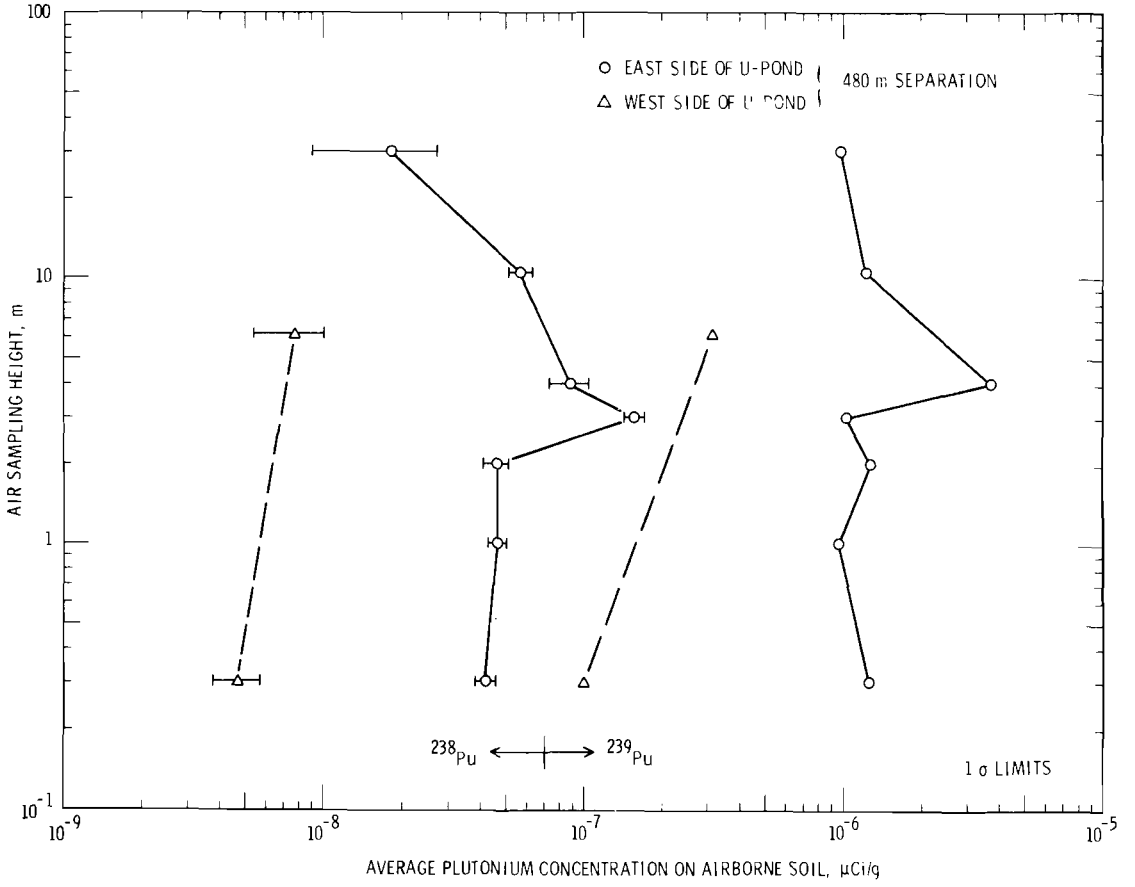

Neg. 7611156-1

FIGURE 7. Airborne Nonrespirable ^{238}Pu and ^{239}Pu Fluxes at U-Pond During February 27-November 10, 1975 (Particles Collected in Cowls)

References

1. G. A. Sehmel and F. D. Lloyd, "Resuspension of Plutonium at Rocky Flats," in Atmosphere-Surface Exchange of Particulate and Gaseous Pollutants, R. J. Engelmann and G. A. Sehmel coordinators, CONF-704921, available from National Technical Information Service, Springfield, VA, pp. 757-779, January 1976.

2. P. Krey, E. Hardy, H. Volchok, L. Toonkel, R. Knuth, M. Coppes, and T. Tamura, Plutonium and Americium Contamination on Rocky Flats Soil--1973, HASL-304, Health and Safety Laboratory, New York, N.Y.

WIND-CAUSED PARTICLE RESUSPENSION RATES

G. A. Sehmel and F. D. Lloyd

Wind-caused tracer resuspension rates were measured experimentally and calculated. They ranged from 10^{-11} to 10^{-7} fraction resuspended/sec for respirable particles. Resuspension rates for nonrespirable particles were on the order of 10^{-11} fraction resuspended/sec. Respirable particles resuspension rates increased as the 4.8th power of wind speed. Resuspension rates were independent of weathering time.

INTRODUCTION

Radioactive particles deposited on surfaces can be resuspended by wind and mechanical activity. These resuspended particles are transported downwind and, in sufficient concentration, could become a potential radiological hazard to man. Resuspension mechanisms are poorly understood and, consequently, resuspension rates and potential airborne inhalation hazards cannot be adequately predicted. The need for such predictions is not new: resuspension has long been known to occur where radioactive materials are released to the environment.

Resuspension release rates are needed for source terms in calculating total downwind diffusion and transport of resuspended particles. Only recently in this research have particle resuspension rates been directly measured. Experimental values of wind-caused resuspension rates of tracer particles from environmental surfaces have been determined from mass balance techniques.[1-6]

Some data were initially obtained using 8 μm aerodynamic equivalent diameter (AED) ZnS particles and average wind speeds from 1 to 5 m/sec. Average resuspension rates for ZnS particles were measured for resuspension from an asphalt surface[2] and a cheat grass surface.[7] For average wind speeds of 1 to 4 m/sec, wind resuspension rates from an asphalt surface ranged from 5×10^{-9} to 6×10^{-8} fraction resuspended/sec. For average wind speeds of 1 to 5 m/sec, wind resuspension rates from a cheat grass surface ranged from 1×10^{-9} to 10^{-8} resuspended/sec.

EXPERIMENTAL

Wind-caused resuspension was measured for submicrometer $CaMoO_4$ tracer particles deposited in a lightly vegetated area on the Hanford Reservation. The tracer particles were deposited in the area of a 23-m radius around the air sampling tower shown in Figure 1. Resuspended particles were measured at the tower as a function of wind speed increments for respirable particle diameters and for nonrespirable particles at all wind speeds. Respirable particles were collected within particle cascade impactors while nonrespirable particles were collected by impaction and gravity settling within rotating cowls.[8] "Respirable" particles as used in this report consist largely of particles 10 μm and smaller, although some larger particles will be collected on the first impactor stage, which has an effective 50% aerodynamic equivalent diameter cut-off of 7.7 μm.

RESULTS

Wind-caused resuspension rates for respirable particles are shown in Figure 2 as a function of wind speed. As wind speed increased, resuspension rates increased from about 10^{-11} to 10^{-7} fraction resuspended/sec. Different functional dependencies of resuspension rates on wind speed can be obtained from these data, depending upon which set of wind speed increments are used. During January to February the air was sampled during three rather large wind speed increments, while in subsequent experiments wind speed increments activating selected samplers were smaller. The least squares straight lines shown in Figure 3 were calculated for all

Neg. 743881-1

FIGURE 1. Wind-Tracer Resuspension Site on the Hanford Reservation

data points (both larger and smaller wind increments). In these cases, resuspension rates increased with the 1.0 to 4.8 power of wind speed. However, when only data taken for the smaller wind speed increments are used, wind-caused resuspension rates increased with wind speed to the 4.8 power for 7, 3.3, 2.0 and 1.1 μm/dia particles as well as for the smaller particles collected on the cascade impactor backup filter.

For comparable wind speed increments, tracer resuspension rates were nearly independent of the time the tracer was on the ground surface. It is often assumed in theoretical modeling that particles become less available for resuspension with time. The assumption in these models is that pollutant particles become fixed or attached to soil particles and subsequently "migrate" into the ground surface by rain or other weathering processes. The lesser availability of particles lowers resuspension rates.

The constancy of wind-caused resuspension rates with time over about 9 months is a significant deviation from the limited literature for radioactive particle resuspension. Radioactive particle resuspension literature indicates that airborne fission products from nuclear weapons testing decreases with a weathering half-life of 35 days.[9] In contrast, if there is a weathering half-life for the controlled tracer experiments described above, the weathering half-life must be on the order of years. Some differences in weathering reported by others might be explained by how air samples were collected. In early work, air concentrations were measured without regard for wind speed or diameter. However, in these tracer experiments air concentrations and hence resuspension rates were measured as a function of wind speed increments and particle diameters. In establishing a weathering half-time it would be mandatory to make airborne concentration measurements under nearly identical wind conditions. Obviously, factors other than wind speed also influence weathering, which yet is poorly understood.

Average wind-caused tracer resuspension rates are reported for both respirable and nonrespirable particles in Figure 3. In these cases, "respirable" refers to all particles collected within cascade impactors while "nonrespirable" refers to particles collected by gravity settling in the inlet cowl assembly upstream of the cascade impactor. Nonrespirable particle resuspension rates were nearly independent of time and were on the order of 10^{-11} fraction resuspended/sec. Resuspension rates for respirable particles ranged from about 10^{-11} to 4×10^{-8} fraction resuspended/sec. These resuspension rates did not decrease with time. For the first two sampling periods, resuspension was measured for all wind speeds. In succeeding experiments, resuspension rates were measured only for wind speeds above 1 and above 4 m/sec. The upper or solid line portion of the respirable particle curve corresponds to resuspension rates calculated only for the periods when wind speed fell within prescribed limits. These periods corresponded, in one case, to three wind speeds between 1.3 and 20 m/sec, and in the other case, 4.5 to 9.4 m/sec. The lower limit of the respirable particle curve corresponds to resuspension rates calculated by assuming resuspension

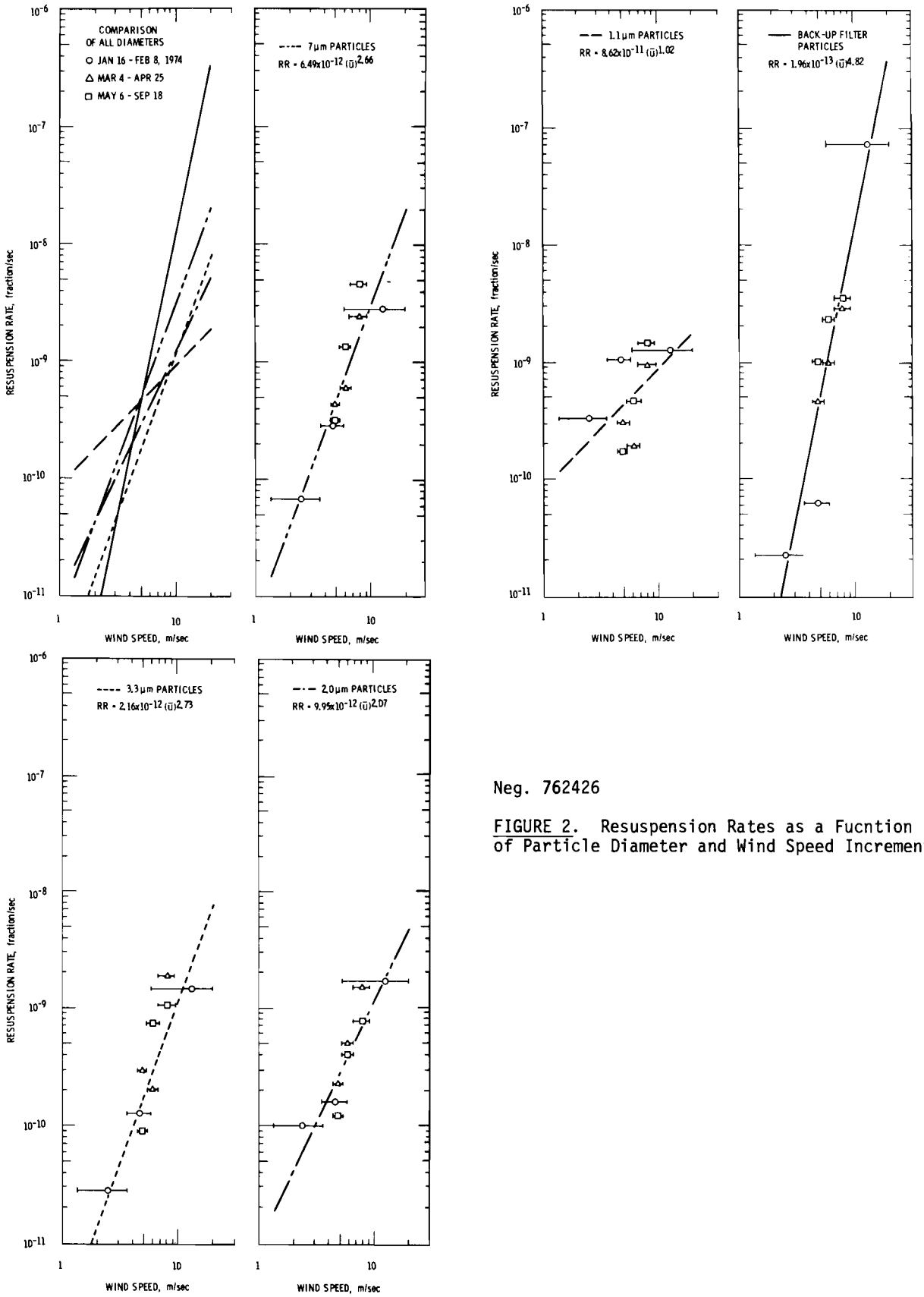

Neg. 762426

FIGURE 2. Resuspension Rates as a Fucntion of Particle Diameter and Wind Speed Increments

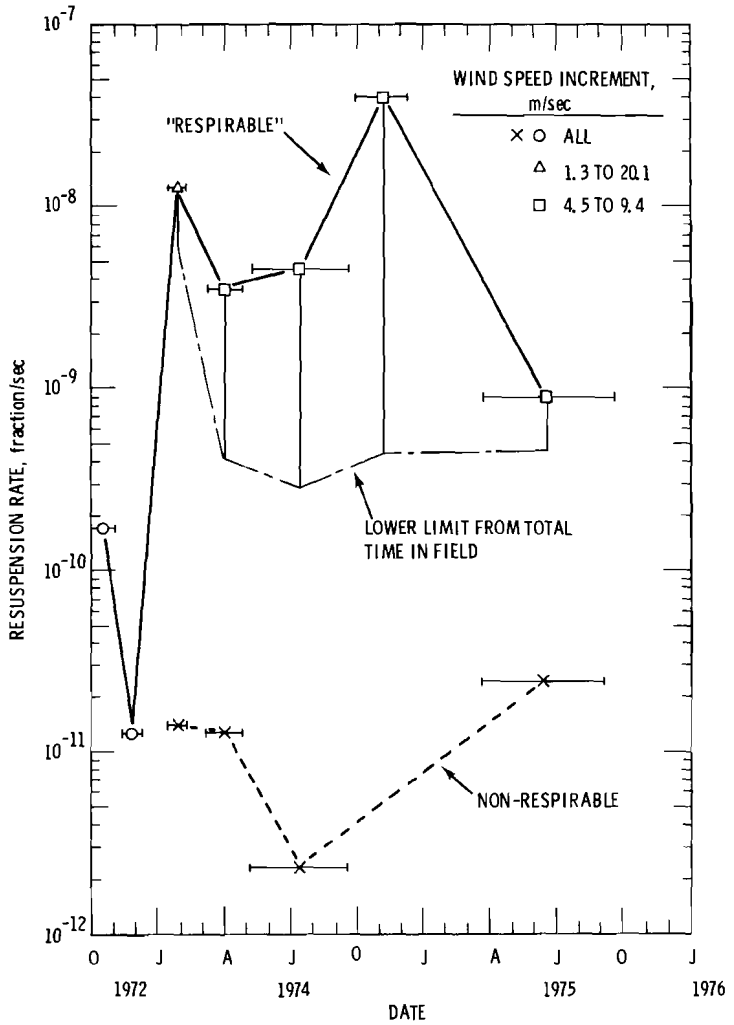

Neg. 762426-16

FIGURE 3. "Average" Wind Caused Resuspension Rates (Lightly Vegetated Desert on Hanford Reservation)

times corresponding to the total time that cascade impactors were in the field (i.e., time included for winds less than 1 and less than 4 m/sec).

CONCLUSIONS

Resuspension rates are needed as source terms in atmospheric diffusion and transport equations; however, atmospheric transport model predictions are no better than the uncertainty in the source data. Uncertainties in resuspension rates are very large. Much research is needed to develop resuspension models which predict particle resuspension rates for any situation.

The change in airborne concentration of a pollutant as a function of time is often attributed to a weathering half-life, the fixation of the pollutant particle into the ground surface soil. For radioactivity, the weathering half-life has been determined by others to be on the order of 35 days. In contrast, weathering half-lives for respirable tracer particles are now estimated in the current study as being on the order of years. Predictions using weathering half-lives of months versus years could have a significant implication in environmental hazards evaluations. Credit for decreased airborne radioactivity from resuspension is now attributed to a weathering half-life

of months. If a weathering half-life of years were applicable, the potential downwind inhalation hazard from resuspended particles would be significantly increased. Additional experimental data are needed to determine the correct weathering half-life to be used in hazards evaluations.

References

1. G. A. Sehmel and F. D. Lloyd, "Particle Resuspension Rates." In Atmosphere-Surface Exchange of Particulate and Gaseous Pollutants. R. J. Engelmann and G. A. Sehmel, coordinators, CONF-740921, National Technical Information Service, Springfield, VA 22151, pp. 846-858, January 1976.

2. G. A. Sehmel and F. D. Lloyd, "Tracer Particle Resuspension Caused by Wind Forces Upon an Asphalt Surface." Pacific Northwest Laboratory Annual Report for 1971: Atmospheric Sciences. BNWL-1651-1, Battelle, Pacific Northwest Laboratories, Richland, WA 99352, pp. 136-138, 1972.

3. G. A. Sehmel and F. D. Lloyd, "Initial Particle Resuspension Rates--A Field Experiment Using Tracer Particles." Pacific Northwest Laboratory Annual Report for 1971: Atmospheric Sciences. BNWL-1950-3, Battelle, Pacific Northwest Laboratories, Richland, WA 99352, pp. 203-207, 1975.

4. G. A. Sehmel and F. D. Lloyd, "Resuspension Rates from a Circular Field Source." Pacific Northwest Laboratory Annual Report for 1975: Atmospheric Sciences. BNWL-2000-3, Battelle, Pacific Northwest Laboratories, Richland, WA 99352, pp. 92-93, 1976.

5. G. A. Sehmel, "Initial Correlation of Particle Resuspension Rates as a Function of Surface Roughness Height." Pacific Northwest Laboratory Annual Report for 1974: Atmospheric Sciences. BNWL-1950-3, Battelle, Pacific Northwest Laboratories, Richland, WA 99352, pp. 209-212, 1975.

6. M. M. Orgill, M. R. Petersen, and G. A. Sehmel, "Some Initial Measurements of DDT Resuspension and Translocation from Pacific Northwest Forest," In Atmosphere-Surface Exchange of Particulate and Gaseous Pollutants. R. J. Engelmann and G. A. Sehmel, coordinators, CONF-740921, National Technical Information Service, Springfield, VA 22151, pp. 813-834, January 1976.

7. G. A. Sehmel, "Particle Resuspension from Truck Traffic in a Cheat Grass Area." Pacific Northwest Laboratory Annual Report for 1975: Atmospheric Sciences. BNWL-2000-1, Battelle, Pacific Northwest Laboratories, Richland, WA 99352, pp. 96-99, 1976.

8. G. A. Sehmel, Plutonium and Tracer Particle Resuspension: An Overview of Selected Battelle-Northwest Experiments, BNWL-SA-6022, Battelle, Pacific Northwest Laboratories, Richland, WA 99352, 1976.

9. R. H. Wilson, R. G. Thomas and J. N. Stannard, Biomedical and Aerosol Studies Associated with a Field Release of Plutonium. WT-1511, Sandia Corporation, Albuquerque, NM, 1961, p. 51.

APPLICATION OF SOIL EROSION DATA TO PARTICLE WIND RESUSPENSION

M. M. Orgill

An appraisal of W. S. Chepil's research work in five areas of wind erosion has been made as it relates to particle wind resuspension research. His research on dynamics of wind erosion and influence of soil properties on wind erosion is relevant to our problem. However, the wind erosion equation as formulated has limited application to particle wind resuspension problems, and a more general and applicable equation needs to be formulated.

INTRODUCTION

Much data concerning wind erosion and translocation has been obtained through wind erosion studies in agricultural fields. This information has and may still provide important insights into the problem of particle resuspension, especially where submicrometer radioactive particles become attached to host soil particles prior to resuspension.

A prolific contributor to erosion studies has been Dr. W. S. Chepil of the Agricultural Research Service, Manhattan, KS. He has written 61 or more research papers on the subject of wind erosion.[1-61] Although the main goal of his research was a practical wind erosion equation for determining annual potential soil loss from agricultural fields, a portion of his basic research is generally fundamental for particle wind resuspension.[62]

His major contributions range from 1939 to 1965, and can be classified into five categories: (1) dynamics of wind erosion; (2) soil properties that influence wind erosion; (3) sedimentary characteristics of dust storms; (4) wind erosion control; and (5) the wind erosion equation. Survey papers on wind erosion were written in 1943[9], 1963[59], and 1965.[61]

Study methods used by Chepil include wind tunnel experiments, laboratory techniques and some field measurements. A significant share of his research was analyzing soil properties that hindered or favored soil erosion, and designing and implementing methods to control the loss of fertile soil in the Great Plains.

This report contains a fairly complete list of Chepil's research contributions (see references) and appraises this information in relation to particle wind resuspension research. In this short summary the principal emphasis is to evaluate briefly the five categories of wind erosion research to which Chepil contributed, and indicate some possible research that might extend the application of this information for particle wind resuspension research. One of those aspects is to consider the possibility of developing a more general wind erosion equation (or equations) for predicting soil or particle translocation.

DYNAMICS OF WIND EROSION

Chepil contributed much to understanding equilibrium forces on soil grains[44,50] during wind movement, which is pertinent to particle wind resuspension. In a turbulent wind he has shown that the threshold drag per unit horizontal area of a soil bed is:

$$\bar{\tau}_c = 0.66\ g\ D\rho'\ \tan\phi\ \eta(1 + 0.75\ \tan\phi)T, \qquad (1)$$

where the mean threshold drag required to move the top soil grains ($\bar{\tau}_c$) is influenced by gravity (g), diameter of soil grains (D), the immersed density of the grains, (ρ'), angle of repose of the grains, (ϕ), closeness of packing of top grains on the soil bed, (η). and the ratio of maximum to mean lift and drag on the soil grains exerted by the turbulent wind, (T). The mean critical threshold drag can be related to critical threshold velocity, i.e., a velocity that just starts the most erodible grains in motion by:

$$\bar{\tau}_c = C_d \ \rho(V_*)_c^2 \qquad (2)$$

and

$$V_* = \frac{V_z}{5.75 \ln \frac{Z}{k}}, \qquad (3)$$

where V_* is the drag velocity, C_d is a drag coefficient which varies with aerodynamic surface roughness, ρ is the density of air, V_z is wind velocity at height Z; k is an index of the aerodynamic surface roughness. These relationships imply that a threshold velocity, V_t, at any height Z is

$$V_t = 5.75 \left[\frac{0.66}{C_d} g \ D \frac{\rho'}{\rho} \tan \phi \ \eta(1 + 0.75 \tan \phi)T \right]^{1/2} \ \ln \frac{Z}{k} \cdot \qquad (4)$$

When the wind velocity exceeds the threshold velocity, then the most erodible grains will start to move, and as the winds increase, the wind shear near the ground will also increase the lift on soil grains causing them to jump into the air and eventually fall to dislodge other grains. This type of movement is saltation. Impacts from the most erodible grains moving in saltation cause the movement of larger and smaller particles called surface creep and suspension, respectively.

The threshold velocity at 1 ft (30 cm) for a soil may vary from 4 to 13 ms^{-1}, depending on soil type and conditions. Equation (4) does not reflect all the factors that could determine the threshold velocity. The effects of moisture and other properties of the soil are not present, and the contribution of convective turbulence to the lift and drag on soil grains has been ignored. Further study and evaluation of the equilibrium forces on soil grains is important for particle wind resuspension research.

SOIL PROPERTIES THAT INFLUENCE WIND EROSION

When the wind velocity exceeds that required barely to move the soil grains, then the rate of soil movement (total weight of soil material moved past a unit width normal to the direction of movement and of unlimited height per unit time) for dry conditions is

$$q = \rho \frac{C_s}{g} \sqrt{D_e} (V_*')^3. \qquad (5)$$

Equation (5) shows that the rate of soil movement varies directly with the square root of the average equivalent diameter, D_e, and the cube of the drag velocity, V_*', where

$$V_*' = \frac{V_z - V_t}{5.75 \ln \frac{Z}{k}}, \cdot \qquad (6)$$

The average equivalent diameter is given by

$$D_e = 2.65 \ \rho_e \ D, \qquad (7)$$

in which ρ_e is the bulk density of the erodible soil particles, and D is their diameter as determined by dry sieving. C_s is a coefficient that varies greatly with the various soil properties. This coefficient covers a multitude of factors and varies with the size distribution of the erodible particles,[5] the proportion of fine dust particles present in the soil mixture,[13] the proportion and size of nonerodible fractions,[20] position in the field,[4] and the amount of moisture in the soil.[34] Other factors of importance are the soil texture,[27] water-stable structure,[28] organic matter,[29,31] soil microorganisms[29] and various products of organic matter decomposition, calcium carbonate,[29] water-soluble salts, and soil colloids.

Chepil spent considerable time and energy analyzing these different soil properties as expressed in the coefficient C_s. Some soil properties, and erodibility by wind have been correlated by statistical data and simple mathematical relationships have been found. Yet, it appears that considerable research is still needed to determine the complex mathematical relationships that relate the basic soil properties to wind erosion.

SORTING, COMPOSITION AND SIZE OF SOIL PARTICLES IN DUST STORMS

The wind erosion process is composed of two major phases,[54] sorting various primary and secondary soil fractions, and disintegration of the secondary fractions to the primary particles by the abrasive action of wind-eroded grains.

The respirable fraction ($< 5\mu$) of wind eroded soil particles is of particular interest in particle wind resuspension. Chepil[37] showed that soil material transported by wind in a single wind storm is characterized by a predominant or peak diameter ($\sim 50 \ \mu$) of discrete particles. The peak diameter varies from one graded material to another depending on the physical composition of the soil and other factors. Depending on soil class, generally 31 to 78% of particles smaller than 100 μm (diameter) are suspended in a wind storm. However, of these only 10 to 20% may be in the respirable size range.

Chepil's data on airborne soil particle sizes near the respirable size range is limited since his primary interest was the analysis of soil properties and other factors. He does emphasize saltation as the primary wind

erosion process. The suspension of soil particles of the respirable size range is the direct result of saltation, surface creep, and the abrasize action of small soil grains on secondary soil fractions. Suspension is primarily the principal visual effect of the saltation mechanism. Research is underway at PNL and other research laboratories to determine particle size distributions in dust storms and to evaluate the role of saltation, surface creep and abrasion in causing suspension of soil particles.

WIND EROSION CONTROL

Soil stabilization proceeds under natural conditions or is accomplished by man, usually in these major successive stages; (1) trapping of moving soil particles; (2) consolidation and aggregation of trapped soil particles; and (3) revegetation of the surface.[54]

Emergency methods of stilling wind erosion are known, but their effects are only temporary. Once erosion is stilled, plant cover must be established or plant residues must be maintained for more permanent control.

Chepil and his co-workers did considerable research on this phase of wind erosion[40,45,49,55,60] and although the concepts apply mainly to agriculture many of the ideas should be useful in most wind erosion problems that require stabilization of the soil.

THE WIND EROSION EQUATION

The development of the wind erosion equation resulted from 30 years of research by Chepil and his associates. The equation embodies the major primary factors that govern wind erodibility of land surfaces and was designed to determine potential erosion from a particular field, and the field conditions of soil cloddiness, roughness, vegetative cover, and sheltering by barriers necessary to reduce potential erosion to a tolerable amount.

The wind erosion equation contains 11 primary variables known to govern soil erodibility; they are reduced to 5 equivalent variables. The general functional relationship is:

$$E = f(I', C', K', L', V), \qquad (8)$$

where E is the potential average annual soil loss in tons per acre, I' is a soil erodibility index; C' is a climatic factor; K' is a soil ridge roughness factor; L' is a field length along the prevailing wind erosion direction; and V is equivalent quantity of vegetative cover. Details of the wind erosion equation have been reviewed by Chepil[59], Woodruff and Siddoway[63] and Skidmore.[64]

The wind erosion equation has been a useful guide to wind erosion control for agricultural fields. Some other uses have been: (1) determining spacing for wind breaks, (2) estimating fugitive dust emmission, (3) predicting horizontal soil fluxes, and (4) estimating effects of wind erosion on productivity.[63,64]

The wind erosion equation in its present format is not very useful for particle wind resuspension. A number of changes to improve the equation have been suggested:[64] (1) modify the equation so it can be applied to single wind storms, (2) modify or adjust the equation so it is applicable on a larger scale than an agricultural field, (3) try to include time dependency in the various soil and meteorological parameters, and (4) extend its application to a variety of soil and climatic conditions.

CONCLUSIONS

The research contributions of W. S. Chepil on wind erosion have been briefly examined as they may apply to particle wind resuspension. A certain amount of his basic research is pertinent to the particle wind resuspension problem, expecially to the dynamics of wind erosion and the influence of soil properties on wind erosion.

The wind erosion equation, because of its deterministic and climatological aspects, has limited applicability to the particle wind resuspension problem and will need considerable modification and additional research in order for it to be useful for a wide range of soil and climatic conditions.

There is a need for a more general wind erosion equation or equation which could be applied to a variety of soil and climatic conditions for particle wind resuspension problems. Present overall research in this field is directed toward that goal.

References

1. W. S. Chepil, R. A. Milne (1939). "Comparative Study of Soil Drifting in the Field and in a Wind Tunnel," Sci. Agr. 19:249-257.

2. W. S. Chepil, (1940). The Relation of Wind Erosion to Some Physical Soil Characteristics, Ph.D. Thesis, University of Minnesota.

3. W. S. Chepil, and R. A. Milne (1941). "Wind Erosion of Soil in Relation to Roughness of Surface", Soil Sci. 52: 417-431.

4. W. S. Chepil, and R. A. Milne (1941). "Wind Erosion of Soils in Relation to Size and Nature of the Exposed Area", Sci. Agr. 21:479-487.

5. W. S. Chepil (1941). "Relation of Wind Erosion to the Dry Aggregate Structure of a Soil", Sci. Agr. 21:488-507.

6. W. S. Chepil (1942). "Measurement of Wind Erosiveness of Soils by Dry Sieving Procedure", Sci. Agr. 23:154-160.

7. W. S. Chepil (1943). "Relation of Wind Erosion to the Water-Stable and Dry Clod Structure of the Soil", Soil Sci. 55: 275-287.

8. W. S. Chepil, and F. Bisal (1943). "A Rotary Sieve Method for Determining the Size Distribution of Soil Clods", Soil Sci. 56:95-100.

9. W. S. Chepil (1943). Soil Erosion by Wind -- Report of Investigations, Soil Research Lab., Dominion Dept. of Agriculture, Swift Current, Canada.

10. W. S. Chepil (1944). "Utilization of Crop Residues for Wind Erosion Control", Sci. Agr. 24:307-319.

11. W. S. Chepil (1945). "Dynamics of Wind Erosion -- I. Nature of Movement of Soil by Wind", Soil Sci. 60:305-320.

12. W. S. Chepil (1945). "Dynamics of Wind Erosion -- II. Initiation of Soil Movement", Soil Sci. 60:397-411.

13. W. S. Chepil (1945). "Dynamics of Wind Erosion -- III. The Transport Capacity of the Wind", Soil Sci. 60:475-480.

14. W. S. Chepil (1945). "Dynamics of Wind Erosion -- IV. The Translocating and Abrasive Action of the Wind", Soil Sci. 61:167-177.

15. W. S. Chepil (1946). "Dynamics of Wind Erosion -- V. Cumulative Intensity of Soil Drifting Across Eroding Fields", Soil Sci. 61:257-263.

16. W. S. Chepil (1946). "Dynamics of Wind Erosion -- VI. Sorting of Soil Material by the Wind", Soil Sci. 61:331-340.

17. W. S. Chepil, and A. W. Zingg (1950). "Aerodynamics of Wind Erosion", Agr. Eng. 31:279-282-284.

18. W. S. Chepil (1950). "Methods of Estimating Apparent Density of Discrete Soil Grains and Aggregates", Soil Sci. 70:351-362.

19. W. S. Chepil (1950). "Properties of Soil Which Influence Wind Erosion -- I. The Governing Principle of Surface Roughness," Soil Sci. 69:149-162.

20. W. S. Chepil (1950). "Properties of Soil Which Influence Wind Erosion -- II. Dry Aggregate Structure as an Index of Erodibility", Soil Sci. 69:403-414.

21. W. S. Chepil (1951). "Properties of Soil Which Influence Wind Erosion -- III. Effect of Apparent Density on Erodibility", Soil Sci. 71:141-153.

22. W. S. Chepil (1951. "Properties of Soil Which Influence Wind Erosion -- IV. State of Dry Aggregate Structure", Soil Sci. 72:387-401.

23. W. S. Chepil (1951). "Properties of Soil Which Influence Wind Erosion -- V. Mechanical Stability of Structure", Soil Sci. 72:465-478.

24. W. S. Chepil (1951). "An Air Elutriator for Determining the Dry Aggregate Soil Structure in Relation to Erodobility by Wind", Soil Sci. 71:197-208.

25. W. S. Chepil, C. L. Englehorn, and A. W. Zingg (1952). "Effect of Cultivation on Erodibility of Soils by Wind", Soil Sci. Soc. Amer. Proc. (1951) 16:19-21.

26. W. S. Chepil (1942). "Improved Rotary Sieve for Measuring State and Stability of Dry Soil Structures", Soil Sci. Soc. Amer. Proc. (1951) 16:113-117.

27. W. S. Chepil (1953). "Factors that Influence Clod Structure and Erodibility of Soil by Wind -- I. Soil Texture", Soil Sci. 75:473-483.

28. W. S. Chepil (1953). "Factors that Influence Clod Structure and Erodibility of Soil by Wind -- II. Water Stable Structure", Soil Sci. 76:389-399.

29. W. S. Chepil (1954). "Factors that Influence Clod Structure and Erodibility of Soil by Wind -- III. Calcium Carbonate and Decomposed Organic Matter," Soil Sci. 77:473-480.

30. W. S. Chepil (1955). "Factors that Influence Clod Structure and Erodibility of Soil by Wind -- IV. Sand, Silt, and Clay", Soil Sci. 80:155-162.

31. W. S. Chepil (1955). "Factors that Influence Clod Structure and Erodibility of Soil by Wind -- V. Organic Matter at Various Stages of Decomposition," Soil Sci. 80:413-421.

32. W. S. Chepil, and N. P. Woodruff (1954). "Estimations of Wind Erodibility of Field Surfaces", J. Soil and Water Conserv. 9:257-265, 285.

33. W. S. Chepil, N. P. Woodruff, and A. W. Aingg (1955). Field Study of Wind Erosion in Western Texas, USDA, SCS-TP-125, 60 pp.

34. W. S. Chepil (1956). "Influence of Moisture on Erodibility of Soil by Wind", Proc. Soil Sci. Soc. Amer. 20:288-292.

35. W. S. Chepil, and N. P. Woodruff (1956). "Implements for Wind Erosion Control", Agric. Eng. 37:751-754.

36. W. S. Chepil, (1957). "Dust Bowl -- Cause and Effects", J. Soil and Water Conserv. 12:108-111.

37. W. S. Chepil (1957). "Sedimentary Characteristics of Dust Storms -- I. Sorting of Wind-Eroded Soil", Amer. J. Sci. 25:12-22.

38. W. S. Chepil, and N. P. Woodruff (1957). "Sedimentary Characteristics of Dust Storms -- II. Visibility and Dust Concentration, Amer. J. Sci. 255:104-114.

39. W. S. Chepil (1957). "Sedimentary Characteristics of Dust Storms -- III. Composition of Suspended Dust", Amer. J. Sci. 255:206-213.

40. W. S. Chepil (1957). Width of Field Strips to Control Wind Erosion, Kansas State College, Agric. Exper. Sta. Tech. Bull. 92.

41. W. S. Chepil (1958). Soil Conditions that Influence Wind Erosion, USDA Tech. Bull. No. 1184.

42. W. S. Chepil (1958). "The Use of Evenly Spaced Henispheres to Evaluate Aerodynamic Forces on a Soil Surface", Trans. Amer. Geographic Un. 39:397-404.

43. W. S. Chepil, and F. H. Siddoway (1959). "Measurement of Wind Turbulence with Strain Gauge Assembly", J. Meteor. 16(4): 417-418.

44. W. S. Chepil (1959). "Equilibrium of Soil Grains at the Threshold of Movement by Wind", Soil Sci. Soc. Amer. Proc. 23:422-428.

45. W. S. Chepil (1959). "Wind Erodibility of Farm Fields", J. Soil-Water Conserv. 14:214-219.

46. W. S. Chepil, and N. P. Woodruff (1959). Estimation of Wind Erodibility of Farm Fields, USDA Prod. Res. Rpt. No. 25, 1-21.

47. W. S. Chepil (1960). "Conversion of Relative Field Erodibility to Annual Soil Loss by Wind", Soil Sci. Soc. Amer. Proc. 24:143-145.

48. W. S. Chepil, N. P. Woodruff, F. H. Siddoway, and L. Lyles (1960). "Anchoring Vegetative Mulches", Agr. Engn. 41:754-765, 759.

49. W. S. Chepil (1960). "How to Determine Required Width of Field Strips to Control Wind Erosion", J. Soil-Water Conserv. 15:72-75.

50. W. S. Chepil (1961). "The Use of Spheres to Measure Lift and Drag on Wind-Eroded Soil Grains", Soil Sci. Soc. Amer. Proc. 25(5):343-345.

51. W. S. Chepil, N. P. Woodruff and F. H. Siddoway (1961). How to Control Soil Blowing, USDA Farmers' Bulletin 2169, 16 pp.

52. W. S. Chepil, F. H. Siddoway, and D. V. Armburst (1962). "Climatic Factor

for Estimating Wind Erodibility of Farm Fields", J. Soil-Water Conserv. 17:162-165.

53. W. S. Chepil (1962). "A Compact Rotary Sieve and the Importance of Dry Sieving in Physical Soil Analysis", Soil Sci. Soc. Amer. Proc. 26:4-6.

54. W. S. Chepil, and N. P. Woodruff (1963). The Physics of Wind Erosion and its Control", Advances in Agron, 15:211-302.

55. W. S. Chepil, N. P. Woodruff, F. H. Siddoway, D. W. Fryrear, and D. V. Armburst, (1963). "Vegetative and Nonvegetative Materials to Control Wind and Water Erosion", Soil Sci. Soc. Amer. Proc. 27:86-89.

56. W. S. Chepil, F. H. Siddoway, and D. V. Armburst (1963). "Climatic Index of Wind Erosion Conditions in the Great Plains", Soil Sci. Soc. Amer. Proc. 27:449-452.

57. W. S. Chepil, D. V. Armburst, and F. H. Siddoway (1964). "Effects of Ridges on Erosion of Soil by Wind", Soil Sci. Soc. Amer. Proc. 28:557-560.

58. W. S. Chepil, F. H. Siddoway and D. V. Armburst (1964). "In the Great Plains Prevailing Wind Erosion Direction", J. Soil-Water Conserv. 19:67-70.

59. W. S. Chepil, F. H. Siddoway, and D. V. Armburst (1964). Wind Erodibility of Knolly and Level Terrains", J. Soil-Water Conserv. 19:179-181.

60. W. S. Chepil, F. H. Siddoway, and D. V. Armburst (1965). "Effect of Kind, Amount, and Placement of Residue on Wind Erosion Control", Trans. Amer. Soc. Agr. Engin. 8:327-331.

61. W. S. Chepil (1965). "B. Transport by Wind: Transport of Soil and Snow by Wind", Agric. Meteor., Meteorological Monographs, Vol. 6, No. 28.

62. G. R. Hilst, and P. W. Nickola (1959). "On the Wind Erosion of Small Particles", Bull. of AMS, Vol 40, No. 2, 73-77.

63. N. P. Woodruff, and F. H. Siddoway (1965). "A Wind Erosion Equation", Soil Sci. Soc. Amer. Proc. 29:602-608.

64. E. L. Skidmore (1974). A Wind Erosion Equation: Development, Application, and Limitations, ERDA Symposium Series 38, Atmospheric-Surface Exchange of Particulate and Gaseous Pollutants, CONF-740921, Richland, WA.

WEATHERING OF SURFACES AS MEASURED BY AIRBORNE RADIOACTIVE PARTICLE CONCENTRATIONS ON THE HANFORD RESERVATION

G. A. Sehmel

Respirable air concentration ranges measured between 1972 and 1975 at resuspension study sites are summarized and compared with fallout levels measured at the Hanford Reservation boundary. Results indicated that maximum airborne concentrations were substantially less than the maximum permissible airborne concentration (MPC) for uncontrolled areas. The weathering half-life, determined in this study, was 5 months in one area for ^{137}Cs, but much longer than 5 months for a second area. These reductions with time are much slower than data reported by others showing airborne concentrations decreasing with a half-life of 35 to 40 days.

INTRODUCTION

Resuspension occurs when wind blowing over a surface moves particles from that surface up into the air and transports them downwind. Resuspension occurs at radioactively contaminated sites on the Hanford Reservation.[1] Sites of low-level waste disposal where resuspension was measured include U-pond area, S-16 area, and Z-19 ditch leading into U-pond, all of which are within or near 200-West Area; the B-C Crib area south of the 200-East Area; the Gable Mountain Pond area; and an area close to the Hanford Meteorological Station (HMS) Tower, near 200-West Area. The study reported here observed the airborne concentrations as a function of time over three years. One objective of these experiments was to determine weathering rates.

EXPERIMENTAL PROCEDURE

The earliest and simplest experiments were performed at Gable Mountain Pond and near the HMS Tower. Later in the study more extensive experiments with more sophisticated instruments were conducted at the remaining areas. In these experiments meteorological sensing instruments were used to activate air samplers automatically as functions of wind speeds and direction. These experiments were designed to collect and measure increased airborne radioactivity concentrations at higher wind speeds, determine resuspension physics, and gather data for estimating a mass balance across a contaminated zone. Upwind airborne concentrations were simultaneously measured with downwind airborne concentrations to determine whether resuspension increased activity levels between upwind and downwind arrays of air sampling towers. In initial experiments, air samples were collected and total radioactivity was determined. In later experiments, air filters were weighed before use. After sample collection, air filters were again weighed, making it possible to determine the amount of airborne soil particles present and thus to calculate the radioactivity concentration per gram of airborne solid collected.

RESULTS

Extensive data were obtained on airborne radioactivity concentrations around the resuspension sites studied. The concentrations were expressed both in $\mu Ci/cm^3$ of air and $\mu Ci/g$ of airborne solids. Data have been summarized[1] without detailing the airborne concentration profiles measured in each experiment. This report summarizes some weathering data by showing ranges of measure airborne ^{137}Cs and plutonium concentrations as a function of time between 1972 and 1975.

Airborne ^{137}Cs concentrations were measured at U-pond, B-C Crib, Z-19, S-16, and HMS Tower areas. Results of these experiments are summarized in Figure 1. Airborne

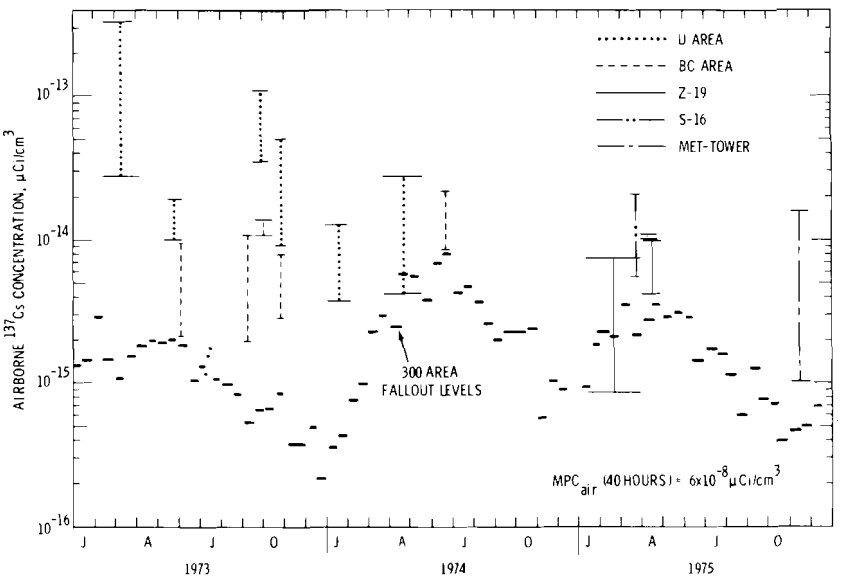

Neg. 765724-7

FIGURE 1. Range of "Downwind" Airborne ^{137}Cs Concentrations at Resuspension Sites Compared to Fallout Levels

^{137}Cs concentrations are shown in $\mu Ci/cm^3$ as a function of time from 1973 to 1975. These concentrations are compared with 300 Area fallout levels[2], shown by horizontal dashed lines. Measured airborne concentrations at the different sites are all above fallout levels. The data symbols for each experiment are plotted to represent the range of measured airborne concentrations and the time over which the experiment was conducted. The maximum airborne ^{137}Cs concentration was 3×10^{-13} $\mu Ci/cm^3$, which is more than two orders of magnitude greater than fallout levels but significantly less than the MPC_{40HR}[3] of 6×10^{-8} $\mu Ci/cm^3$.

Airborne concentrations at U-pond decreased from 1973 through mid-1974. On the average, air concentrations decreased about 50% over 5 months. This is much greater than the 35 to 40 days weathering half-time often quoted in resuspension literature.[4] B-C Crib air concentration data do not show any such short fixation half-life. Airborne concentrations at B-C Crib were constant from May 1973 to June 1974, suggesting a long fixation half-life.

Airborne plutonium concentration ranges for both ^{238}Pu and ^{239}Pu measured in these resuspension experiments are shown in Figure 2, and are compared with 300 Area fallout levels. Airborne peak plutonium concentrations at resuspension study sites were significantly greater than 300 Area fallout levels, and airborne ^{239}Pu concentrations in general were greater than airborne ^{238}Pu concentrations. Although resuspension was occurring at these sites, measured airborne concentrations were significantly less than MPC.

After 1972, plutonium concentrations were measured only at U-pond. Any decrease in airborne concentrations with time was not statistically significant. Concentrations were too near fallout levels, thus precluding a well defined weathering half-time. The indication is that the weathering half-time is long.

CONCLUSIONS

Wind resuspension of ^{238}Pu, ^{239}Pu, ^{241}Am, ^{90}Sr, and ^{137}Cs occurred[1] at the study sites during the 1972-1975 study period. Air concentrations near sites of resuspension exceeded fallout levels measured at the 300 Area during the same time intervals, but were still far below occupational maximum permissible air concentrations (MPC).

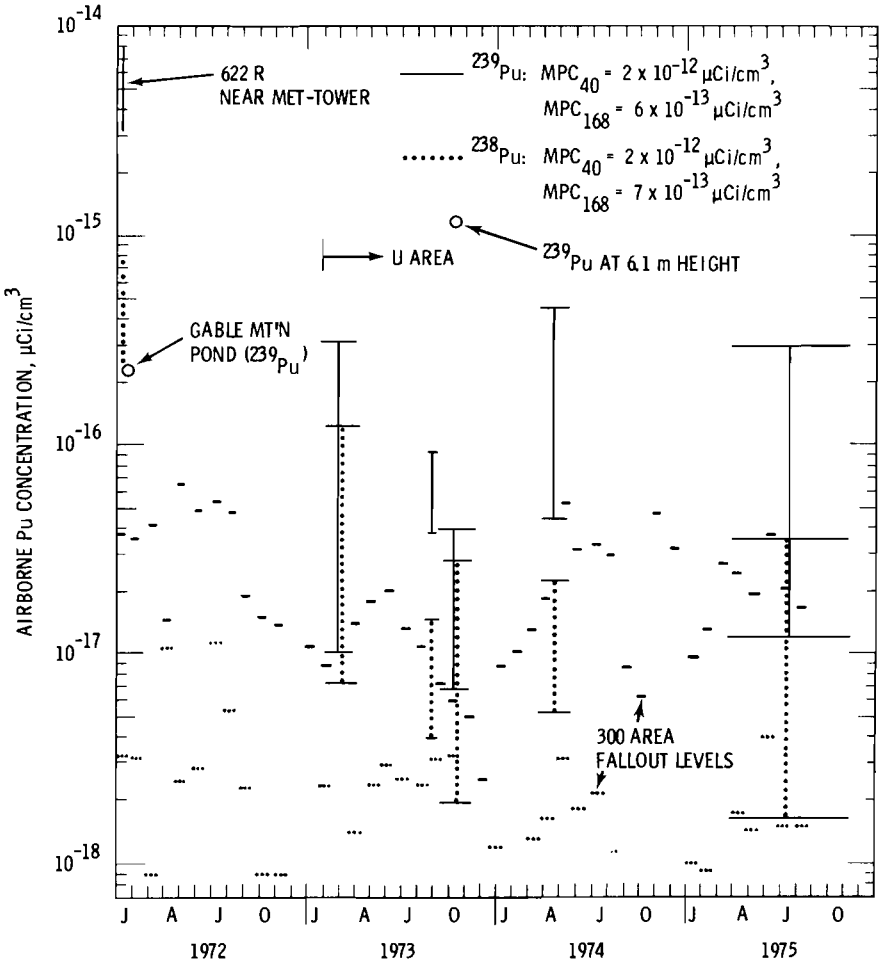

Neg. 765724-4

FIGURE 2. Range of Airborne Pu Concentration at Resuspension Sites Compared to Fallout Levels

Results of the studies reported here indicate the weathering half-life is from 5 months to a very long time. Knowledge of this ill-defined half-life is important in modeling efforts to describe long term airborne effects of surface contamination. The longer weathering times found in this study are supported by results of tracer studies in an area near the U-pond.[a]

(a) See "Wind-Caused Resuspension Rates", this annual report.

References

1. G. A. Sehmel, Radioactive Research Experiments on the Hanford Reservation, BNWL-2081, Battelle, Pacific Northwest Laboratories, Richland, WA 99352, 1977

2. C. W. Thomas, "Atmospheric Fallout During 1975 at Richland, Washington and Point Barrow, Alaska." In: Pacific Northwest Laboratory Annual Report for 1975,

BNWL-2000-PT 3, Battelle, Pacific Northwest Laboratories, Richland, WA 99352, pp. 16-19, 1976.

3. Recommendations of the International Commission on Radiological Protection, ICRP Publication 2, Report of Committee II on Permissible Dose for Internal Radiation, Pergamon Press, New York, NY, 1959.

4. R. H. Wilson, R. G. Thomas and J. N. Stannard, Biomedical and Aerosol Studies Associated with a Field Release of Plutonium. WT-1511, Sandia Corporation, Albuquerque, NM, 1961.

RADIOACTIVITY IN FOREST FIRE SMOKE PLUMES

G. A. Sehmel and M. M. Orgill

Smoke from two forest logging slash burns was sampled with an air filter mounted on a Cessna 411 airplane. Radioactivity concentrations in the smoke plumes were compared to concentrations in background air outside these smoke plumes. In both smoke plumes, ^{137}Cs concentration was higher than in background samples. In one plume the ^{137}Cs was 11 times greater than background. Concentrations of other fission product nuclides in the plumes was equal to or less than background concentrations. This observation supports a hypothesis that surface air of low concentration is drawn into the smoke plume. Confirmation of this explanation was not possible with the limited data.

INTRODUCTION

In an earlier study, smoke plumes from crop land fires[1] and one forest logging slash burn[2] were sampled for airborne radioactive particles. Results from those experiments indicated that radioactive particles concentrations within the smoke plume were greater than in ambient background air, showing that radioactive surface contamination from prior deposition could be resuspended by the fire. Release rates could not be calculated from the measured air concentrations since the entire smoke plume was not sampled. The maximum ratio of concentration in smoke to concentration in background air was obtained for ^{137}Cs. In this case, the measured ^{137}Cs concentration in the smoke plume was 22 times the ambient background air concentration. Consequently, additional smoke plumes were sampled to determine the variability of air concentration within smoke plumes versus ambient background air concentrations. This paper presents the results of these additional measurements.

EXPERIMENTAL PROCEDURE

Smoke from two forest logging slash burns in Idaho were sampled using a Cessna 411 airplane to obtain IPC filter paper samples. For each sample, approximately 1.5×10^5 ft^3 (4.3×10^3 m^3) of air were filtered.

The first fire was near the North Fork of Slate Creek approximately 20 miles (30 km) south of Grangeville, Idaho. Ignition occurred about 1000 PDT, October 8, 1976, and the fire burned some 70 acres of old logging slash on a steep south-facing slope. A dense smoke plume was present by 1130 and was moving toward the northeast, extending some 20 miles (50 km). The smoke plume, sampled between 1135 and 1408, was approximately 300 m above the terrain. The top of the smoke plume varied between 7000 ft

(2134 m) and 8000 ft (2438 m) MSL. The smoke sample was taken between 7000 ft (2134 m) and 7300 ft (2225 m) MSL. After smoke sampling, a background air filter sample was obtained approximately 10 miles (15 km) west of the fire site and over the Salmon River between 1531 and 1800. The sample was taken at around 6500 ft (1981 m) MSL. Total sample volume was determined with a vane anemometer which integrated total flows.

The second fire sampled occurred on October 12, 1976, about 15 miles (25 km) north-northwest of Kellogg, Idaho. The fire burned small bulldozed slash piles which released relatively small amounts of smoke. The resultant smoke plume extended approximately 5 miles (8 km) to the north and east. The plume was sampled between 1500 and 1728 PDT. The altitude of sampling was between 500 ft (152 m) and 2000 ft (609 m). A background filter was taken prior to smoke plume sampling about 5 miles (8 km) to the west of the fire site between 1056 and 1332 PDT, at about 6500 ft (1981 m) MSL. A flow rate of 1026 ft^3/min (29.1 m^3/min), which is a typical average sampling rate, was used to calculate total volume sampled.

Radioactive nuclides on filter samples were measured by multichannel gamma counting.

RESULTS

Ratios of smoke sample concentration to background concentration are shown in Table 1 for eight radionuclides. Airborne concentrations of some of these radionuclides may have been influenced by the fallout plume from a Chinese nuclear test that had occurred on September 26, 1976.

For the Slate Creek fire, the concentration ratio was corrected for the time the airplane was not in the smoke plume during the smoke plume sampling period. For this

TABLE 1. Ratio of Concentration of Smoke Plume to that in Background Air

Isotope	(Background-Corrected Smoke Sample)/(Background Sample)[a] Slate Creek 10-8-76	(Total Smoke Sample)/(Background Sample)[b] Slate Creek 10-8-76	(Total Smoke Sample)/(Background Sample)[b] Kellogg 10-12-76
^{144}Ce	0.5	0.7	0.7
^{141}Ce	0.3	0.5	0.8
^{131}I	0.4	0.6	0.9
^{7}Be	1.0	1.1	1.0
^{103}Ru	0.2	0.4	0.9
^{137}Cs	10.6	11.0	(c)
^{95}Zr	0.2	0.4	0.7
^{95}Nb	0.2	0.4	0.7

a. Corrected smoke sample has background collection when outside the smoke subtracted from total smoke plume sample.
b. Total smoke sample includes radioactivity collected while outside the smoke plume.
c. Background sample was less than ^{137}Cs radiochemical detection limit.

calculation, ambient air concentrations immediately adjacent to the smoke plume were assumed equal to air concentrations in the background filter run. This seems to have been a reasonable assumption for the Slate Creek fire; however, for the Kellogg fire, a correction factor would have indicated negative air concentrations for some of the isotopes in the smoke plume. Consequently, a corrected ratio is not shown for the Kellogg fire in the table.

Concentration ratios in Table 1 range from 0.2 to 11.0. For six of the radioactive isotopes, the airborne concentration in the smoke plume was less than in the background air sample. Based upon these data, one hypothesis is that relatively clean air (decreased concentration of radioisotopes) was entrained from low levels by the smoke plume. The relatively clean air at ground level could have been caused either by prior deposition, and/or by fission product nuclides at air sampling levels from the Chinese nuclear test air plume. The data are insufficient to determine which, if either, of these two explanations is valid. Had these results been anticipated, additional air samples at other elevations might have helped clarify experimental results.

^{7}Be concentrations in the smoke plume were equal to the ambient background level, but ^{137}Cs was 11 times the ambient background level. Equality of ^{7}Be concentrations in both smoke and ambient air might be expected since ^{7}Be is a relatively short-lived cosmic-ray induced radioisotope. At the Kellogg fire, ^{137}Cs was also released but the ratio cannot be shown since the background sample was below radiochemical detection limits.

CONCLUSIONS

Surface deposited ^{137}Cs can be released by burning vegetation. Other isotopes may also be released. However, reported data may have been influenced by airborne fission products from a Chinese atmospheric nuclear test. The concentration ratio data are consistent with a hypothesis that relatively clean air near ground level is entrained into the smoke plume.

Additional results to be obtained from these samples include concentrations of airborne plutonium. Samples are currently being analyzed for plutonium.

References

1. G. A. Sehmel and M. M. Orgill, "Resuspension of Radioactive Isotopes Induced by Burning Forest Logging Slash," PNL Annual Report for 1975, to USAEC DBER, BNWL-2000 PT 3, Battelle, Pacific Northwest Laboratories, Richland, WA, March 1976.

2. G. A. Sehmel and M. M. Orgill, "Resuspension of Radioactivity Induced by Burning Crop Stubble", PNL Annual Report for 1974, to USAEC DBER, BNWL-1950 PT 3, Battelle, Pacific Northwest Laboratories, Richland, WA, February, 1975.

THE CROSSWIND DISTRIBUTION OF CONTAMINATION RESUSPENDED FROM A SURFACE AREA SOURCE[(a)]

T. W. Horst

The crosswind distribution of atmospheric contamination due to resuspension from a surface area source may be adequately predicted from the contamination directly upwind of the receptor alone, if the surface distribution has roughly the same extent in all directions. This is demonstrated with a hypothetical, Gaussian distribution of surface contamination, and with a real distribution, the BC-Crib controlled area.

Research has been conducted to develop simple methods of estimating the air concentrations of surface contamination resuspended by the wind. Approximate relations have been reported[1] which predict the crosswind-integrated air concentration C(x,z) for a generalized area source, based on the exact result for a uniform area source. That these same equations can in many practical cases also be used to predict the crosswind distribution of the resuspended contamination has been verified.[2] This is done using the surface contamination distribution G(x,y) directly upwind of the receptor as input, rather than the crosswind-integrated surface contamination G(x), and is based on the fact that only sources within a narrow, diffusion-plume-shaped upwind sector contribute significantly to the air concentration at a given point.[3]

SENSITIVITY STUDY

The limits on source configuration and receptor location necessary for this approximation to be valid have been investigated by comparing the resuspended air concentrations predicted by both the approximation and by a numerical solution of the exact equations from which it was derived. A hypothetical Gaussian distribution of surface contamination was used;

$$G(x,y) = G_0 \exp\left[\frac{-(x-x_0{}^2}{2\sigma_1{}^2} - \frac{y^2}{2_2{}^2}\right]$$

(a) This research was partially supported by the Atlantic Richfield Hanford Company.

Figure 1 shows the results from one such set of calculations, for Pasquill D atmospheric conditions. Here the air concentration C, normalized by the mean wind speed u, the resuspension rate Λ and the peak surface contamination G_0, is plotted as a function of downwind distance from the contamination peak $x-x_0$. Curves are shown for two surface contamination distributions: one symmetric about the peak, $\sigma_1 = \sigma_2$, and the other elongated in the downwind direction, $\sigma_1 = 10\sigma_2$. Separate cross sections parallel to the downwind direction are shown at the peak, y = 0, and at distances of one, two and three standard deviations crosswind of the peak. The analytical approximation, shown as discrete points, applies to both surface contamination distributions.

Figure 1 shows that for $\sigma_1 = \sigma_2$ the analytical approximation is good, especially upwind of and directly downwind of the peak. As σ_2 decreases the agreement deteriorates, e.g., $\sigma_1 = 10\sigma_2$ in Figure 1. The approximation is still good upwind of the peak, but deteriorates rapidly downwind of the peak. However, as σ_2 becomes greater than σ_1, the air concentrations at crosswind distances of two and three times σ_2 approach the close match with the numerical solution displayed at y = 0 for $\sigma_1 = \sigma_2$.

Since the approximation is based on the surface contamination distribution directly upwind of the receptor, the agreement with the numerical solution depends on the effectiveness of the crosswind diffusion. The least lateral diffusion occurs for Pasquill F,

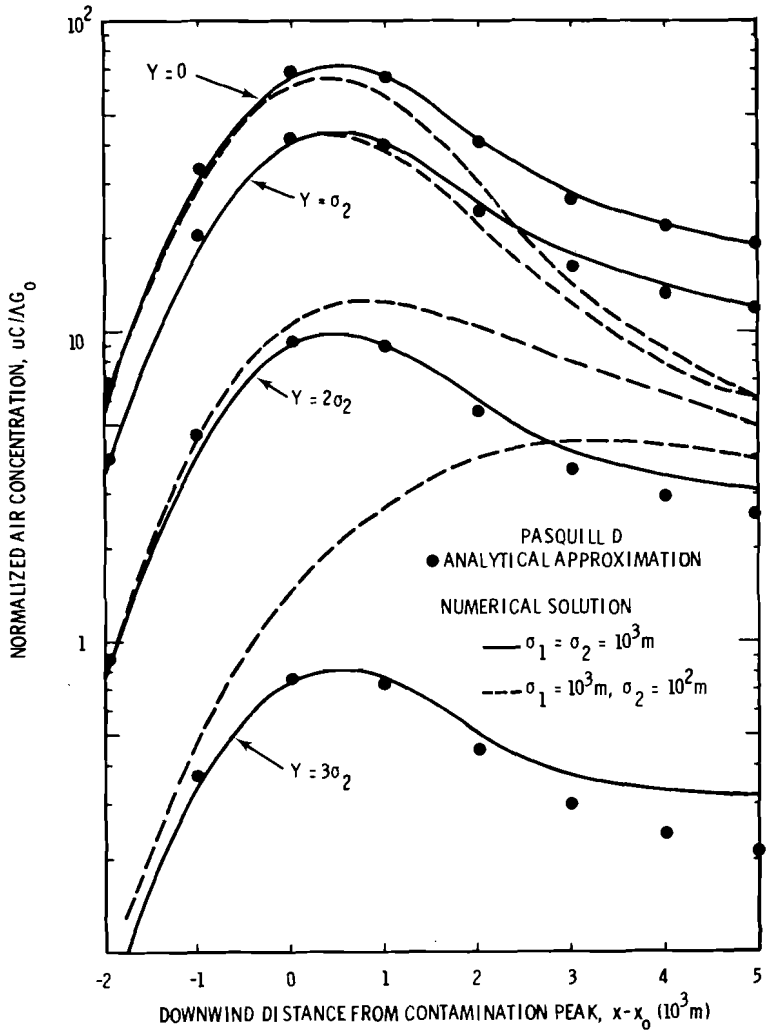

Neg. 73374-1

FIGURE 1. Comparison of Resuspension Models for Gaussian Distributions of Surface Contamination

and hence for $\sigma_1 = \sigma_2 = 10^3$ m the air concentrations at crosswind distances of two and three times σ_2 match the predictions as well as for y = 0. There is also a modest improvement from Pasquill D in the match for $\sigma_2 = 10^2$ m, especially for y = 0 and $y = \sigma_2$. On the other hand the match for Pasquill A and $\sigma_1 = \sigma_2 = 10^3$ m is considerably poorer at $y = 2\sigma_2$ and $y = 3\sigma_2$ than for Pasquill D. The predictions at $3\sigma_1$ downwind of the peak are low by factors of roughly 1.5 and 2.5, respectively. Calculations were also made for $\sigma_1 = 10^2$ m, $\sigma_2 = 10^2$ m and $\sigma_2 = 10$ m with results very similar to those for $\sigma_1 = 10^3$ m, $\sigma_2 = 10^3$ m and $\sigma_2 = 10^2$ m.

BC-CRIB CONTROLLED AREA

Figure 2 shows the crosswind distribution of resuspended air concentration predicted for the BC-Crib controlled area, an area of low-level surface contamination on the Hanford Reservation. Calculations were made by both methods for two downwind distances: x = 900 m, the peak of the crosswind-integrated distribution, and x = 2000 m, the downwind edge of the distribution. The meteorological conditions are again Pasquill D, and the effect of deposition has been included with a deposition velocity v_d equal to 10^{-2} u. At 900 m the approximation agrees excellently with the numerical solution. At 2000 m the

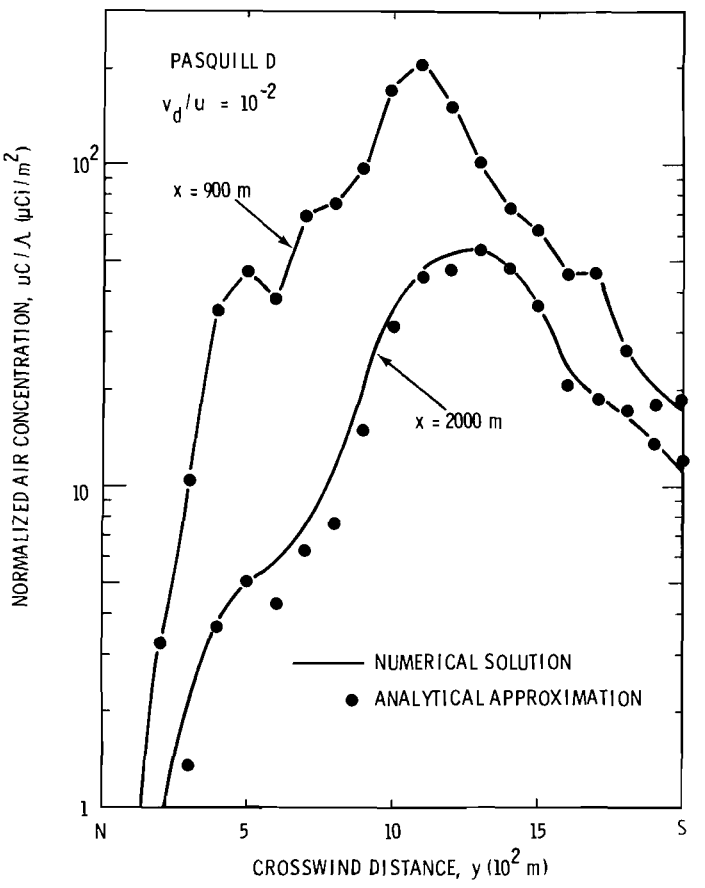

Neg. 73374-4

FIGURE 2. Comparison of Resuspension-Deposition Models for BC-Crib Controlled Area

agreement is poorer, within about 50% at worst, but in most cases within 15%. The approximation underpredicts worst north of the peak where x = 2000 m is distant from the surface contamination directly upwind but where the receptor is on the north edge of the central contamination pattern.

CONCLUSION

In summary, the anylytical approximation is adequate to predict the suspended air concentrations, based only on the contamination directly upwind of the receptor, to within several tens of percent if the distribution has roughly the same extent in all directions. The peak air concentration is predicted with an error of less than 10%. The percent errors increase with increasing distance from the peak of the surface distribution, but the air concentration is at the same time decreasing with distance from the peak. The error may be greater than a factor of two beyond a distance of about three standard deviations from the peak, especially for unstable atmospheric conditions, but where this occurs the air concentration is usually less than 10% of the peak concentration.

References

1. T. W. Horst, "Resuspension from a Generalized Area Source," Pacific Northwest Laboratory Annual Report for 1975 to the USERDA Division of Biomedical and Environmental Research, Part 3 Atmospheric Sciences, BNWL-2000 PT 3, Battelle-Northwest, Richland, WA, March 1976.

2. T. W. Horst, The Estimation of Air Concentrations Due to the Suspension of Surface Contamination by the Wind, BNWL-2047, Battelle-Northwest, Richland, WA, March 1976.

3. F. Gifford, "Computation of Pollution from Several Sources," Int. J. Air Pollut., 2, pp. 109-110, 1959.

POLLUTANT SCAVENGING

The removal of atmospheric pollutants by clouds and precipitation can largely determine budgets of pollutants distributed on a regional scale. The amounts and patterns of pollutants delivered by precipitation to sensitive ecosystems, as well as the distributions remaining in the air as inhalation hazards, can only be estimated realistically with knowledge gained by a thorough investigation of precipitation scavenging processes.

During this reporting period the entire precipitation scavenging program at PNL has been reoriented to meet the goals of the Multistate Atmospheric Power Production Pollution Study (MAP3S), a major research program of ERDA's Division of Biomedical and Environmental Research. The scavenging program is now primarily focused on these two areas: incloud scavenging in frontal and convection storms; and development and management of a precipitation chemistry network.

The reports in this section describe the theoretical and computational modeling efforts as well as the field experiments run to provide the data needed for verification and improvement of the incloud scavenging models. A synergistic balance between the utilization of diagnostic models and field experiments is the goal of this research. The establishment of the four station operational network of precipitation chemistry stations in the northeastern United States, the analysis procedures for the samples and the rapid turnaround of computer-printed analyses reports were significant accomplishments during this reporting period. Such results demonstrate that the cooperation needed for success in MAP3S is achievable.

- PRECIPITATION SCAVENGING IN MAP3S

PRECIPITATION SCAVENGING PROGRAM DESIGN FOR FY 1977

B. C. Scott

A general overview of the precipitation scavenging program is presented including a description of the basic scavenging hypothesis to be investigated during the winter of 1976-1977. The modeling and field experiments to be conducted during the coming year are also described.

INTRODUCTION

The overall objectives of the precipitation scavenging program are to determine those precipitation mechanisms which effectively remove power plant pollutants from the atmophere, and to provide the necessary field data for computing transformation of pollutants into different chemical configurations. In support of the MAP3S program, a major goal of the scavenging program is determining those events causing the removal and transformation of SO_2 and $SO_4^=$ by cloud systems. Although the following discussion emphasizes the removal and transformation of SO_2 and $SO_4^=$, the program is not limited to investigating sulfur compounds. The effectiveness of precipitation in removing other industrial and power plant pollutants such as NH_3, NO_x, O_3, etc., will also be examined.

The field program for the winter of 1976-77 has been designed primarily to determine if a Lake Michigan site is adequate for accomplishing the overall objectives of the scavenging program. Is the field site accessible for aircraft flights and ground crews, are the snow storms sufficiently predictable to enable frequent and periodic probing, and are the ambient concentrations of gaseous power plant pollutants and trace metals sufficient for their transformation and removal to be observed within the experimental time frame?

SCAVENGING HYPOTHESIS

Our basic hypothesis, to be examined during the winter experiments of 1976-77, is that most of the scavenging of $SO_4^=$ and SO_2 in cold cloud storms (precipitation either reaches the surface as snow or melts just above the surface) occurs by riming in the lower portions of the clouds. The hypothesis assumes that most SO_2 and $SO_4^=$ enters the cloud through cloud base (i.e., only a small fraction of this material is entrained through the sides of the clouds). Therefore, understanding precipitation scavenging requires adequate descriptions of the nucleation process and of the histories of the cloud droplets nucleated at cloud base.

The cloud drop size distribution is known to be determined by the updraft velocity and the maximum cloud supersaturation within the first 100 meters above cloud base. After these tiny cloud droplets have risen 4 to 5 min (about 200 m above cloud base) they will have grown large enough (by condensation) to be captured by large falling ice particles. This capture (or riming) process then prevents, through freezing, any further SO_2 to $SO_4^=$ transformation within or on the surface of the falling ice particle. Thus

most of the sulfate contained within those cloud droplets, which eventually contribute water mass to the surface precipitation from cold cloud storms, is either present at nucleation or is transformed from SO_2 within the first few hundred meters of cloud base (4 to 5 min after droplet nucleation).[a] Similarly adsorption or desorption of SO_2 by the cloud droplets must occur within the first few minutes of droplet lifetime if SO_2 is to be removed from the cloud by falling ice particles.

To test this hypothesis and to develop better hypotheses relating precipitation scavenging to aerosol and gas characteristics, to precipitation intensity and types, and to cloud characteristics, we hope to conduct a multi-year study closely collaborating between modeling and systematic field experiments.

MODELING EFFORTS

During the first year, mesoscale modeling of the airflow over Lake Michigan will be done with the Lavoie model. This model predicts 1) convergence and divergence associated with the mesoscale flow fields, and 2) depth and spatial distribution of the mixing layer. The model output should also be valuable for determining optimal locations of surface sampling stations and aircraft sampling tracks. The output will be input for a convective scale model to be developed in stages over the next few years. This convective scale model will include detailed ice and water cloud microphysics and should enable careful examination of the relationships between precipitation scavenging and cloud dynamics and microphysics. Observations of the convective activity obtained from the field experiments at Lake Michigan will determine if the model will be kinematic or time dependent, and one or two dimensional.

FIELD MEASUREMENTS

Field experiments are planned to coincide with the occurrence of snow at the surface. Snowflakes and individual crystals within the flakes often provide considerable information about their life histories. For example, the shape of crystals growing by deposition is determined primarily by cloud temperature. Thus, by knowing the temperature profile in the cloud (either as a result of direct observations or through model predictions) a nucleation region (in terms of height above the surface) for crystals of particular shapes can be established. In addition, ice crystals must also grow to a critical size before they can begin to accrete cloud water. Again, by knowing the cloud's thermal structure, the time interval for crystal growth by deposition may be computed. Once the crystals obtain their critical riming size, the accretion of cloud water, which already contains pollutants, becomes the dominant capture mechanism. The degree of riming indicates the mass of pollutant obtained by the accretion mechanism and is dependent upon cloud water content and droplet size distribution; both parameters will be measured by aircraft.

Clearly none of these growth and capture mechanisms can be distinguished with samples of liquid precipitation. Thus, careful examination of the precipitation in wintertime snowstorms should provide a unique opportunity to unravel many of the details of precipitation scavenging.

Little is known about the microphysical and dynamical details of the lake effect snowstorms (i.e., those snowstorms that occur on the lee shore of Lake Michigan). Figure 1 shows the main dynamical features expected during these snowstorms. As cold polar air moves over the warm lake, eddy fluxes transport heat and moisture into the mixing layer and thereby increase its thickness. Small convective clouds are expected over the lake in the relatively shallow mixing layer near the windward shore, but as the depth of the mixing layer increases, convective activity is expected to intensify and become more extensive. By the time the polar air reaches the lee shore, the mixing layer is expected to be 3 to 4 km deep and to contain one or more bands of cloudiness. Each band is expected to be composed of several areas of intense activity with each area containing several active convective cells. We do not expect to find any abrupt downwind edge to these bands of precipitation. Rather we anticipate that the clouds glaciate at their downwind edges and eject streamers of ice crystals which advect to the east. These ice crystals are expected to continue to grow even though the water

---

[a] Some $SO_4^{=}$ aerosol may also be attached by other capture processes during this time interval, and some cloud droplets may escape capture by ice particles and grow by coalescence to large cloud drops which subsequently freeze and fall out. Our theoretical studies will estimate the magnitude of these assumed secondary sources of scavenged material at the surface.

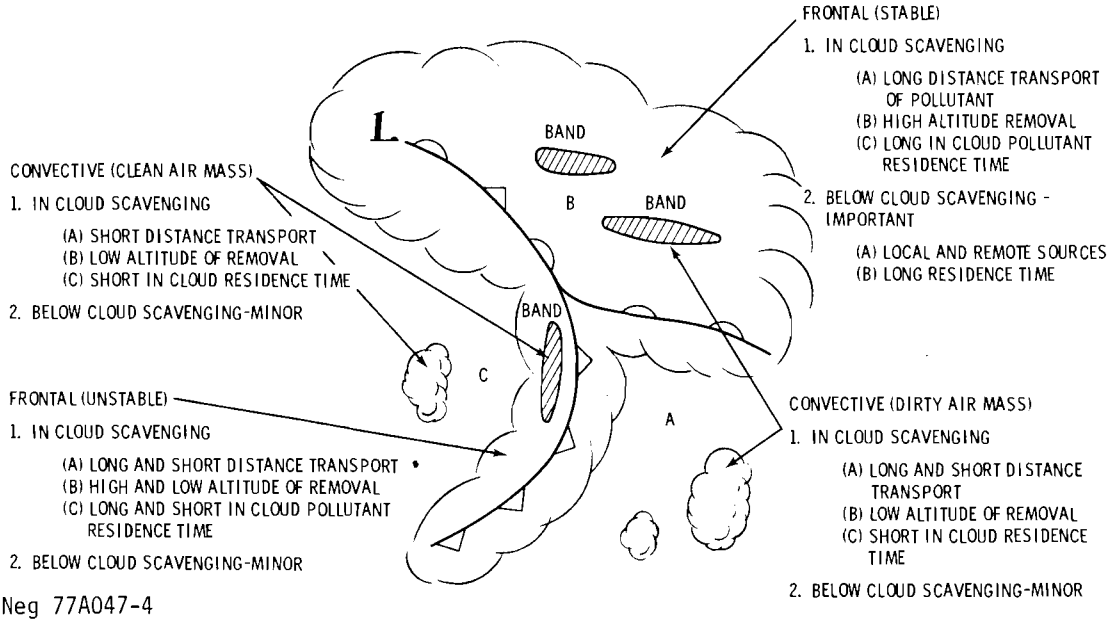

Neg 77A047-4

FIGURE 1. Anticipated Dynamic and Microphysical Features of a Lake Michigan Snowstorm

cloud has completely evaporated and the environment is subsaturated with respect to water. If a lake effect snowstorm should occur at our field site, extensive probing with radar and aircraft will be attempted.

Since this year's field work has been delayed by aircraft engine failure, it is likely that a lake effect snowstorm will not occur during our scheduled sampling interval (February-March). During this late winter period, the intensity and duration of snow at the surface depends strongly on the orientation of extratropical cyclones relative to the observer. The precipitation in these extratropical cyclones is dominated by embedded precipitating bands; the heaviest precipitation being associated with mesocale areas of convective activity within these bands. Figure 2 illustrates the spatial orientation of the major pollutant removal regions in an extratropical cyclone. If our field site lies in regions B or C of Figure 2 during February and March, snow is likely to be observed at the surface. As is the case for a lake effect snowstorm, such periods of snow will provide detailed records of the life-history of individual precipitating particles. However, as is evident in Figure 2, the extratropical cyclone provides a much larger variation in space and time scales for scavenging than does the simpler lake effect snowstorm. One goal of our 1977 field studies will be to determine if intense mesoscale areas can be identified and probed independently from the surrounding lighter precipitation areas.

This year's field work will be limited primarily to a characterization study of those Michigan snowstorms that occur during our sampling period. Aircraft measurements of aerosols and gases will be taken with our DC-3 upwind, below cloud base, and downwind of major snow producing bands. These "clear air" measurements will include determination of concentrations of SO_2, NH_3, NO_x, O_3, sizing and chemical characterization of aerosols, determination of the deliquescent nature of the larger aerosols, and measurement of the CCN spectrum. Hopefully these measurements can be supplemented with bulk water samples obtained directly from within the clouds. Cloud liquid water content will be measured near cloud base, near cloud top, and at the middle of the cloud. Cloud droplet size distributions will be taken near cloud base.

At the surface two sequential sampling sites will be established on a line approximately normal to the precipitating band. At one surface site a multi-stage impactor will run continuously for 5 to 7 days at a time. At both sites sequential samples of snow will be collected at fixed intervals and later analyzed for $SO_4^=$, HSO_3^-, $SO_3^=$ and others. The snow will be characterized

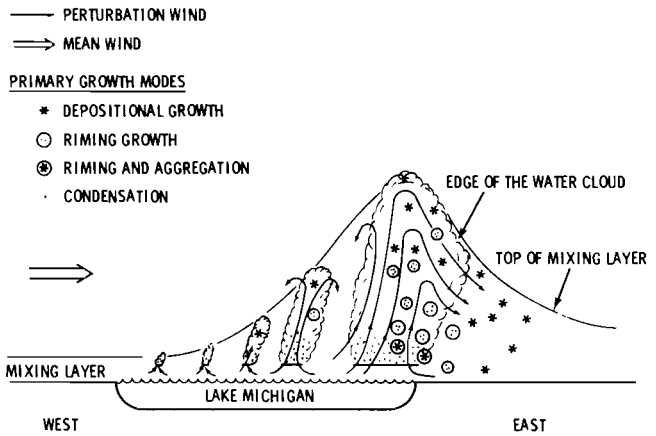

Neg 77A047-5

FIGURE 2. Removal Regions in an Extratropical Cyclone

according to primary growth habit, degree of aggregation and riming, precipitation rate, etc. Formvar replicas of the falling snow will be obtained. If possible, core samples of snow will be obtained.

Additional support will be obtained from the PPI and RHI displays from a LWR 74C weather radar at Muskegon (range of 230 km), and from the visual and IR synchronous and nonsynchronous satellite data received at Detroit.

THE MAP3S PRECIPITATION CHEMISTRY NETWORK

M. Terry Dana, D. R. Drewes, D. W. Glover, J. M. Hales
and J. E. Rothert

A precipitation chemistry sampling network, with four initial sites, is operating in the northeastern United States. Samples are collected on a precipitation event basis by local cooperating organizations, and sent to Richland for chemical analysis. Samples are being analyzed for all the expected ionic pollutant species, using automated wet chemical, ion chromatography, and atomic absorption spectrophotometry methods. Analysis results are printed out in standard form and distributed monthly to interested parties.

An important component of the Multi-state Atmospheric Power Production Pollutant Study (MAP3S) is the collection of reliable precipitation chemistry data at carefully selected sites in the northeastern United States. These data will be used to identify trends in precipitation quality over the region as power production using fossil fuels increases; the data will also aid in developing and verifying models of regional transport, diffusion and deposition. The network is one task of the MAP3S Precipitation scavenging program; the responsibilities of Battelle include coordination of field operation (selecting and equipping sites, specifying sampling methods, and providing sampling and shipping materials), laboratory analysis, and data dissemination.

FIELD OPERATION

Battelle-developed wet deposition collectors[1] have been installed at the four initial network sites, and sampling began in October 1976. The collection area (of about 450 cm^2) is covered by a mechanized lid during fair weather, and is exposed automatically when a precipitation sensor is activated. A funnel and bottle arrangement can collect as much as 2 ℓ (4.4 cm of precipitation) per sample. The collectors are designed to accommodate a mechanism for immediate freezing of the collected precipitation, but all samples are now being handled as liquids until after analysis.

The four present sites and cooperating organizations are listed in Table 1. Local personnel (graduate students) at each site collect samples on a precipitation event basis, but the minimum sample collection time is now 24 hr. The samples are weighed and the pH taken before being divided into portions for local analysis and for shipment to the Battelle laboratory in Richland, Washington. Precipitation gauge data and sample pH and volume measurements are logged and a copy is sent to Battelle along with the samples.

CHEMICAL ANALYSIS

Table 2 lists chemical species analyzed and methods used at the network laboratory. This list encompasses essentially all of the ionic species expected to be in the samples. Total conductivity and acidity/alkalinity measurements are also made to check the completeness of the analyses for individual pollutants. The samples, sent by air freight in insulated containers, are kept at a temperature of 4°C until analysis is completed; the remaining volumes are stored in a freezer at -18°C.

DATA DISSEMINATION

An important objective of the study is rapid analysis and dissemination of analysis data to network participants and other interested parties. A computer program has

TABLE 1. MAP3S Precipitation Chemistry Network Sites

Site Number	Location	Cooperating Organization
1	Whiteface Mountain, NY	Atmospheric Sciences Research Center State University of New York at Albany
2	Ithaca, NY	Section of Ecology and Systematics Cornell University
3	State College, PA	Department of Meteorology Pennsylvania State University
4	Charlottesville, PA	Department of Environmental Sciences University of Virginia

TABLE 2. Chemical Species Analyzed and Methods

Specie	Method
Common Anions SO_4^{2-}, NO_2^-, NO_3^-, Cl^-, PO_4^{3-}	Ion Chromatography or Automated Wet Chemistry
Cations NH_4^+ Na^+, Mg^{2+}, K^+, Al^{3+}, Ca^{2+}	Automated Wet Chemistry Flame Emission Atomic Absorption Spectrophotometry
SO_2 (dissolved)	Automated Wet Chemistry
Conductivity	Conductivity Cell
Free Acidity	pH Electrode
Acidity/Alkalinity	Titration

been developed which organizes all relevant data and prints out summaries in a standard format. The analyses performed during each calendar month are printed out and distributed. In addition, a summary of each year's activities and data will be compiled and issued as an ERDA report.

REFERENCES

1. D. W. Glover, "Development of a No-deposition (sic) Precipitation Sampler," PNL Annual Report for 1975 to ERDA DBER, Part 3, Atmospheric Sciences, BNWL-2000 PT 3, pp. 187-188, Battelle-Northwest, Richland, Washington, available from NTIS, Springfield, Virginia, 1976.

AN ALGORITHM FOR PROCESSING AND ANALYZING DATA FROM THE MAP3S PRECIPITATION NETWORK

D. R. Drewes

Computer software has been written which organizes and tabulates the precipitation chemistry data to be collected for the MAP3S regional scavenging program. The algorithm has two modes of operation. The first mode analyzes raw laboratory data and reduces them for storage on standard IBM cards. In the second mode, stored data are used as input and the program generates tables of data in a format specified by the user.

Data management for an extended project such as the MAP3S precipitation scavenging network presents several complications. Because of the length of the project, future needs must be anticipated and included as early as possible. Since future needs cannot always be anticipated, the data management system must be flexible enough to meet the needs as they arise. Furthermore, the volume of data expected requires a rather compact data storage format. As in all problems of this type, certain trade-offs must be considered in order to maximize the utility of the system: flexibility is obtained by increasing the size and complexity of the system, etc.

The software written to handle the precipitation network data operates in two different modes, and has been set up to recognize the input data being supplied and choose the appropriate mode. In the first mode, raw data from the laboratory may be input (e.g. the values of % T from the colorimetric NH_4^+ analysis). These data are first fed to a subprogram which converts them to appropriate units (e.g. concentration), and then the converted data are stored in an array. After all such input has been received, the storage array is used to output the data in tables and on punched cards for permanent storage.

The second mode of operation results when the cards produced under the first mode are used as input. It allows tabulation of data as performed above, and also affords the user the opportunity to perform any desired calculations on the data. This is done by encoding the appropriate calculations in a subprogram unit, inserting it into the program deck, and running with an appropriate data deck.

The modular construction of the program allows easy adaptation to changes in the analytical methods and the data output. For example, since the reduction of the 'raw' NH_4^+ data to NH_4^+ concentration is handled exclusively by one subroutine, a change from a colorimetric procedure to an ion-chromatographic one would require only replacement of this single unit, and nothing else would be affected. The dual nature of the code allows it to respond to both the immediate needs of data reduction and storage and also to more detailed examination of any portion of the data base.

APPLICATION OF A MESOSCALE MODEL FOR DETERMINING TRANSPORT AND SCAVENGING IN LAKE-EFFECT SNOWSTORMS

B. C. Scott and W. J. Eadie

To examine the intricacies of scavenging processes, it is necessary to realistically simulate cloud dynamics and microphysics. Such simulations require adequate knowledge about the locations and the environments in which cloud clusters are likely to develop. Therefore, an existing mesoscale model is being modified to meet these theoretical and experimental needs. Model calculations of mixing layer depth and vertical velocities are presented for two meteorological situations expected to occur frequently during our planned field programs.

INTRODUCTION

Vast amounts of precipitation originate from bands of clouds associated with the convergence from frontal motions, orographic features, or turbulent fluxes of heat and moisture from the surface. Indeed, the total surface precipitation at most mid-latitude sites is almost entirely composed of precipitation associated with convective instability (e.g., thundershowers) or transient extratropical cyclones (e.g., frontal passages). Furthermore, the precipitation from these extratropical cyclones is dominated by embedded precipitating bands; the heaviest precipitation within these bands being associated with mesoscale areas of convective activity.[1] Since the ultimate consideration in predicting the removal of pollutants by precipitation is the amount of water deposited at the surface, it pays to closely examine those cloud systems contributing the most precipitation; that is, individual convective clouds or mesoscale clusters of convective clouds. One objective of the precipitation scavenging studies is therefore to develop a model which can adequately resolve the time and space scales associated with the attachment of pollutant to cloud water within these convective systems. Such a model will then enable investigation of the intricacies of the scavenging processes and determination of the dominant pollutant capture and removal processes.

To simulate realistic cloud dynamics, which through a strong interaction with cloud microphysics ultimately determine cloud lifetimes and precipitation at the surface, one must specify the location and the environment in which convective cloud clusters grow. To provide this information, we are currently adapting an existing mesoscale model to meet our theoretical and experimental needs.

The lake effect mesoscale model developed by Lavoie[2] has been selected to predict the winter air flow patterns, the thickness of the mixing layer, and the regions of convec-development near our field experimental site in western Michigan. In addition to providing the environmental parameters necessary for the smaller scale convective modeling, the model should be valuable in determining trajectories of power plant pollutants, variations in storm intensity with changes in inflow conditions, and for siting field crews.

MODEL DESCRIPTION

The model consists of three layers; a superadiabatic surface layer, a neutral mixing layer, and a stable upper layer. The neutral mixing layer is the only layer whose physical characteristics are time dependent. In this mixing layer, responses to heat and moisture fluxes and frictional forcing enable

the thickness of the layer to vary in space and time, and to produce various wind accelerations.

The grid resolution of the model (10 km) is too crude to resolve individual convective elements. However, several schemes have been developed[3,4,5] to parameterize the condensation process and allow the subsequent heat release to feed back into the energy equation. Regardless of the parameterization used, the major effect of latent heat release is to more sharply define and amplify the upward deformation of the initial mixing layer thickness. The thickness of the mixed layer and the vertical velocity at the top of the layer are the most meaningful output fields of the model in interpreting the location and intensity of convective development. A shallow mixed layer indicates shallow clouds and short cloud lifetimes, whereas a thick mixed layer implies deep clouds, longer cloud lifetimes, and greater opportunities for precipitation development. Similarly, a region of maximum upward vertical motion indicates an area favorable for convective development through upslope flow and/or convergence in the mesoscale wind field. Additional output from the mesoscale model will provide the temperature, moisture content, and divergence within the mixed layer--all important components in determining cloud development.

The case studies presented below have been selected to show the influence of Lake Michigan on the mesoscale air mass features near our experimental field site headquarters at Muskegon. The model has been run without considering latent heat release, but the thickness of the mixing layer and the computed vertical motion can be considered proportional to the intensity of convection and to the likelihood of precipitation development. Thus, probable washout locations of the projected plumes are expected to be within 50 km downwind from the regions with maximum upward vertical motion.

RESULTS

In these case studies, the water temperature of Lake Michigan was taken to be 0°C to simulate conditions in late winter or early spring. The initial potential temperature of the mixed layer was assumed to be -6°C. The initial thickness of the mixed layer was taken to be 2 km and the mixed layer was assumed to be capped with 2°C inversion. Results are presented for initial wind directions of 225° and 270°, and an initial wind speed of 10 m sec^{-1}.

Figure 1 shows the steady solution obtained with a prevailing wind of 225° for the deformation of the inversion surface capping the mixed layer. Note the depression of the inversion surface in the vicinity of the western shoreline and the upward deformation over and downwind of the eastern shoreline. With this southwesterly wind direction, lake-effect snow is frequently observed in the Muskegon-Holland area,[6] where the thickness of mixed layer is a maximum. The location of the second maximum in upper Michigan is frequent area of heavy snows.[7] The vertical motion at the top of the mixed layer is shown in Figure 2. Both the subsidence over the upwind (western) shoreline and upward motions over the eastern shoreline reveal the sensitivity of the model to the detailed configurations of the land-lake boundaries.

The deformation of the inversion obtained for a prevailing wind of 270° is shown in Figure 3. Both the southern and northern Michigan maxima in the inversion surface have shifted south and west from the locations of the maxima shown in Figure 1. The vertical motion at the top of the inversion surface for the 270° wind shown in Figure 4 is a graphic example of the response of the model in the detailed configuration of Lake Michigan.

In the coming months, the model will be extended to include the effects of latent heat release. A library of mesoscale modeling results for various wind directions will be completed as an aid in planning the field studies. Included within this library will be the trajectories of those plumes emitted from the various power plants and urban areas located on the shores of Lake Michigan.

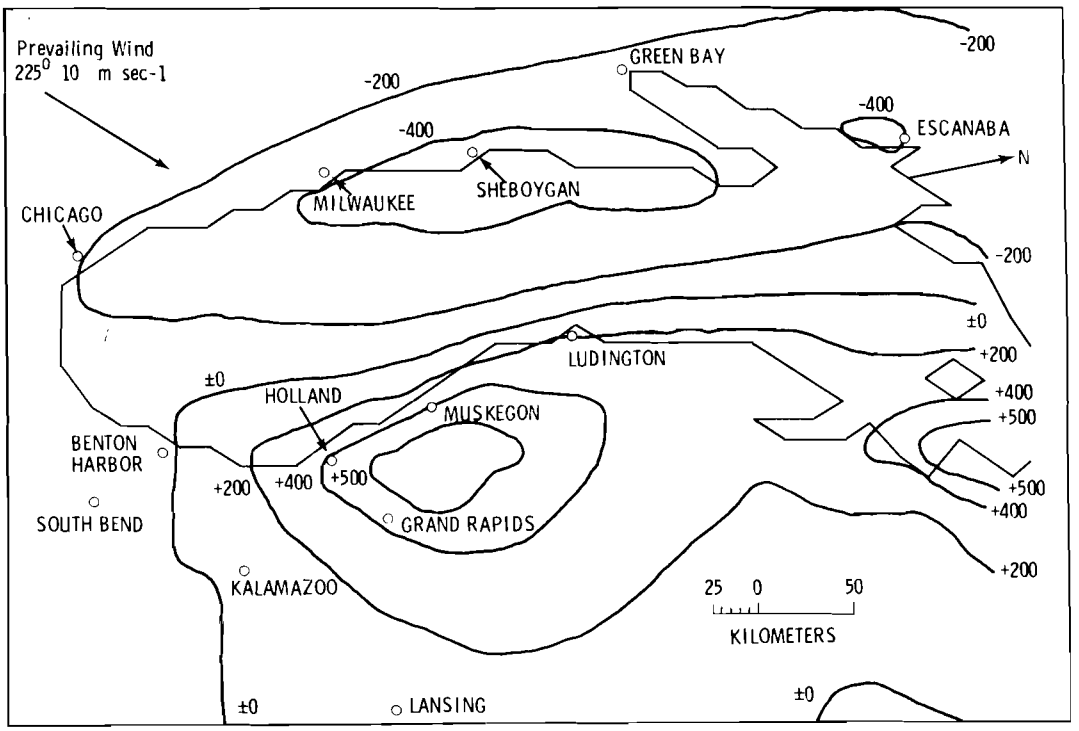

FIGURE 1. Inversion Deformation (m) from an Initial Height of 2000 m for a 225° Wind Direction

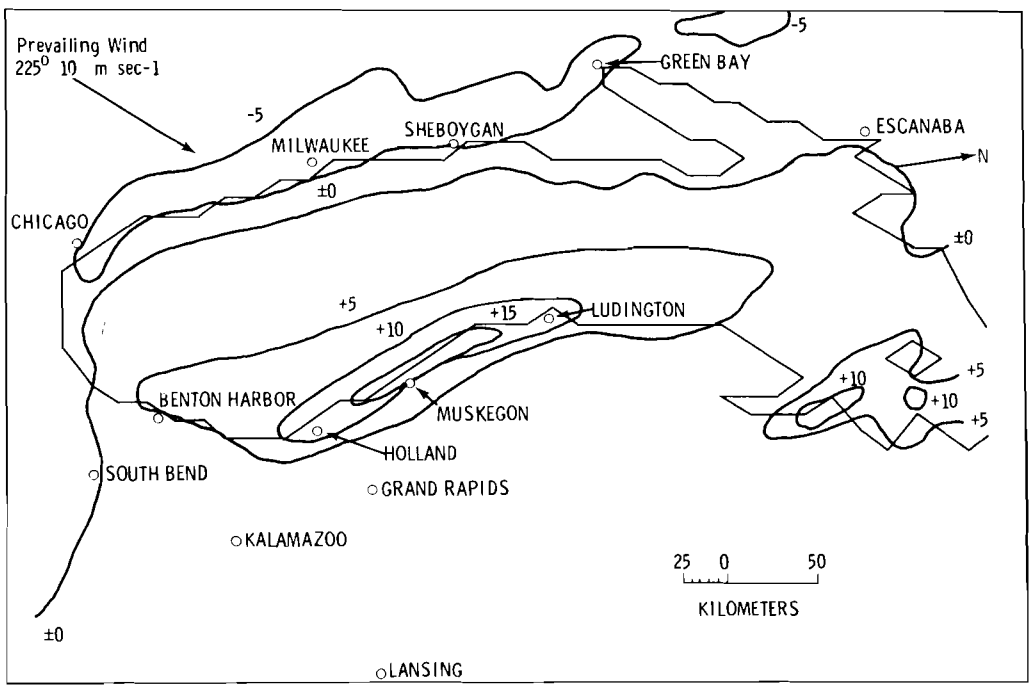

FIGURE 2. Vertical Motion (cm sec^{-1}) at Inversion Surface for a 225° Wind Direction

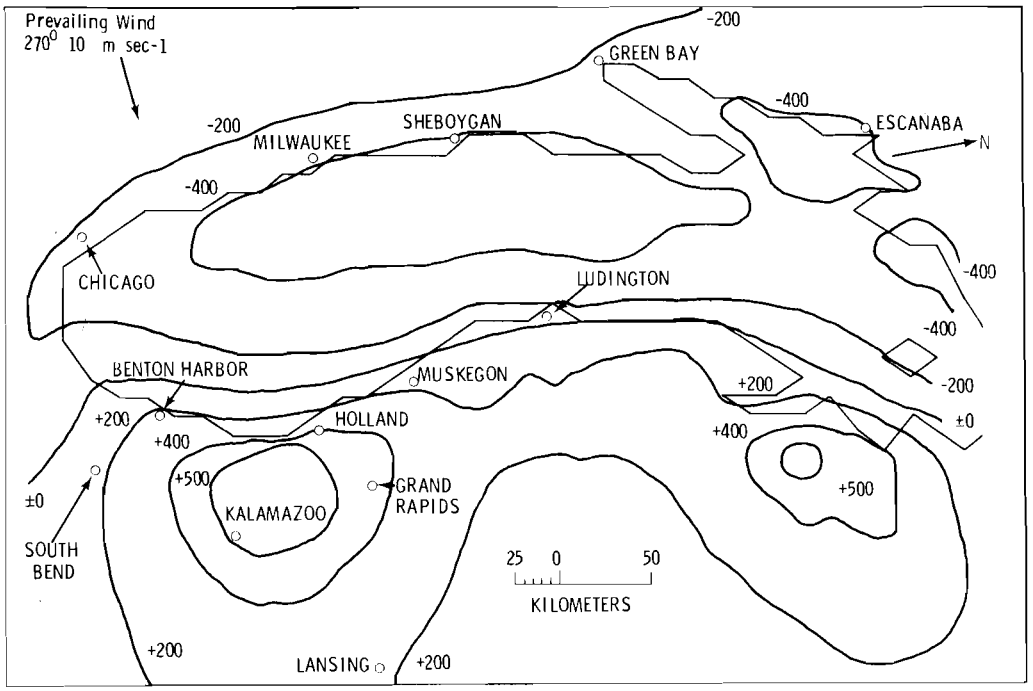

FIGURE 3. Inversion Deformation (m) from an Initial Height of 2000 m for a 270° Wind Direction

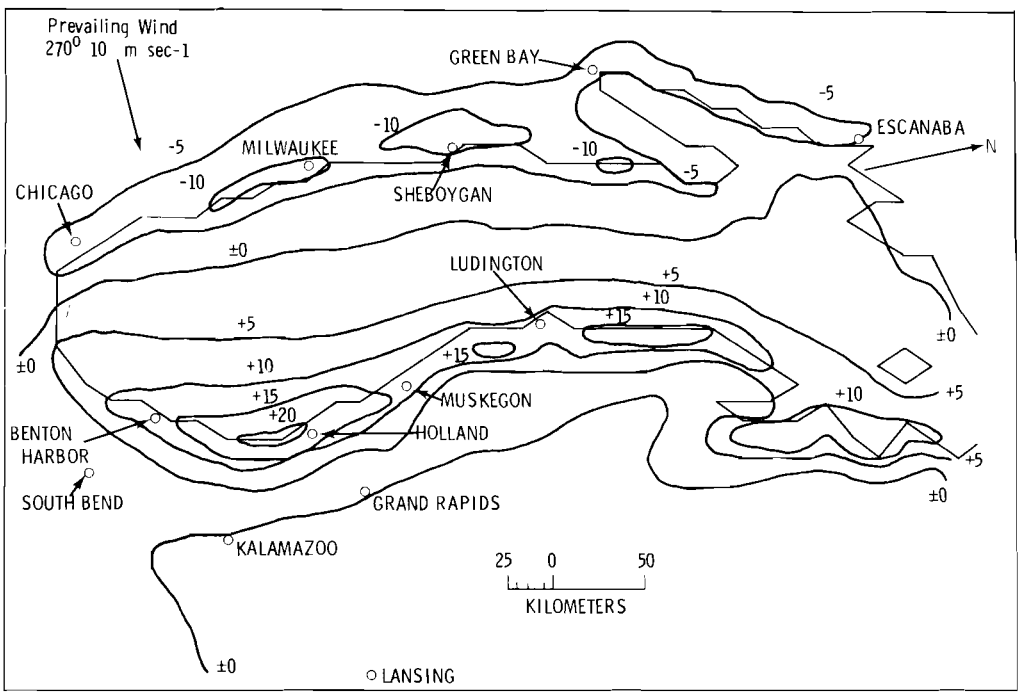

FIGURE 4. Vertical Motion (cm sec^{-1}) at Inversion Surface for a 270° Wind Direction

References

1. P. V. Hobbs and R. A. Houze, Jr. "Mesoscale Structure of Precipitation in Extratropical Cyclones." From preprints from International Cloud Plysics Conference, July 1976, Boulder, CO, available from the Amer. Meteor. Soc., pp. 488-493, 1976.

2. R. Lavoie. A Mesoscale Numerical Model and Lake Effect Storms. Ph.D. Thesis, Pennsylvania State University, available from University Microfilms, Ann Arbor, MI, p. 102, 1968.

3. C. W. Kreitzberg and D. J. Perkey, "Release of Potential Instability: Part 1. A Sequential Plume Model Within a Hydrostatic Primitive Equation Model." J. Atmos. Sci., 33, pp. 456-475, 1976.

4. R. Lavoie, "A Mesoscale Numerical Model of Lake-Effect Storms." J. Atmos. Sci., 29, pp. 1025-1040, 1972.

5. E. L. Magaziner, "A Numerical Model of the Effects of Seeding on the Evolution of a Lake-Effect Storm." J. Appl. Metero., 12, pp. 948-954, 1973.

6. V. L. Eichenlauls and E. Garrett. "Climatic Modification and Lake-Effect Snowfall Along the Lee Shore of Lake Michigan: A Classic Month as Viewed by Radar and Weather Satellite." Weatherwise, 24-12, 268-275, 291, 1972.

7. V. L. Eichenlauls, "Lake Effect Snowfalls to the Lee of the Great Lakes: Its Role in Michigan." Bull. Amer. Meteor. Soc., 51, 403-412, 1970.

RESULTS OF FLARE RELEASE OF AgI AND In INTO A SUPER COOLED CLOUD

W. E. Davis and J. M. Thorp

Initial analyses are presented of an incloud tracer release by flare of indium and silver iodide into a supercooled cloud on March 31, 1972, on the Olympia Peninsula, Washington. The analysis of surface samplers revealed greater than 12% of the indium was deposited. A preliminary analysis found values of silver only slightly higher than background.

INTRODUCTION

From 1971 to 1975, precipitation scavenging field studies were conducted on the Olympic Peninsula in Washington. The primary purpose of these field studies was determining whether a tracer released from aircraft into frontal storms would be removed by precipitation in sufficient quantities to be measured in ground collectors. Further, the tests were designed to indicate what atmospheric conditions enhance removal of the tracer by precipitation. One of these experiments, a flare release of silver iodide and indium into a supercooled cloud, was carried out on March 31, 1972.[1,2]

EXPERIMENTAL METHOD

The tracer test on March 31, 1972, had two objectives:

1. To see whether a non-nucleating tracer injected simultaneously with a nucleating agent into a stable supercooled area of cloud would be removed in sufficient quantities to be detected at the ground;

2. To predict a ground target for the precipitation falling from the seeded area.

The design of the experiment called for a prefrontal supercooled cloud layer with stable lapse rate to assure nucleation by the AgI, and steady precipitation at the ground to minimize evaporation of the seeded precipitation.

On March 31, 1972, at 1600 PST, an occluded front was west of the Olympic Peninsula (Figure 1). Rain in advance of this storm began on the northwest coast before noon and continued into the evening. Continuous rain at 0.01-0.02 in./10 min was occurring at both Quillayute and Forks, before, during, and well after the experiment (Figure 2).

The assigned position of the aircraft for the tracer release was based on Quillayute radiosonde data taken at 1500 PST (Figure 3). This position was picked such that the initial deposition was expected to occur at or near Forks, WA (Figure 4). A mean wind was computed for the 12,000 ft layer and an estimated average precipitation fall velocity of ∿2.0 m/sec throughout the layer was used. The position for aircraft tracer release was then calculated.

At 1635 PST, the University of Washington B-23 airplane ignited flares releasing 1200 g of AgI and 500 g of In at 12,000 ft (MSL) for 14 min over a triangular track at an atmospheric temperature of -6.6°C in the prefrontal clouds (Figure 4).

The result of the seeding was the development of a "hole-in-the-cloud" with observable ice fall occurring as the hole was forming.[3] Various solar optical phenomena were reported, i.e., a lower tangent arc. Visual observations and a foil sample taken by the aircraft after tracer release indicated that ice crystals were in the seeded area.

The airplane made several position measurements within the hole and was able to determine the drift of the hole to be from ∿204° true. This drift direction was assumed to be the release level wind direction and helped determine the expected arrival position of the tracers on the ground.

The next radiosonde data after the release at 1653 PST (Figure 5) were not available until nearly 1700 PST. This sounding showed a shift in the wind from 240° to 260° had occurred at the release height of 12,000 ft since the 1500 PST sounding. This

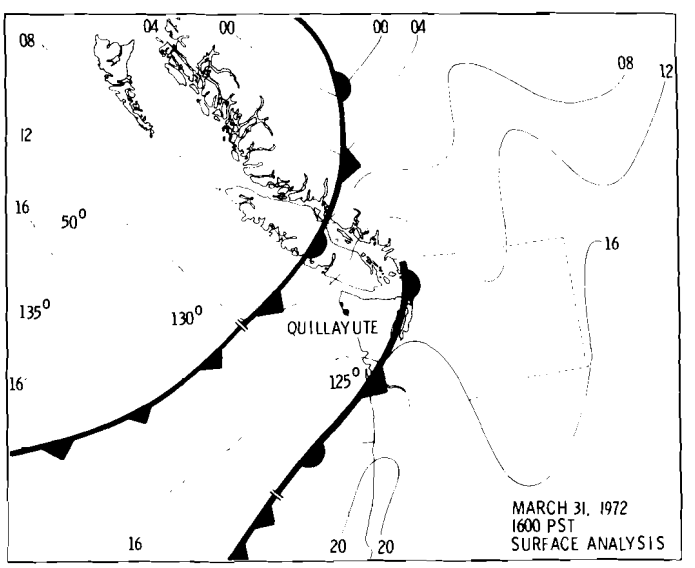

FIGURE 1. Surface Analysis for March 31, 1972, 1600 PST

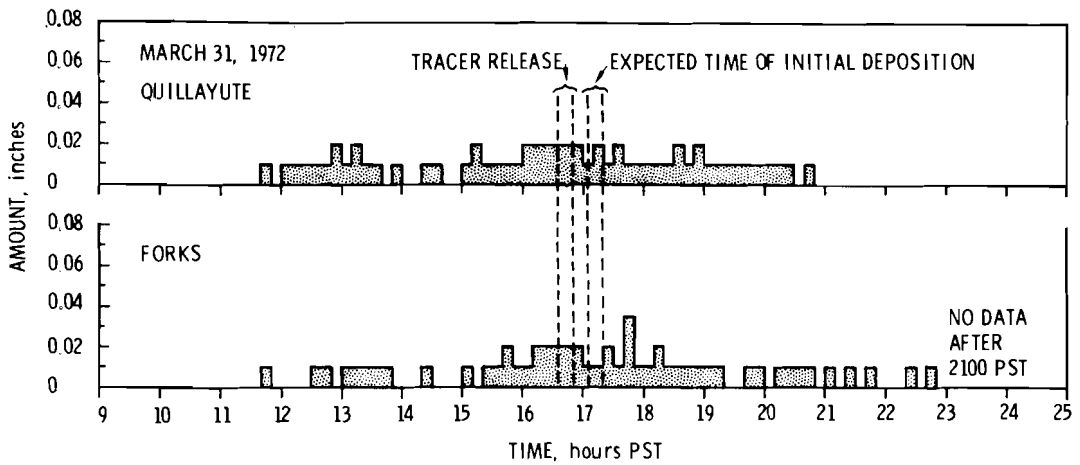

FIGURE 2. Ten-Minute Averages of Precipitation at Forks and Quillayute for March 31, 1972. (Note: no data recorded for Quillayute after 2100 PST)

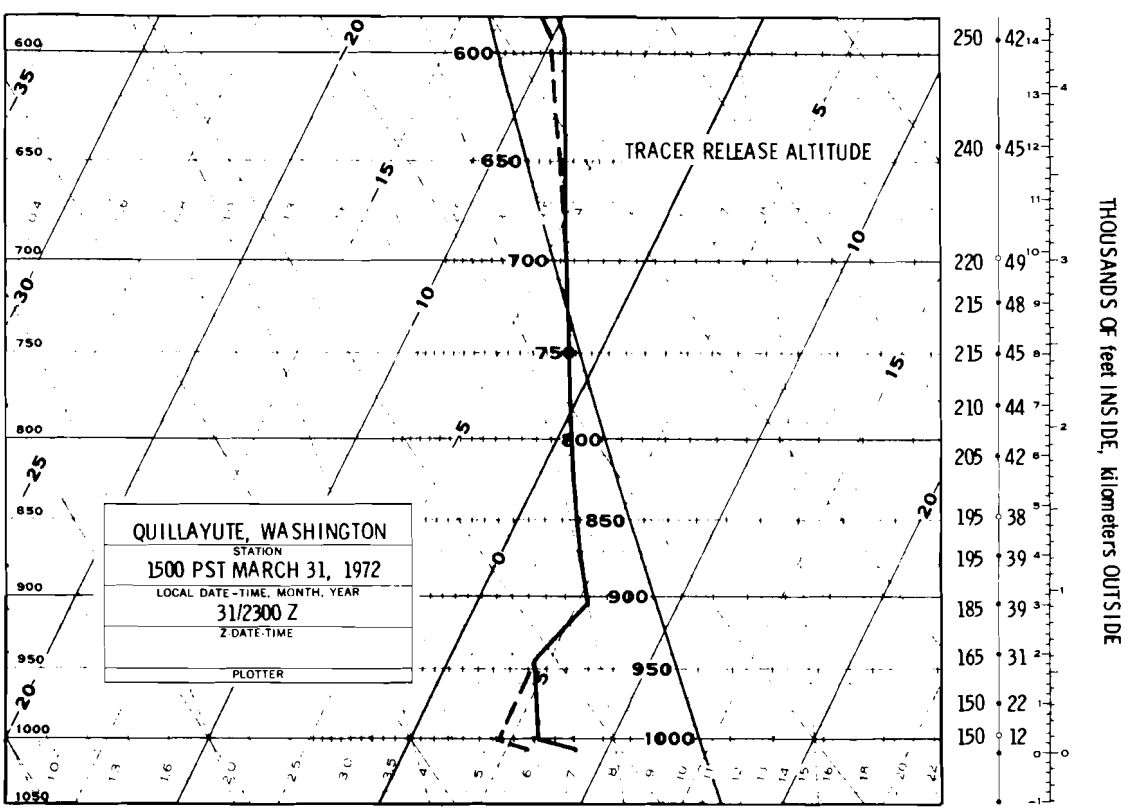

FIGURE 3. Plot of Radiosonde Data Taken at 1500 PST March 31, 1972, at Quillayute, WA (wind speeds on right are in knots)

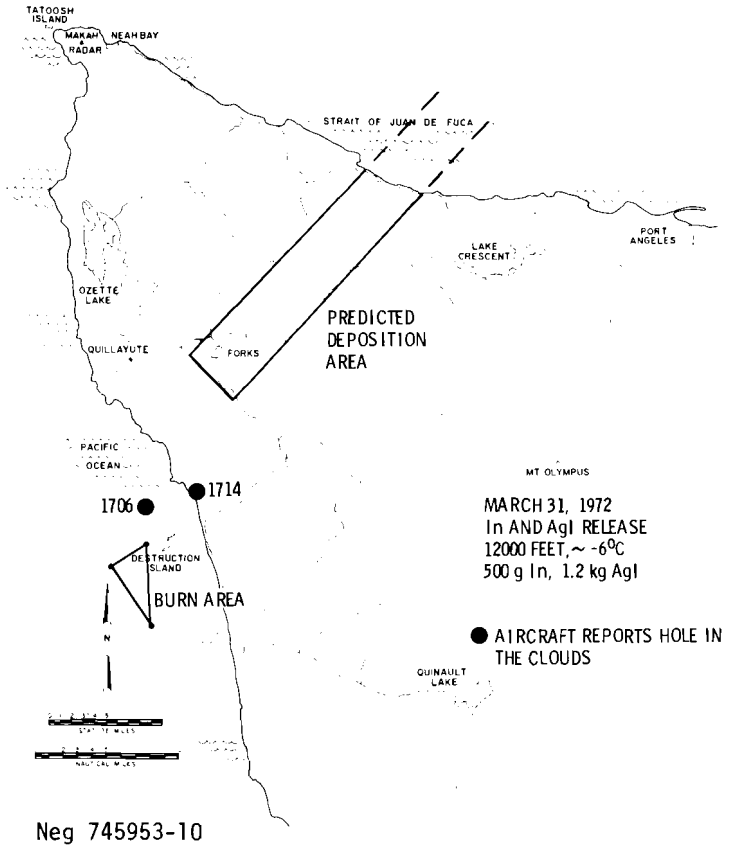

Neg 745953-10

FIGURE 4. Map of Olympic Peninsula with Tracer Release Position and Predicted Deposition area

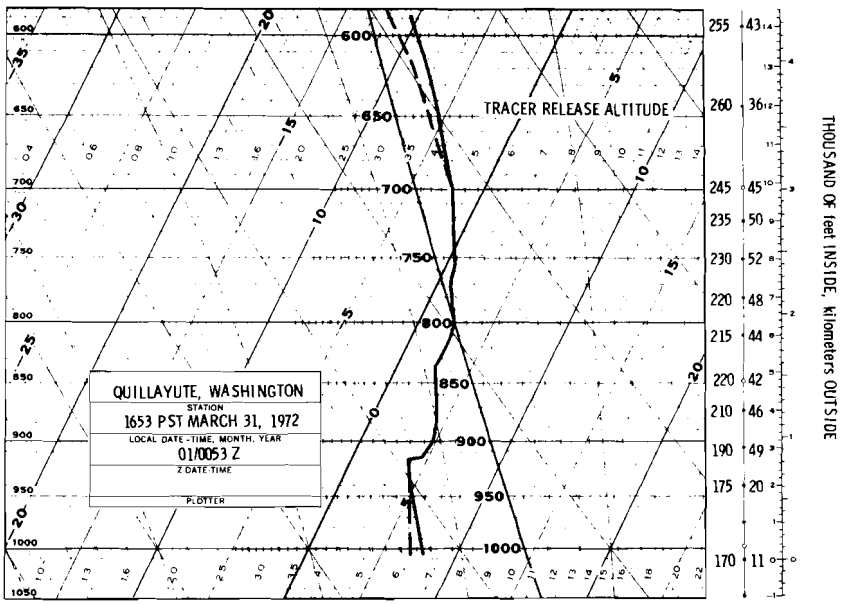

FIGURE 5. Plot of Radiosonde Data Taken at 1653 PST March 31, 1972, at Quillayute, WA (wind speeds on right are in knots)

wind shift could have altered the ground deposition pattern considerably from that predicted.

ANALYSIS

To determine the ground deposition pattern, 221 rain samplers were set out along roads on the Olympic Peninsula. Water samples from 85 of these have been analyzed for indium using neutron activation techniques.

The neutron activation analysis revealed the presence of indium in samplers west of Forks, WA. Samples which contained significant indium were then reanalyzed for silver. Preliminary analysis for silver showed greatly reduced amounts compared to indium (Table 1) considering equal amounts of the two tracers were released. It may be significant that Ag above background (>1.0 ng) does appear in areas of positive indium deposition. Additional analysis is required to determine the deposition pattern for Ag.

The estimated deposition pattern based on the indium analysis is shown in Figure 6. Approximately 12% of the indium released was accounted for. It is quite possible that more was deposited; we cannot tell how much because the deposition pattern extended to the north where there were no samplers. Two samples in the area of deposition have been removed from the analysis because of inadvertent duplication of the sample numbers. At this time it appears that the removal of these two samples will not affect the basic deposition pattern as shown.

CONCLUSIONS

The pattern based on these analyses shows:

1. A non-nucleating tracer, indium, injected simultaneously with a nucleating agent, AgI, into a supercooled area of a cloud was removed by precipitation in sufficient

TABLE 1. Samples with >1 ng of In

Sample #	Ng (In)	Ng (Ag)	Wt (grams)
67	15.9 ± 0.5	2.63 ± 0.63	173
68	2.6 ± 0.4	1.12 ± 0.48	206
69	23.3 ± 0.7	1.31 ± 0.50	221
70	4.0 ± 0.5	1.62 ± 0.04	213
71	10.2 ± 1.1	1.92 ± 0.47	188
72	10.8 ± 0.6	1.42 ± 0.54	159
73	9.4 ± 0.6	1.76 ± 0.41	242
74	2.1 ± 0.2	1.04 ± 0.63	266
81	3.3 ± 0.3	NA	162
82	26.2 ± 0.5	"	124
83	2.6 ± 0.3	"	146
84	6.8 ± 0.4	"	131
85	4.2 ± 0.4	"	148
87	33.8 ± 0.9	"	129
88	16.5 ± 6.0	"	114
90[a]	<0.8	0.61 ± 0.35	140
413	1.18± 0.69	NA	

a.This sample is an example of general background.
NA - not analyzed for AG

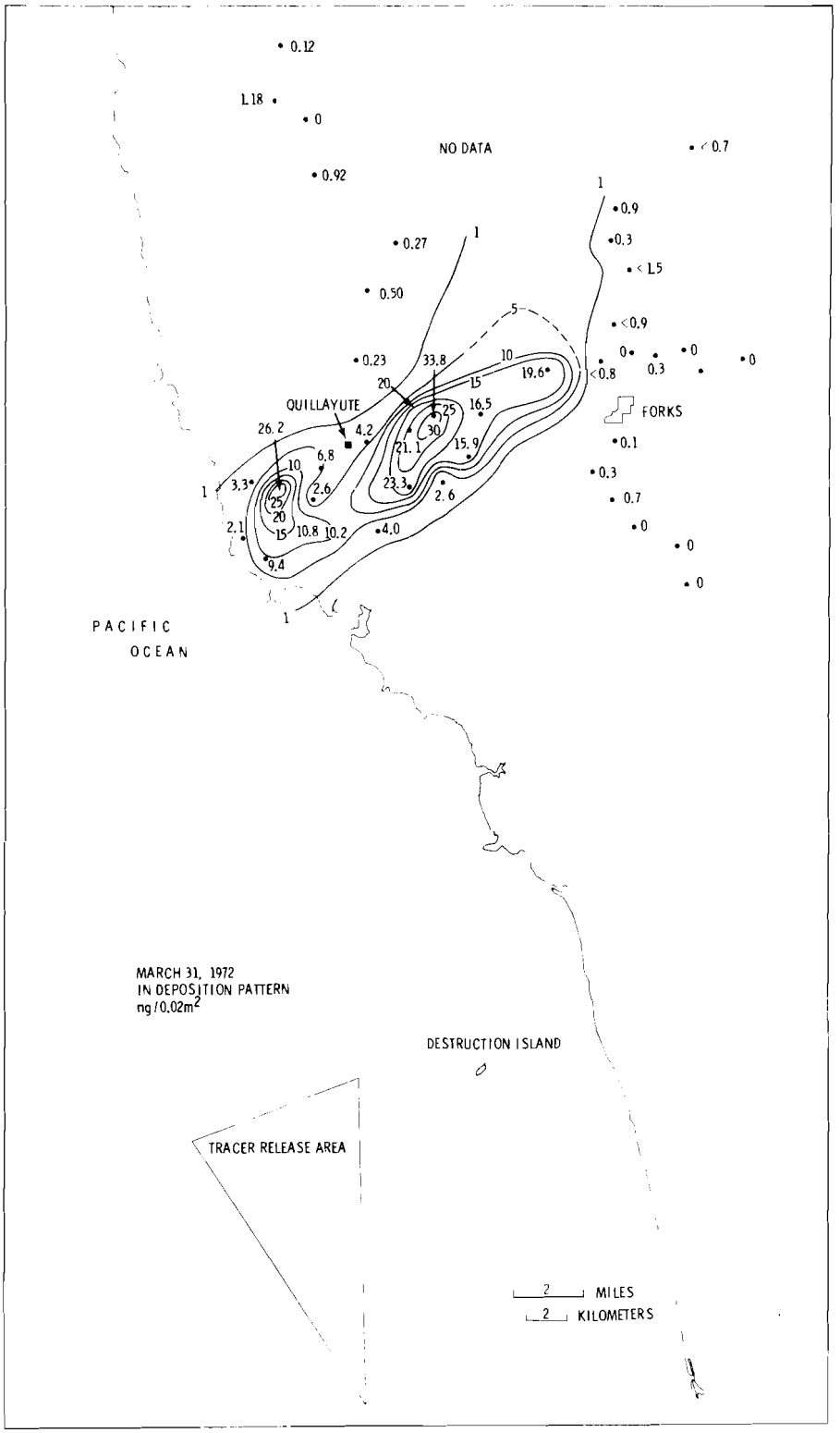

FIGURE 6. Analysis of In Deposition. Isolines are ng/sampler (0.02 m^2)

quantities to be detected at the ground. Approximately 12% of the amount released has been accounted for.

2. Targeting of the precipitation as indicated by the tracer analysis did not occur in the Forks area, but further to the west. This result indicates the continuing need for an expanded sampling system to cover the variability in the winds associated with frontal storms.

ACKNOWLEDGMENTS

This experiment reflects the efforts of a large task force: J. C. Draper, W. G. N. Slinn, T. M. Tanner, S. R. Garcia, C. L. Wilkerson, D. J. Newland, O. P. Gifford, M. T. Dana, D. W. Glover, J. W. Sloot, M. C. Miller, C. W. Thomas, R. N. Lee, V. T. Henderson, F. B. Steele, R. E. Erwin, F. O. Gladfelder, J. M. Baily, J. A. Young, N. A. Wogman, and students and staff at the University of Washington and Washington State University, especially Professor Lawrence F. Radke, Cloud Physics Group, of the University of Washington. We are grateful for the assistance of the 758th USAF Radar Squadron.

References

1. W. E. Davis and J. A. Young. "Results of In-Cloud Tracer Releases in Frontal Storms." In Proceedings of Symposium "Precipitation Scavenging - 1974," Champaign, IL (to be published - 1976).

2. W. G. N. Slinn, "In-Cloud Scavenging Studies," PNL Annual Report for 1972 to the USAEC Division of Biology and Medicine, Atmospheric Sciences, BNWL-1751 PT 1, Battelle, Pacific Northwest Laboratories, 76-79, 1973.

3. L. F. Radke. Personal communications 1972, 1976.

IN-FLIGHT AIRCRAFT EXHAUST AND TRACER SIZE DISTRIBUTION MEASUREMENTS

B. C. Scott and N. S. Laulainen

Preliminary results are presented from an experiment designed to determine the size distribution and the nucleation ability of an europium tracer. Large concentrations (2×10^4 cm^{-3}) of tracer aerosol with diameters ≤ 0.04 μm were produced. Whereas previous experiments had identified no tracer particles with dimensions ≥ 0.1 μm, this experiment identified significant numbers. A small fraction of the europium appeared to act as a CCN.

INTRODUCTION

A multi-tracer release of aerosol particles into a precipitating cloud system is an attractive way to compare the effectiveness of a variety of pollutant attachment and removal mechanisms. However, the attachment of tracer aerosols to cloud water depends strongly on the size distribution and solubility of the aerosol. For example, a soluable aerosol such as ammonium sulfate can be activated as a condensation nuclei

at typical cloud supersaturations, if its dimensions exceed some critical value (generally 0.01 to 0.1 μm). Less soluble tracers can also be effectively incorporated into the cloud drops through capture mechanisms such as Brownian and turbulent diffusion, phoretic transport, and impaction. In contrast to the nucleation events where attachment rates to cloud water are essentially infinite, the attachment rates for less soluble particles are highly size dependent and range from 0.01% h^{-1} for phoretic attachment to about 100% h^{-1} for inertial impaction.[1] Thus, for an in-cloud tracer release experiment to provide information about attachment and removal of natural pollutants, it is absolutely essential that the size distribution and microphysical characteristics of the tracer be known. This report describes our first attempt to characterize one tracer thought to be well suited for in-cloud scavenging experiments.

THE EXPERIMENT

The experiment was performed with two airplanes flying in tandem; the lead airplane flying about 100 m ahead of the trailing airplane and simulating a normal tracer release by burning the tracer from Brad Patton aerosol generators. The tracer examined was europium, an insoluble material, thought to be in its pure form, an ineffective condensation nucleus. Previous releases of tracer materials with these aerosol generators had produced aerosols distributed over dimensions less than 0.1 μm.[2] The trailing aircraft was equiped with a Whitby electrical aerosol analyzer and a Royco optical particle counter for measuring aerosol size distribution, an integrating nephelometer for indication of particles greater than 0.1 μm in diameter, a TECO model 14 analyzer for indication of and monitoring of the lead aircraft's exhaust (NO/NO_x), and a device for continuous cloud condensation nuclei (CCN) measurements.[3] Filter samples were also obtained to verify that the aerosol measured was indeed the tracer released by the lead aircraft.

RESULTS

Figure 1 summarizes the raw, non-normalized aerosol size distributions obtained in the ambient atmosphere (26 samples), in the environment containing aircraft exhaust (10 samples), and in the environment containing both aircraft exhaust and tracer material (5 samples).

Figure 2 illustrates the aerosol size distributions after each curve was normalized so that the aerosol concentrations are equivalent at 0.075 μm. As seen in Figure 1, the 0.075 μm size is the first size interval where aerosol concentrations are essentially identical regardless of what was being measured; i.e., tracer, exhaust, or ambient air. In addition, the selection of 0.075 μm as a normalization size produces very close correspondence between aerosol concentrations of exhaust and ambient air for sizes $\geq$ 0.075 μm, despite the use of the Whitby instrument to obtain concentrations for sizes < 0.23 μm while the Royco was used for larger aerosol sizes. The error bars illustrate the variability of the concentrations and represent one standard deviation.

Nuclepore filters (pore size 0.2 μm) were exposed during the ambient, exhaust and exhaust plus tracer phases of the experiment. Because of the small pore size, flow rates were typically low--around 0.4 cfm; consequently few particles were actually found on the filters. For this reason, only preliminary analysis of the particles was attempted.

An example of scanning electron microscope micrograph is shown in Figure 3a and micrographs of increased magnification of selected areas of Figure 3a are shown in Figures 3b and 3c. Two distinct types of particles are seen in the micrographs; one type is nearly spherical while the other type is irregular. Occassionally, some of the irregularly shaped particles appear as conglomerates of smaller spherical particles. It had been hoped that enough particles would be found on the filters so that independent size information could be obtained, but with so few particles such attempt was considered futile.

However, one particle of each type was further examined by X-ray fluorescence. The results of this analysis are shown in Figures 4a through 4c, where the elemental spectra of the irregular particle, the spherical particle and a blank area of the filter are shown, respectively. The irregular particle appears to be of crustal origin because of the large peaks due to silicon and iron in its spectrum. The spherical particle is clearly the tracer, Eu. It is also noted that the tracer particle is around 0.7 μm in size. The spectrum of the blank area indicates the presence of zinc as a contaminant, either as a result of handling or present in the filter material itself. It should also be pointed out that carbonaceous particles, which one might expect from the exhaust, cannot be seen by this fluorescence technique.

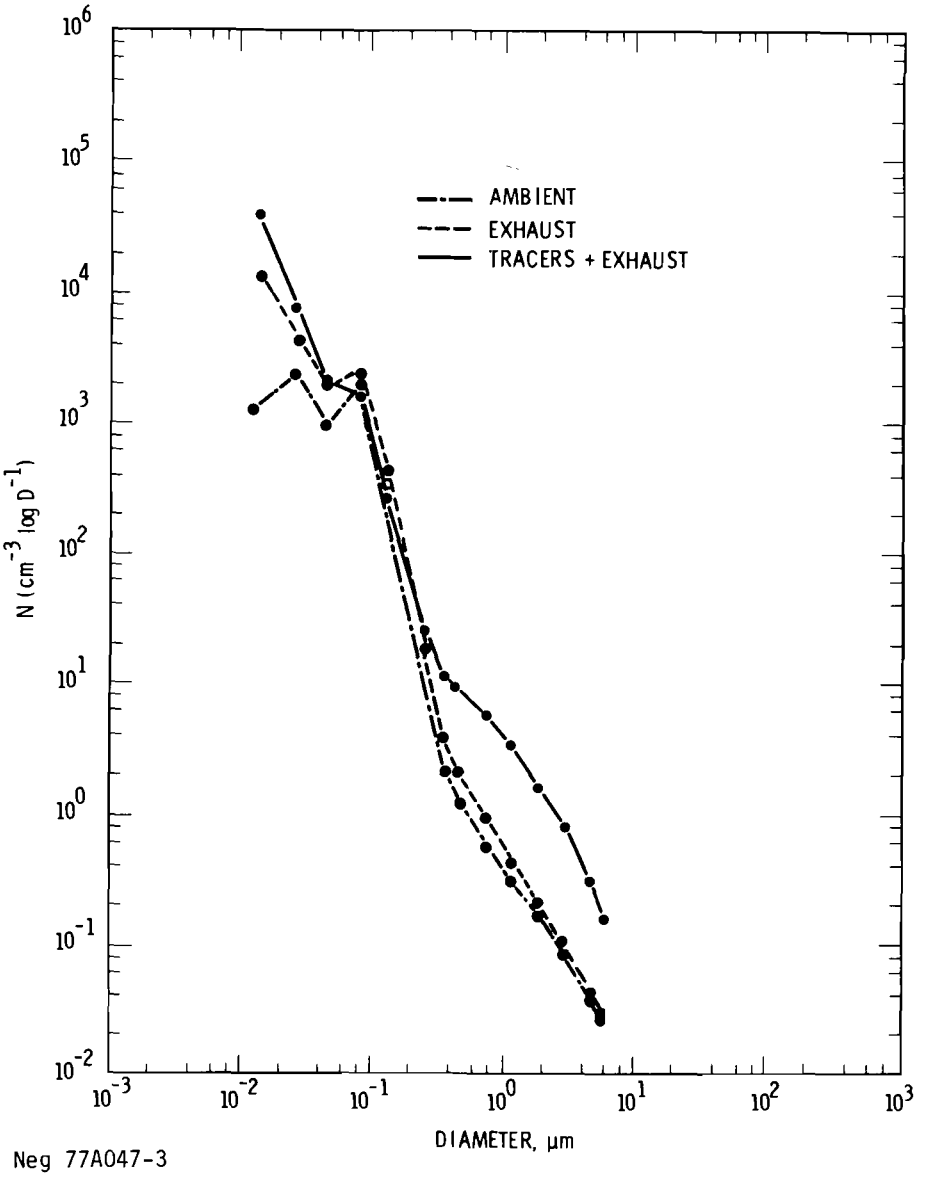

Neg 77A047-3

FIGURE 1. Aerosol Concentrations for Ambient Air, Aircraft Exhaust and Exahust Plus Tracer. Raw Data.

DISCUSSION

The Whitby aerosol analyzer works by applying a given voltage, and then capturing charged particles on an absolute filter and measuring the resultant current. Particle size distributions are then obtained by taking the differences between the currents obtained at different voltages. For typical aerosol concentrations in the boundary layer, the largest measured currents are on the order of 0.1 pA. However, to reduce the influence of background particle concentrations, the experiment was performed at an altitude of approximately 3.4 km. At this altitude, the largest measured currents due to ambient aerosol were on the order of 0.01 pA. Instrument error and noise are on the order of 0.001 pA. Thus, subtraction of current values in two successive size intervals at these low current readings could potentially produce differences near the noise level of the instrument. However, for the tracer and the exhaust samples, the

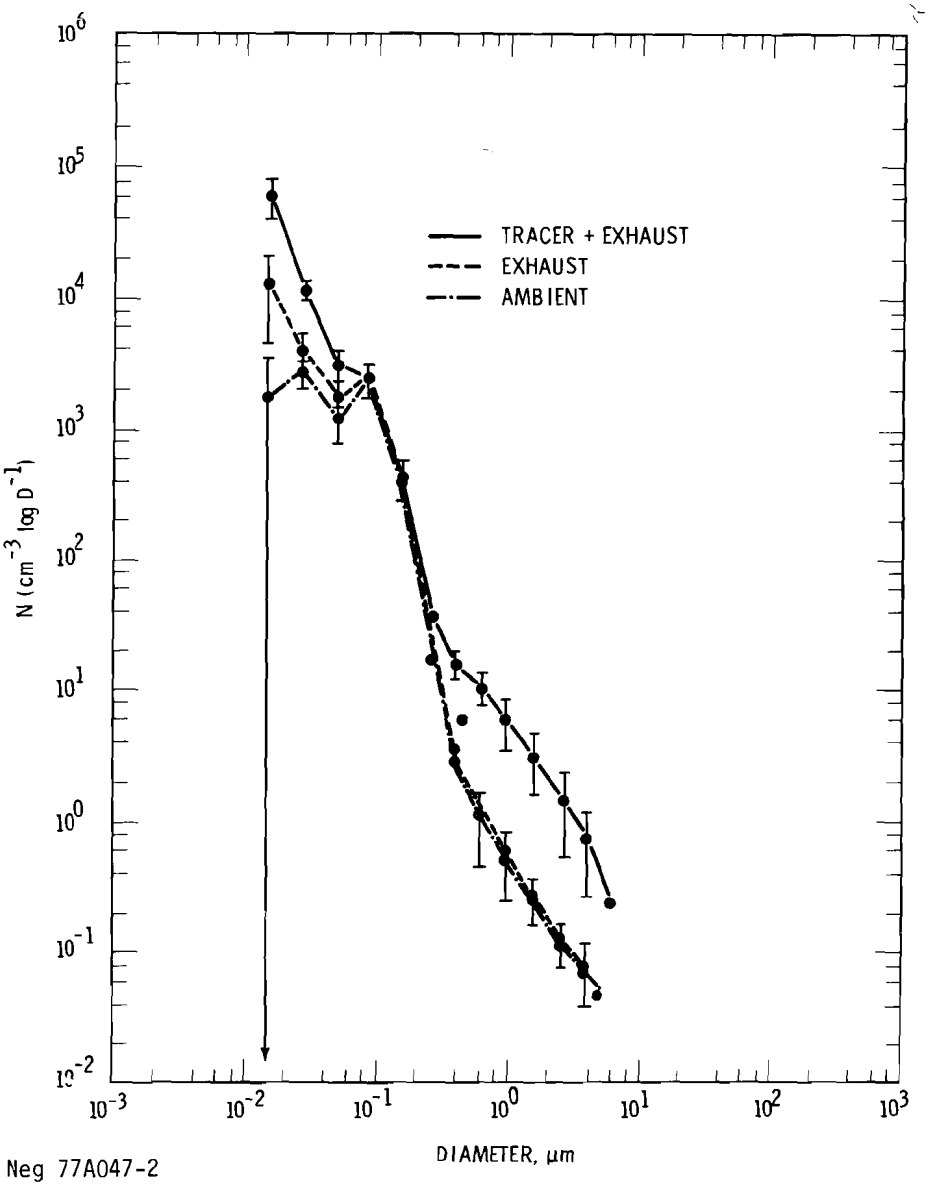

Neg 77A047-2

FIGURE 2. Aerosol Concentrations for Ambient Air, Aircraft Exhaust and Exhaust Plus Tracer. Concentrations Normalized to be Equal at 0.075 μm.

uncertainty in aerosol concentrations produced by instrument noise are, for all Whitby size intervals, less than the natural variation (i.e., one standard deviation) of the particle concentrations produced as the aircraft moved in and out of the exhaust or tracer plume. Therefore, we can say with a large degree of confidence that the differences in the three curves of Figure 2 are the result of measuring three distinctly different aerosol populations.

The exhaust from the lead airplane produced aerosols with concentrations in excess of ambient aerosols for sizes less than 0.04 μm. Large concentrations (2×10^4 cm^{-3}) of small tracer particles were produced with concentrations exceeding those of the exhaust aerosol at similar sizes by factors of 2 to 5. No information could be obtained about the size distribution of tracer particles with dimensions between 0.04 μm and 0.36 μm because the tracer concentrations decreased

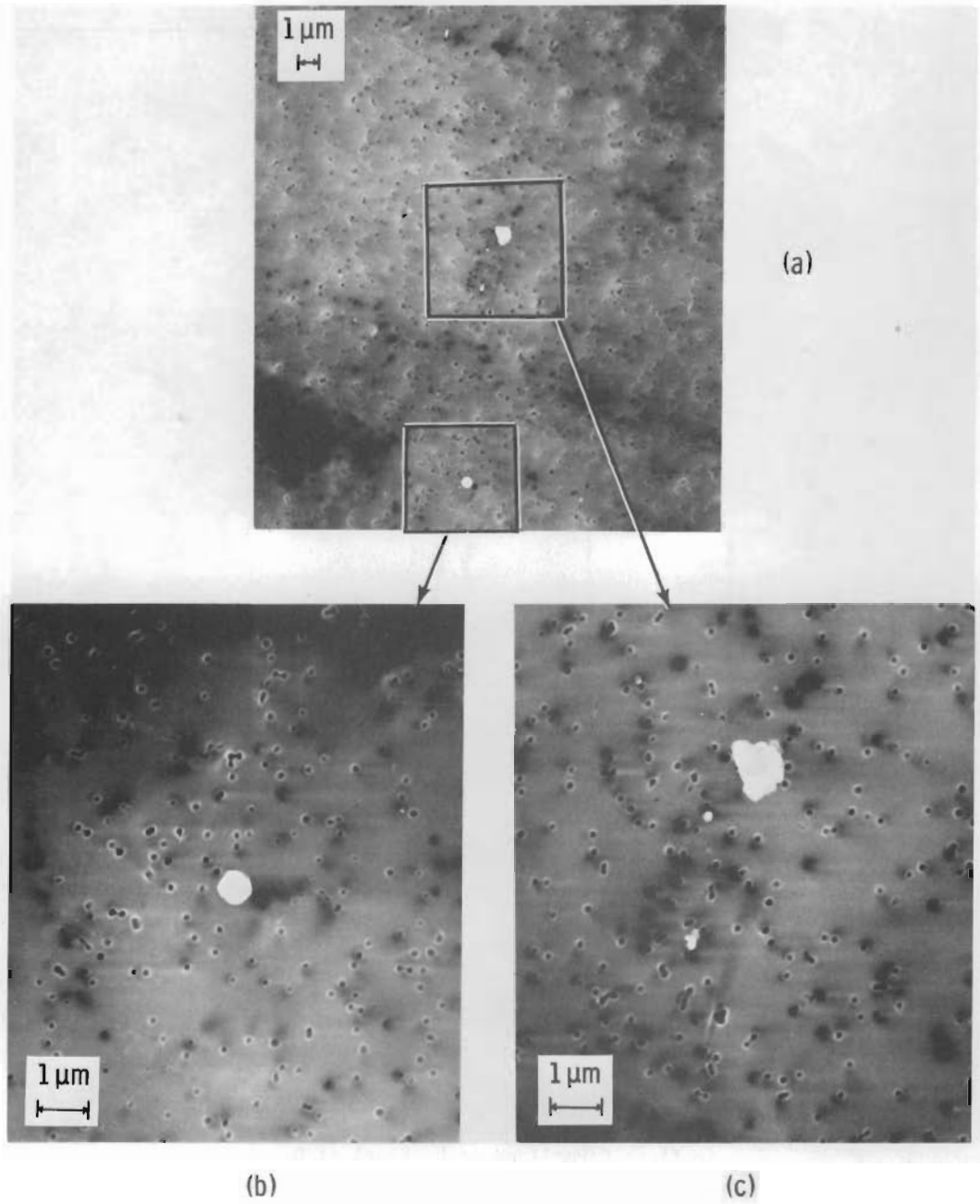

Neg 77A047-1

FIGURE 3. Electron Microscope Micrographs of Tracer/Exhaust Filter Sample:
a) Magnification at 2400X showing soil and tracer particles,
b) Magnification at 8000X of tracer particle, diameter ∿0.7 µm,
c) Magnification at 8000X of soil particle, diameter ∿1 µm.
Pore size of nuclepore filter is 0.2 µm.

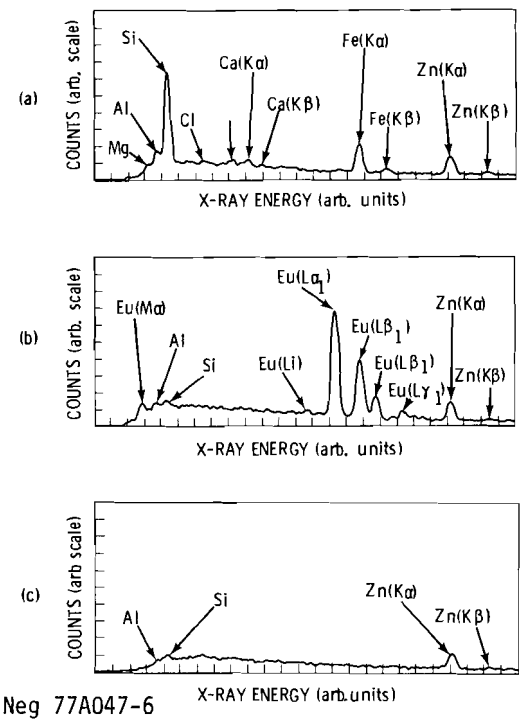

Neg 77A047-6

FIGURE 4. X-ray Fluorescence Spectra of Tracer and Soil Particles of Figure 3:
a) Soil particle showing large peaks for silicon and iron and small peaks for Al, Ca, and K,
b) Tracer particle showing large peaks for europium,
c) Filter blank with an indication of zinc contamination.

to below that of the ambient aerosol. Unexpected results, however, were the generation of large tracer particles with dimensions greater than 0.36 μm.

Observations of the generator burners during the flight indicate that one burner was not atomizing the tracer solution correctly. Additionally, in those burners appearing to fire correctly, some tracer material was observed to bubble and fizzle in a slag heap at the bottom of the burners and to occasionally fall away in big chunks. It is quite likely that some or all of the tracer particles greater than 0.36 μm were produced from these malfunctioning burners.

These findings are further substantiated from the filter analysis, where at least some of the large particles are composed of tracer material. Since X-ray fluorescence analysis of particles smaller than 0.1 μm is not possible, the elemental composition of these smaller particles can only be conjectured.

Preliminary results from the CCN measurements suggest that CCN concentrations increased by a factor of three during the tracer burn. By assuming that all of the big (> 0.36 μm) tracer particles acted as CCN, we would account for only about 10% of the CCN increase. Thus, if the CCN measurements prove to be reliable after further reduction, they imply that a small fraction of the tracer aerosol with dimensions < 0.36 μm behaves as CCN.

CONCLUSIONS

This single experiment was not expected to conclusively define the size distribution and the CCN characteristics of the tracer material. Clearly, the experiment must be repeated several times to verify the measurements. Rather, this experiment should be considered as a prototype to test the feasibility of tracer characterization with aircraft sampling. The major difficulty with the tandem aircraft approach was remaining in the tracer plume long enough to obtain a relatively undiluted sample where aerosol concentrations were significantly above background concentrations. Experiments for the future are designed to overcome this difficulty by using a single aircraft. The tracer generators will be located below the fuselage in the main part of the aircraft and the tracer material will be sampled through a probe located in the aircraft tail.

In the coming year, we will continue our efforts to characterize our tracer materials in terms of size distribution and microphysical properties. In addition, we will attempt to develop techniques for changing the size distribution and microphysical characteristics of the tracer materials. By being able to generate, at will, tracers with various microphysical properties, we will develop a powerful tool for examining, first hand, the scavenging ability of clouds.

References

1. W. G. N. Slinn and J. M. Hales, "Phoretic Processes in Scavenging," Proc. Symp. Precipitation Scavenging, Series 22. USAEC Symp., pp. 411-422, 1970.

2. A. J. Alkezweeny and L. F. Radke, "Airborne Measurements of the Size Distribution of AgI Particles," Pacific Northwest Laboratories Annual Report for 1972 to the USAEC Division of Biology and Medicine, BNWL 1650, Vol. II, Physical Sciences, Part 1 Atmospheric Sciences, BNWL 1650, pp. 79-82, 1972.

3. V. K. Saxena and N. Fukuta, "Field Applications of a New Cloud Condensation Nucleus Spectrometer: Investigation's of Continental and Maritime Aerosols," Preprints, International Conference on Cloud Physics, July, 1976, Boulder, Colorado. Avail, from Amer. Meteor. Soc., pp. 607-612, 1976.

A MICROPHYSICAL MODEL OF SCAVENGING BY ICE PARTICLES

B. C. Scott

Results are presented from case studies designed to examine the importance of particle configuration in determining the rate of growth and the scavenging ability of ice particles. The scavenging effectiveness of precipitation particles is linked to their ability to accrete pollution containing cloud water. Planar and columnar ice crystals are found to grow by deposition for several minutes before they begin to accrete cloud water. Conversion to spherical graupel takes an additional 9-10 min. By contrast, initially spherical ice particles are able to accrete cloud water almost immediately after their formation and are thus predicted to be the more effective scavengers.

INTRODUCTION

Understanding the details of incloud microphysics is important in describing the removal of pollutants by precipitation. Determination of the time available for pollutant to be incorporated into the cloud water and determination of how much of the cloud water contributes to precipitation at the surface are essential for describing the chain of events that lead to pollutant deposition at the ground. Numerical modeling is necessary for achieving these goals. The model described here is the first step in the development of a detailed microphysical, Eulerian model, where the effects of sedimentation, turbulence, and pollutant depletion can be combined with the growth, collection, and fallout of hydrometeors. A model with these features will be valuable in determining experimental design and interpreting field data.

The completed model will incorporate a variety of attachment mechanisms including Brownian diffusion, phoretic processes, impaction, nucleation and ad(de)sorption. The model will enable investigation of the

attachment of a gas or a polydispersed aerosol to a polydispersed spectrum of cloud particles which may be either water or ice. The model will also compute cloud supersaturation which will determine if the cloud particles are evaporating or growing, and hence, may have a significant influence on the dominant attachment mechanism. The ice phase will be incorporated into the model if preliminary modeling and field studies justify its importance as an effective scavenger. The tiny cloud droplets and ice particles in the model (which will develop on specified size distributions of CCN) will be allowed to evolve into precipitation through condensational (depositional) growth, coalescence, riming, and aggregation.

MODEL DESCRIPTION

At this stage of development, the model is a kinematic, Lagrangian model in which a single air parcel rises with constant velocity in a moist adiabatic environment. The parcel does not entrain surrounding environmental air and does not interact with parcels above or below through turbulent eddy fluxes. The initial cloud droplet spectrum is specified, is polydisperse, and is allowed to evolve with time through condensation only. The parcel is assumed to be imbedded within an existing cloud at an initial temperature of -9°C. The cloud supersaturation is computed and determines the depositional growth rates of the ice and water particles.

To determine which cloud particle type grows more rapidly (and hence effectively converts the greatest amount of pollutant containing cloud water into precipitation) several tests were made in which an initial "precipitation" particle was assumed to have different shapes and phases. Because of the myriad of ice particle shapes that can naturally occur in clouds, the selection of a representative ice particle shape is somewhat arbitrary. Generally the cloud temperature during the depositional growth phase determines the basic crystal shape (i.e., whether the crystal is planar or columnar) while cloud supersaturation and riming serve to decorate the crystal. Here, however, we assume a particular crystal shape regardless of temperature and supersaturation and examine the growth of that ice particle in an environment which is the same for each shape selected.

As the ice particles rime and become more irregular in shape, it is necessary to specify the particle dimensions so that proper fall velocities, capacitance values, and cross-sectional capture areas are known. The procedure outlined by Scott[1] is used to determine these values. Essentially, this procedure assumes that the length of the major axis is determined only by the depositional mass of the ice particle. The length of the minor axis is then allowed to slowly increase during riming until it equals the major axis length (i.e., the particle becomes spherical) when the riming mass equals seven times the depositional mass.

RESULTS

The results presented here are preliminary results from case studies designed to examine the significance of the shape and phase of individual water particles in determining the rate of growth to precipitation sized particles. The process is truely stochastic in nature, but because of the uncertainties involved in the dimensions and the collection efficiencies of the particles, the "continuous" growth mode due to capture has been assumed. The particular process being considered is the accretion or riming process. Here larger precipitation sized particles falling relative to the tiny cloud droplets (which may contain large amounts of pollutants) collide with and capture these small cloud droplets and ultimately transport them to the ground. Later studies will determine the amount of pollutant in these cloud droplets and will enable a more exact determination of scavenging ability.

Figure 1 illustrates the change in droplet size distribution produced by condensation in the ascending air parcel. The initial droplet size distribution has maritime characteristics and is bimodal with concentration peaks near 4.0 and 32.0 μm in diameter. The final size distribution, produced after about 12 min of ascent at 1.5m/sec, has a single mode at a diameter of 40 μm. During this vertical rise, the liquid water content associated with the cloud droplets has increased from 1.0 g m^{-3} to 1.6 g m^{-3}. For the case illustrated here, riming columns with a concentration of 1 ℓ^{-1} have reduced the droplet concentration from 70 cm^{-3} to 68 cm^{-3}.

The final droplet spectrum shown in Figure 1 is typical of a droplet population growing by condensation alone. If entrainment of air from outside the cloud had been included, the final droplet spectrum would have been broadened toward the smaller sizes. If coalescence, vertical mixing, and sedimentation had been considered, the final spectrum would have had an increased concentration of larger droplets.

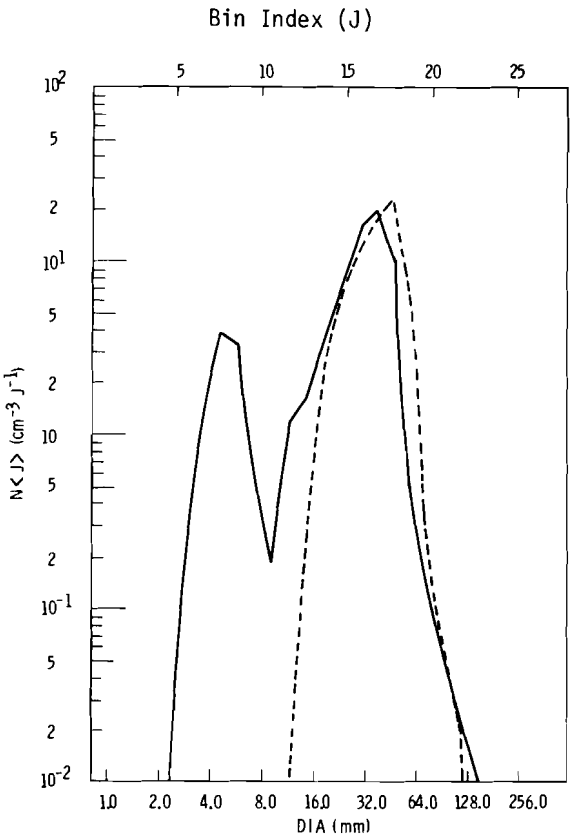

FIGURE 1. Initial Droplet Size Distribution (———) and Droplet Size Distribution at 700 Sec (-----).

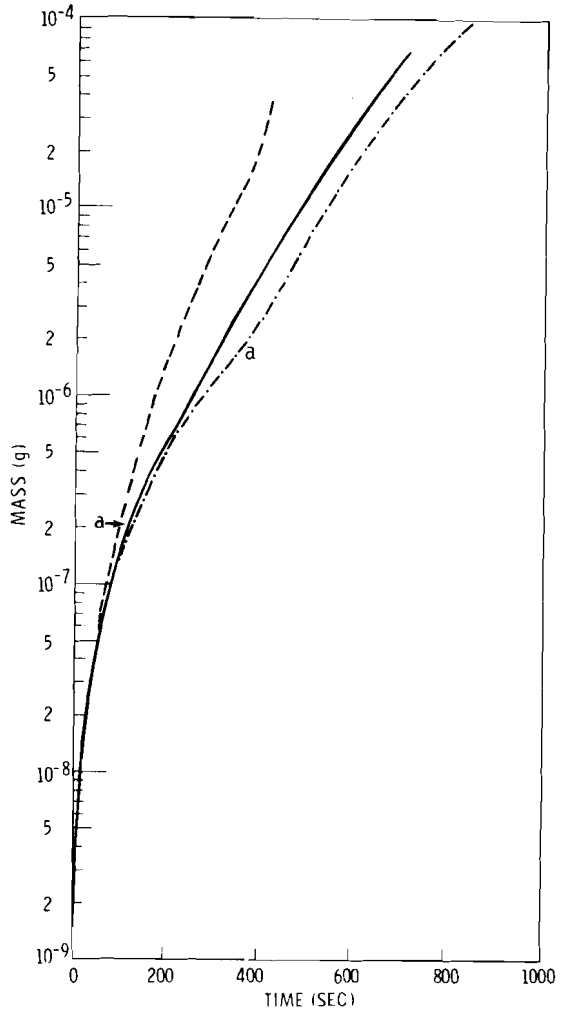

FIGURE 2. Ice Particle Mass as a Function of Time for (—·—) Plates; (———) Columns; and (- - - - -) Spherical Particles.

Figure 2 illustrates the mass growth rates of ice particles with initially identical masses, but with three different initial configurations. The character a drawn on the curves for the planar and columnar crystals indicates when the crystals have grown large enough by deposition to begin to accrete cloud droplets (riming).

As shown in Figure 2, the column crystals must grow by deposition for about 2 min before they begin to rime while the plate-like crystals must grow for 5 min before riming commences. Once both crystals are simultaneously riming, they accrete droplet mass at the same rate enabling the ratio of column mass to plate mass to remain nearly constant at 1.6. The plate and column crystals rime to spherical shapes (graupel) within 2 min of each other after about 13 min of growth. The initially spherical ice particles are, however, the more efficient rimers, and are able to accrete cloud water earlier and more rapidly than either crystalline particle. These spherical ice particles (assumed to be initially frozen droplets) behave similarly to liquid droplets and begin to accrete cloud water almost immediately after their formation. Indeed, after 7 min of growth, each spherical particle has accreted nearly 10 times the mass accreted by either a riming plate or column.

The primary difference between an ice phase and a liquid phase spherical particle is the rate of depositional (condensational) mass growth. Because of the difference in vapor pressure over water and ice, the depositional mass growth rate of the spherical ice particle is enhanced nearly a factor of

100 over that of the liquid drop. Thus, within 2 min, the spherical ice particle has grown from its initial diameter of 8 μm to about 95 μm and is beginning to accrete substantial amounts of cloud droplets. By contrast, a liquid droplet takes roughly 10 min to grow to the same 95 μm dimension under similar environmental conditions.[1]

CONCLUSIONS

These results are important for two reasons. First, they demonstrate that ice particle shape must be considered when considering growth of ice particles in natural clouds; and secondly, they help to identify the time scales available for different attachment mechanisms. An ice particle growing by deposition alone is likely to acquire aerosol pollutant mass primarily by Brownian diffusion and inertial capture. An ice particle growing primarily by accretion of cloud water can acquire additional large amounts of pollutants, both soluble and insoluble, contained within the cloud water. That is, riming should significantly enhance the apparent scavenging ability of ice particles. The results indicate that under typical cloud conditions and within 5 min of nucleation, most ice particles should begin to rime. The initially spherical particles will be the favored scavengers. However, within 15 min of ice nucleation, and in a relatively moist cloud (1 g m^{-3} of liquid water) all ice particles should have rimed to quasi-spherical or irregular shapes. Further studies will determine the significance of drop size distribution and liquid water content on these conclusions.

References

1. B. C. Scott, "Theoretical Study of the Evolution of Mixed-Phase Cumulus Clouds." PhD Dissertation, University of Washington, 269 pp., 1976.

PRECIPITATION SCAVENGING OF TRITIATED WATER VAPOR: A CONTROLLED-RELEASE FIELD EXPERIMENT

M. Terry Dana, M. A. Wolf, N. A. Wogman

A precipitation scavenging field experiment, using tritiated water vapor as the tracer, was conducted on the Hanford diffusion grid. The release mechanism was designed to promote thorough evaporation and mixing of the vapor before introduction into the humid ambient air. Concentration results compare favorably with estimates made from reversible gas scavenging theory.

Radioactive gaseous emissions from nuclear facilities have been the subjects of considerable research in assessment of environmental effects and development of control technologies. Increasing concern is being expressed over the effects of release of ^{85}Kr, ^{131}I, and the compounds of tritium (^{3}H); this is due to the general proliferation of fission power plants, but it is also due to the proposed expansion of fuel

reporcessing activities, and the projected use of controlled thermonuclear reactors (CTR) for power production. Current CTR designs promise that large amounts of tritium will be available for release under accident conditions, and that regular emissions will be somewhat greater than those from existing fission plants.[1]

The precipitation scavenging properties of tritium have been treated in detail theoretically[2] and the consequences of regular release and accident situations assessed.[1] There remains, however, a paucity of field experimental data on below-cloud scavenging of tritium. The only available data concerns long-range scavenging of tritium from bomb test debris.[3]

A model program of controlled-release field experiments was instituted as one task of the Precipitation Scavenging program. This effort is an attempt to acquire some experimental data which will be useful in testing the validity of gas scavenging theories.

The tritium compound chosen for the initial experiments was tritiated water vapor (HTO). Tritium is expected to be primarily in this form in the atmosphere, particularly during rainy conditions.[1] The experimental design--details of which will be described in a forthcoming publication[4]--involves the release of a controlled amount of HTO (about 0.5 Ci mixed with a few mℓ of H_2O) from the Hanford Meteorology Tower, and collection of precipitation on downwind sampling arcs of the existing diffusion grid. Samples collected cross-plume at two distances downwind are subjected to standard radiation counting techniques; the resulting concentrations and deposition patterns then may be interpreted in terms of scavenging rates and compared with theoretical estimates.

Since HTO behaves similar to H_2O chemically, the release must be done such that the tracer is completely vaporized on release, and subject to sufficient diffusion so that condensation does not occur immediately. This is accomplished by injecting the liquid at a slow rate (about 0.2 mℓ/min) from a syringe into the air stream from an electric heat gun. The air stream is confined to a 2.5 cm diameter plastic tube long enough that the injected water becomes thoroughly mixed and evaporated in the hot dry air stream prior to release to the humid ambient atmosphere.

The one experiment conducted to date, called HTO-1, was held on April 8, 1976, during a period of light prefrontal rain. Meteorological and source data are listed in Table 1, and concentration results, expressed in pCi/cm^3 (adjusted to the volume of rain collected during the release) are listed in Table 2.

Theoretical estimates for the run conditions were calculated using the EPAEC gas scavenging model described elsewhere.[2,5] A bivariate normal plume model was employed in the model, with plume parameters derived from the wind record for the source height. Standard deviations of plume spread were assumed to be the product of sampling distance and the standard deviations of wind angles. The experimental results compared favorably with the two reversible scavenging limiting cases shown in Table 2. While the actual concentrations are closest to the "stagnant drop" case (limited liquid phase mixing), the difference between the two cases is comparable to uncertainties arising from the use of idealized plume and raindrop size spectrum parameters, so no conclusions can be drawn about the preferability of one case or the other. Calculations based on irreversible scavenging, or perfect solubility of HTO in H_2O, led to concentration estimates much larger than those observed, however.

TABLE 1. Experimental Data, Run HTO-1

HTO Release Rate Q	3.3×10^{-4} Ci/sec
HTO Release Height h	60 m
Mean Wind Velocity[a]	5.4 m/sec
Predominant Wind Direction[a]	281 degrees
Downwing Sampling Distances x	400,800 m
Standard Deviation of Wind Angles[a]	
Elevational σ_ϕ[b]	0.035 radian
Azimutal σ_θ	0.140 radian
Ambient Temperature[a] T	11 C
Rainfall Rate J	0.6 mm/hr

a. At release height
b. Estimated

TABLE 2. Observed Concentration Results and EPAEC Model Estimates, Run HTO-1

Sampling Distance x, m	Sample Position,[a] degrees	HTO Concentration, pCi/cm³ Observed[b] NF[c]	Observed[b] F[d]	Theoretical Gas Phase Controlled	Theoretical Stagnant Drop
400	82	0		18	8.6
	90	41.8		79	38
	98	77.0	80.0	130	68
	106	67.4		79	38
	114	1.7	0.8	18	8.6
	122	0		0	0
800	82	0		16	8.5
	88	4.8		22	10
	94	25.1		50	23
	100	27.5	31.3	67	33
	106	24.9		50	23
	112	2.9	3.7	22	10
	118	0		16	8.5

a. Bearing from source point, relative to true north
b. Corrected to volume of rain collected during HTO release and background of 0.3 ci/cm³
c. Nonfreezing collector
d. Freezing collector (collector bottle packed in dry ice).

References

1. D. S. Renne, W. F. Sandusky and M. Terry Dana, An Analysis of Tritium Releases to the Atmosphere by a CTR, BNWL-1938, Battelle-Northwest, Richland, Washington, 1975.

2. J. M. Hales, Scavenging of Gaseous Tritium Compounds by Rain, BNWL-1659, Battelle-Northwest, Richland, Washington, 1972.

3. M. H. Dickerson and T. V. Crawford, In-Cloud Precipitation Scavenging of Tritiated Water Vapor, UCRL-51283, Lawrence Livermore Laboratory, Livermore, California, 1972.

4. M. Terry Dana, N. A. Wogman and M. A. Wolf, "Precipitation Scavenging of Tritiated Water Vapor: Field Experiment," submitted to Atmos. Environ., 1976.

5. J. M. Hales, M. A. Wolf and M. Terry Dana, "A Linear Model for Predicting the Washout of Pollutant Gases from Industrial Plumes," AIChE Journal, 19(2), pp. 292-297, 1973.

SUBMICRON AEROSOL WASHOUT EXPERIMENT: PROGRESS SUMMARY[a]

N. S. Laulainen

Progress of an experiment designed to measure submicron aerosol precipitation scavenging rates by monitoring changes in the particle size distribution of ambient atmospheric aerosols as a function of time during a precipitation event is summarized. Inspection of some preliminary data collected during the winter season at the Hanford Meteorological Station indicates that such an experiment is feasible.

INTRODUCTION

This report describes an experiment to study precipitation scavenging of submicron aerosol in the atmosphere and summarizes efforts to date to carry out this experiment. The experiment attempts to infer scavenging rates from changes in the ambient aerosol size distribution during precipitation episodes. Preliminary discussions of this type of experiment have appeared elsewhere.[1,2]

Efforts so far have been largely devoted to experimental setup, testing several sampling and analysis procedures and examining weather records for frequency of favorable precipitation events. Continuation of this effort is planned for the winter season 1976-77, contingent upon favorable weather conditions.

The key experimental features of the experiments discussed in this report are:

1. Quantitative estimates of true scavenging are made by direct use of the continuity equation.

2. Improved submicron aerosol scavenging estimates are determined by measurement of primary (dry) and secondary (wet) particle sizes and application of existing scavenging theory.

3. Practical methods for estimating scavenging of submicron aerosol from the atmosphere should be a direct result of this study.

The simplest example of an experiment based on the continuity equation is the case of a stationary air mass with no sources external to the sampled volume and no net introduction of particles by transport. Stagnant air parcels, such as those found in basins, may represent an example of such a condition. Prefrontal overrun, although bringing in new upper-level air, is not mixed with the trapped parcel. Precipitation can descend through the test parcel without being diluted or altered except by scavenging. Situations simular to those described occur frequently in the Columbia Basin area of Central Washington during the winter months.[3]

Only a few below-cloud scavenging experiments have been conducted on ambient atmospheric aerosol. Radke et al.[4] sampled the particle size distribution in a plume downwind from a Kraft-process paper mill before and after a rain shower. Scavenging efficiencies as a function of particle size were inferred from differences in the two size distributions, along with measurements of the raindrop distribution. Graedel and Franey[2,5] have carried out experiments similar to those discussed in this paper, to infer scavenging rates during both rain and snow events. Their results indicate, however, that air mass or source changes may have contaminated some of their data. Willeke et al.[6] also have reported changes in measured aerosol size distributions during precipitation events which they attribute to scavenging.

EXPERIMENTAL SETUP

A versatile sampling system capable of meeting the requirements imposed by the

a. A more complete version of this report appears as BNWL-2176.

scavenging experiment outlined above has been assembled and installed in the Battelle/Atmospheric Sciences motor laboratory. The motor laboratory gives the experiment mobility; an optimum sampling location can be chosen without having to provide external electrical power to run the sampling instrumentation since an onboard generator is available. Moreover, it provides shelter for the equipment as well as personnel.

Sampling Line. A schematic diagram of the sampling manifold is shown in Figure 1. The practical feature of this manifold is the all-glass segmented construction; sampling port configurations may be easily modified by replacing a 3 ft section with the desired section. Provision for monitoring temperature and relative humidity in the sample stream is also possible. Air is continuously drawn through the sampling line by a Dayton Air Pump, nominally rated at 160 cfm.

Aerosol Samplers. Complete characterization of the ambient aerosol requires extensive particle sampling using a variety of samplers or sampling techniques, depending on the type of information about the particles desired. In this study, information on the time evolution of the aerosol size spectrum, as well as knowledge about that aerosol component which is active through condensational growth are of particular interest. To monitor aerosol concentrations in various size classes, the instrumentation listed in Table 1 has been chosen. With the exception of the scanning electron microscope, which will be discussed separately, data collected by these instruments allows more or less real-time analyses of the particle spectra.

AEROSOL CHARACTERIZATION STUDIES

Aerosol characterization studies were carried out while assembling and testing the sampling system. The days during which both Whitby and Royco aerosol size distribution data were taken are summarized in Table 2.

All air samples, except those taken in March 1976, were taken in the vicinity of the 622 R Meteorology Building. Effects of local vehicular traffic were easily seen on chart recordings of the CN-count. Samples were taken only when the CN-count was near its background level. The March samples were obtained near the 122 m meteorology tower, 500 m east of the weather station. Effects of local traffic were minimized to some extent, although on 12 March, the sampling site was occasionally downwind of a smoke stack located in the 200-West area.

As can be seen in Table 2, a wide range of meteorological conditions were encountered during the sampling period. Aerosol loading and the character of the particle size distribution were also quite variable during this same period, as indicated in columns 6 and 7, where dN/dlogD is the number size distribution evaluated at a particle diameter D_p=1 μm and β' is the exponent of a power law fit to the data in the region 0.4 μm to 5 μm of the form:

$$\frac{dN}{d\log D} \propto D_p^{-\beta'} \qquad (1)$$

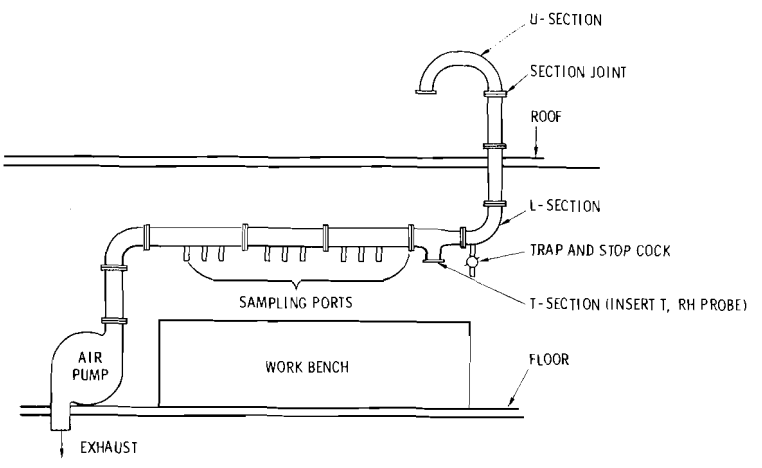

Neg 75182-1

FIGURE 1. Schematic Diagram of Sampling System, Installed in Battelle Motor Laboratory

TABLE 1. Particle Measurement Instrumentation

Type	Particle Size Range (μm)	Response or Sampling Time (min)	Comment
CE Condensation Nucleus Counter (Optical)	≲0.01	<0.1	
Whitby Electrostatic Aerosol Analyzer	0.01-0.5	1-2	9 useful size channels
Royco Model 220 Optical Particle Analyzer	0.5-5.0	~1	12 or 13 useful size channels plus total
Integrating Nephelometer (MRI)	0.01-1.0	<0.1	Total light scatter in 0.1 to 1.0 μm range
Scanning Electron Microscope (SEM)	≳0.1	10-60	Nuclepore filter samples

TABLE 2. Summary of Sampling Times, Aerosol Characteristic and Meteorological Conditions

Date Da Mo Yr	Time Interval (PST)	No. of Samples	RH-Range (%)	T-Range (°F)	$dN/d\log D\|_{1\mu m}$ (#/cm^3)	β'	Comments
17-12-75	0953 - 1410	3	80 - 60	29 - 37	4.5 - 3.5	2.4 - 2.2	Clear to scattered
18-	0844 - 1440	4	92 - 68	22 - 35	4.5 - 3.5	2.7 - 2.4	Clear
19-	0837 - 0849	2	99	20	2.0	3.7	Fog
22-	0838 - 1252	3	94 - 80	29 - 35	6.0	3.3	Fog, overcast
23-	0913 - 1300	5	88 - 92	30 - 32	4.0	4.1	Snowing, fog
29-	1116 - 1409	5	92 - 86	92 - 86	~10	~3	Overcast
30-	1129 - 1300	2	46 - 36	43 - 46	1.7 - 1.2	1.9 - 1.8	Very clean air, windy, broken
31-12-75	0922 - 1250	2	62 - 52	38 - 40	0.4	1.7 - 1.4	Overcast, KFR 0300
05-01-76	1000 - 1005	1	86	32	1.4	3.1	Overcast
07-	1431 - 1436	1	99	31	2.0	3.5	Snowing
08-	0821 - 1340	3	99 - 92	27 - 32	0.4 - 0.8	3.1	Fog to, clear
09-	0935 - 1316	4	98 - 67	21 - 39	0.5 - 1.0	3.3 - 1.3	Light ground fog, clear
12-	1116 - 1342	2	60 - 47	41 - 45	3.5 - 1.6	2.5 - 1.9	Clear
13-	0856 - 1433	3	85 - 66	30 - 34	0.9	2.1	Overcast
14-01-76	0831 - 1458	5	96	28 - 36	0.8 - 2.0	2.8	Overcast, fog
15-01-76	1106 - 1111	1	70	40	0.2	2.7	Overcast
16-	1328 - 1455	3*	72	50	2.0	3.1	Clear
19-	0855 - 1120	8*	92 - 75	26 - 36	1.0 - 0.9	2.8 - 2.3	High, broken
20-	0841 - 1307	3*	92 - 64	80 - 39	4.0 - 1.6	3.1	Clear to scattered
21-	0850 - 1349	7*	99 - 98	29 - 30	8.0 - 5.0	3.3 - 3.5	Fog, freezing drizzle
22-	1007 - 1253	2	99 - 94	29 - 30	4.5	3.7	Fog, overcast
23-	1055 - 1100	1	82	33	1.7	3.7	Clear
26-01-76	1355 - 1410	2	98 - 97	29	~4	~3.8	Fog
02-02-76	1006 - 1330	3	95 - 89	32 - 33	1.6	4.4	Overcast, calm
03-	0837 - 1439	3	80 - 58	31 - 40	0.6 - 1.9	3.8 - 2.0	Snowing lightly, pm, KFB 1555
05-	0911 - 1442	3	72 - 22	24 - 32	~1	~1.8 - 2.7	Clear
06-02-76	0941 - 0946	1	59	27	2	2.3	Clear
08-03-76	0857 - 0902	1	78	36	4	2.5	High, scattered
09-	1055 - 1523	2	52 - 58	54 - 64	3.5 - 0.7	2.7 - 2.2	High, overcast
11-	0829 - 1453	3	48 - 20	43 - 50	1.8 - 2.0	2.0 - 0.6	Blowing dust, pm, clear
12-	0840 - 1404	6	68 - 43	29 - 50	~3.0	~1.5	Overcast, KFR 1820

*Explained in text.

Scanning Electron Microscope Analysis of Filter Samples

Several experiments were conducted to determine the best means of collecting the particle samples. One of the goals of the direct collection approach was to achieve at least some particle size separation on the filters so that giant particles or droplets (size $\gtrsim$ 5 μm) could be distinguished from submicron particles. Another goal was to select a method which allowed a sample to be obtained in 10-60 min.

Of the several methods tested, a multistage Nuclepore filter assembly with filters of decreasing pore size was finally chosen. Several tests were conducted under different meteorological conditions and with different combinations of pore sizes, number of filter stages, and filter types. Filter samples were then analyzed with a scanning electron microscope. An exposure taken under dry and dusty conditions, on 26 April 1976, using a three stage assembly of 5.0 μm, 0.8 and 0.2 μm Nuclepore filters and a sampling time of 60 min, is shown in Figure 2. There appears to be a general tendency for particles smaller than ∿1 μm to be roughly spherical while those larger than ∿1 μm to be irregularly shaped.

The idea of using nuclepore filters as crude particle size classifiers is not unique. Spurny et al.,[7] investigated particle discrimination by three identical filters of pore size 2 μm in series, each filter operating at a different face velocity, and found that a nearly monodisperse component can be extracted from a polydisperse aerosol stream. They have also found that any sort of particle detector sampling the aerosol stream before and after passage through a single filter at a given face velocity, can indicate the size distribution.

During the preliminary tests, there were a few precipitation episodes which may have been suitable to conduct a scavenging experiment; these events occurred before the entire sampling system was completed. The data on some of these occurances give some qualitative indication that the technique could yield scavenging rates. On 25 December 1975, precipitation occurred in the form of a light snow (3.1 in. total over an 11 hr period beginning at 0600). Winds were out of the NW at 5 mph. Size distributions measured at ambient humidity during this episode are shown in Figure 2, where a clear decrease in concentrations for particles larger than ∿2 μm is seen over the time interval of the measurements. The submicron particle concentrations show either no or irregular changes during the same time interval, the latter presumably due to changes in particulate sources and/or air mass change, perhaps by advection.

Fog and trace freezing drizzle occurred on 21 January 1976. A significant decrease in particle concentration occurred for all measured size classes between the morning and afternoon observations (see Figure 3). Because there was little or no wind during that same interval, the decrease appears to relate to relative humidity changes or attachment of aerosol particles to fog droplets. Scavenging by the freezing drizzle was probably negligible.

Clearly, these examples only represent a fraction of the data collected and summarized in Table 2. On the other hand, the examples were selected to be representative of the kinds of changes of aerosol size distributions encountered during the winter months. For scavenging work, it is of course vital to be able to distinguish scavenging effects from all the other effects--a task which is by no means trivial.

INTERPRETATION OF SCAVENGING DATA

A general approach to the scavenging problem is to make use of a form of the continuity equation, such as

$$\frac{\partial N_i}{\partial t} = -\nabla \cdot N_i V_i - w_i + G_i, \quad i = 1,2,\ldots n \tag{2}$$

where w_i and G_i are wet removal and generation rates, respectively, of aerosol in the size range a_i to $a_i + da$. Usually w_i is set equal to $\psi_i N_i$, where ψ_i is the differential washout coefficient for this size range. The generation term may contain mechanisms such as condensation, coagulation and nucleation. The divergence term includes advection and diffusion of aerosol into and out of the study volume.

For the case where there are no external sources and no net introduction of particles by transport into the sampled volume element as well as no condensational growth (e.g. growth started prior to the experiment) or other generation during the precipitation episode, Equation 2 reduces to the familiary Equation 3.

$$\frac{dN_i}{dt} = -\psi_i N_i \tag{3}$$

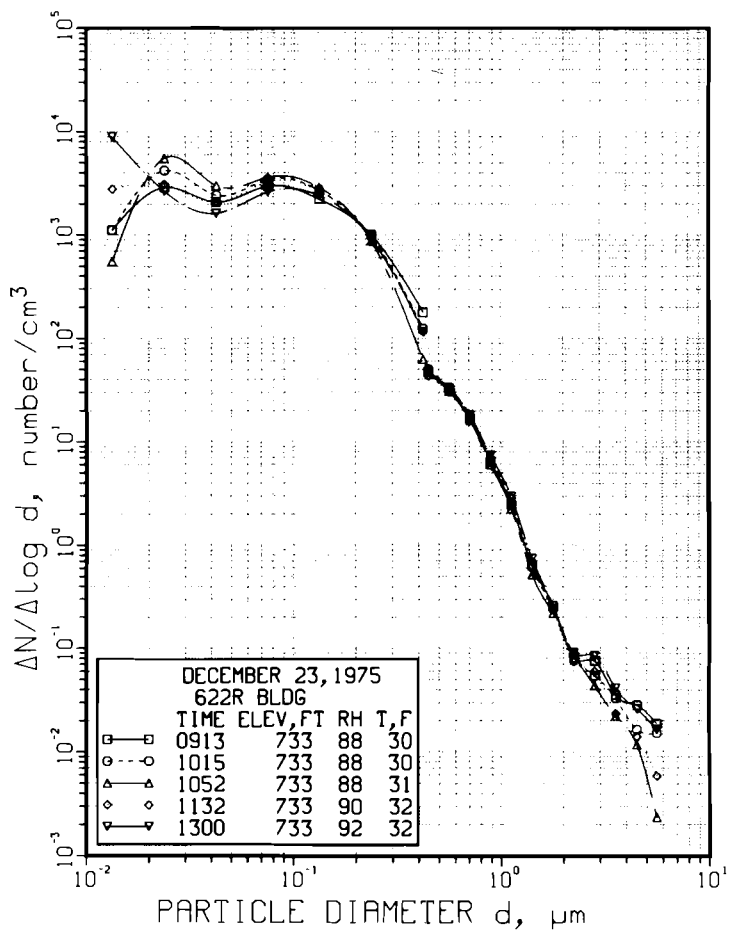

FIGURE 2. Aerosol Number Size Distributions for 23 December 1975

If some of the preceeding restrictions are relaxed to allow for a nonnegligible generation term, then Equation 2 takes the form

$$\frac{\partial N_i}{\partial t} = -w_i + G_i. \qquad (4)$$

By using a known functional relationship between w_i and $\hat{a}_i$ (e.g. Reference 3), where $\hat{a}$, is the size of the secondary (wet) aerosol, Equation 4 can be used to verify w_i ($\hat{a}_i$) as well as to study the character of G_i from measurements of both primary and secondary aerosol sizes.

A more general situation may be examined in the case where outside sources are significant and constant. Prior to the precipitation episode, a steady state condition may be assumed to exist such that

$$-\nabla \cdot N_i \cdot V_i + G_i = 0, \qquad (5)$$

where some type of generation (e.g. photochemical) may be occurring in the sampled volume. With the onset of precipitation, a transient mode is established and the aerosol concentration is governed by the equation

$$-\nabla \cdot N_i V_i - w_i + \hat{G}_i = \frac{\partial N_i}{\partial t} \qquad (6)$$

which explicitly shows the effect of scavenging and the fact that more than one type of generation may be present. Eventually, assuming steady precipitation conditions, a new equilibrium may be established such that

$$-\nabla \cdot N_i V_i - w_i + \hat{G}_i = 0. \qquad (7)$$

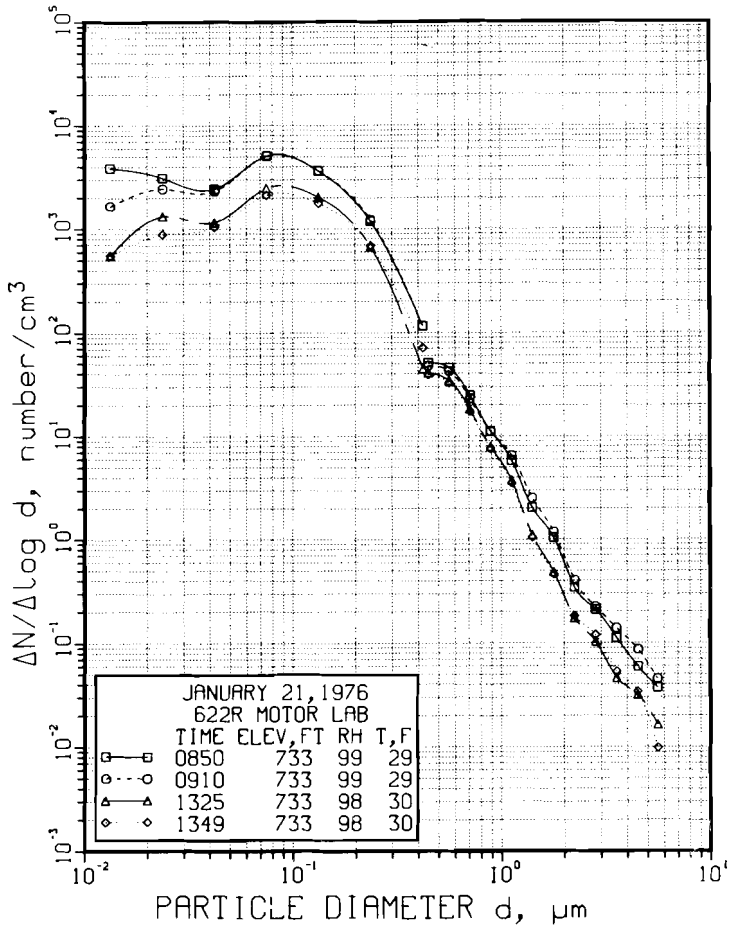

FIGURE 3. Aerosol Number Size Distributions for 21 January 1976

Suitable combination of Equations 5-7, along with measurements of both primary and secondary aerosol size spectra before and during a precipitation event, should provide valuable insights for verifying the functional relationship of w_i $(\hat{a}_i)$ as well as studying the importance of G_i and D_i relative to scavenging. Procedures for analyzing this type of experiment will be developed in a later report.

The possibility remains that the w_i are so small for submicron aerosol that the $\frac{dN_i}{dt}$ cannot be measured before the weather changes. In this case, it may only be possible to monitor the primary and secondary aerosol under no source conditions and to try to match the measured scavenging rates (normalized with respect to precipitation rate) with those obtained from theory by accounting for growth (or attachment) in a phenomenological or empirical manner and incorporating the particle size changes into the theory.[8] By examining both primary (dry) and secondary (wet) aerosol, the fraction of particles which are active in the growth processes can be estimated. This information also can be used to keep track of the size classes the particles start out from and the size classes from which they are eventually scavenged.

References

1. N. S. Laulainen, "Below Cloud Scavenging of Aerosols: Some Ideas for Improved Measurements," Pacific Northwest Laboratory Annual Report for 1974 to the USAEC Division of Biomedical and Environmental Research, Part 3, Atmospheric Sciences, BNW-1950 PT3, Battelle Northwest, Richland, Washington, February 1975, pp. 109-113, 1975.

2. T. F. Graedel and J. P. Franey, "Field Measurements of Submicron Aerosol Washout by Rain," R. W. Beadle and R. G. Semonin, coords., Precip. Scav. - 1974. ERDA Sympos. Series, (Available as CONF-74014 from NTIS, Springfield, Virginia), 1975.

3. J. M. Thorp, "Characterization of Pre-Frontal Winter Precipitation in Eastern Washington," in this report.

4. L. F. Radke, E. E. Hindman, II and P. V. Hobbs, "A Case Study of Rain Scavenging of Aerosol Particles from an Industrial Plume," (ibid Reference 2), 1975.

5. T. F. Graedel and J. P. Franey, "Field Measurements of Submicron Aerosol Washout by Snow," Geophys. Res. Letters, 2, pp. 325-328, 1975.

6. K. Willeke, W. E. Whitby and V. A. Marple, "Size Distributions of Denver Aerosols--A Comparison of Two Sites," Atmos. Environ., 8, pp. 609-633, 1974.

7. K. R. Spurny, J. P. Lodge, Jr., E. R. Frank and D. C. Sheesley, "Aerosol Filtration by Means of Nuclepore Filters: Aerosol Sampling and Measurement," Environ. Sci. Technol., 3, pp. 464-468, 1969.

8. W. G. N. Slinn, "Some Approximations for the Wet and Dry Removal of Particles and Gases from the Atmosphere," BNWL-SA-5489, to be published in Proc. 1st Int. Symp. on Acid Precipitation and the Forest Ecosystem and J. Air, Water and Soil Pollution, in press, 1976.

POLLUTANT TRANSFORMATIONS AND INTERACTIONS

Comprehensive assessment of atmospheric pollution effects is not possible unless the pollutant transformations, both physical and chemical, which occur between source and receptor are known. The efficiency with which the pollutants are removed from the atmosphere depends on the physical and chemical state of the pollutants. Health and ecological hazards depend on the nature of the pollutants reaching the receptors, regardless of the pollutants leaving the sources.

The primary pollutant transformation reported here is the SO_2 to sulfate particulate transformation in power plant and urban plumes. Reports describe: a field measurement program in which the Milwaukee plume was sampled over Lake Michigan; measurements of physical characteristics such as particle size distributions, and related phenomena such as light scattering and turbidity; models which complement and guide field measurements; and hardware and software developments. We are also involved in the MAP3S program; contributions include airborne measurements of pollutants in the northeastern United States and subsequent analysis and modeling efforts.

- AEROSOL AND TRACE GAS TRANSFORMATIONS
- RESEARCH AIRCRAFT OPERATIONS

ESTIMATION OF TRANSFORMATION RATE OF SO_2 TO SO_4 FROM ATMOSPHERIC CONCENTRATION DATA[a]

A. J. Alkezweeny and D. C. Powell

The transformation rate of SO_2 to sulfate is estimated from data collected by aircraft following a tetroon northeast of St. Louis, Missouri, on August 10 and 11, 1975. Assuming deposition velocities of 1 cm s^{-1} and 0.1 cm s^{-1} for SO_2 and sulfate, respectively, the analysis including 90% confidence limits, yields a rate of 0.14 ± 0.04 hr^{-1} for the first day, and 0.10 ± 0.02 hr^{-1} for the second. The confidence limits do not preclude the likelihood that the rate was the same for both days, in which case it would have been 0.10 to 0.1 hr^{-1}.

INTRODUCTION

Within the last few years, several estimates have been made of the transformation rate of SO_2 to sulfate in the ambient atmosshere. Some of these estimates include a range of an order of magnitude. For example, Cox[1] estimated a transformation rate of 0.01 to 0.10 hr^{-1} in an urban plume for photo-oxidation with NO_x and hydrocarbons, or thermal oxidation with ozone and olefins. Roberts and Friedlander[2] found the total oxidation rate to vary from 0.012-hr^{-1} to 0.13 hr^{-1} in the Los Angeles basin. A recent review of oxidation rates[3] gave a rate of 0.016 to 0.133 hr^{-1} for the homogeneous gas phase reaction and 0 to 0.06 hr^{-1} for heterogeneous catalyst oxidation. Since these rates are additive, they imply that the transformation rate can be anywhere from 0.02 to 0.20 hr^{-1}. Other investigators seem to favor the lower ends of such ranges. Eliassen and Saltbones[4] imply a transformation rate of about 0.007 hr^{-1}. Smith and Jeffrey[5] present a graph plotting conversion to sulfate as a function of relative humidity. Interpretation of their graph indicates rates of about 0.03 hr^{-1} at 75% r.h. and about 0.12 hr^{-1} for 88% r.h. Between those two figures the relation is depicted as roughly linear, and no figures are given for lower levels of r.h. Dana, et al.[6] found that under some circumstances, a significant portion of the SO_2 in a power plant plume is converted to sulfate within 0.4 km of the stack during rain. Other work on the transformation of SO_2 to sulfate in urban plumes is being conducted in St. Louis[7,8] as part of the EPA-MISTT program. Unfortunately, the transformation rate was not reported.

This paper presents preliminary results of a field experiment conducted near St. Louis, Missouri, and the subsequent modeling effort directed toward estimating a transformation rate. Since the transformation rate is apparently influenced by conditions in a manner not well understood, those pertaining to the particular flights are described in detail so that this article may aid in bringing about a future consensus.

---

a. Atmospheric Environment in Press.

THE EXPERIMENT

The experiment was conducted northeast of St. Louis, Missouri, during the summer of 1975. The sampling equipment was carried onboard a DC3 airplane, and the measurements were made while the airplane was following a 0.94 m^3 tetroon[9]. The tetroon was launched from the Civic Memorial Airport in Alton, Illinois, and rose to an altitude of 900 to 1200 m above sea level. The procedure for deploying the tetroon was that described by Hoecker[10]. Before and during each flight, pibal data were collected to determine wind speed and direction. The tetroon was launched an hour after the DC3 took off to allow for instrumentation calibration and stabilization.

Two flights were initiated at approximately 1400 CDT, one on August 10, and the other on August 11. August 10 was characterized by clear to scattered cumulus in the morning, and brief scattered to broken altocumulus in the afternoon. The mean wind speed was about 7 ms^{-1}, and the mixing depth about 1400 m. The average temperature and relative humidity were 21°C and 60%, respectively. The tetroon traveled to the north at first. About 1-1/2 hr later, it drifted to the northeast and passed over Springfield, Illinois. August 11 was mostly clear, with some broken altocumulus and cirrus in the afternoon. The wind speed was about 6 ms^{-1} and the mixing depth was about 2400 m. The average temperature and relative humidity were 26°C and 53%, respectively. The flight path was to the northeast for the first 3 hr; after that the tetroon path changed toward the north.

The SO_2 concentration was measured with a flame photometric detector, the detectable limit being about 5 ppb. Particles were collected on IPC filters subject to an airflow rate of 50 cfm and later were analyzed by an X-ray fluorescence technique to determine the total sulfur in the aerosol. The SO_2 measurements were considered to have a standard error of 10%, and the sulfate measurements an error of 8.5%.

Figure 1 gives the concentrations of sulfur in SO_2 and sulfur in combined SO_2 and sulfate as a function of time for each of the two days. These concentrations are 20-min averages. The ozone level during the flights increased slightly with distance, and its concentration was about 200 ppb on August 10 and about 250 ppb on August 11. The NO and NO_2 levels were below 20 ppb.

The sulfur concentrations (Figure 1) shows a decrease in time reflecting the effects of diffusion, transformation and deposition.

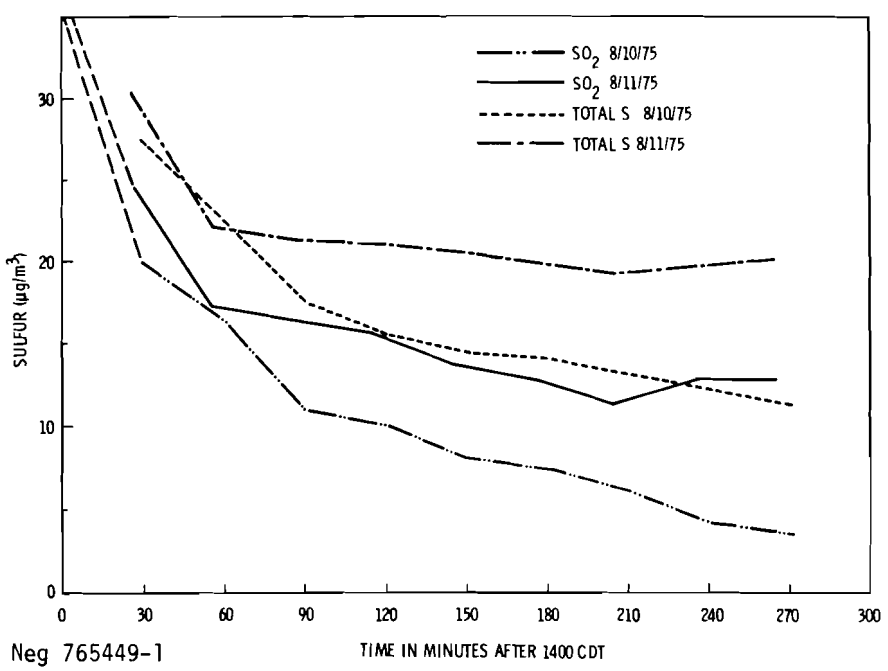

Neg 765449-1

FIGURE 1. Sulfur in SO_2 and Sulfur in Combined SO_2 and Sulfate as a Function of Time

After about 3.5 hr of flight time on August 11, an increase in the SO_2 concentration indicated entrainment of pollutant from a new source. This entrainment was also detected by a sudden decrease of the ozone level and an increase of the NO/NO_2 ratio.

ANALYTICAL METHOD

The variables used in the analysis are the logarithms of the ratios of sulfur in SO_2 to total sulfur as a function of time along a path following the tetroon. These data are shown in Figure 2. There is a least squares regression line through the points for each of the two dates. Here we assumed that the plot of points shows sufficient organization that further analysis is justified.

In the analysis to follow we make the following assumptions:

1. The diffusion of the SO_2 and the sulfate is the same.
2. The transformation of SO_2 to sulfate is a first order reaction.
3. The pollutant is evenly distributed vertically throughout the mixing layer at the times of sampling. This assumption seems reasonable for the slightly unstable conditions prevailing (see Deardorff and Willis)[11].

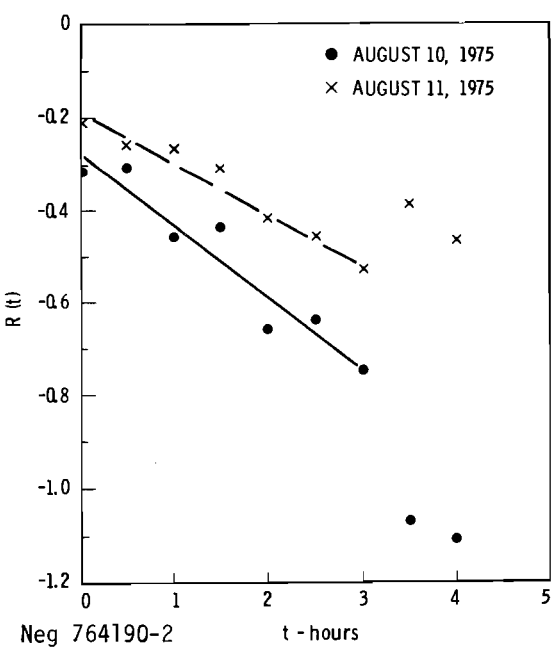

FIGURE 2. Logarithms of the Ratio of Sulfur in SO_2 to Total Sulfur as a Function of Time

The problem is treated as if the samples were collected within the same air parcel. The pertinent equations are those for the conservation of mass.

We employ the following definitions:

$X(t)$ = mass of sulfur in a "followed air parcel" in the form of SO_2

$Y(t)$ = mass of total sulfur in a "followed air parcel" in the form of sulfate and SO_2

k_g = dry removal rate for SO_2 (hr^{-1})

k_a = dry removal rate for sulfate (hr^{-1})

k = transformation rate of SO_2 to sulfate (hr^{-1}).

Equations for the conservation of sulfur mass are:

$$\frac{dX(t)}{dt} = -(k_g + k)X(t) \quad \text{and} \tag{1}$$

$$\frac{dY(t)}{dt} = -k_g X(t) - k_a[Y(t) - X(t)]. \tag{2}$$

Combining Equation (1) and (2) we get:

$$\frac{1}{r(t)}\frac{dr(t)}{dt} = -k - [1 - r(t)](k_g - k_a), \tag{3}$$

where $r(t) = X(t)/Y(t)$. Rearranging Equation (3), and integrating from $t = o$ to $t = T$ yields:

$$K = \frac{1}{T}\ln\frac{r(o)}{r(T)} - (k_g - k_a)\left[1 - \frac{1}{T}\int_o^T r(t)dt\right]. \tag{4}$$

Since the original data are in units of concentration, we wish to solve for a descriptor defined from concentrations. Let $C_g(t)$ and $C_a(t)$ be the concentrations of sulfur in SO_2 and sulfur in sulfate, respectively. Then the final descriptor is defined as:

$$R(t) = \ln\frac{C_g(t)}{C_g(t) + C_a(t)} \tag{5}$$

However, since the diffusion is always assumed to be the same, the concentrations refer to the same volume, $V(t)$, that is:

$$X(t) = C_g(t)V(t) \quad \text{and} \tag{6}$$

$$Y(t) = C_g(t)V(t) + C_a(t)V(t) \tag{7}$$

Therefore,

$$R(t) = \ln \frac{X(t)}{Y(t)} = \ln r(t). \quad (8)$$

To calculate k_g and k_a, we divide the deposition velocities by the depth of the mixing layer Δz to get:

$$k_g - k_a = \frac{1}{\Delta z}(V_g - V_a), \quad (9)$$

where V_g and V_a are the deposition velocities of SO_2 and sulfate. Substituting Equations (8) and (9) into (4), we get:

$$k = \frac{1}{T}[R(o) - R(T)] - \frac{1}{\Delta z}(V_g - V_a)$$

$$\left[1 - \frac{1}{T}\int_0^T e^{R(t)}\, dt\right], \quad (10)$$

where k is assumed to be independent of time or averaged over the time period T. A similar equation was derived by Roberts and Friedlander[2].

The equations for the least square regression lines on Figure 2 are in the form of

$$R(t) = -a - bt, \quad (11)$$

where a is equal to 0.276, and 0.190 and b is equal to 0.150 hr^{-1} and 0.108 hr^{-1} for August 10 and 11, respectively. Equation (11) is valid only for the first 3 hr of sampling time. For both days, data points beyond the seventh ones do not fit the linear regression. The last two points for August 10 are below the estimated detectable limit of the instrument, therefore, they are not expected to fit. On the other hand, the last two points measured on August 11 reflect excess entrained SO_2 as pointed out earlier. Substituting Equation (11) into (10) and using known values of a, b, t and z for each day, the final expressions for k are

August 10:

$$k_1 = 0.150 - 0.010(V_g - V_a) \quad (12)$$

and August 11:

$$k_2 = 0.180 - 0.004(V_g - V_a), \quad (13)$$

where V_g and V_a are in units of cm s^{-1} and k in hr^{-1}. The equations are plotted in Figure 3.

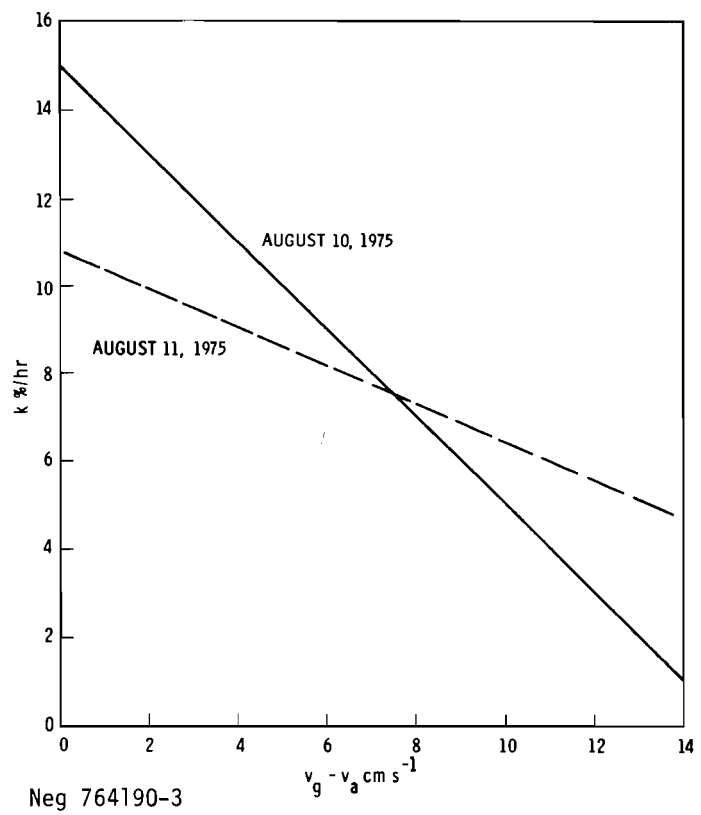

Neg 764190-3

FIGURE 3. Dependence of the Calculated Transformation Rate on the Deposition Velocities of SO_2 and Sulfate

RESULTS AND DISCUSSION

Figure 3 shows that the calculated transformation rate of SO_2 to sulfate depends on the deposition velocities of SO_2 and sulfate. A mean deposition velocity of about 0.8 cm s^{-1} was estimated by Owers and Powell[12] over the British Isles. Smith and Jeffrey[5] have independently arrived at the same result. Since these estimates are for a mixture of terrain and vegetation types, not significantly different from St. Louis area, they can be assumed to apply to the conditions of the present study. Other estimates are available. Garland, et al., (1974) obtained a value for short grass less than 1 cm s^{-1}. On the other hand, current estimates of the dry removal rate of sulfate place this figure at about one-tenth of the rate for SO_2.

If we assume a deposition velocity of 1 cm s^{-1} for SO_2 and 0.1 cm s^{-1} for sulfate, then from Figure 3, the transformation rates are 0.14 hr^{-1} and 0.10 hr^{-1} for August 10 and 11, respectively. These figures agree reasonably well with previous estimates given by Roberts and Friedlander[2] and by Levy, et al.[3]

The large difference in the transformation rates between the two days cannot be explained. This is partly because of the limited number of parameters measured during this experiment and partly because a dominant mechanism for the transformation of SO_2 to sulfate has not been established. However, one can speculate about the causes based on the meteorological conditions. The day with the higher transformation rate was characterized by higher relative humidity and lower temperature than the day with the lower transformation rate. If one assumes catalytic oxidation of SO_2 in the plume, these results are in agreement with the dependence of the oxidation rate on the temperature and relative humidity.[14]

Another possible cause for the difference is that the exponential function of time chosen to model the ratio (see Figure 2) may not be appropriate.

Examining Equations (10) and (11) we find, for the assumed deposition velocities, that the calculated values of k are dominated by the value of the linear regression slopes b. The 90% confidence limits for b are calculated from the data points and found to be 0.150 ± 0.037 hr^{-1} for August 10, and 0.108 ± 0.021 hr^{-1} for August 11. The corresponding values of k are k_1 = 0.14 ± 0.04 hr^{-1} and k_2 = 0.10 ± 0.02 hr^{-1}. From these figures we see that the confidence limits for k are not narrow enough to reject the hypothesis that the transformation rate was actually the same on both days. In this case, it would have to be between 0.10 hr^{-1} and 0.12 hr^{-1}.

The transformation rates calculated above are based on the actual data collected inside the urban plume. However, the suggestion has been made to subtract the sulfate background from the data before performing the calculation. The background sulfur in aerosol measured on the ground was 0.875 $\mu g/m^3$. This value was subtracted from the sulfate measurement and the calculation was then repeated. The transformation rates under the same assumed deposition velocities for SO_2 and sulfur are k_1 = 0.125 ± 0.023 hr^{-1}. Here again, if we assume the transformation rates are the same for both days, it will be 0.093 hr^{-1}.

CONCLUSIONS

Samples of SO_2 and sulfate taken by aircraft following the tetroon northeast of St. Louis, Missouri, on August 10 and 11 were analyzed to yield a transformation rate of SO_2 to sulfate. The rate depends on the deposition velocities used in the calculation. Assuming deposition velocities of 1 cm s^{-1} for SO_2 and 0.1 cm s^{-1} for sulfate, the analysis (including 90% confidence limits) yields a transformation rate of 0.14 ± 0.04 hr^{-1} for the first day and 0.10 ± 0.02 hr^{-1} for the second. The confidence limits do not preclude the likelihood that the rate was the same for both days, in which case it would have been 0.10 to 0.12 hr^{-1}.

ACKNOWLEDGMENTS

The authors wish to express their appreciation to Drs. R. L. Drake, J. M. Hales, and L. L. Wendell for their review of this paper and many helpful suggestions.

References

1. R. A. Cox, "Particle Formation from Homogeneous Reactions of Sulphur Dioxide and Nitrogen Dioxide." Tellus, XXVI, 235-240, 1974.

2. P. T. Roberts and S. K. Friedlander. "Conversion of SO_2 to Sulfur Particulate in the Los Angeles Atmosphere." Env. Health Perspectives, 10, 103-108, 1975.

3. A. H. Levy, D. R. Drewes and J. M. Hales. "SO_2 Oxidation in Plumes: A Review and Assessment of Relevant Mechanistic and Rate Studies." EPA report under preparation, 1976.

4. A. Eliassen and J. Saltbones. "Decay and Transformation Rates of SO_2, as Estimated from Emission Data, Trajectories and Measured Air Concentrations." Atmospheric Environment 9, 425-429, 1975.

5. F. B. Smith and G. H. Jeffrey. "Airborne Transport of Sulphur Dioxide from the U.K." Atmospheric Environment, 9, 643-659, 1975.

6. M. T. Dana, J. M. Hales and M. A. Wolf. "Rain Scavenging of SO_2 and Sulphate from Power Plant Plumes." Jour. of Geo. Res., 80, 4119-4129, 1975.

7. R. B. Husar, J. D. Husar, N. V. Gillani, S. B. Fuller, W. H. White, J. A. Anderson, M. W. Vaughn, and W. E. Wilson, Jr. "Pollutant Flow Rate Measurement in Large Plumes: Sulfur Budget in Power Plant and Areas Source Plumes in the St. Louis Region." Presented at 171 A.C.S. meeting, New York City, April 4-9, 1976.

8. W. H. White, J. A. Anderson, D. L. Blumenthal, R. B. Husar, N. V. Gillani, S. B. Fuller, K. T. Whitby, and W. E. Wilson, Jr. "Formation of Ozone and Light-Scattering Aerosols in the St. Louis Urban Plume." Atmospheric Environment, 9, 1975.

9. A. J. Alkezweeny, "The Growth of Aerosol in an Urban Plume." Paper prepared for presentation at the 12th International Symposium of Atmospheric Pollution, Institute National de Recherche Chemique Appliquee, Paris, France, May 5-7, 1976.

10. W. H. Hoecker. "A Universal Procedure for Deploying Constant - Volume Balloons and for Deriving Vertical Air Speeds from Them." Jour. Appl. Met., 14, 1118-1124, 1975.

11. J. W. Deardorff and G. E. Willis. "A Parameterization of Diffusion in the Mixed Layer." Jour. of App. Met., 14, 1459-1477, 1975.

12. M. J. Owers and A. W. Powell. "Deposition Velocity of Sulphur Dioxide on Land and Water Surface Using a ^{35}S Tracer Method." Atmospheric Environment, 8, 63-67, 1974.

13. J. Freiberg. "Effects of Relative Humidity and Temperature on Iron-Catalized Oxidation of SO_2 in Atmospheric Aerosols." Environmental Science & Technology, 8, 731-734, 1974.

SO_2 TO SULFATE CONVERSION IN AN URBAN PLUME

A. J. Alkezweeny

A pseudo-first order oxidation rate of 9.8% per hour is calculated from SO_2 and sulfate data. The data was collected by an airplane sampling in the vicinity of a tetroon downwind of St. Louis, Missouri.

An experiment made on August 17, 1975 near St. Louis, Missouri, was run to determine the conversion rate of SO_2 to sulfate. The experiment was conducted in a Lagrangian frame of reference. The trajectory of an air parcel containing the pollutant was approximated by the movement of a constant volume balloon. An instrumented DC3 airplane was used to sample the pollutant in the vicinity of the balloon. The SO_2 concentration was measured by a flame photometric detector. The aerosol particles were collected on a quartz filter at the rate of 8.2 cfm for a period of 50 min, and were later analyzed for sulfate by turbidometric method.

The balloon was launched from the Civic Memorial Airport in Alton, Illinois, northeast of St. Louis, at about 1230 CDT and rose to about 600 m MSL, headed toward St. Louis. The balloon descended to 300 m and rose again to 1000 m at about 1255 CDT. At this point, the balloon was near the base of cumulus clouds. At 1300 CDT, the balloon changed direction and headed back toward the airport and south of it. Then it drifted around the airport in a counterclock fashion, ending north of the airport at about 1620. During this time the balloon altitude fluctuated between 750 to 1000 m. The visibility was estimated to be in the range of 6 to 16 km with scattered clouds based at about 1000 m and broken clouds whose bases were at 1100 m. The top of the mixing was estimated at 1300 m MSL. The average temperature and relative humidity at the sampling level were 23°C and 76.3%, respectively. The vertical profiles of wind speed and direction taken from a series of pibal launched from the airport show a very light wind of less than 5 knots with a variable direction.

Table 1 shows the concentrations of SO_2 and sulfate measured during this flight. In the table, R represents the ratio of sulfur in SO_2 to the total sulfur in the form of SO_2 and sulfate. O_3, NO, and NO_2 were also measured during the flight with standard commercial instruments. Their average concentrations were 250 ppb for O_3, 5 ppb for NO, and 15 ppb for NO_2. The range of sulfate level, between 24.5 to 39.7 $\mu g/m^3$, found for this area, is about three times the sulfate level (8 to 12 $\mu g/m^3$) which was found by the EPA-CHESS program to have a substantial relationship with some types of morbidity.

TABLE 1. SO_2 and Sulfate Data Collected on August 17, 1975, Downwind of St. Louis, Missouri

Sample Number	Time CDT	SO_4 ($\mu g/m^3$)	SO_2 ($\mu g/m^3$)	R
1	1230-1320	27.6	33.06	0.642
2	1330-1420	39.7	83.3	0.759
3	1430-1520	35.2	47.8	0.671
4	1530-1620	24.5	25.9	0.613

To estimate the transformation rate of SO_2 to sulfate from the data in Table 1, a few assumptions must be made. It is assumed that the reaction leading to SO_2 oxidation is a first order reaction with respect to SO_2, and that the ratio of SO_2 to sulfate is independent of diffusion. Therefore, the rate of change with time of the sulfur mass in the form of SO_2, X(t), and the rate of change of total sulfur Y(t) in the combined gas and aerosol are:

$$\frac{d\,X(t)}{dt} = -\,(k_g + k)\,X(t) \qquad (1)$$

and

$$\frac{d\,Y(t)}{dt} = -\,k_g\,X(t) - k_a\,[Y(t) - X(t)] \qquad (2)$$

where k is the transformation rate, and k_g and k_a are the removal rates of SO_2 and sulfate, respectively.

Combining Equation (1) and (2) and integrating from time t_1 to t_2 yields the following equation:

$$\frac{1}{t_2-t_1}\int_{t_1}^{t_2} k\,dt = \frac{1}{t_2-t_1}\ln\frac{r(t_1)}{r(t_2)}$$

$$-\,(k_g-k_a)\left[1 - \frac{1}{t_2-t_1}\int_{t_1}^{t_2} r(t)\,dt\right] \qquad (3)$$

where r = X/Y. Since the diffusion of SO_2 and sulfate is the same, therefore r = R.[1] For a well mixed pollutant, as found during this experiment, the removal rates can be calculated from the following relation:

$$k_g - k_a = \frac{V_g - V_a}{H} \qquad (4)$$

V_g and V_a represent the deposition velocities of SO_2 and sulfate particles and H is the height of the mixing layer. Therefore, Equation (3) takes the following form:

$$k_{a_v} = \frac{1}{t_2-t_1}\ln\frac{R(t_1)}{R(t_2)} - \frac{V_g - V_a}{H}(1-R_{a_v}) \qquad (5)$$

k_{a_v} and R_{a_v} are average values of the time period t_1 and t_2.

The deposition velocity of SO_2 has been determined by several investigators, and it is generally[2] around 1.0 cm/sec, and a tenth of this for sulfate aerosol. Substituting the appropriate values for the parameters in Equation (5), the average transformation rate between samples 2 and 3 is 11.5% per hour; 8% per hour between Samples 3 and 4. The first sample was not used in the calculation because between it and the second sample a new material was entrained into the air parcel.

The transformation rates obtained in this study, generally agree with the finding of others (see Table 2). For instance, Benarie et al.[3] estimate of the rate in the industrial Rouen region in France to be in the range 6 to 25% per hour. Roberts and Friedlander[4] find the rate varying from 1.2 to 13% per hour in the Los Angeles basin, California. Rates of 10 and 14% per hour are reported by Alkezweeny and Powell[1] for St. Louis, Missouri.

Other rates for St. Louis may be estimated from Breeding et al.[5] data using the same above assumptions. They have found the half-life time of SO_2 to range 2 to 3.5 hr, based on ground measurements made on April 11, 1973, and 2.4 to about 6.5 hr calculated from aircraft data collected on April 14 and 17, 1973. The half-life time T is related to the combined sum of $(k_g + k)$ in the following manner:

$$K = k_g + k = \frac{\ln 2}{T}. \qquad (6)$$

Therefore, K is in the range of 19.8 to 34.7% per hour, and 10.7 to 28.9% per hour based on the ground and the aircraft data, respectively. To calculate k_g, the height of the mixing layer is needed. These are given by Haagenson and Morris.[6] They reported the top of the mixing layer to be at 1200 m AGL on April 11, and at about 600 AGL on April 14 and 17. Using these values, the transformation rates will range 17.1 to 32% per hour and 5.3 to 23.5% per hour, resulting from their ground and aircraft data, respectively.

TABLE 2. Comparison of the SO_2 Transformation Rates in Urban Plumes Determined by Various Investigators

k% per hour	Location	Data Collected at	Reference
6 - 25	Rouen, France	Ground	Benarie et al (1972)
17.1 - 32	St. Louis, Missouri	Ground	Breeding et al (1976)*
5.3 - 23.5	St. Louis, Missouri	Aircraft	Breeding et al (1976)*
1.2 - 13.0	Los Angeles, California	Ground	Roberts and Friedlander (1975)
10 - 14	St. Louis, Missouri	Aircraft	Alkezweeny and Powell (1976)
8 - 11.5	St. Louis, Missouri	Aircraft	This work

*Calculated from that data, see text.

ACKNOWLEDGEMENTS

The author wishes to thank Dr. Roger Tanner of Brookhaven National Laboratory for his analysis of Hi-Vol filter samples.

References

1. A. J. Alkezweeny and D. C. Powell, "Estimation of Transformation Rate of SO_2 to SO_4 from Atmospheric Concentration Data," Atmospheric Environment, in press, 1976.

2. B. Fisher, "The Transport of Sulphur Dioxide over a Long Distance," Atmospheric Environment, 8, p. 89, 1974.

3. M. Benarie, A. Nonat and T. Menard, "The Transformation of Sulphur Dioxide into Sulphuric Acid in Relation to the Climatology of an Urban/Industrial Area (Rouen, France)," Clean Air Conference, Melbourne, Australia, May 15-18, 1972.

4. P. T. Roberts and S. K. Friedlander, "Conversion of SO_2 to Sulfur Particulate in the Los Angeles Atmosphere," Environ. Health Perspectives, 10, pp. 103-108, 1975.

5. R. J. Breeding, H. B. Klonis, J. P. Lodge, J. B. Pate, D. C. Sheesley, T. R. Engler and D. R. Sears, "Measurements of Atmospheric Pollutants in the St. Louis Area," Atmospheric Environment, 10, pp. 183-194, 1976.

6. P. L. Haagenson and A. L. Morris, "Forecasting the Behavoir of the St. Louis, Missouri, Pollutant Plume," J. Appl. Meteor., 13, pp. 901-909, 1974.

AIRBORNE MEASUREMENTS OF POLLUTANTS OVER URBAN AND RURAL SITES[a]

A. J. Alkezweeny and D. R. Drewes

Trace gas measurements made during a flight from Alton to Springfield, Illinois showed an increase in the O_3 level with distance from the city. When a power plant plume was encountered, a sharp decrease in the O_3 level was observed.

This note presents the results of simultaneous measurements of trace gases and aerosol during an airplane flight from Alton, Illinois, to Springfield, Illinois. The flight was initiated on August 16, 1975, at 1335 CDT from the Civic Memorial Airport in Alton and terminated at 1413 CDT northeast of Springfield. The sampling altitude was maintained at about 600 m MSL. The sky condition above the flight path was characterized by broken clouds with bases estimated at about 1000 m MSL. The wind speed at the flight altitude was about 3 m sec^{-1} from the southwest, estimated by a series of pilot balloon ascents at the Alton airport. The average temperature and relative humidity along the flight path were 24°C and 71%, respectively. Ground fog in the morning and haze with light wind throughout the day were reported for Alton and St. Louis.

Concentrations of O_3 (with the Bendix Ozone Monitor), NO and NO_2 (TECO-NO_x Monitor), SO_2 (AID gas chromatograph with Meloy flame photometric detector), and total aerosol (General Electric Condensation Nuclei Counter) were measured. Except for SO_2, the data were recorded continuously at the rate of 5 sec^{-1}, and later reduced to 15 sec averages. The aerosol data were further reduced by dividing each concentration by the initial concentration to eliminate a relative calibration uncertainty. The SO_2 data were taken at discrete intervals, and each measurement was made on a 5-sec sample.

Figure 1 shows the concentrations of the various pollutants along the flight path. In general, the concentrations of NO, NO_2, SO_2, and aerosol decrease with distance from the city reflecting the effect of physical and chemical transformations and removal processes. On the other hand, the O_3 shows an opposite trend. This should be expected because of photochemical production of this species, and indeed similar behavior has been reported by other investigators. For instance, aircraft measurements by Gloria et al.,[1] in air masses advected over the Pacific Ocean show a build-up of O_3 in an aged air mass. Furthermore, Cleveland and Kleiner[2] reported that ground level O_3 concentrations at sites from 27 to 49 km downwind from an urban complex were higher than at the urban site. Recent measurements of pollutants by White et al.[3] in the St. Louis plume also showed the build-up of O_3 downwind of the city. These measurements were made from an aircraft between 460 and 760 m MSL across the urban plume at various distances. They measured O_3 concentrations of 110 ppb at 160 km northeast of St. Louis, about half the value from Figure 1 for about the same distance and altitude. The difference may be due primarily to a difference in wind speed, as the present measurements were made with a 3 m sec^{-1} wind speed compared to about 13 m sec^{-1} wind speed during their experiment. Low wind speed reduces the dispersion of pollutants which react to form O_3 in a photochemical system.

In conclusion, these limited data show clearly the increase of O_3 with distance from an urban source under light wind conditions. This build-up results in levels significantly higher thant he 80 ppb Federal 1-hr ambient air standard for oxidant. Furthermore, they show the dramatic decrease in the O_3 level and the corresponding increases in SO_2, NO_x, and particule levels encountered in a power plant plume.

---

a. Submitted for publication to the Journal of Applied Meteorology.

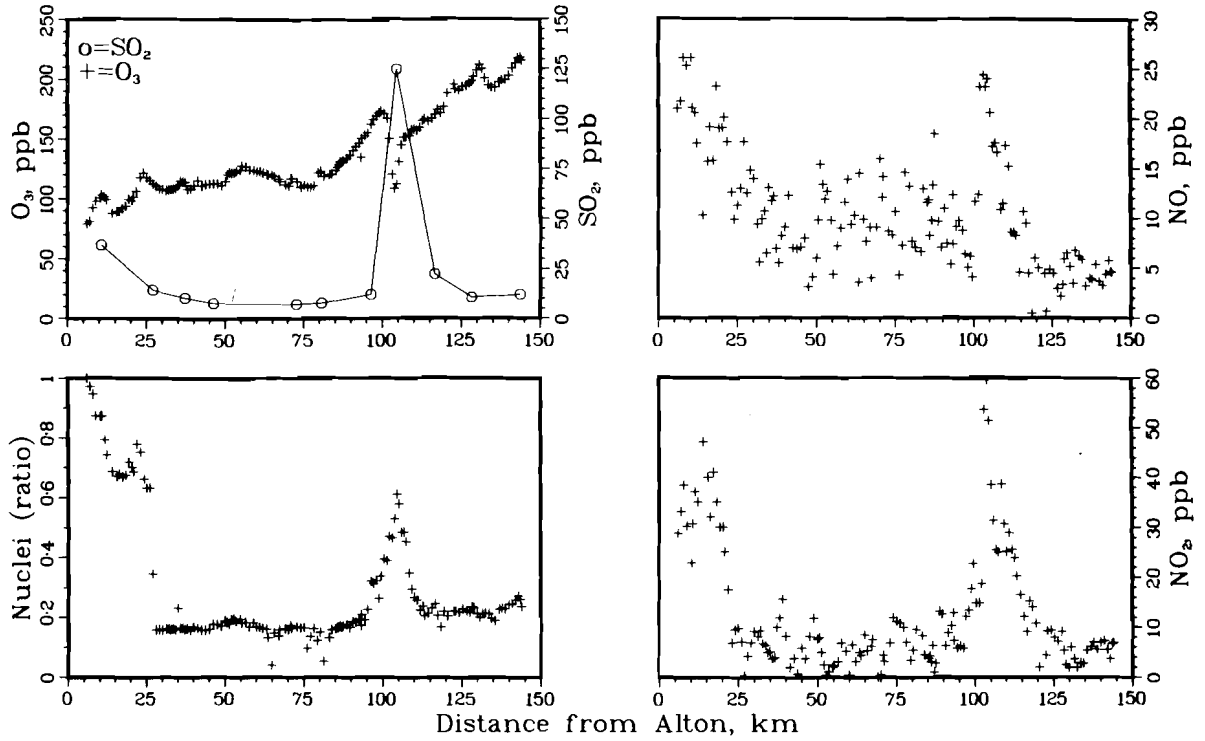

FIGURE 1. Concentrations of O_3, SO_2, NO, NO_2, and Aerosol Northeast of St. Louis

References

1. H. R. Gloria, G. Bradburn, R. F. Reinisch, J. N. Pitts, Jr., J. V. Behar and L. Zafonte, "Airborne Survey of Major Air Basins in California," J. Air Pollut. Control. Assoc., 24, pp. 645-652, 1974.

2. W. S. Cleveland and B. Kleiner, "Transport of Photochemical Air Pollution from Camden-Philadelphia Urban Complex," Environ. Sci. and Tech., 9, pp. 869-872, 1975.

3. W. H. White, J. A. Anderson, D. W. Blumenthal, R. B. Husar, N. V. Gillani, S. B. Fuller, K. T. Whitby and W. E. Wilson, Jr., Formation of Ozone and Light-Scattering Aerosols in the St. Louis Urban Plume, Paper presented at the 171st National Meeting of the American Chemical Society, New York, New York, April 4-9, 1976.

REVIEW OF SO_2 OXIDATION RATES IN PLUMES

A. J. Alkezweeny

The SO_2 oxidation in a polluted atmosphere is discussed in light of field observations and some related laboratory experiments. It is concluded that heterogeneous reaction is probably the dominant mechanism for the oxidation, with lead being the leading catalyst. Evidence indicates that the rate in a power plant plume is lower than an urban plume and depends on plant location and degree of mixing of outside air with the plume.

The oxidation rate of SO_2 in a polluted atmosphere is determined from field observations or atmospheric simulation experiments ranging over several orders of magnitude. Several experimental difficulties are involved. The lack of instrumentation able to detect low-level sulfur with sufficient sensitivity and time response is a considerable problem; a particularly severe one in power plant plumes where aircraft plume traverse time is on the order of a few seconds. The data collected may not represent the actual concentrations, since, for instance, instrumented aircraft attempting to penetrate the plume through its centerline may pass through the edges or miss the plume. Under light and variable wind, it is difficult to estimate the pollutant transport time. This time is required to calculate the oxidation rate. Finally, the lifetime of SO_2 in the plume, even after being corrected for effect of diffusion, is controlled by transformation to particulate and removal processes. The latter depend strongly on the nature of ground surface, i.e. grass, water, snow, etc., and may well change with distance from the source. Even in elevated plumes, there is some evidence of sulfate particles falling out of the plumes.[1]

In the following sections, the oxidation rates of SO_2 in urban plumes will be reviewed and compared with those from power plant plumes. Then, the oxidation mechanism will be discussed in the light of field observations and some related laboratory experiments.

First, let us compare the rates found in urban plumes. Benarie et al.,[2] found the conversation rate of SO_2 to H_2SO_4 to vary from 6 to 25% per hour, and the average of 15 measurements is 16.6% per hour. The rates were calculated from SO_2 and H_2SO_4 data collected at seven ground stations in the industrial area of Rouen, France. In the Los Angeles basin, Roberts and Friedlander[3] obtained a rate of 1.3 to 13% per hour from eleven pairs of measurements taken at two sites, with an average value of 7.1% per hour. In their calculations, they assumed a pseudo-first order rate constant and deposition velocities of 0.7 cm/sec and 0.03 cm/sec for SO_2 and sulfate, respectively. From three separate aircraft measurements of SO_2 and sulfate, made following a tetroon downwind of St. Louis, Missouri, Alkezweeny and Powell[4] and Alkezweeny[5] estimated the rates to be 19, 14, and 9.8% per hour. The removal rates were calculated from assumed deposition velocities of 1 cm/sec for SO_2 and 0.1 cm/sec for sulfate. Assuming the same deposition velocities, Alkezweeny[5] estimated the oxidation rates to be in the range 5.3 to 32% per hour in the St. Louis plume using SO_2 half-life time values from Breeding et al.[6] Their results were based on aircraft and ground measurements of SO_2 and other trace gases downwind of the city.

Others have also estimated the conversion rate of SO_2 to sulfate from emission data, aircraft or ground measurements, and long range air trajectory calculations. Eliassen and Saltbones[7] estimated in the range 0.28 to 1.73% per hour, and 1.1% per hour was estimated by Prahm et al[8] These two studies cover a horizontal extent of about 1000 km over Europe and the British Isles. Smith and Jeffrey[9] found the rate to depend on the

relative humidity. The rate is near zero at 60% and about 2.4% per hour at 72% relative humidities.

Table 1 summarizes the SO_2 oxidation rates determined by the various investigators. The first five values are comparable with each other; their average values are within a factor of 2.5. On the other hand, the last three rates are much smaller. The difference between the two groups may be attributed to pollutant transport distances. In the first group, the data were collected within about 150 km from the source; in the second group, the transport distances ranged 400 to 1000 km. Therefore, the pollutants which are active in the oxidation processes may have been depleted, reducing the rate. It is well known that the oxidation rate in clean air masses is much lower than that for polluted air. The former ranges 0.03 to 0.2% per hour.[10] In fact, Smith and Jeffrey[9] did not rule out the possibility that most of the oxidation took place near the source.

Estimates of the oxidation rates in stack plumes are highly variable, and are generally much lower than those for urban plumes. Lower rates may be explained in terms of the SO_2 oxidation mechanisms. Two possible routes for the SO_2oxidation in polluted atmosphere are homogeneous and/or heterogeneous chemical reactions. Homogeneous reactions consist of photo-oxidation of SO_2 in the presence of NO_x and hydrocarbons or thermal oxidation with ozone and olefins.[11] Ozone concentrations in power plant plumes are usually much lower than urban plumes, and hydrocarbons are mostly produced by automobiles,

TABLE 1. Conversion Rates of SO_2 to Sulfate in Urban Plumes

Range	Average	Location	Reference
6-25	16.6	Rouen, France	Benarie et al, (1972)
1.2-13.0	7.1	Los Angeles, California	Roberts and Friedlander (1975)
10-14	12	St. Louis, Missouri	Alkezweeny and Powell (1976)
8-11.5	9.8	St. Louis, Missouri	Alkezweeny (1976)
5.3-32	16.4	St. Louis, Missouri	Breeding et al, (1976)[a]
0.28-1.73	0.72	Western Europe	Eliassen et al, (1975)
-	1.1	Faroe Islands & British Isles	Prahm et al, (1976)
-	0(60% R.H.) 3(72% R.H.)	British Isles	Smith and Jefferey (1975)

a. Calculated from their data by Alkezweeny (1976)

therefore this mechanism is more operative in urban plumes. Free radicals have also been proposed as possible SO_2 oxidizing agents. However, free radicals are scavenged by nitric oxide[12] which is normally high in power plant plumes. The second route, the heterogeneous reaction, is the catalytic oxidation of SO_2 on surfaces of wet or dry metal particles. However, some of the potential catalysts have major emission sources other than power plant coal or oil fuels.[13] Furthermore, the presence of ozone has been shown to increase the SO_2 oxidation in solution droplets.[14-15] Therefore, whether the oxidation is homogeneous or heterogeneous, the rates in urban plumes are expected to be higher than those in power plant plumes.

If this is the case, then the rates in a power plant plume should depend upon its location, i.e., rural or urban area, and the degree of mixing of the plume with ambient air. Some of the recent plume studies seem to suggest this. For instance, the oxidation rate determined by the University of Utah group[16] in the Four Corners power plant plume is 0.37% to 0.76% per hour. The plant is far away from large urban sources, therefore the air mixed with the plume is relatively free of pollutants. Whitby et al.[17] reported the oxidation rate in the Labadie power plant plume, near St. Louis, to be 1.5% per hour at 10 km from the stack, and to increase with distance. A 4.9% per hour rate was found at a distance of 45 km.

Most of the oxidation rate calculations are based on the assumption of a first order reaction with respect to SO_2. However, not all investigators agree on this. Stephens and McCaldin[18] plotted log of the ratio of particulate to SO_2 against plume age, and fitted the data with a straight line, which is indicative of a first order reaction. Their data were collected via aircraft traversing a power plant plume on the Gulf Coast, 80 miles north of Tampa, Florida. Additional support for a quasi-first order reaction was the experimental results of Roberts and Friedlander.[3] However, other experiments indicated that the reaction is of higher order. Newman et al.[19] made several aircraft measurements in an oil-fired power plant plume. They have found that a pseudo second-order reaction fit their data quite well. Even a complex order reaction with respect to SO_2 was found in the laboratory for the reaction of SO_2, O_3, and olefins.[20]

Let us turn to other controversial problems. Is the SO_2 oxidation a homogeneous or heterogeneous reaction? Hidy and Burton (1975)[21] reviewed processes which lead to aerosol formation in the atmosphere and discussed recent observations from the Los Angeles Basin. They concluded that homogeneous reactions are the most significant for the production of submicron sulfate aerosols. Cox[11] estimated the conversion of SO_2 to sulfate to be 1.0 to 10% per hour in urban plumes for photo-oxidation with NO_x and hydrocarbons, or thermal oxidation with ozone and olefins. His estimate is based on extrapolation of the Cox and Penkett[20] laboratory experiments in which adding aerosol of iron oxide particles did not significantly affect sulfuric acid formation. Iron oxide is a potential catalyst for the SO_2 oxidation. A recent review of oxidation rates in power plant plumes by Levy et al.[16] has given a rate of 1.6 to 13.3% per hour for homogeneous gas phase reaction and 0 to 6% per hour for heterogeneous catalytic reaction. Calvert[22] discussed several possible homogeneous reaction routes, and a total potential rate of 1.7 to 4.7% per hour was estimated. However, he did not rule out the importance of heterogeneous reaction.

Heterogeneous reactions are supported by the results of several experiments. Katz[23] concluded from his measurements in a nickel smelter plume, near Sudbury, Canada, that metallic oxide particles which act as catalysts are very important to the SO_2 oxidation. Furthermore, the oxidation may take place at night as well as in sunlight. Benarie et al.[2] reported no correlation between ground measurement of NO_2 and sulfuric acid, but a strong correlation (correlation coefficient 0.72) between the latter and airborne particles. They concluded that the oxidation is dominated by catalytic effect of solid aerosol. Newman et al.[19] measured the oxidation rate in plumes and found no correlation between it and the time of day. They have also postulated catalytic oxidation on particles. Giles et. al.[24] examined data for sulfur dioxide and smoke collected during summer and winter months in a residential and industrial area in Great Britain and found deficiencies of SO_2 relative to smoke in winter compared with summer. After discussing several possible causes, they have suggested adsorption of SO_2 on solid particles followed by catalytic oxidation.

Two interesting experiments were made in Los Angeles which demonstrate the importance of aerosol particles to the SO_2 oxidation in the atmosphere. Roberts and Friedlander[3] filled a 96 m^3 Teflon bag with unfiltered air, and added a small amount of SO_2, 1-heptene, and NO_x. The mixture then was irradiated with sunlight. A pseudo-first order conversion rate of 21 to 99% per hour was found. However, when the experiment was repeated with the addition of SO_2 alone the rate was up to 11% per hour. In a similar experiment, Clark et al.[25] filled a 14 m^3 bag with filtered air near the freeway and exposed it to sunlight. The conversion rate was estimated to range from 0.55 to 1.3% per hour.

Clearly, the results of several experiments discussed in the proceeding reactions favored the heterogeneous catalysis oxidation for SO_2 in the atmosphere with the enhancement by the photochemical reaction processes.

Several trace metals have been proposed as possible catalysts, such as V,[19] Fe and Mn,[26,27] carbon (soot) particles[28] and others. When SO_2 is oxidized on the particle surface or in solution droplets, the particles which contain sulfur must contain the catalyst. Table 2 shows typical concentrations, and the percentages of masses below one micron particle diameter for various trace metals. Each point is a yearly average of the data collected by Lee et al.,[29] at six cities in the eastern United States. Young[30] found that 96% of the total mass of sulfur aerosol contained in particles, less than one micron in diameter, in St. Louis. However, from Table 2, only 17% of the mass of iron particles are in this size range. Therefore, based on the above argument, iron is not expected to act as a catalyst in the atmosphere, nor are zinc, copper and manganese. On the other hand, it is possible that lead and vanadium are effective as catalysts. Studies of the reaction of SO_2 with lead and vanadium compounds in the laboratories has shown that V_2O_5 to be ineffective in the SO_2 oxidation,[31,32] yet oxidized lead gave high oxidation rates.[31,33] Furthermore, lead has higher mass concentration than any other trace metals (see Table 2) and 67% of this mass lies in the size range below 0.3 microns,[30] therefore, it offers a much larger surface area. In addition, the lead sources are outside power plant plume, and since the oxidation rate is higher in urban plume than power plant plume, lead is a very strong candidate for the catalyst oxidation of SO_2 in the atmosphere.

TABLE 2. Typical Concentrations of Trace Metals in Urban Atmospheres

Species	Percent of Mass of Size <1 μm	Concentration in μg/m^3
Iron	17	1.0
Lead	68	1.9
Zinc	40	0.55
Copper	35	0.18
Manganese	25	0.053
Vanadium	64	0.10

References

1. L. Newman, J. Forrest and V. Manowitz, "The Application of an Isotopic Ratio Technique to a Study of the Atmospheric Oxidation of Sulfur Dioxide in the Plume from a Coal-Fired Power Plant," Atmos. Environ., 9, pp. 969-977, 1975a.

2. M. Benarie, A. Nonat and T. Menard, "The Transformation of Sulfur Dioxide into Sulfuric Acid in Relation to the Climatology of an Urban/Industrial Area (Rouen, France)," Clean Air Conference, May 15-18th, Melbourne, Australia, 1972.

3. P. T. Roberts and S. K. Friedlander, "Conversion of SO_2 to Sulfur Particulate in the Los Angeles Atmosphere," Environ. Health Perspec., 10, pp. 103-108, 1975.

4. A. J. Alkezweeny and D. C. Powell, "Estimation of Transformation Rate of SO_2 to SO_4 from Atmospheric Concentration Data," Atmos. Environ., in press, 1976.

5. A. J. Alkezweeny, "SO_2 to Sulfate Conversion in Urban Plume," in this report, 1976.

6. R. J. Breeding, H. B. Klonis, J. P. Lodge, Jr., J. B. Pate, D. C. Sheesley, T. R. Engler and D. R. Sears, "Measurements of Atmospheric Pollutants in the St. Louis Area," Atmos. Environ., 10, pp. 181-194, 1976.

7. A. Eliassen and J. Saltbones, "Decay and Transformation Rates of SO_2, as Estimated from Emission Data, Trajectories and Measured Air Concentrations," Atmos. Environ., 9, pp. 425-429, 1975.

8. L. P. Prahm, V. Torp and R. M. Stern, "Deposition and Transformation Rates of Sulphur Oxides During Atmospheric Transport Over the Atlantic," Tellus, XXVIII, pp. 355-372, 1976.

9. F. B. Smith and G. H. Jeffrey, "Airborne Transport of Sulphur Dioxide from the U.K.," Atmos. Environ., 9, pp. 643-659, 1975.

10. C. Junge, "The Cycle of Atmospheric Gases - Natural and Man Made," Q.J.R. Met. Soc., 98, pp. 711-729, 1972.

11. R. A. Cox, "Particle Formation from Homogeneous Reactions of Sulphur Dioxide and Nitrogen Dioxide," Tellus, XXVI, pp. 235-240, 1974.

12. S. P. Sander and J. H. Seinfeld, "Chemical Kinetics of Homogeneous Atmospheric Oxidation of Sulfur Dioxide," Environ. Sci. & Tech., 10, pp. 1114-1123, 1976.

13. J. W. Winchester and G. D. Nifong, "Water Pollution in Lake Michigan by Trace Elements from Pollution Aerosol Fallout," Water, Air, and Soil Pollution, 1, pp. 50-64, 1971.

14. S. A. Penkett, "Oxidation of SO_2 and Other Atmospheric Gases by Ozone in Aqueous Solution," Nature Physical Science, 240, pp. 105-106, 1972.

15. L. A. Barrie and H. W. Georgii, "An Experimental Investigation of the Absorption of Sulphur Dioxide by Water Drops Containing Heavy Metal Ions," Atmos. Environ., 10, pp. 743-749, 1976.

16. A. Levy, D. R. Drewes and J. M. Hales, "SO_2 Oxidation in Plumes: A Review and Assessment of Relevant Mechanistic and Rate Studies," EPA-450/3-76-022 report, 96 pages, September 1976.

17. K. T. Whitby, B. K. Cantrell, R. B. Husar, N. V. Gallani, J. A. Anderson, D. L. Blumenthal and W. E. Wilson, "Aerosol Formation in a Coal-Fired Power Plant Plume," Presented before the Division of Environmental Chemistry, American Chemical Society, New York, April 4-9, 1976.

18. N. T. Stephens and R. O. McCaldin, "Attenuation of Power Station Plumes as Determined by Instrumented Aircraft," Environ. Sci. & Tech., 5, pp. 615-621, 1971.

19. L. Newman, J. Forrest and V. Manowitz, "The Application of an Isotopic Ratio Technique to a Study of the Atmospheric Oxidation of Sulfur Dioxide in the Plume from an Oil-Fired Power Plant," Atmos. Environ., 9, pp. 959-968, 1975b.

20. R. A. Cox and S. A. Penkett, "Aerosol Formation from Sulphur Dioxide in the Presence of Ozone and Olefinic Hydrocarbons," J. Chem. Soc. Farody Transections I, 68, pp. 1735-1753, 1972.

21. G. M. Hidy and C. S. Burton, "Atmospheric Aerosol Formation by Chemical Reactions," International J. of Chem. Kinetics, Symp. No. 1, 1975.

22. J. Calvert, Interactions of Air Pollutants - X. The Effect of SO_2 Addition of the Reactions in the Simulated Polluted Atmosphere. National Academy of Sciences, Conference on Health Effects of Air Pollutants, Washington, D.C., October 3-5, 1973.

23. M. Katz, "Photoelectric Determination of Atmospheric Sulfur Dioxide, Employing Dilute Starch-Iodine Solutions," Analytical Chem., 22, pp. 1040-1047, 1950.

24. C. H. Giles, S. D. Forrester and B. J. Hojiwala, "Adsorption and Catalysis at the Solid/Sulfur Dioxide Interface in the Atmosphere. An Examination of Statistical Data," J. Colloid and Interface Science, 50, pp. 588-601, 1975.

25. W. E. Clark, D. A. Landis and A. B. Harker, "Measurements of the Photochemical Production of Aerosols in Ambient Air Near a Freeway for a Range of SO_2 Concentrations," Atmos. Environ., 10, pp. 637-644, 1976.

26. P. M. Foster, "The Oxidation of Sulphur Dioxide in Power Station Plumes," Atmos. Environ., 3, pp. 157-175, 1969.

27. J. Freiberg, "Effect of Relative Humidity and Temperature on Iron-Catalyzed Oxidation of SO_2 in Atmospheric Aerosols," Environ. Sci. & Tech., 8, pp. 731-734, 1974.

28. T. Novakov, S. G. Chang and A. B. Harker, "Sulfates as Pollution Particles: Catalytic Formation on Carbon (Soot) Particles," Science, 186, pp. 259-261, 1974.

29. R. E. Lee, Jr., S. S. Goranson, R. E. Enrione and G. B. Morgan, "National Air Surveillance Cascade Impactor Network, II. Size Distribution Measurements of Trace Metal Components," Environ. Sci. & Tech., 6, pp. 1025-1030, 1972.

30. J. A. Young, Private Communication, 1973.

31. P. H. Urone, P. H. Lutsep, C. M. Noyes and J. F. Parcker, "Static Studies of Sulfur Dioxide Reactions in Air," Environ. Sci. & Tech., 2, pp. 611-618, 1968.

32. M. Corn and R. T. Cheng, "Interactions of Sulfur Dioxide with Insoluble Suspended Particulate Matter," J. Air Poll. Cont. Ass., 22, pp. 870-875, 1972.

33. B. M. Smith, J. Wagman and B. R. Fish, "Interaction of Airborne Particles with Gases," Environ. Sci. & Tech., 3, pp. 558-562, 1969.

34. P. T. Roberts and S. K. Friedlander, "Photochemical Aerosol Formation, SO_2 1-Heptene, and NO_x in Ambient Air," Environ. Sci. & Tech., 10, pp. 573-580, 1976.

THE DESIGN OF THE LAKE MICHIGAN EXPERIMENT

A. J. Alkezweeny

A study of pollutant interactions in urban plumes was relocated from St. Louis to Lake Michigan. The advantages of the relocation and the experimental method are described here.

The objective of the Aerosol and Trace Gases Transformation program is to study pollutant interactions in urban plumes. Emphasis is placed on SO_2 to sulfate conversion, oxidation rates and mechanisms responsible for the formation of sulfate aerosol. The method of investigation is a field experiment conducted in a Lagrangian frame of reference, supported by diagnostic modeling. In the past, the field operation was located in the St. Louis area during the METROMEX program. The decision to relocate the experiment over Lake Michigan, and to study the Milwaukee plume as it is transported over the lake, was made because:

- The lake is a source-free region. No entrainment of a new material enters the plume from other sources, in contrast to the several sources scattered around St. Louis.
- The lake surface represents a uniform terrain. Therefore, the dry removal of pollutants is constant along the transport path and depends only on the physical and chemical composition of the pollutants. Furthermore, aircraft sampling can be made close to the surface.
- The temperature over the lake is uniform.
- Milwaukee is a large metropolitan area. It is isolated from other large urban areas when the wind direction is from other than the south.

The advantages of the lake area described above make plume modeling much easier. A disadvantage in this area is the lake breeze circulation across the lake shore. However, the lake breeze occurs only one-third of the time, on the west shore, during the summer. Therefore, the experiment may be conducted on days without lake breeze; measurements may also be taken beyond the boundary of the circulation.

The first experiment was conducted during 3 weeks in August of 1976. Four research platforms were used; the BNW DC-3 and Cessna 411 airplanes, and two boats. The DC-3 made penetrations through the Milwaukee plume at different altitudes within the mixing layer. Then the same procedure was repeated at a new location. The new location was determined by the wind speed and direction recorded from instrumentation onboard the aircraft. Meanwhile, the second aircraft was collecting high volume (H.V.) aerosol samples and measuring SO_2 upwind and outside the plume. The boats were stationed on both sides of the lake, within the urban plume. Lundgren impactors, H.V. samplers, SO_2 bubblers, and freon collection bottles were used onboard the boats.

The data collected in real-time onboard the DC-3 aircraft were: temperature, dew point temperature, wind speed, wind direction, standard aircraft parameters (altitude, air speed, etc.), O_3, SO_2, NO, NO_2, light scattering, particle concentration, flow rate of H.V. sampler, and aircraft location (longitude, latitude). All these data were recorded on a magnetic tape, and can be displayed at will on a digital readout. Some of the parameters were also recorded on a chart recorder.

Several bottles were filled with air samples for later freon analysis. Air samples were also captured in bags and sent to the EPA laboratory for hydrocarbon determination. Three different H.V. samplers were used to determine the chemical composition of aerosol. The first one samples at the rate of 50 cfm on IPC filters. These filters will be analyzed for trace metals by X-ray fluorescence and neutron activation techniques. The second H.V. sampler was supplied by the Brookhaven National Laboratory; it consisted of three filter packs which are chemically treated. Its purpose is to determine the SO_2 concentration and composition of sulfate aerosol by wet chemistry technique. The third sampler used a 47 mm fluropore filter. Some of these filters were sent to the Argonne National Laboratory to be analyzed by infrared spectroscopy, and others were sent to the Lawrence Berkeley Laboratory to be analyzed by Electron Spectroscopy for Chemical Analysis (ESCA).

During 1 week of this study, a NASA group flew their airplane over the lake with a remote CO sensor mounted onboard, oriented downward. Measurements of O_3, NO/NO_x, and solar radiation were made by a group from the University of Michigan at several fixed sites along the eastern shore of the lake. Figure 1 shows the various activities during last summer's experiment.

Data collected from these experiments are currently being analyzed, and the results will be reported later. Although the experiment is designed to study the transformation of SO_2 to sulfate, the data collected from the aircraft on the surface instrumentation should give information on the following:

a) Transport and interaction of other pollutants such as oxidant.

b) Dry removal rates of various trace metal as a function of particle size over water surfaces.

c) Diffusion characteristics of an urban plume.

d) Emission rates of various metals in the Milwaukee area.

e) Possible information on metal catalysis oxidation of SO_2.

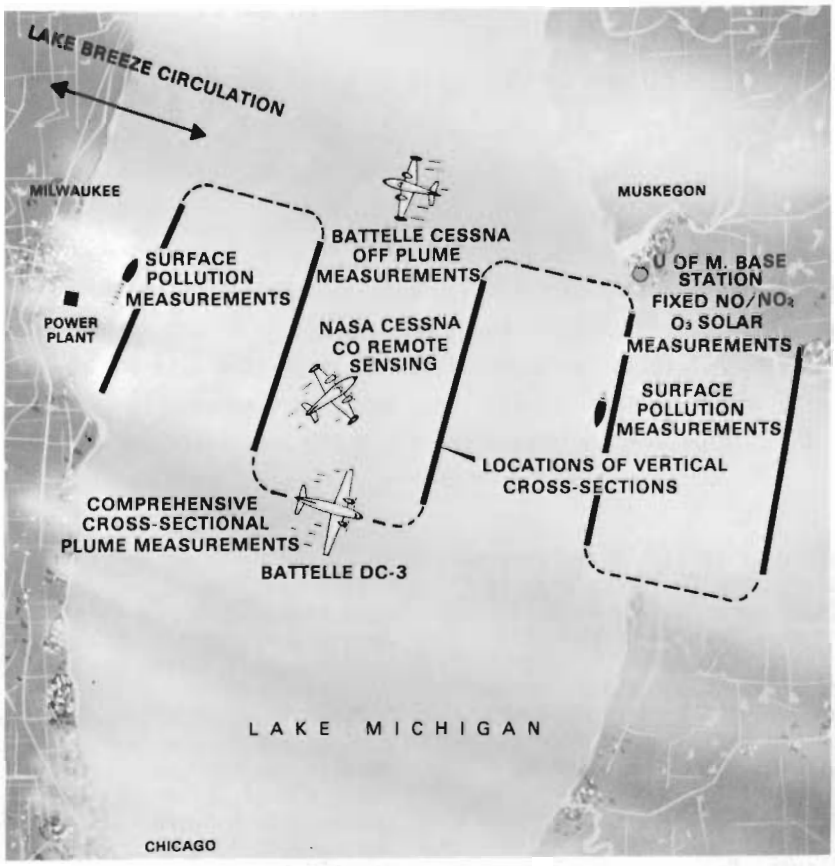

Neg 77350-2

FIGURE 1. Composite: Long Range Plume Transformation Study

AIRBORNE MEASUREMENTS OF HYDROCARBONS IN THE ST. LOUIS PLUME

A. J. Alkezweeny and R. N. Lee

Results are reported for two hydrocarbon sampling methods used during this study of the St. Louis urban plume in August of 1975. Samples secured in Tedlar bags yielded concentration data for carbon monoxide and volatile organics. Less volatile species were captured on a solid absorbent and identified via GC/MS analysis.

During the summer of 1975, a field experiment was conducted in the St. Louis area to study SO_2 to sulfate transformation in an urban plume. The experiment was conducted in a Lagrangian frame of reference using the BNW DC-3 aircraft, and a constant volume balloon (tetroon) to identify the plume trajectory. The tetroon was launched from the ground to an altitude within the plume. Since laboratory experiments have shown some hydrocarbons to be potential contributors to the SO_2 oxidation processes, a few samples were collected for later analysis using ground base instrumentation. Samples were collected on August 6, 12, and 17, 1975. On the 6th, the tetroon was launched from Weiss Airport and traveled to the southwest of St. Louis. On the 12th and 17th, the launch site was Alton Civic Airport, northeast of the city.

Two methods were used to capture samples for hydrocarbon analysis. Each of these methods was directed toward a different segment of the hydrocarbon spectrum. Light paraffins and olefins (through C_6) were measured quantitatively by gas chromatographic analysis of air samples collected in 70 ℓ Tedlar bags. These samples, obtained over periods of 8 to 11 min, were analyzed at the RAPS laboratory in St. Louis. Concentration data for samples collected on August 12 and 17, 1975, are presented in Table 1.

The second technique, focusing on heavier hydrocarbons and oxygenated species, employed a solid adsorbent (chromosorb 102) to concentrate these components from an unfiltered air stream over a period of 30-60 min. Analysis of these samples were conducted by GC/MS at the Battelle-Columbus Laboratory. Incomplete examination of the mass spec data for 6 samples collected on August 6, 1975, indicates the presence of the compounds listed in Table 2.

The limited number of bag samples does not ensure easy interpretation of the analytical results. Indeed, any discussion of the resulting data which goes beyond simply noting concentration trends and speculating reasons for unexpected trends would be unjustified. The two flights referred to in Table 1 occurred on days which differed significantly in the prevailing meteorological conditions. The greater hydrocarbon concentrations recorded for August 17, a day characterized by very weak and variable winds, is most likely due to the dominant influence of a nearby refinery. On that day, all sampling was done within 2 miles of Civic Airfield. The first three samples were taken downwind of the refinery before a wind shift brought the constant volume balloon back over the refinery. The dramatic increase in hydrocarbon concentration in sample number four is no doubt due to fresh hydrocarbon input from this source.

General concentration trends observed for specific species or compound classes are noted in Table 1. The high, uniform concentration of methane is very similar to earlier ground level data at both urban and rural sites, and is in keeping with the absence of a significant urban source and methane's relatively inert behavior. Carbon monoxide concentrations were low relative to surface measurements in the St. Louis metropolitan area and decreased with time, presumably because of diffusion

TABLE 1. Hydrocarbons in Bag Samples, ppb C_1

	Aug. 12		Aug. 17			
	1235 → 1247	1604 → 1612	1350 → 1400	1450 → 1500	1600 → 1608	1647 → 1655
I. TOTAL HYDROCARBONS	2120	2160	2560	2260	2130	2540
II. CARBON MONOXIDE	830	760	530	470	400	550
III. SATURATED HYDROCARBONS						
A. Alkanes						
Methane	1700	1710	1680	1670	1660	1690
Ethane	12.1	13.6	15.0	13.5	8.5	14.0
Propane	7.9	9.0	30.1	21.4	10.3	23.1
Isobutane	3.3	3.7	19.6	15.6	3.8	24.9
N-Butane	5.9	7.0	58.3	40.8	16.3	64.3
Isopentane	5.6	6.8	61.7	52.0	17.6	56.1
N-Pentane	4.0	4.0	24.3	19.4	9.6	23.3
2,2-Dimethylbutane	0.2	-	1.9	1.2	0.6	1.4
2,3-Dimethylbutane + Trans-4-methylpentene-2	0.5	1.1	8.8	5.5	3.3	7.8
2-Methylpentane	1.5	2.9	19.5	13.5	6.6	17.2
3-Methylpentane + (Hexene-1 + 2-Ethylbutene-1)	0.7	1.8	13.5	9.3	3.9	11.1
N-Hexane	5.9	-	45.4	20.2	12.6	18.1
B. Cyclic Compounds						
Cyclopentane	0.5	1.1	3.0	2.8	2.3	3.3
Methylcyclopentane + (3,3-Dimethylpentene-1)	20.1	19.7	36.1	28.9	27.5	24.3
Cyclohexane + (Cis-4-Methylhexene-2)	2.9	-	18.8	-	12.6	12.6
IV. UNSATURATED COMPOUNDS						
A. Olefins						
Ethylene	2.9	2.8	8.7	17.9	4.6	4.7
Propylene	0.4	0.5	1.9	1.9	1.2	1.1
Isobutylene + Butene-1	0.7	1.7	1.2	1.6	0.5	0.5
Trans-Butene-2	0.2	0.5	0.9	0.8	-	1.3
Cis-2-Butene	0.2	0.1	0.5	0.2	0.5	0.5
3-Methylbutene-1	0.4	0.3	0.2	0.3	0.4	0.1
Pentene-1	1.6	-	0.6	0.8	-	1.1
2-Methylbutene-1	0.2	-	0.1	0.3	0.2	0.1
2-Methylpentene-1 + 4-Methylpentene-1	-	-	0.2	0.1	0.4	0.1
2,4-Dimethylpentene-2	-	3.6	42.0	19.6	23.7	47.4
2,4-Dimethylpentene-1	40.0	21.3	67.4	12.1	-	-
Trans-Hexene-3	-	-	19.8	21.2	8.2	15.8
V. AROMATIC						
Benzene	-	-	67.4	-	-	-
VI. ACETYLENE	0.9	1.3	1.0	1.6	1.8	1.4

TABLE 2. Organics Identified in the Urban Plume (August 6, 1975) by GC/MS Data

Sampling Times →	1618 -1648	1652 -1722	1726 -1756	1759 -1829	1833 -1903	1906 -1934
Cyclopentadiene	(x)					
Cyclohexadiene	(x)					
Benzene	(x)	(x)	(x)	(x)		(x)
Toluene	x	x	x	x	x	x
Xylene						(x)
Styrene	x	x	x	x	x	x
Trimethylbenzene		(x)				
Methylstyrene	x	x				
Allylbenzaldehyde					x	x
Benzaldehyde	x	x		(x)	x	x
Phenylacetate	(x)	(x)	(x)	(x)		(x)
Acetophenone		x	x	x	x	x
Naphthalene	x	x	x	x		
Terephthaldehyde	x	x	x	x	x	x
Phenol	x	x	x	x	x	x
Methylnaphthalene	x	x	x			
Benzylalcohol	(x)					
C_5-Benzene	(x)	(x)	(x)	(x)		
C_2-Naphthalene	x	x	x	x		
Biphenyl	x	x	x	x	x	
Acenaphthylene	x					
Anthracene	x	x				
Methylanthracene	x					

x indicates >0.06 ppb ( ) tentative identification

and chemical transformation. The concentrations of acetylene were also quite low in comparison to urban surface data, but increased with time. Contrary to carbon monoxide the major source of acetylene is the automobile, hence the increase may reflect entrainment of surface air. The concentration of paraffins, other than methane, shows a slight increase with time on August 12 and a decrease on August 17. This is the opposite of what might be expected from knowledge of the respective flight paths. The concentration changes observed on August 12 are for only two samples widely separated in terms of both time and space, and may reflect the influence of a non-urban source. The progressively lower paraffin concentrations observed in samples 1, 2 and 3, on August 17 may be attributed to dilution via diffusion. As opposed to the somewhat larger changes in paraffin concentrations, the olefin levels are generally low and rather uniform. This observation raises questions regarding the possible transformation of these more reactive materials during the period between capture and analysis. The four most abundant olefins (2,4-Dimethylpentene-1, 2,4-Dimethylpentene-2, Trans-Hexene-3 and Ethylene) display a somewhat irregular concentration profile.

GC SYSTEM FOR THE ON-SITE ANALYSIS OF HYDROCARBONS AT AMBIENT CONCENTRATIONS

R. N. Lee

Solid absorbent traps offer an alternative to the use of bags for sampling atmospheric hydrocarbons. An analytical system consisting of an adsorbent trap coupled to a gas chromatograph has been built for onsite concentration and analysis of ambient hydrocarbons.

Growing interest in the fate of atmospheric injections of SO_2 has enhanced interest in the mechanisms of SO_2 oxidation. Plume studies of the sulfate product evolution have dealt in varying detail with the qualitative and quantitative identification of a host of primary and secondary plume constituents. These studies have employed concentration profiles obtained via airplane-mounted instruments to reveal features of the chemical processes occurring within the plume. Although instrumentation is available for real-time surveys of many plume components, analytical limitations require the use of integrated sampling techniques for some species. Laboratory evidence has suggested that some hydrocarbons may play a major role in the SO_2-sulfate transformation.[1] Hydrocarbon data is thus essential to studies which seek to resolve the atmospheric oxidation process. Furthermore, the wide range of hydrocarbon concentrations and reactivities encountered in ambient air require the application of sampling techniques which do not alter composition.

Most investigations have employed Tedlar bags for the capture and storage of air samples prior to chromatographic analysis.[2] This procedure incorporates a cryogenic concentration step to bring the sample into the detection range of the flame ionization detector. Concentration is typically followed by analysis using a temperature programmable gas chromatograph to permit elution of the complex hydrocarbon mixture. Although widely employed, the following sources of error must be considered since they are capable of obscuring hydrocarbon concentration trends:

- Hydrocarbon loss may occur during storage via adsorption on container walls.
- The hydrocarbon content may be depleted via chemical reaction within the bag. Exposure to sunlight, variable temperatures and storage periods contribute to a non-uniform sample history. These factors may have a dominant influence on concentration data.

In view of the potential difficulties inherent in the use of plastic bags, it is important to consider alternative approaches for obtaining ambient hydrocarbon data. One such method employs a solid adsorbent for the capture of these materials. This technique has been successfully employed to remove and concentrate organics from water and ambient air as the first step in their quantitative measurement.[3-4]

A system which uses this approach has been designed and constructed for use in aircraft studies. This system, depicted in Figure 1, can be mounted in the aircraft to allow in-flight analysis. The traps may also be used in the same way as bags and individual samples analyzed with a ground based chromatograph. This latter procedure has the advantage of excluding sunlight and providing a more uniform and definable sample history than possible with the use of sample bags.

The system described in Figure 1 consists of the following components:

1) U-tube trap (1/8-in. O.D. x 11-in. stainless steel) wrapped with heating wire and packed with the solid adsorbent.

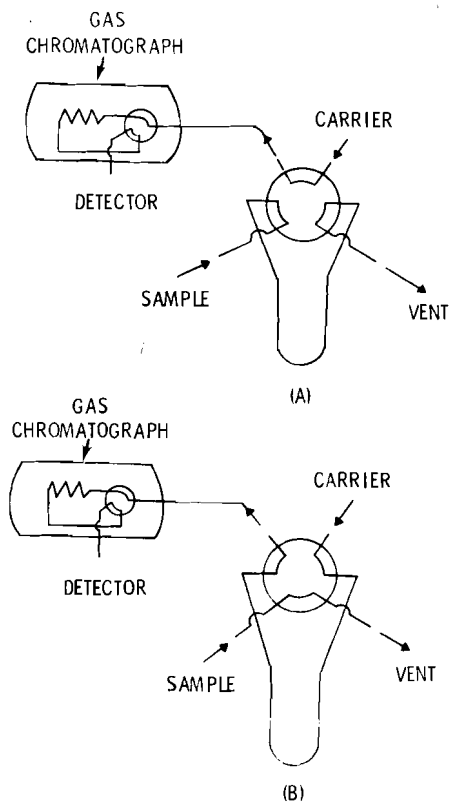

FIGURE 1. Flow Schematic for the Concentration and Analysis of Ambient Hydrocarbons.
a) Sampling Mode
b) Backflush of Adsorbent Trap

2) Six-port valve used to channel sample flow through the trap and carrier gas to the chromatograph while in the sampling mode. When switched to the inject mode, carrier flow is diverted to the trap which is electrically heated to desorb the organics and drive them onto the chromatograph column.

3) Four-port valve used to backflush the column.

4) Gas chromatograph equipped with a flame ionization detector.

This system was constructed by interfacing a Chromalytics Model 1047 concentrator (Chromalytics Corp., Unionville, Pennsylvania) with an Analytical Instrument Development Model 511 gas chromatograph. A column backflush capability was introduced by mounting a four-port valve to the interior of the column oven.

While it is not possible to cover a broad spectrum of atmospheric hydrocarbons with this system, it does offer an opportunity to evaluate the relative merits of solid adsorbent and bag sampling techniques for aircraft sampling missions. Satisfactory operation depends on the ability of the trap to capture the hydrocarbons of interest within a shallow layer of the adsorbent. This feature is necessary to permit sample release to a small volume of carrier and hence, achieve efficient separation of the sample components. Laboratory and field tests are currently in progress to determine the operational characteristics of the system. In addition to capture and release efficiency, these tests must consider the possibility of chemical transformations accompanying interaction with the solid adsorbent.

References

1. R. A. Cox, and S. A. Penkett, "Aerosol Formation from Sulfur Dioxide in the Presence of Ozone and Olefinic Hydrocarbons," J. Chem. Soc. Far. Trans. I, Vol. 68, pp. 1735-1753, 1972.

2. W. A. Lonneman, S. L. Kopczynski, P. E. Darley and F. D. Sutterfield, "Hydrocarbon Composition of Urban Air Pollution," Environ. Sci. Tech., Vol. 8, pp. 229-236, 1974.

3. J. P. Mieure, and M. W. Dietrich, "Determination of Trace Organics in Air and Water," J. Chromatogr. Sci., Vol. 11, pp. 559-570, 1973.

4. A. J. Murray, and J. P. Riley, "The Determination of Chlorinated Aliphatic Hydrocarbons in Air, Natural Waters, Marine Organisms and Sediments," Anal. Chim. Acta., Vol. 65, pp. 261-270, 1973.

ESTIMATING AEROSOL OPTICAL PROPERTIES FROM SIZE DISTRIBUTIONS MEASURED BY OPTICAL PARTICLE COUNTERS

N. S. Laulainen

Mie theory calculations indicate the response of the Royco Model 220 optical particle counter as a function of particle size is rather insensitive to the real part of the particle refractive index. However, size measurements appear to be somewhat sensitive to the imaginary part of the refractive index. This sensitivity can significantly affect the calculation of other aerosol optical properties, such as the extinction coefficient, when size distributions determined by this technique are used as input data.

INTRODUCTION

Recent years have seen considerable effort to determine the physical and chemical properties of atmospheric aerosols, both of natural and anthropogenic origin. The reasons for this effort are clear; atmospheric aerosols profoundly affect precipitation development and can significantly modify the climate by altering the solar radiation field. The fundamental parameters which are required from measurements of aerosol systems are the size distribution, complex index of refraction, particle solubility and relative humidity, and some as-yet-unspecified parameter describing particle shape.

Many optical systems have been developed to measure aerosol size distributions. These systems take advantage of light-scattering properties of aerosols as a function of size. Most of their shortcomings occur because the light scattering is also sensitively dependent on particle refractive index and shape, such that the size measurements can only be referenced to equivalent spheres of known index and size of the type used in calibrating the measurement systems. When inferring the effects of particles on precipitation development, ambiguities in specifying the true size distribution may be unimportant. However, when specifying the effects of aerosols on solar radiation, these ambiguities must be resolved. An earlier paper[1] examined the interpretation of optical measurements in terms of those parameters which appear to have important climatological implications. In this paper, we address the specific aspect of interpreting aerosol size distributions measured by a Model 220 Royco optical particle counter and estimating various aerosol optical properties from these data.

THEORETICAL ASPECTS

The theoretical basis of size distribution determination with the Model 220 Royco optical particle counter is the relationship between light scattering intensity at a scattering angle of $\pi/2$ (see Figure 1) and particle diameter, namely (see for example, Reference 2)

$$\sigma(D_p, \tfrac{\pi}{2}) = \frac{\pi D_p^2}{4} \phi(D_p, \pi/2), \qquad (1)$$

where $\sigma(D_p,\pi/2)$ is the light scattering coefficient per particle of diameter D_p for scattering angle $\pi/2$, $\frac{\pi D_p^2}{4}$ is the geometric cross-section of the particle with diameter D_p, and

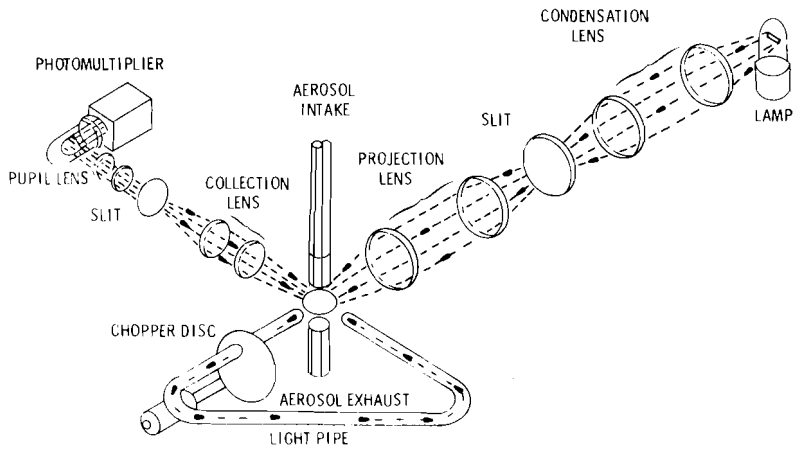

FIGURE 1. Schematic Representation of the Royco Model 220 Optical Particle Counter Detection System

$\phi(D_p,\pi/2)$ is the light scattering phase function for a particle of diameter D_p and scattering angle $\pi/2$.

This relationship assumes that the particles are spherical in shape and that the particle refractive index is known and uniform for all the particles. Hodkinson[3] also discusses the response of optical particle counters.

Calibration of the optical particle counter (OPC), while implicitly using Equation (1), actually is based on the response of the instrument to light scattered from latex spheres of known size and refractive index (n = 1.6). The actual shape and size of the latex particles is established independently by standard scanning electron microscopy. Particle sizes derived from the OPC for aerosols whose refractive index is different than n = 1.6, are then in fact referenced to the response the instrument would have for latex spheres of equivalent sizes.

The response given by Equation (1) is sensitive not only to particle refractive index, but also scattering angle and wavelength of light. The actual response of the Model 220 Royco OPC is supposedly less sensitive to these parameters, particularly particle refractive index, because instrument responds to light scattered at angles[3] of $\pi/2 \pm 0.4$ rad ($\pm 24°$) instead of exactly $\pi/2$ and because the instrument uses an incandescent bulb or "white" light instead of monochromatic source for illumination of the particles.

INSTRUMENTAL RESPONSE AND PARTICLE REFRACTIVE INDEX

Since the response of the OPC is sensitive to particle refractive index, scattering angle and wavelength of the illuminating light, we examine this response for two cases. In the first case, we assume that the effective response wavelength of the system is $\lambda = 0.5$ μm and that the instrument accepts light scattered exactly at $\pi/2$ and we calculates the response for several particle refractive indices. In the second case, the same calculations are made except that the wavelength of the illumination is smeared out over a wide spectrum $\lambda = 0.5 \pm 0.1$ μm, and that a finite solid angle detection cone of ± 0.1 rad ($\pm 5°$) centered at a scattering angle of $\pi/2$ is allowed for (this choice is more conservative than that suggested by Hodkinson[3]).

For case 1, the response function $\sigma(D_p,\pi/2)$ given by Equation (1), is shown in Figure 2 for the reference refractive index, n = 1.6, and two other refractive indicies, n = 1.5 and n = 1.5 - 0.1i, respectively. Except for the region 1 to 2 μm and beyond 7 μm, the response function for n = 1.5 is 20 to 30% smaller than for the reference index n = 1.6. Alternatively, for the same response, the particle diameters for n = 1.5 are ∿15 to 20% larger than the corresponding diameters for n = 1.6. The inclusion of an absorptive term (imaginary part of the refractive index) increases the discrepancy between the reference diameters and those for the refractive index n = 1.5 - 0.1i. These results are also summarized in Table 1 for each channel of the Model 220 OPC.

The response function for case 2 for the same set of refractive indicies as in case 1 is shown in Figure 3. The bars associated with each curve indicate the range of values for the response when the wavelength varies from 0.4 to 0.6 μm and the scattering angle varies from 85 to 95°. The curves are drawn through the median of each range. If a scattering angle of 90 ± 24° is used in the calculations, the range of values is increased dramatically, as indicated by the dashed bars for D_p = 2.24 μm. The practical significance of these results indicate that the response as a function of particle size is roughly independent of the real part of the refractive index, but is somewhat sensitive to the imaginary part. Thus, for aerosols which have an absorptive term, scaling of the actual particle diameters appears necessary if the measured particle size distributions are to be used in subsequent calculations for other optical parameters. The results for case 2 are also summarized in Table 1.

DISCUSSION

Since atmospheric aerosols can have a wide range of refractive index (n = 1.3) for water droplets to n∿2-i for carbon particles), it is important to scale the measured size distributions properly. Unfortunately, the refractive index is not generally known a priori (indeed the objective of many experiments is to determine this and other parameters). Often, however, the general composition of the particles can be determined by other means. This information, along with ambient relative humidity, can provide a reasonable estimate of refractive index. For example, sulfate

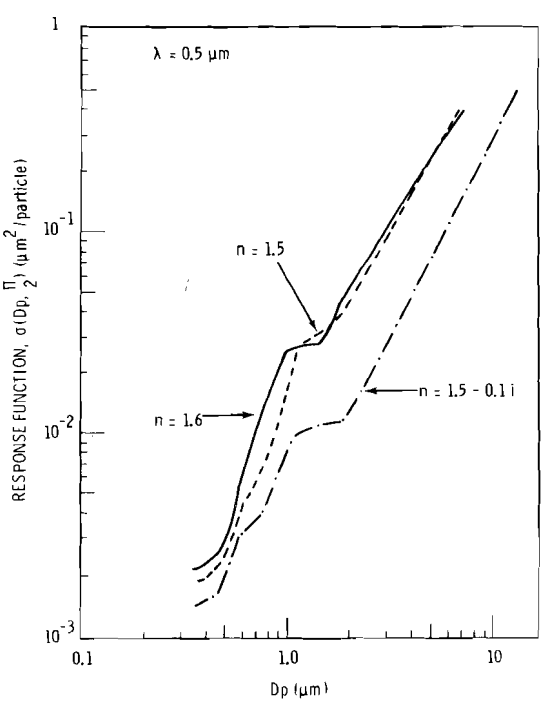

FIGURE 2. Ideal Response Function as a Function of Size of a π/2-Light Scattering OPC for Various Refractive Indicies

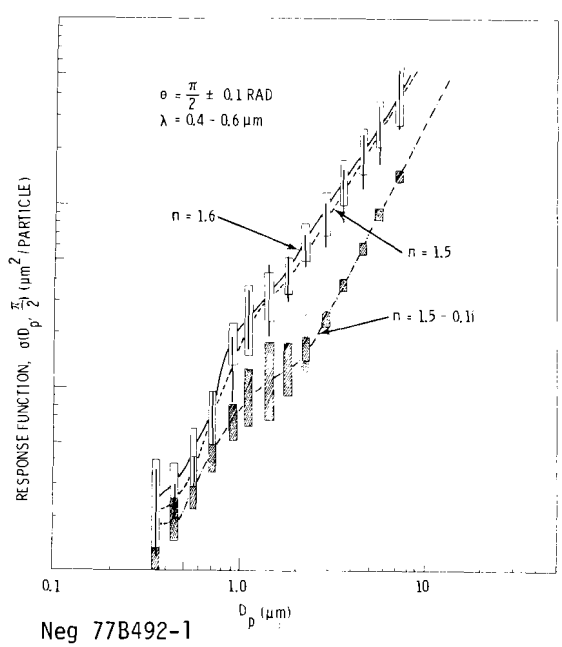

Neg 77B492-1

FIGURE 3. Response Function of a π/2-Light Scattering OPC with Finite Apertures (θ = π/2 ± 0.1 rad) and White Light Illumination for same Refractive Indicies of Figure 2. The bars indicate the spreading of the response function from ideal.

TABLE 1. Particle Diameters as a Function of Refractive Index Referenced to Latex Spheres with n=1.6 for the Royco Model 220 OPC

Ch. No.	Ref. Diameter (μm)	Calculated Particle Diameter (μm) Case 1 n=1.5	Case 1 n=1.5-0.1i	Case 2 n=1.5	Case 2 n=1.5-0.1i
2	0.355	0.46	0.52	0.46	0.53
3	0.447	0.50	0.54	0.52	0.58
4	0.562	0.66	0.82	0.62	0.76
5	0.71	0.82	1.0	0.73	0.76
6	0.89	1.01	2.6	0.98	2.35
7	1.12	1.12	3.0	1.18	2.85
8	1.41	1.41	3.2	1.48	3.3
9	1.78	1.98	3.9	1.9	3.8
10	2.24	2.45	4.7	2.5	4.7
11	2.82	3.2	5.8	3.2	5.6
12	3.55	3.8	6.8	4.0	6.8
13	4.5	4.7	8.0	5.0	8.3
14	5.6	5.9	10.0	6.0	10.0
15	7.1	7.1	12.0	7.4	12.0

aerosol is one of the dominant components in the urban atmosphere and has a real part of the refractive index of ∿1.5. The imaginary part of refractive index of sulfate aerosol is uncertain. For our calculations, we have assumed that the range n = 1.5 to n = 1.5 - 0.1i is representative. It should be noted that many of the difficulties mentioned in an earlier paper[1] encountered in calculating aerosol optical properties are still present--namely the problem of nonspherical particles and nonuniform refractive index (i.e., different kinds of particles or particles of complex composition).

To illustrate the effect of refractive index, we calculate the extinction coefficient from a particle size distribution measured over Seattle at 2000 ft on 18 June 1976, by assuming a) that the measured size distribution is independent of refractive index, and b) that the measured size distribution is scaled appropriately to the refractive index, as discussed in the preceding section.

Curves for extinction coefficient per particle $\sigma(D_p)$ as a function of particle size at wavelength λ = 0.5 m and refractive indices n = 1.6, n = 1.5, n = 1.5 - 0.1i are shown in Figure 4. Notice that for particles larger than ∿2 μm, the extinction coefficient is proportional to D_p^2. Also note that scattering and total extinction are equal when the refractive index is entirely real. Using these curves and the results of Table 1, the extinction coefficient per unit volume can be easily computed for the measured size distribution, according to

$$b_{ext} = \sum_i \frac{\Delta N_i}{\Delta \log D_p} \cdot \sigma(D_{p_i}) \cdot \Delta \log D_p$$

where $\frac{\Delta N}{\Delta \log D_p}$ is the number of particles per unit volume in size channel i of width $\Delta \log D_p$ and the sum is over all channels and $\Delta \log D_p$ = 1/10 for the OPC. (In this calculation we also include particle size

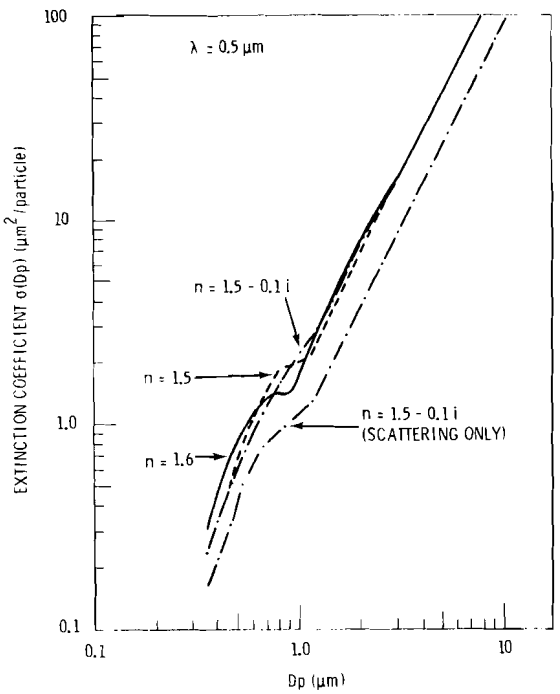

FIGURE 4. Extinction Coefficient per Particle as a Function Size for Various Refractive Indicies

measurements made with the Whitby Electrical Aerosol Analyzer where $\Delta \log D_p = 1/4$. The contributions from those measurements are shown separately.) The results of these computations are summarized in Table 2.

An inspection of Table 2 reveals that the calculation for n = 1.6 and n = 1.5 (both cases) produces essentially the same extinction coefficient--even when the scaled diameters are used. However, for n = 1.5 - 0.1i the extinction coefficient is much larger for the scaled diameters than for the reference diameters. A similar calculation can be carried out for the scattering coefficient using the scaled diameters; the result is $b_{scatt} = 0.28 \times 10^{-4}\ m^{-1}$. As a point of reference, both turbidity and light scattering coefficient ($\lambda = 0.525\ \mu m$) were also measured with multiwavelength sunphotometer, and an integrating nephelometer, respectively, at the same time the size distributions were obtained. These measurements gave an extinction coefficient $b_{ext} = 0.7 \pm 0.4 \times 10^{-4}\ m^{-1}$ and a scattering coefficient $b_{scatt} = 0.4 \pm 0.1 \times 10^{-4}\ m^{-1}$, respectively. While the measurements admittedly have rather large uncertainties, the inclusion of an absorptive (imaginary) term in the refractive index (perhaps unrealistically large) improves the agreement between measured and calculated extinction.

SUMMARY

In this report, we have examined the effect of aerosol refractive index on particle size distribution measurements with optical particle counters and on subsequent calculations of aerosol optical properties using these measured distributions. For no absorption by the particles, size distributions are relatively insensitive to particle refractive index. On the other hand, the distributions appear to be somewhat sensitive to the imaginary part of the refractive index and thus, when properly scaled, can have a significant effect on the calculation of other aerosol optical properties, e.g. extinction coefficient.

ACKNOWLEDGMENT

The author acknowledges, with appreciation, Marcia Baker of the University of Washington for the computer algorithm to compute extinction parameters.

References

1. N. S. Laulainen, "Comments on the Determination of Aerosol Optical Properties," Pacific Northwest Laboratory Annual Report for 1975 to the USERDA Division of Biomedical and Environmental Research, Part 3 Atmospheric Sciences, BNWL 2000 PT3, Battelle-Northwest, Richland, Washington, March 1976, pp. 268-271, 1976.

2. D. Deirmendjian, Electromagnetic Scattering on Spherical Polydispersions, Elsevier, New York, 1969.

3. J. R. Hodkinson, "The Optical Measurement of Aerosols," Aerosol Science, C. N. Davies, Ed., Academic Press, New York, pp. 287-357, 1966.

TABLE 2. Calculated Extinction Coefficient for Several Refractive Indicies Referenced to Latex Spheres with n=1.6 for a Size Distribution Measured at 2000 ft over Seattle on 18 June 1976 with the Whitby Electrical Aerosol Analyzer (EAA) and Royco Optical Particle Counter (OPC)

EAA Ch. No.	Ref. Diameter (μm)	$\frac{\Delta N}{\Delta \log D_p}$ (#/cm^3)	Extinction n=1.6	Coefficient n=1.5		($\mu m^2/cm^3$) n=1.5-0.1i	
3	0.0133	2840	0	0		.01	
4	0.0237	33200	0	0		.63	
5	0.0422	34400	0.31	0.24		4.13	
6	0.075	12400	3.50	2.49		11.3	
7	0.133	4160	28.6	19.7		37.3	
8	0.237	167	16.7	12.1		13.9	
9	0.422	11	6.61	5.91		5.23	
OPC Ch. No.		Sum x $\frac{1}{4}$	13.94	10.11		18.12	
4	0.562	6.26	6.70	6.32[a]	7.39[b]	5.23[a]	9.08[b]
5	0.71	3.64	5.02	5.86	6.08	4.77	7.39
6	0.89	2.23	3.21	4.35	4.48	4.01	22.7
7	1.12	1.71	3.86	3.61	3.90	4.21	25.3
8	1.41	1.13	4.94	4.24	4.46	4.35	22.2
9	1.78	1.03	5.97	6.88	7.73	6.32	26.8
10	2.24	0.76	7.35	6.81	8.28	7.12	29.6
11	2.82	0.74	10.7	11.0	13.6	10.8	41.4
12	3.55	0.63	14.3	14.4	18.0	14.3	52.3
13	4.5	0.50	17.9	18.0	22.0	17.9	60.0
14	5.6	0.34	18.7	18.7	21.8	18.7	60.2
15	7.1	0.088	7.7	7.68	8.62	7.67	22.0
		Sum x $\frac{1}{10}$	10.64	10.79	12.63	10.54	37.9
		Total	24.6	20.9	22.7	28.7	56.0
TOTAL EXTINCTION (10^{-4} m^{-1})			0.25	0.21	0.23	0.29	0.56

a. Using the extinction coefficient per particle (Figure 4) at the reference diameters.

b. Using Figure 4 and the scaled diameters (Case 2 of Table 1).

AIRBORNE MEASUREMENTS OF PARTICLE SIZE DISTRIBUTION, LIGHT SCATTERING AND TURBIDITY AT DIFFERENT ALTITUDES

A. J. Alkezweeny and N. S. Laulainen

Aircraft measurements of particle size distributions, light scattering extinction coefficients, and turbidity over the Pacific Northwest are presented. The size distributions are found to be bi-modal. The extinction coefficients calculated from the size distribution do not agree with that measured by the nephelometer and the sunphotometer.

Simultaneous measurements of particle size distributions, light scattering extinction coefficients and turbidity (aerosol optical depth) over the Pacific Northwest were made in June 1976 using an instrumented DC-3 airplane. The particle size distributions were measured in the range of 0.01 to 5 μm with an electrical aerosol analyzer[1] and a Royco Optical Sensor, Model 220. The optical sensor was interfaced with a 15-channel pulse height analyzer and printer. Aerosol light scattering data were obtained with an MRI integrating nephelometer, Model 1562.[2] A multiwavelength sunphotometer was employed to measure solar intensities in five wavelength bands; only the turbidities derived from the channel at λ = 500 nm were used in this study.

Data were collected at different altitudes from ground level to 10,000 ft MSL. Aerosol extinction coefficients were derived from sunphotometer turbidity measurements using the relationship,

$$b = \Delta\tau/\Delta h$$

where $\Delta\tau$ is the difference between turbidities measured at h and h + Δh. The integrating nephelometer measured aerosol scattering extinction coefficient, b_{scatt}, directly at wavelength λ = 525 nm. For comparison, aerosol extinction coefficients were calculated from the measured size distributions at each altitude using tabulated Mie extinction efficiencies $Q(\alpha_i,n)$ for refractive index n = 1.6 - 0i and a wavelength of λ = 500 nm from the expression

$$b = \sum_i Q(\alpha_i,n)\ \Delta S(D_{p_i}) \cdot \frac{10^6}{4},$$

where $\alpha_i = \pi D_{p_i}/\lambda$ is the size parameter and $\Delta S(D_{p_i})$ is the measured particle surface area ($\mu m^2/cm^3$) in the geometric mean particle diameter size class D_{p_i}. The summation is over all size intervals from about 0.04 to 5 μm. Figure 1 shows the particle volume distributions measured over the Tri-Cities, Sunnyside, and Seattle, Washington. It can be seen that the size distributions are bi-modal with a peak at 0.1 - 0.2 μm particle diameter and a second peak greater than 1 μm. According to Whitby,[3] the submicron mode is characteristic of the polluted atmosphere while the second mode is caused by mechanically produced aerosol such as resuspension and sea spray; there is no interaction between the two modes. The latter can be seen easily by comparing the distributions from Sunnyside and Seattle. Sunnyside is a small community in eastern Washington with no major sources of pollution in contrast to the large metropolitan city of Seattle, where many sources exist. Since the first mode is a result of chemical reactions, it is expected that the peak of this mode should be higher for Seattle than for Sunnyside. On the other hand, the second mode is not related to the pollution level and therefore the two locations ought to have similar values. Actually, the peak of the second mode at Sunnyside is higher than Seattle, indicating resuspension of dust as a possible cause. On June 8, there was a temperature inversion over the Tri-Cities between 5000 and 6000 ft, MSL, resulting in a reduction of concentration of all particle size classes above the inversion. Similar effects were observed in St. Louis in 1975 by others.[4]

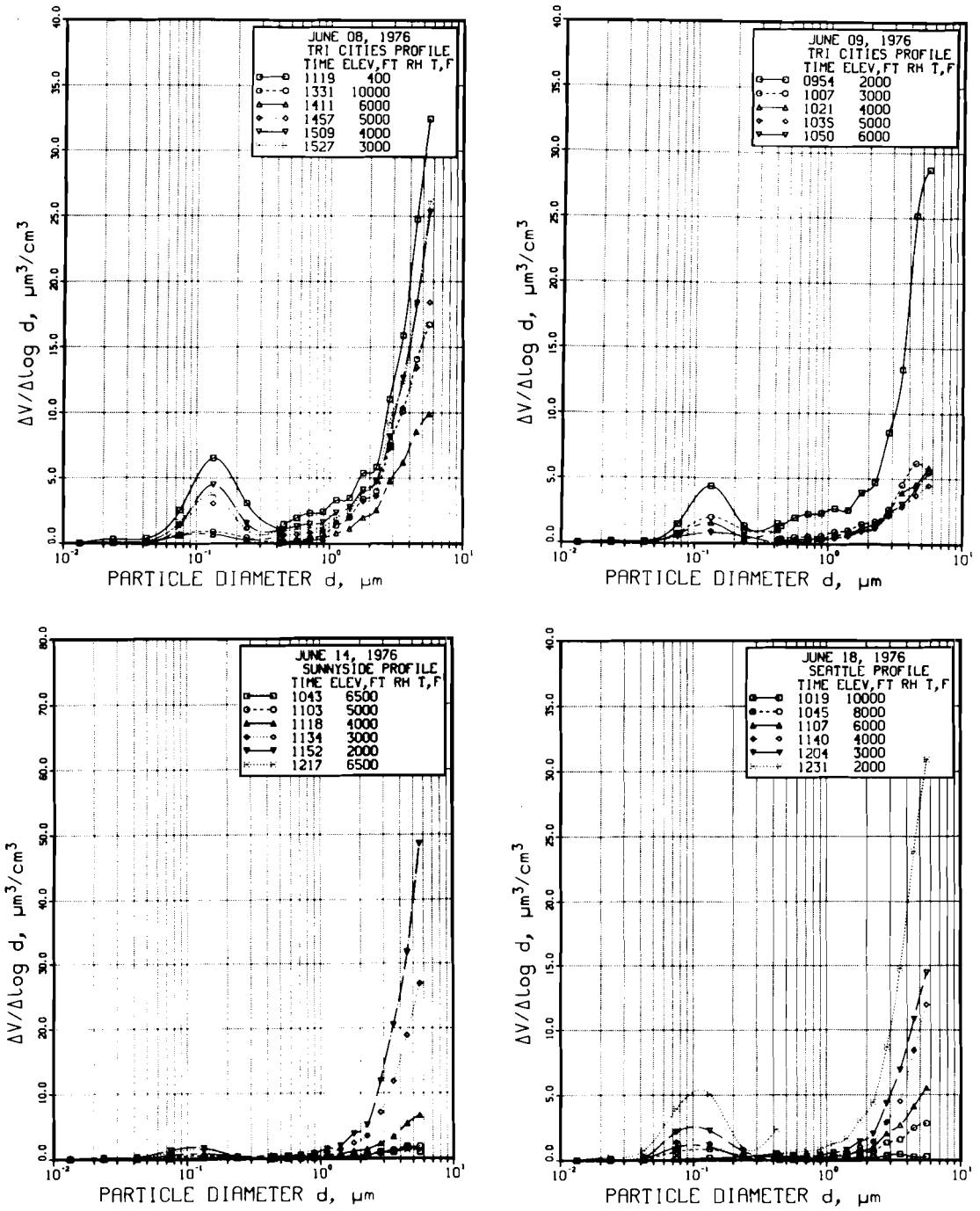

FIGURE 1. Aerosol Volume Distributions

Comparison of the calculated aerosol scattering extinction coefficients using a refractive index of 1.6 and the measured extinction coefficients obtained with the integrating nephelometer and the sunphotometer are shown in Figure 2. In all cases, the calculated values are smaller than the measured values. The poor agreement between measured and calculated extinction was also found for the data obtained over St. Louis during August 1975, even when a substantial imaginary aerosol refractive index was included in the calculations. In many cases, the extinction coefficients derived from the sunphotometer measurements are larger than those obtained with the nephelometer, which measures only aerosol light scattering, while the sunphotometer optical depths contain both light scattering and absorption by the aerosol. Although the measured and calculated b_{scatt} do not agree, the two quantities are well correlated. A correlation coefficient of 0.93 was determined for this set of data. Such behavior was also found by Ensor, et al.,[5] for Los Angeles aerosol. The error in the aerosol extinction coefficients derived from the sunphotometer turbidity measurements is very large in a clear air case because of instrumental resolution and it is consequently difficult to compare them with the nephelometer and calculated values.

On the basis of these limited data and those obtained by the authors at St. Louis, it is not practical to derive particle size distributions from multiwavelength sunphotometer measurements alone; the situation is particularly poor for clean air case.

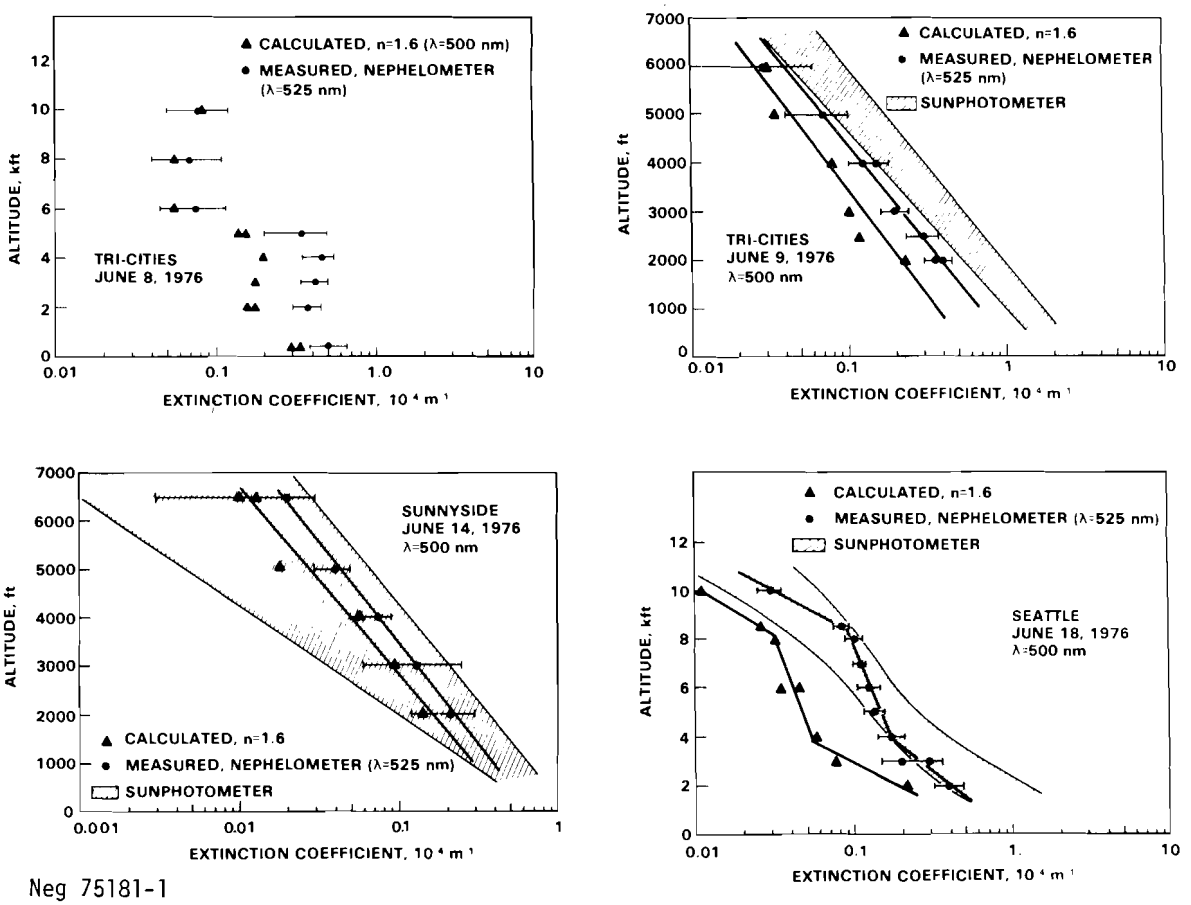

Neg 75181-1

FIGURE 2. Calculated and Measured Extinction as a Function of Altitude

References

1. B. Y. H. Liu, and D. Y. H. Pui, "On the Performance of the Electrical Aerosol Analyzer," J. Aerosol Sci., 6, 249-264, 1975.

2. N. C. Ahlquist, and R. J. Charlson, "A New Instrument for Evaluating the Visual Quality of Air," J. Air. Poll. Control Assoc., 17, 467-469, 1967.

3. K. T. Whitby, "On the Multimodal Nature of Atmospheric Aerosol Size Distributions," Presented at VII International Conference on Nucleation, Leningrad, U.S.S.R., September, 1973.

4. A. J. Alkezweeny, and N. S. Laulainen, "Simultaneous Aerosol Size Distributions and Turbidity Measurements Over a Metropolitan Area," Pacific Northwest Laboratory Annual Report for 1975 to the USERDA Division of Biomedical and Environmental Research. Part 3, Atmospheric Sciences, 202-205, 1976.

5. D. S. Ensor, R. J. Charlson, N. C. Ahlquist, K. T. Whitby, R. B. Husar, and B. Y. H. Liu, "Multiwavelength Nephelometer Measurements in Los Angeles Smog Aerosol. 1. Comparison of Calculated and Measured Light Scattering," J. Coll. Interf. Sci., 39, 242-251, 1972.

SOME ASPECTS OF THE "STATIONARY STATE" APPROXIMATION AND ITS USE IN MODELING KINETIC PHENOMENA

J. M. Hales

The stationary state assumption is examined using some simple examples, and criteria for evaluating when such conditions exist are presented. A practical example - that of application to gas-scavenging calculations- is discussed. Similar treatments should apply beneficially to reaction kinetics problems, especially in situations where difficult differential equations occur.

DESCRIPTION OF THE STATIONARY STATE ASSUMPTION

The stationary state approximation is an important and often utilized tool for modeling transient behavior in composite, chemically reacting systems. It was first applied in the field of chemical reaction kinetics by Bodenstein[1] in his 1908 analysis of rate behavior of the hydrogen-bromine reaction, and has been employed extensively in the field of reaction kinetics since that time. A major use of the stationary state approximation is now modeling of multicomponent, reactive plumes of pollutants in the atmosphere. Other atmospheric applications of lesser importance include modeling of various mass-transfer phenomena.

Some important aspects of stationary state approximations can be illustrated by a simple example. Suppose a chemical species (denoted here by A) is being depleted by competing elementary chemical reactions, one reversible and one irreversible:

$$A \underset{k_2}{\overset{k_1}{\rightleftarrows}} B \qquad (1)$$

$$A \xrightarrow{k_3} C \qquad (2)$$

The rates of formation of A, B, and C in a well mixed system are given by

$$\frac{dA}{dt} = -(k_1 + k_3)\ A + k_2\ B \qquad (3)$$

$$\frac{dB}{dt} = k_1\ A - k_2\ B \qquad (4)$$

$$\frac{dC}{dt} = -\ k_3\ A\ . \qquad (5)$$

These equations may be integrated, subject to appropriate initial conditions A_o, B_o, and C_o, to provide expressions for the concentrations A, B, and C as functions of time. This may be accomplished in a straightforward manner by LaPlace transformation. Transforming (3) and (4) and eliminating L(B)

$$L(A) = \frac{A_o\ s + k_2(A_o + B_o)}{s(s + k_1 + k_2 + k_3) + k_2\ k_3} \qquad (6)$$

which, for a system initially close to equilibrium, i.e.,

$$\frac{B_o}{A_o} \approx K_{eq} \qquad (7)$$

(6) becomes

$$L(A) = \frac{A_o\ (s + k_1 + k_2)}{s(s + k_1 + k_2 + k_3) + k_2\ k_3}\ . \qquad (6a)$$

Equation (6) may be inverted to obtain the rather cumbersome expression

$$A(t) = \frac{1}{a - b}\left\{\left[k_2(A_o + B_o) + a\ A_o\right] e^{at} - \left[k_2(A_o + B_o) + b\ A_o\right]\ e^{bt}\right\}\ ; \qquad (8)$$

$$a,b = -\frac{(k_1 + k_2 + k_3) \pm \sqrt{(k_1 + k_2 + k_3)^2 - 4\ k_2\ k_3}}{2}$$

plus similar forms for B(t) and C(t).

A number of simplifying assumptions can be applied to reduce the complexity of Equations (8), and these various approximations have been denoted as stationary-state assumptions. Radically different predictions of kinetic behavior arise as consequences of these various assumptions, as the following case examples indicate:

Case 1: Near-Equilibrium Conditions

In this case reactions (1) occur so rapidly compared to (2) that the condition

$$\frac{B}{A} \approx K_{eq} \qquad (9)$$

is upheld throughout the course of the reaction; this implies that $k_2, k_1 >> k_3$, and the transformed problem becomes

$$L(A) = \frac{A_o\ (s + k_1 + k_2)}{s(s + k_1 + k_2) + k_2\ k_3}\ . \qquad (6b)$$

Inversion of (6b) and subsequent rearrangement gives the following, much simpler set of expressions for A, B, and C:

$$C(t) = A_o + B_o + C_o - (A_o + B_o)\ \exp\left(-\frac{k_3 t}{1 + K_{eq}}\right)\ ;$$

$$A(t) = \frac{A_o + B_o + C_o - C(t)}{1 + K_{eq}}\ ;$$

$$B(t) = K_{eq}\ A(t)\ . \qquad (10)$$

Several important aspects of this type of approximation should be emphasized. First, it should be noted that invocation of (9) effectively eliminated differential Equation (4), leading directly to a simplification of the problems; in fact, (9) can be derived from (4) by setting the derivative equal to zero. It is extremely important to realize, however, that applying (4) in this manner is not equivalent to setting dB/dt = 0. Note that the final solution (10) dictates that B should indeed vary with time. Disregarding this point can lead to serious errors in interpreting reaction phenomena.

A second important aspect of this example concerns the conditions for which the Case 2-type approximations are valid. The transformed Equations (6) and (6b) provide specific information in this regard; by inspection one can deduce that the critical conditions that must be satisfied is

$$k_2 >> k_3 \quad . \tag{11}$$

Moreover, the obvious condition that the initial concentrations A_0 and B_0 must be close to equilibrium must be upheld. These two conditions correspond, respectively, to perturbations on the equilibrium by the forcing function k_3 A and by the initial conditions. In problems involving air pollution chemistry, one usually can ignore the second condition. This is not universally true, however, and caution should be exercised to ensure that both conditions are upheld whenever Case 1 - type approximations are applied.

Criterion (11) applies specifically to system (1), and cannot be extended directly to more general cases. This example is pertinent, however, in its demonstration that such criteria often may be deduced more readily by inspection of the transformed equations, rather than the equations or the solutions, themselves.

Finally, it should be noted that typical kinetics software packages usually yield Case 1 solutions when steady states are stipulated. This can be seen by noting the system.

$$\frac{dA}{dt} = -(k_1 + k_3) A + k_2 B \tag{3}$$

$$B = K_{eq} A \tag{9}$$

$$\frac{dC}{dt} = k_3 A \quad . \tag{5}$$

Proceeding from (3) - (9) - (5) in a sequential fashion typical of Runge-Kutta or most other applicable finite-difference approximations yields results that correspond directly to Equations (10).

Case 2: Near-Equilibrium Conditions and Low Intermediate Concentrations

This case is of little practical significance to reaction system (1) - (2), but it is extremely important for application to more complex systems involving short-lived, transient intermediates. The previously-mentioned application of Bodenstein[1] belongs to this class.

Modification of (3) - (5) corresponding to this assumption can be accomplished by the following steps:

- replace (4) with (9)
- substitute (9) into (3).

This provides the system

$$\frac{dA}{dt} = -k_3 A \tag{3a}$$

$$B = K_{eq} A \tag{9}$$

$$\frac{dC}{dt} = k_3 A \tag{5}$$

with the solutions

$$A(t) = A_0 e^{-k_3 t}$$

$$B(t) = K_{eq} A(t)$$

$$C(t) = C_0 + A_0 (1-e^{-k_3 t}) \tag{12}$$

It is especially important to note here that, even though solutions (12) are based essentially on assumption (9), they still vary radically from Solutions (10). One must be careful in applying steady-state approximations that Case 2 assumptions are not inadvertently applied when Case 1 approximations are desired.

Case 3: Zero-Derivative Conditions

Readdressing Equations (1) - (3), it is interesting to consider one further case. Since (9) was based on the idea that $k_1 A - k_2 B$ (= dB/dt) = 0, one can attempt to examine the effect of replacing (4) with

$$\frac{dB}{dt} = 0 \tag{13}$$

to obtain the set

$$\frac{dA}{dt} = (-k_1 + k_3) A + k_2 B \tag{3}$$

$$\frac{dB}{dt} = 0$$

$$\frac{dC}{dt} = k_3 A \qquad (5)$$

with the solutions

$$A(t) = \frac{1}{(-k_1 + k_3)} \left\{ -k_2 B + \left[(-k_1 + k_3) A_o + k_2 B\right] \exp \left[(-k_1 + k_3) t\right] \right\}$$

$$B(t) = B_o$$

$$c(t) = C_o + A_o - A(t) \qquad (14)$$

Case 3 is the only example in which dB/dt is actually set equal to zero. It makes little sense in a physical sense, and thus it is not useful for practical interpretation. It is important, however, to recognize that this type of substitution can be made inadvertently, and to guard against this occurring in practice.

Several other cases of these types can be considered; and the stationary state assumption emerges as a class of asymptotic approximations to behavior under limiting conditions. Class 1 conditions are of primary interest to this discussion, and will be considered individually in the remaining text.

For situations where analytical solutions are sought, use of the steady-state approximation bears the advantage of considerable mathematical simplification. This is true also for numerical solutions; in such cases however, a second advantage of avoidance of stiff differential equations is usually more important. Stiffness in ordinary differential equations--when present--is a particularly annoying aspect of most common numerical techniques, and it can often be avoided by use of the stationary state approximation.

The question of zeroing dB/dt in Equation (4) has led to several misconcepts in the past. Many established texts[2,3,4,5] suggest that applying the stationary state assumption is indeed equivalent to holding the concentration of a specific intermediate (B in this case) constant. Several rather involved--and ofter erroneous--arguments have been advanced in support of this concept. It has been reasoned, for example, that transient, intermediate species occur at such low concentrations that their time rates of change are negligible, thus allowing their derivatives to be set equal to zero to formulate stationary state relationships. Such reasoning, however, is superfluous and unnecessary for Case 1 conditions. It is much less confusing and misleading to visualize this type stationary state approximation solely as an asymptotic approach of a reacting system to dynamic equilibrium conditions.

CRITERIA FOR VALIDITY OF THE STATIONARY STATE APPROXIMATION

Granted the convenience of the stationary state approximation, it is of obvious interest to obtain some reliable criterion to ascertain conditions under which this assumption is valid. In qualitative terms, use of this approximation should be acceptable whenever:

1) the rate constants of the reactions in the "stationary state" process are much greater than those in competing reactions;[a] and

2) sufficient time has passed to allow for the effects of initial conditions to decay.

Several investigators (cf. Rice[6]) have derived criteria for validity of the stationary state approximation, but these have been confined largely to simple well-mixed systems where initial conditions were assumed unimportant. Furthermore, no serious attempt has been made to develop criteria useful for switching to or from the stationary state approximation at intermediate points in a computational algorithm.

One method of ascertaining the validity of stationary state assumptions is to solve a given kinetics problem, both with and without help of the approximation, and simply compare the results. This has been

[a] "Competing reactions" are viewed here as any mechanisms, physical or chemical, that may perturb the local concentration. An example of a physical effect in this regard is turbulent mixing.

accomplished by previous authors, both analytically for simple systems (cf. Leighton[7]) and numerically for more complex problems (cf. Hecht, et al.[8]). It is a somewhat unsatisfying approach in that it requires solution of the rigorous equations - precisely what was to be avoided in the first place. Once such an exercise has been conducted, however, certain insights are gained which may be applied for other problems. Thus a stationary state approximation may be applied with reasonable confidence to a subsequent but similar system once it has been proven a valid approximation for the original problem.

Other criteria for stationary state application can be developed by examination for the differential equations themselves. On an intuitive basis, for example, in the well-mixed reaction described by the rate equation

$$\frac{dA}{dt} = R_g - R_d$$

where R_g and R_d are the generation and decay reactions of component, A should be expected to approximate stationary state behavior whenever

$$\frac{dA/dt}{R_g} << 1 \text{ and } \frac{dA/dt}{R_d} << 1.$$

Since R_g and R_d essentially require solution of the differential equations for their evaluation, however, this criterion is of limited value.

The criteria discussed above tend to apply primarily to well-mixed systems, where the rate coefficients are constant and the only mechanism for effecting concentration change is chemical reaction. They are useful for establishing whether or not to implement a stationary-state approximation prior to performing a calculation, but are of limited application to problems where switching to a stationary state is desirable at points during the course of computation.

More flexibility in this respect is provided by a somewhat different approach, which utilizes a partial solution to a linearized version of the rate expression. The procedure is as follows:

Consider once again

$$\begin{array}{l} A \overset{k_1}{\rightarrow} B \\ B \overset{k_2}{\leftarrow} A \end{array} \qquad (1)$$

where the concentration of component A varies because of reactions 1 and additional unspecified competing processes (reaction, mixing,...), A rate equation for B can be written as follows:

$$\frac{dB}{dt} = - k_2 B + k_1 A. \qquad (4)$$

Since not all processes for changing the concentrations of A are specified, we cannot write a corresponding equation for its rate of change. For the present analysis we will simply approximate this unknown entity by an appropriate constant value Γ:

$$\frac{dA}{dt} \cong \Gamma. \qquad (15)$$

Differentiating (4) and substituting $dB/dt = \xi$, the following form is obtained:

$$\frac{d\xi}{dt} + k_2 \xi = k_1 \frac{dA}{dt} \cong k_1 \Gamma. \qquad (16)$$

This may be integrated between the limits (o,t) and (ξ_o,ξ) to obtain

$$\xi = -\left(\frac{k_1}{k_2}\Gamma - \xi_o\right)\exp(-k_2 t) + \frac{k_1}{k_2}\Gamma \qquad (17)$$

where $\xi_o = k_1 B_o + k_1 A_o$, A_o and B_o being the initial concentrations. The concentration at any time, t, is obtained by integrating (21) from 0 to t:

$$\int_o^t \xi \, dt = \int_o^t \frac{dB}{dt} dt = B(t)$$

$$= \left\{\left(\frac{k_1}{k_2^2} - \frac{k_1}{k_2} A_o + B_o\right)[\exp(-k_2 t) - 1] + B_o\right\}$$

$$+ \left\{\frac{k_1}{k_2}\Gamma t\right\} \qquad (18)$$

Now, under conditions where the stationary state approximation is valid

$$B(t)|_{ss} = \frac{k_1}{k_2} A = \frac{k_1}{k_2}(\Gamma t + A_o) \qquad (19)$$

A reasonable criterion for approach to steady state concentrations is

$$\frac{B(t) - B(t)_{ss}}{B(t)_{ss}} << 1 \qquad (20)$$

thus from (16) and (19)

$$\frac{\left(\frac{\Gamma}{k_2} - A_o + \frac{k_2}{k_1} B_o\right) \exp(-k_2\, t) - \frac{\Gamma}{k_2}}{\Gamma\, t} << 1. \quad (21)$$

This criterion has some advantage over its counterparts because it reflects any perturbations caused by initial conditions, and also because it allows more convenient assessment of nonreactive mechanisms.

Equation (21), or variations of it, may be utilized as practical criteria for determining validity of the stationary state assumptions, provided, of course, that some means for estimating Γ exists. This is often difficult to accomplish prior to computation, but can be satisfied concurrently with many numerical calculations, thus allowing the possibility of switching on or off the stationary state approximation during the course of a computation. Although this course of action would seem to offer advantages in providing more efficient computation, it is a practice that has not been employed extensively up to now.

A few comments regarding criterion (21) are in order. First it should be noted that the first bracketed term in (18) provides the transient response, both to the initial conditions and to the forcing function $\Gamma \cong \frac{dA}{dt}$.

For small t the initial conditions tend to dominate the transient behavior of the system. For larger t the initial conditions tend to become unimportant and it is primarily Γ that dictates transient response. These features are evident in Equation (18) as well as in the criterion (21).

APPLICATION OF STATIONARY STATE APPROXIMATIONS TO GAS SCAVENGING COMPUTATIONS

As has been described in previous work,[9] the response of pollutant concentration in a falling raindrop to a corresponding gas-phase pollutant environment may be expressed by the equation

$$\frac{dc}{dz} = \frac{3k_y}{av_t}(y - H'c) \quad (22)$$

where c and y are the aqueous-phase and gaseous-phase pollutant concentrations, z is the vertical location of the drop, a is the drop radius, v_t is its fall velocity, k_y is a mass-transfer coefficient, and H' is a solubility parameter. Letting $k_2 = 3\, H'\, k_y/av_t$ and $k_1 = 3\, k_y/av_t$ we have

$$\frac{dc}{dz} = -\, k_2 c + k_1 y. \quad (23)$$

y, on the other hand, varies rather independently of c, and depends upon plume geometry, wind speed, and raindrop fall velocity. Equation (23) often becomes extremely stiff, and a stationary state approximation would facilitate the computation process. This approximation is

$$c = \frac{k_1}{k_2}\, y \text{ at s.s.} \quad (24)$$

Now, to draw things into direct correspondence with the previous derivation, we let y = A and c = B. Equations (23) and (24) then become

$$\frac{dc}{dz} = k_1 A - k_2 B$$

and $B = K_{eq}\, A$.

Denoting dy/dz by Γ, one can use criterion (21) to evaluate stationary state behavior. Upon resubstituting the original variables the result is

$$\left\{\left[\frac{av_t}{3\, H'\, K_y} - \frac{(y_o + H'\, c_o)}{-\, dy/dz}\right] \exp\left[\frac{3\, H'\, K_y}{av_t}(z - z_o)\right] - \frac{av_t}{3\, H'\, K_y}\right\} \frac{1}{z - z_o} << 1 \quad (25)$$

where y_o and c_o are concentrations at location z_o. At the present time a numerical code for solution of (22) is being modified to test automatically for satisfaction of (25) and to compute the subsequent concentration value on the basis of the stationary state approximation if this criterion is satisfied. Otherwise the procedure shifts to the basic predictor-corrector algorithm for solution of (22). Since this test is conducted every step, it is expected to allow a marked increase in the computational step size, with a corresponding savings in computer execution time. This same general approach should benefit reaction kinetics codes where similar problems are encountered.

References

1. M. Bodenstein, Z. Physik. Chem., 35, 329, 1913.
2. K. J. Laidler, Chemical Kinetics, McGraw-Hill, New York, 1965.
3. O. Levenspiel, Chemical Reaction Engineering, Wiley, New York, 1962.
4. J. G. Calvert, and N. J. Pitts, Photochemistry, Wiley, New York, 1966.
5. A. A. Frost, and R. G. Pearson, Kinetics and Mechanism, Wiley, New York, 1961.
6. O. K. Rice, "Conditions for a Steady State in Chemical Kinetics," J. Phys. Chem., 64, 1851-1857, 1960.
7. P. A. Leighton, Photochemistry of Air Pollution, Academic Press, New York, 1961.
8. T. A. Hecht, P. M. Roth and J. A. Seingelf, Mathematical Simulation of Photochemical Reactions, Report R73-28, Systems Applications Inc., San Rafael, California, 1973.

NUMERICAL MODELING IN SUPPORT OF THE LONG RANGE PLUME TRANSFORMATION STUDY

J. M. Hales

This report is a brief, qualitative description of how the PROTEUS computer code is being applied in evaluation of aircraft plume transformation data. Several additional runs in conjunction with the 1976 field data are anticipated for the immediate future.

The PROTEUS computer code, described in an earlier report,[1] is now being applied to analysis of data from the long-range plume transformation study. The current focus of this research is to evaluate postulated homogeneous thermal and photochemical transformation mechanisms for SO_2 conversion.

A schematic representation of the code's application is shown in Figure 1. Here the wind and concentration data from an initial aircraft cross section are interpolated to grid centers on a Y-Z computation grid. These then are utilized as boundary conditions for the differential equations of the computer code, whose solutions are approximated numerically for comparison with values measured by the aircraft at downwind locations.

There have been two major efforts in this area recently. The first effort was the creation of the necessary software to produce magnetic tape records of the gridded data for subsequent use by the PROTEUS code. The second major effort was the adaption of a previously-described parameterized reaction kinetics sequence for use with PROTEUS. This is the 39-step lumped mechanism, published by Hecht, et al.,[2] which is shown for reference in Table 1. It is currently being applied as a driver to generate free-radical concentration values necessary for examination of various photochemical SO_2 conversion mechanisms. A number of test runs in conjunction with the 1976 aircraft plume transformation results are planned for the immediate future.

PROTEUS-FIELD MEASUREMENT INTERACTION

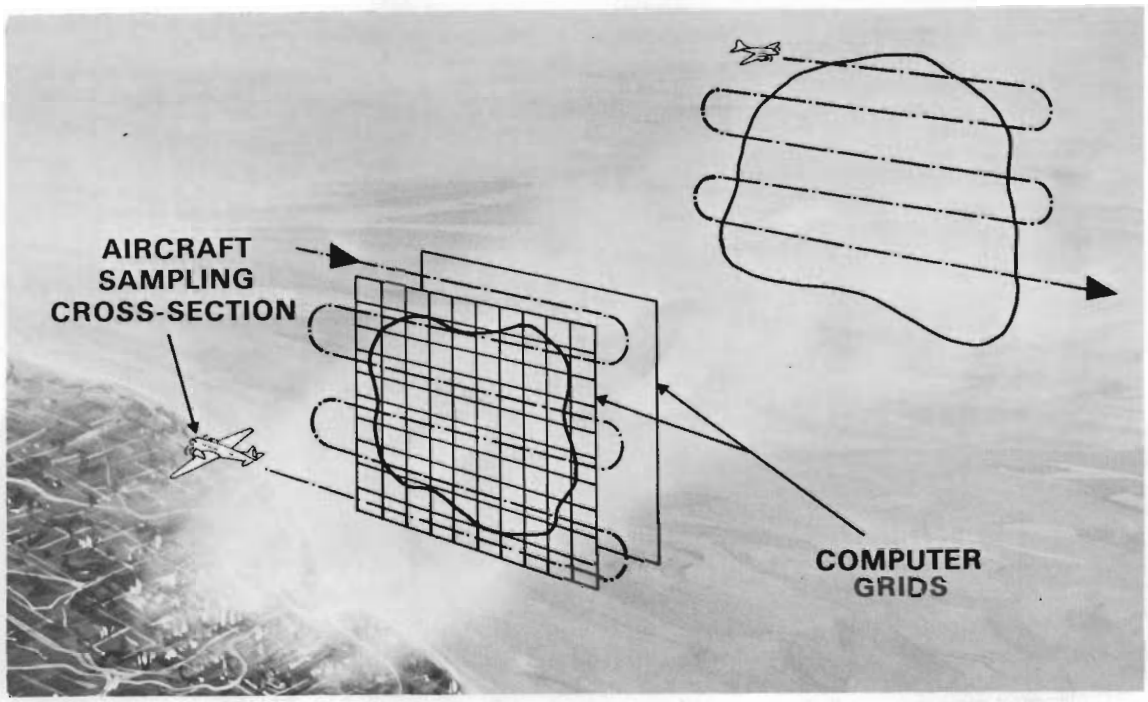

Neg 77350-3

FIGURE 1. Schematic of Proteus Code Application

TABLE 1. Lumped Kinetic Mechanism for Photochemical Smog Developed by Hecht, et al[2]

NO_2-NO-O_3 Cycle

$$NO_2 + h\nu \xrightarrow{1} NO + O$$
$$O + O_2 + M \xrightarrow{2} O_3 + M$$
$$O_3 + NO \xrightarrow{3} NO_2 + O_2$$

Important reactions of O with inorganic species

$$O + NO + M \xrightarrow{4} NO_2 + M$$
$$O + NO_2 \xrightarrow{5} NO + O_2$$
$$O + NO_2 + M \xrightarrow{6} NO_3 + M$$

Chemistry of NO_3, N_2O_5, and HNO_3

$$O_3 + NO_2 \xrightarrow{7} NO_3 + O_2$$
$$NO_3 + NO \xrightarrow{8} 2NO_2$$
$$NO_3 + NO_2 \xrightarrow{9} N_2O_5$$
$$N_2O_5 \xrightarrow{10} NO_2 + NO_3$$
$$N_2O_5 + H_2O \xrightarrow{11} 2HNO_3$$

Reactions of HNO_3 with inorganic species

$$NO + HNO_3 \xrightarrow{12} HNO_2 + NO_2$$
$$HNO_2 + HNO_3 \xrightarrow{13} H_2O + 2NO_2$$

Chemistry of HNO_2

$$NO + NO_2 + H_2O \xrightarrow{14} 2HNO_2$$
$$2HNO_2 \xrightarrow{15} NO + NO_2 + H_2O$$
$$HNO_2 + h\nu \xrightarrow{16} OH + NO$$

Important reactions of OH with inorganic species

$$OH + NO_2 \xrightarrow{17} HNO_3$$
$$OH + NO + M \xrightarrow{18} HNO_2 + M$$
$$OH + CO + (O_2) \xrightarrow{19} CO_2 + HO_2$$

Oxidation of NO by HO_2

$$HO_2 + NO \xrightarrow{20} OH + NO_2$$

Photolysis of H_2O_2

$$H_2O_2 + h\nu \xrightarrow{21} 2OH$$

Organic Oxidation Reactions: HC_1 = olefins, HC_2 = aromatics, HC_3 = paraffins, HC_4 = aldehydes

$$HC_1 + O \xrightarrow{22} ROO + \alpha R\overset{\overset{\|}{O}}{C}OO + (1-\alpha)HO_2$$
$$HC_1 + O_3 \xrightarrow{23} R\overset{\overset{\|}{O}}{C}OO + RO + HC_4$$
$$HC_1 + OH \xrightarrow{24} ROO + HC_4$$
$$HC_2 + O \xrightarrow{25} ROO + OH$$
$$HC_2 + OH \xrightarrow{26} ROO + H_2O$$
$$HC_3 + O \xrightarrow{27} ROO + OH$$
$$HC_3 + OH \xrightarrow{28} ROO + H_2O$$
$$HC_4 + h\nu \xrightarrow{29} \beta ROO + (2-\beta)HO_2$$
$$HC_4 + OH \xrightarrow{30} \beta R\overset{\overset{\|}{O}}{C}OO + (1-\beta)HO_2 + H_2O$$

Reactions of organic free radicals with NO, NO_2, and O_2

$$ROO + NO \xrightarrow{31} RO + NO_2$$
$$R\overset{\overset{\|}{O}}{C}OO + NO + (O_2) \xrightarrow{32} ROO + NO_2 + CO_2$$
$$R\overset{\overset{\|}{O}}{C}OO + NO_2 \xrightarrow{33} R\overset{\overset{\|}{O}}{C}OONO_2$$
$$RO + O_2 \xrightarrow{34} HO_2 + HC_4$$
$$RO + NO_2 \xrightarrow{35} RONO_2$$
$$RO + NO \xrightarrow{36} RONO$$

Other peroxy radical reactions

$$HO_2 + HO_2 \xrightarrow{37} H_2O_2 + O_2$$
$$HO_2 + ROO \xrightarrow{38} RO + OH + O_2$$
$$2ROO \xrightarrow{39} 2RO + O_2$$

References

1. J. M. Hales, "A User Oriented Computer Code for Solution of the General Equations of Continuity for Trace Substances in the Atmosphere." PNL Annual Report for 1974 to USAEC DBER, BNWL-1950, pt. 3, pp. 77-78, 1975.
2. T. A. Hecht, J. H. Seinfeld, and M. C. Dodge, "Further Development of Generalized Kinetic Mechanism for Photochemical Smog," Envi. Sci. Tech., 8, 327-332 1974.

AN ALGORITHM FOR ANALYZING AND DISPLAYING AEROSOL DATA

D. R. Drewes and N. S. Laulainen

Computer software has been written to analyze aerosol data recorded from the Whitby Electrical Aerosol Analyzer (EAA) and the Royco Optical Particle Counter (OPC). Output is both printed and graphical.

The increasing amounts of aerosol data collected under various programs dictated the development of computer software to analyze the data and display the resultant aerosol size distributions. The algorithm which resulted performs basically the same simple but time-consuming computations on the data previously done by hand and produces printed output of both normalized and non-normalized aerosol number, surface, and volume distributions. In addition, the algorithm also generates plots of these various distributions versus particle diameter, as shown in Figure 1. This aspect of the algorithm allows the data to be viewed in a much more meaningful way than the simple printed output, and considerable effort was spent in making the graphical output as useful as possible. The user has several options, including the use of different colors to differentiate between data taken at various times. A legend is included to present other information relevant to the plots. Taken together, the graphical and printed output of the algorithm present a powerful way to analyze and view data on aerosol distributions.

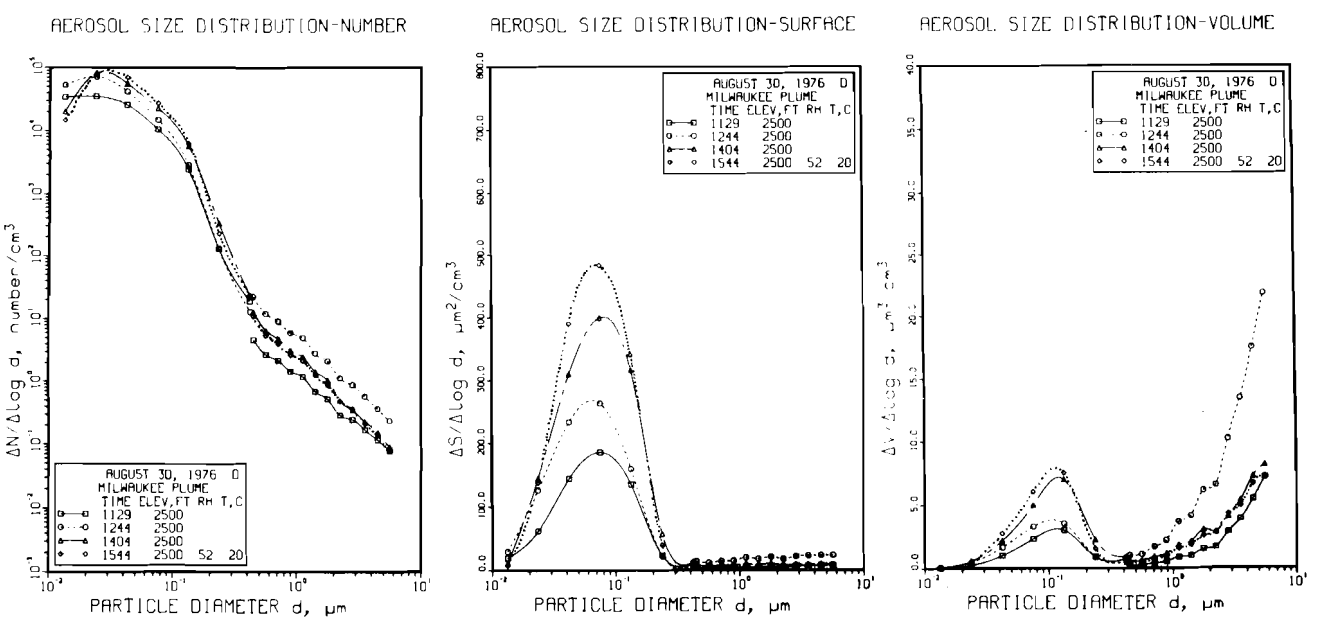

FIGURE 1. Graphical Output from Aerosol Data Analysis Algorithm

AN ALGORITHM FOR PROCESSING AND ANALYZING DATA FROM THE BNW DC-3 RESEARCH AIRCRAFT

D. R. Drewes and A. J. Alkezweeny

The data acquisition system aboard the BNW DC-3 research airplane records data, as voltage signals, in a compact binary format on 7-track magnetic tape. Computer software has been written which converts these data to appropriate units and makes them available for analysis. The user has direct control over the important aspects of the analysis, and the modular nature of the code allows great flexibility in the types of analyses to be performed. In addition to printed output, graphic output may be generated using the highly versatile DISSPLA graphics package.

A flexible algorithm for analyzing and displaying data recorded by the data acquisition system aboard the BNW DC-3 aircraft was described in a previous report.[1] Since that time, instrument changes and the addition of a VLF navigation system have resulted in a need to alter the format in which the data are recorded on the 7-track tape. Data are still recorded in binary form with 12-bit resolution, but to record more parameters, the number of seconds of data per tape record was reduced from 15 to 6. The 42 channels recorded each second under the present configuration are shown in Table 1.

These changes in data format have required some changes in the software used to analyze the information. The modular form in which the algorithm was originally written, however, has greatly simplified these adaptations. The major changes have been in the subprogram units which direct the graphical output. After looking at preliminary plots and printout of the data, it was determined that the most information could be gained from the O_3, NO_x, SO_2, and nephelometer data, and that temperature, dewpoint, humidity, and wind data were also important. Accordingly, a subroutine was written to compose a page containing plots of these data. When inserted into the program as a module, it produces (on film) a display of these data for any time period specified by the user. An example is shown in Figure 1. The VLF navigation system data (latitude and longitude) have been

TABLE 1. Data Recorded by DC-3 Data Acquisition System

Channel	Parameter
1	Day
2	Month
3	Time (minutes)
4	Time (seconds)
5	Altitude
6	Airspeed (M8 system)
7	VOR 1
8	VOR 2
9	DME
10	Temperature
11	Dewpoint
12	Ozone (data)
13	NO (data)
14	NO_2 (data)
15	SO_2 (data)
16	Nephelometer
17	Hi-vol flow
18	Condensation nuclei (data)
19	Condensation nuclei (range)
20	Ozone (range)
21	NO_x (range)
22	SO_2 (range)
23	Aerosol (data)
24	Aerosol (range)
25	Hi-vol status
26-27	Airspeed (VLF system)
28-29	Wind velocity
30-31	Wind direction
32-33	Ground speed
34-37	Latitude
38-41	Longitude
42	Event mark

used to refer the data to a spatial rather than a temporal frame. The flexibility originally designed into the algorithm has allowed modification to accommodate changes in both the input it receives and the output it produces.

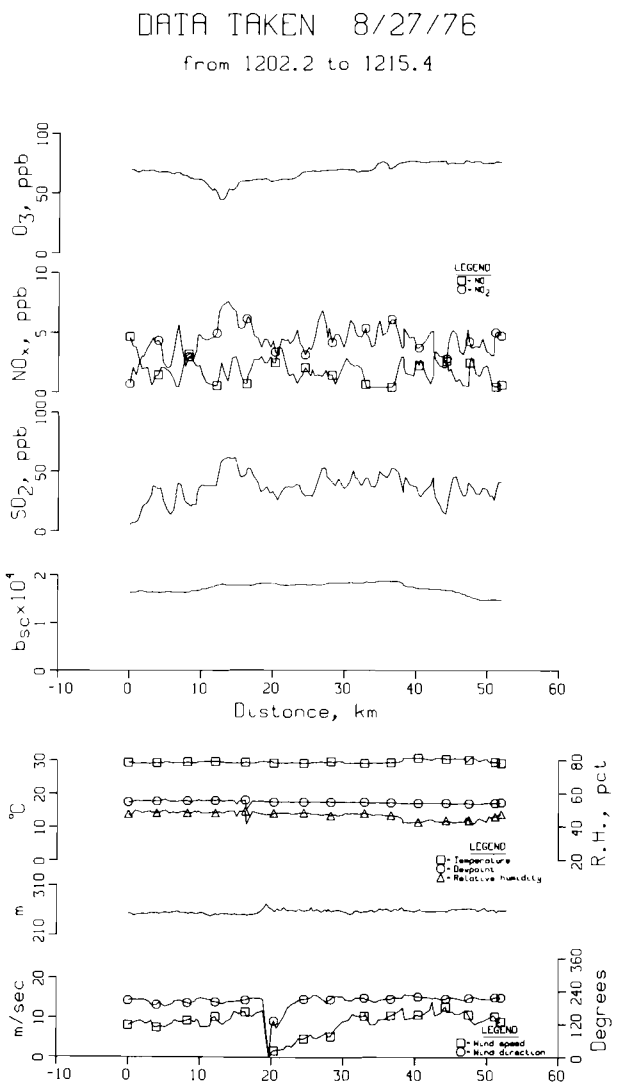

FIGURE 1. Graphical Output from DC-3 Data Analysis Algorithm

Reference

1. D. R. Drewes, "A Computer Algorithm for Reduction and Presentation of Information from the BNW DC-3 Data Acquisition System," PNL Annual Report for 1975 to the USERDA Division of Biomedical and Environmental Research, Part 3, Atmospheric Sciences, BNWL-2000, PT 3, UC-11, pp. 169-171, 1975.

A VERY LOW FREQUENCY NAVIGATION SYSTEM AS A RESEARCH TOOL

R. F. Edwards, F. O. Gladfelder and J. R. Lugar

To provide the researcher with basic parameters, such as time, geographic location, altitude, airspeed, heading, and speed/direction of winds aloft at the time a parcel of air is being sampled, an accurate method of obtaining this information must be provided. This report summarizes the use of a Global VLF GNS-500A Navigational System which has been installed in the BNW Douglas DC-3 airplane to meet this need.

The GNS-500A is a medium and long-range navigation system intended to provide area navigation on a worldwide basis by reference to ground facilities at extreme distances throughout the world.

The GNS-500A operates by phase tracking very low frequency (VLF) communications signals, in addition to OMEGA unique frequencies. An onboard computer continually monitors digitally phase-locked receivers, computing the expected phase angle of each signal with respect to the geographic location of the transmitters and airplane. The distance in meters from each transmitter to the airplane is computed every four-tenths of a second. These and other computations provide the basis for a multitude of fixes of airplane position and change in position.

Aircraft equipped with VLF navigation have greatly simplified the tracking of plumes. VLF features digital readout of Greenwich meantime and date, present position, stored waypoint coordinates, bearing to waypoints, distance and estimated time to waypoint, airplane drift angle, ground speed, true air speed, cross track distance, wind direction and speed.

The VLF system provides Great Circle point to point navigation, independent of the requirement for ground-based radio navigation aids in the surrounding area of flight, thus enabling the research airplane to sample over mountainous terrain and large bodies of water at all elevations.

The VLF system utilizes a digital computer in conjunction with very low frequency (10-30 kHz) radio transmission to provide great circle navigation capability from a known point. Transmissions used by the VLF system are provided by VLF United States Naval Communications Stations and the Omega Navigational Network. The computer automatically selects eight signals which when used simultaneously will optimize the navigation accuracies in the geographical area of flight, therefore, making it possible to precisely pinpoint the geographic locations of the entry and exit point of the plume under study.

In case of plume direction change, the VLF system can provide guidance from its present position to any waypoint selected, create a pseudo-vortac at any waypoint, or to establish an offset parallel course. A new route of flight can be quickly programmed should a change of course be necessary.

Figure 1 shows how the VLF system aids the researcher by giving wind speed/direction and precise coordinates of the parcel of air being sampled, therefore, enabling the researcher to determine in advance where the next downwind crossing should take place.

The VLF system provides up-to-date information with regards to changes in direction and speed of winds aloft.

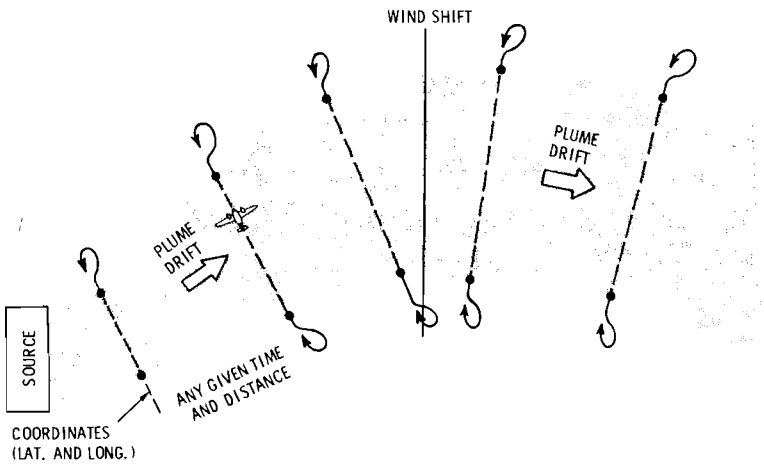

Neg 77517-1

FIGURE 1. The VLF System Enables the Research Airplane to Follow the Same Parcel of Air Downwind from the Source

This on-the-spot information alerts the researcher to any changes in direction or speed of the air parcel being sampled.

All information provided by the VLF system is fed into the airborne data acquisition system which consists of a Data General NOVA 1220 Processor, multiplexer/analog-to-digital converter and 7-track industry-compatible magnetic tape transport.

The NOVA processor contains 8K 16-bit words of core memory. A hardware multiply/divide option permits rapid arithmetic operations for real time engineering unit conversion and data averaging.

Analog parameters from the onboard research instrumentation are acquired via a high level (0-5 volt) multiplexer/analog-to-digital converter (12 bit) which has a capacity of 16 different input channels. The system is capable of conversion rates up to 28 kHz.

The acquired data are formatted and written to 7-track tape, which can be directly processed on other computer systems. The tape medium also serves as input for the acquisition applications programs. The onboard terminal device with paper tape input capability (teletype model ASR33) allows real time examination of the data being collected.

References

1. Project Speckled Trout, Navigation Systems Operation Evaluation, Andrews Air Force Base, Washington, DC.

2. Global Navigation Incorporated, GNS-500 VLF Navigation System, Report 1010, Los Angeles, CA, 1975.

COMPOSITE MODELS FOR ATMOSPHERIC PROCESSES

Consideration of the alternative strategies for using coal-fired electric power plants has caused a pressing need to evaluate the human health and ecological effects of the associated pollution over a multi-state area. As part of the cooperative MAP3S program, PNL has developed an assessment model which simulates atmospheric transport, diffusion, chemical transformation, dry deposition and precipitation scavenging. The model incorporates the results of programs directed specifically at each of these processes, and is being improved and verified.

The reports in this section reflect efforts to make the model more realistic, but at the same time, maintain the economy needed for long-term assessments. Significant effort was applied to converting the hourly precipitation data from the station file format of the National Climatic Center to a synoptic file format required for real time consideration of precipitation patterns in assessment models. Preliminary assessment work is reported for selected combinations of power plants both in the northeast and northwest United States.

- MAP3S MODELING STUDIES
- PACIFIC NORTHWEST REGIONAL ASSESSMENT PROGRAM

A FORMULATION OF TIME-VARYING DEPTHS OF DAYTIME MIXED LAYER AND NIGHTTIME STABLE LAYER FOR USE IN AIR POLLUTION ASSESSMENT MODELS

D. C. Powell

A descriptive two-layer physical model of the vertical enhancements and constraints on mixing of material emitted from ground-based sources is presented. The model allows for stability variation throughout a mixed layer that increases in depth during the daytime and throughout a surface-based stable layer that increases in depth at night. Above these heights moderately stable conditions are assumed to prevail constantly. For grids on the order of $(1000\ km)^2$ the only effective barrier to vertical penetration is the top of the mixed layer, which vanishes as a constraint at night. Incorporation of the above into a computer model facilitates differentiation of the vertical growth of mass increments according to (1) whether or not the effective release height is included within the current depth of the daytime mixed layer or nighttime stable layer and (2) whether the mass increment is a new release confined within the maximum diurnal mixed layer or an older release that has expanded beyond this depth.

INTRODUCTION

Tennekes[1] states that the principal variables in air-pollution dispersal over moderately long distances are the wind-speed vector and the height of the mixed layer. Sophisticated trajectory calculation methods are already well-known[2,3] and are included in the present Battelle Lagrangian puff model. The change in behavior of the mixed layer depth with time has been incorporated in the above model during the preceding year.

The mixed layer height is usually considered an effective barrier to vertical penetration. But different writers present conflicting accounts of the basic behavior of the mixed layer height. Norton and Hoidale[4] depict the mixed layer height as varying sinusoidally in a diurnal cycle, increasing during the daytime and decreasing at night, all of which takes place within 3000 to 4000 m. On the other hand, Carson[5] depicts the mixed layer height as a function that increases during the daytime, following which it loses its definition. This picture is in relative agreement with modeling results by Venkatram and Viskanta[6] and with experimental results by Kaimal, et al.[7] If these latter views are correct, particularly if the mixed layer is undefined at night, there should be significant escape of pollutant material beyond the maximum depth of the mixed layer, since pollutant materials tend quickly to become uniformly distributed through the mixed layer in the afternoon.[8]

The diffusivity profiles of Machta[9] indicate that the tropopause height rather than any height associated with the mixed layer is the appropriate location for modeling a numerical discontinuity in the vertical diffusivity. This implies that if the mixed layer is an effective constraint to vertical penetration, it is not continuously so.

THE PHYSICAL MODEL

Based on the literature cited and our own inspection of radiosonde data, we have developed a computer model of the mixed layer derived from Carson's model.[5] The code puts into effect

- a mixed layer depth that increases during the daytime, and which acts as a constraint to vertical penetration during the day but not at night;
- a surface-based stable layer that increases in depth at night;
- an absolute barrier to further vertical penetration at the tropopause. However, this is not an effective barrier since the mass increments always wander off the map before this spread is attained.

Such a treatment should be a distinct advance over modeling the mixed layer height as a constant since all effects on concentrations of the joint correlation between stability and mixed layer height are lost in such a model.

Carson's work[5] suggests that time-changing heights be defined for a daytime mixed layer and a nighttime surface-based stable layer. These would both be continuous non-decreasing functions up to a time a few hours before definition of the layer is lost, following which there would be a slight decrease, (we are not saying that fidelity to this last feature is essential for our purposes). Such functions could be written as:

$$L_d(t_h) = L_o + (L_{dm} - L_o)\psi_d(t_h - t_d)$$

$$t_d \leq t_h \leq t_{df} \qquad (1)$$

$$L_n(t_h) = L_{nm}\psi_n(t_h - t_n)$$

$$t_n \leq t_h \leq t_{ng} \qquad (2)$$

where the various t's are the following times of day in hours (redefined if necessary to avoid a numerical discontinuity at midnight):

t_h current time

t_d time when mixed layer begins to grow

t_{df} time when mixed layer loses definition

t_n time when stable layer begins to grow

t_{nf} time when stable layer loses its definition

and where L_d is the current mixed layer depth, L_n is the current stable layer depth, L_{dm} is the maximum mixed layer depth, L_{nm} is the maximum stable layer depth, L_o is the initial mixed layer depth, and where ψ_d and ψ_n are suitable functions for relating the current mixed layer and stable layer depths, respectively, to their maximum values.

APPLICATION OF THE MODEL TO VARIOUS CONFIGURATIONS OF RELEASE HEIGHT AND MOVING LID HEIGHT

With the mixed layer height varying from L_o to L_{dm}, the release height of a plume can be either below or above the current level of L_d. (Similar discussion could be written with respect to L_n, but will be omitted.) An illustration of the daytime physical situation is given in Figure 1. At the lower left a ground level release diffuses rapidly up to the limiting height L_d. Further to the right a stack release is shown from a height above the current level of L_d, but below the level of L_{dm}. This material diffuses more slowly in the vertical because of the prevailing stable conditions above the mixed layer. Later when L_d rises above the stack height, the vertical diffusion of this plume will be much more rapid. The line with both dots and dashes represents the vertical expansion of a plume released far upwind on a previous day, and which has expanded above the limit L_{dm}. This plume also continues to expand at a rate compatible with the stable upper layer conditions. At the top of the figure the tropopause limitation to all vertical penetration is shown.

The rate of increase of the standard deviation of vertical dispersion σ_z is modeled differently for each of the three plumes. For recently released plume segments (which may be simulated as puffs), σ_z is increased as an empirical function of travel distance and stability. For the release below L_d the stability varies with the hour. For the release above L_d the stability remains constant until L_d rises above the release height. For the plume

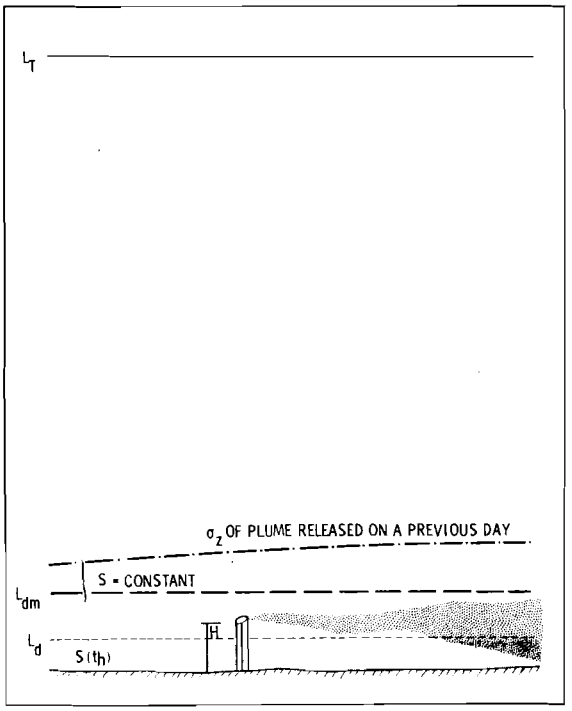

FIGURE 1. Plumes Under Different Vertical Constraints

released on a previous day σ_z is modeled to increase according to the half power of time and vertical eddy diffusitivy. In any of these cases, σ_z is limited by an imposed lid whether it be L_d or L_T.

PARAMETERIZATION

The values given below for the constants and functions in (1) and (2) were derived partly from consideration of values given in the literature[5,6,10] and partly from the advantages of simplicity in a computer code that must be executed and modified. The parameterization now in use consists of:

$$t_d = 6 \quad (3)$$

$$t_{df} = 18 \quad (4)$$

$$t_n = 18 \quad (5)$$

$$t_{nf} = 30 \text{ (effectively 6)} \quad (6)$$

$$L_o = 200 \text{ m} \quad (7)$$

$$L_{dm} = 1500 \text{ m} \quad (8)$$

$$L_{mn} = 400 \text{ m} \quad (9)$$

$$\psi_d = \sin\left[\frac{\pi}{20}(t_h - 6)\right] \quad 6 \leq t_h \leq 18 \quad (10)$$

$$\psi_n = \sin\left[\frac{\pi}{20}(t_h - 18)\right] \quad 18 \leq t_h \leq 30 \quad (11)$$

Other parameter values used are 12,000 m for L_T and 5 m^2/sec for the vertical eddy diffusivity. It should be emphasized that none of this parameterization is considered set

REMOVAL OF THE MIXED LAYER CONSTRAINT

At time t_{df} the mixed layer height loses its definition in the model. Also at this time virtually all the plume elements released during the previous 24 hours are evenly distributed throughout the depth of the mixed layer. Therefore, at time t_{df} the modeling of the vertical expansion changes as follows. The plume elements are no longer constrained by the mixing depth but expand vertically as a function of time:

$$\frac{\partial \sigma_z}{\partial t} = \left(\frac{K_z}{2t}\right)^{1/2} \quad (12)$$

where K_z is the vertical eddy diffusivity and t is travel time. The value of t at which the derivative is computed is the same for all plume elements released from the mixing depth restriction on the same day at time t_{df} since all are assumed to be thoroughly mixed and thus have the same vertical distribution in spite of their different travel times. The assumed value of σ_z at time t_{df} is $L_{dm}(2/\pi)^{1/2}$ since ground level air concentrations computed assuming a Gaussian distribution and this value of σ_z are the same as those computed assuming even distribution through a depth of L_{dm}. Therefore, from this time until the plume element wanders off the map, it will be modeled as a ground-level release distributed vertically in a Gaussian manner with σ_z increasing according to (12) from an initial value of $L_{dm}(2/\pi)^{1/2}$ at time t_{df}.

A GRAPHIC EXAMPLE

Figure 2 shows how the vertical dimension of a plume can increase under the conditions of the previous sections. The graph is for a 48-hr period beginning at 1200. For the sake of clarity the growth of only four plume increments is illustrated, and these at 6-hr release intervals from the source.

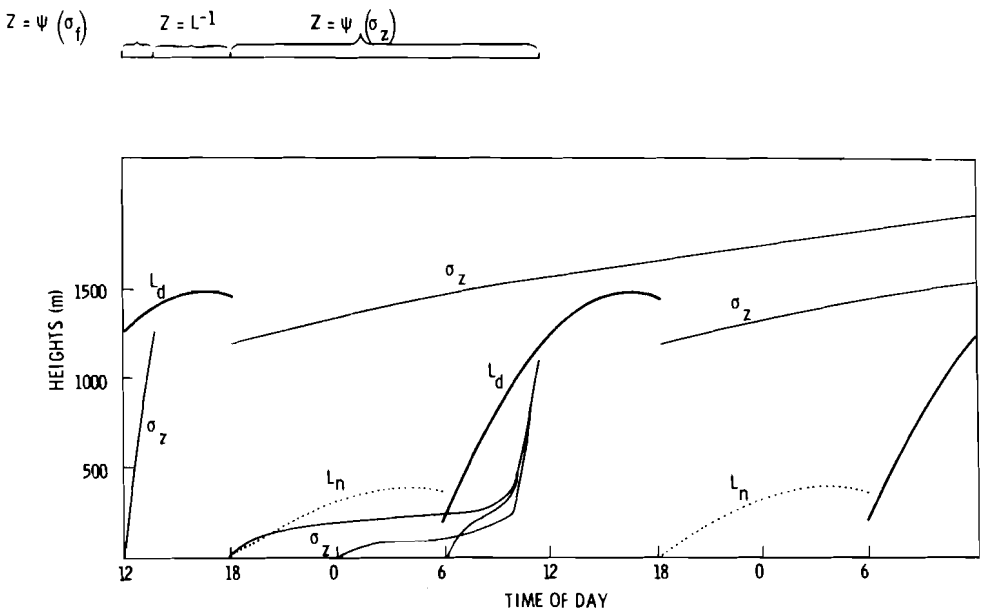

FIGURE 2. Mixed Layer Definition and Plume Expansion

The heaviest black lines are the mixed layer depth, L_d. The dotted line of similar shape but lower height is the nighttime stable layer depth. The lighter solid lines illustrate σ_z at times when the plume element is assumed to be of Gaussian distribution in the vertical. At other times when the lid forms the constraint, the distribution is assumed to be even.

The computation of σ_z as a function of travel distance and stability was facilitated by using formulae by Eimutis and Konicek.[11] Since separate formulae are given for each of the six Pasquill Gifford stability classes, an hourly stability vector was inserted into the program to be used in a diurnal cycle for releases at heights less than the current value of L_d or L_n. The vector may be given as:

F F F F F F D D D D C C C C B B C D

E E E E E E.

This means that stability F is assumed to prevail from 0000 to 0600, that stability D is assumed to prevail from 0600 to 1000 and from 1700 to 1800, etc.

The figure illustrates how plume elements released from the source at different times are quickly mapped into clusters of the same vertical distribution. Considerable computer economy results from this feature, especially since the time interval between releases is usually not every 6 hours, but hourly. Therefore, many more plume elements are mapped into the same vertical distribution than is apparent from the figure.

References

1. H. Tennekes, "The Atmospheric Boundary Layer, Physics Today, 27, 52-63, 1974.

2. G. E. Start and L. L. Wendell. Regional Effluent Dispersion Calculations Considering Spatial and Temporal Meteorological Variations, NOAA Technical Memorandum ERL ARL-44, Air Resources Laboratories, Idaho Falls, ID, May 1974.

3. J. L. Heffter, A. D. Taylor and G. J. Ferber, A Regional-Continental Scale Transport, Diffusion and Deposition Model, NOAA Technical Memorandum ERL ARL-50, Air Resources Laboratories, Silver Springs, MD, June 1975.

4. C. Norton and G. Hoidale, The Diurnal Variation of Mixing Height by Month Over White Sands Missile Range, NM, Report OSD-1366, Atmospheric Sciences Laboratory, U.S. Army Electronics Command, White Sands Missile Range, NM, 1975.

5. D. J. Carson, "The Development of a Dry Inversion-capped Convectively Unstable Boundary Layer," Quart. J. Roy. Meteor. Soc., 99, 450-467, 1973.

6. H. Venkatram and A. Viskanta, Radiative Effects of Pollutants on the Planetary Boundary Layer, EPA-600/4-76-039, Environmental Sciences Research Laboratory, Office of Research and Development, U.S. Environmental Protection Agency, Research Triangle Park, NC, 243 p., 1976.

7. J. C. Kaimal, J. C. Wyngaard, D. A. Haugen, Y. Izumi, O. R. Cote and S. J. Caughey, "Turbulence Structure in a Convective Boundary Layer," to be submitted for publication.

8. J. W. Deardorff and G. E. Willis, "Parameterization of Diffusion into the Mixed Layer," J. of App. Meteor., 14, pp. 1451-1458, 1975.

9. L. Machta, Global Scale Atmospheric Mixing, Turbulence Diffusion in Environmental Pollution, Proceedings of a Symposium held at Charlottesville, VA, April 1973, Advances in Geophyics, Vol. 18B, pp. 33-50, 1974.

10. J. W. Deardorff, Rate of Growth of the Nocturnal Boundary Layer, Proceedings of the Symposium on Air Pollution, Turbulence and Diffusion, December 7-10, 1971, Ed. by H. W. Church and R. E. Luna, Atmospheric Fluid Dynamics Division 5644, Sandia Laboratories, Albuquerque, NM, 183-190, 1972.

11. E. C. Eimutis and M. G. Konicek, "Derivations of Continuous Functions for the Lateral and Vertical Dispersion Coefficients," Atmospheric Environment, 6, pp. 859-863, 1972.

COMPUTATIONAL ECONOMY MEASURES APPLIED TO THE GAUSSIAN PLUME MODEL WITH RESTRICTED VERTICAL MIXING

D. C. Powell

The computation of ground level concentrations according to the Gaussian plume model for a plume spreading between two horizontal surface barriers involves an extended summation of exponential terms accounting for contributions due to multiple reflections. Criteria are given for avoiding the summation subject to an acceptible error level when the plume distribution approaches either of two asymptotic limit conditions--(1) unreflected Gaussian distribution and (2) even distribution.

Consider a plume emitted from a source within the mixed layer defined by a height L. The Gaussian plume equation for ground level concentration at a downwind point $(\tilde{x},\tilde{y},0)$ is given by

$$\chi(\tilde{x},\tilde{y},0) = \frac{Q'Z}{\sqrt{2\pi}\,\sigma_y\,\bar{U}}\, e^{-1/2\left(\frac{y}{\sigma_y}\right)^2}$$

$$\text{where } Z = \frac{\sqrt{2/\pi}}{\sigma_z}\left\{ e^{-1/2\left(\frac{H}{\sigma_z}\right)^2} + \sum_k \left[e^{-1/2\left(\frac{2kL-H}{\sigma_z}\right)^2} + e^{-1/2\left(\frac{2kL+H}{\sigma_z}\right)^2} \right] \right\} \tag{1}$$

where H is the effective stack height and all the other symbols have their conventional meanings.

The discussion is concerned only with the vertical distribution factor Z. There are two asymptotic cases to be considered. Where σ_z is small compared to L, the entire summation over k may be neglected in comparison to the initial term, except possibly the first half of the first term in the summation if H is nearly as large as L. Where σ_z is mathematically large compared to L, the summation is wasteful because many terms are required before the contributions of further terms becomes negligible. Here the physical situation being modeled is that which approaches even distribution in the vertical as an asymptotic limit and for which the value of Z is L^{-1}. In other words, when can we use either

$$Z = \frac{\sqrt{2/\pi}}{\sigma_z}\, e^{-1/2\left(\frac{H}{\sigma_z}\right)^2} \tag{2}$$

or

$$Z = L^{-1} \tag{3}$$

subject to an acceptible level of error?

Suppose we rewrite Z as

$$Z = A + B \tag{4}$$

where A is that part of Z given in (2) and B is the remaining summation. We want to use

$$Z = A \tag{5}$$

subject to an acceptibly low value of error E, given by

$$E = \frac{B}{A + B}\,. \tag{6}$$

It can be shown that (2) or (5) may be used for Z subject to an error level less than E provided that

$$\frac{\sigma_z}{L} < \left[\frac{2\left(1-\frac{H}{L}\right)}{Ln\left(\frac{2}{E}-2\right)}\right]^{1/2}\,. \tag{7}$$

If a 10% error is acceptible, we substitute 0.1 for E, and there results

$$\frac{\sigma_z}{L} < \frac{\left(1-\frac{H}{L}\right)^{1/2}}{1.20}\,. \tag{8}$$

The other asymptotic case is that in which σ_z is large and a criterion is needed for substituting (3) for Z as in (1). It has been found empirically that for calculation of ground level concentrations as in (1) the use of (3) for Z is accurate within 11% provided that

(a) for $0 \le \frac{H}{L} \le 0.5$

$$\frac{\sigma_z}{L} > -\,2.37\left(\frac{H}{L}\right)^2 + 0.489\left(\frac{H}{L}\right) + 0.756;$$

(b) for $0.5 \le \frac{H}{L} \le 1.0$ (9)

$$\frac{\sigma_z}{L} > -\,2.37\left(\frac{H}{L}\right)^2 + 4.25\left(\frac{H}{L}\right) - 1.13\,.$$

The advantages of the criteria for simpler expressions are illustrated in Figure 1. The function given by (8) is shown by dots; the function given by (9) is shown by crosses. The clear area of the figure represents the joint range of σ_z/L and H/L for which the approximation $Z = L^{-1}$ is sufficient. The area with one-way diagonal lines indicates that joint range for which the first term Gaussian approximation (2) is sufficient. The remaining area crossed by diagonals in two directions indicates the joint range for which the more extended expression for must be used. In this case use of the first term in the summation (k = 1) is sufficient.

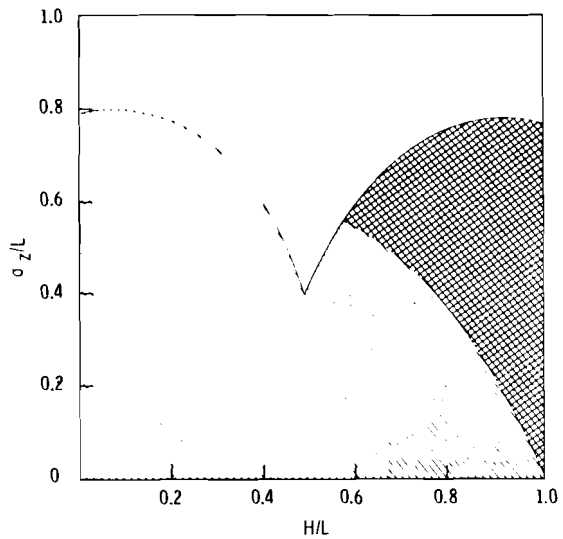

FIGURE 1. Ranges of σ_z/L for Which Asymptotic Definitions Apply

PRECIPITATION DATA BASE MANIPULATION FOR USE IN REGIONAL TRANSPORT AND REMOVAL MODELS

T. D. Fox and L. L. Wendell

A procedure is being developed to prepare large amounts of hourly precipitation data for input to regional atmospheric transport and removal models. The original data are contained on magnetic tape in year-long time series of hourly precipitation for each of approximately 3000 U.S. stations. These data are converted, through a series of sorting, recombining and spatial averaging steps, to arrays of gridded hourly precipitation for use in the transport models.

INTRODUCTION

The importance of using time-changing fields of precipitation rather than climatologically averaged precipitation data in regional transport and removal models has been demonstrated.[1] A procedure producing regional hourly maps of gridded precipitation was tested[2] for a 20-day data interval, using printed data from the National Climatic Center at Ashville, North Carolina. The data were converted to computer punch card data for use in that test. This method of data preparation, although satisfactory for a test case over a specific region for a short time period, is quite inefficient and

time-consuming.[a] It is not suited for general application on a routine basis.

The data are also available from Ashville on magnetic tapes. However, the tapes contain long time series (a full year's worth) of data for each of the approximately 3000 U.S. reporting stations. The sorting and merging of these data to obtain simultaneous precipitation information for all stations which is appropriate for use by pollutant transport and removal models are the objectives of the work discussed here.

PROCEDURE

There are three steps involved in the preparation of this data. First, the coded information for specified states is extracted from the source tapes, and written in binary form to intermediate tapes or permanent files. Second, a SORT routine, using standard CDC SORT/MERGE software[3] is employed to group together the hourly precipitation reports from all of the stations for each day. The data within these groups are arranged according to station number. The daily groups themselves are then arranged chronologically. These data are then written to a second intermediate tape or disk file.

The final step employs the random-to-grid process described in Reference 2 in a program combining the prepared daily precipitation data with station location and time zone information from the card input. Sequential arrays of hourly gridded spatially averaged precipitation for use in the transport models are produced.

a. It was necessary to punch approximately 7,000 cards for the precipitation data from that 20-day period in the northeastern U.S.

Auxiliary programs include one which will combine files of data from different groups of states, which have already been sorted and grouped by day. Use of this program reduces the huge amounts of disk and core space required by the SORT/MERGE software to extract each day's precipitation from the year-long data strings.

Another program produces a compacted set of the location and time zone card input data for a specified region, which is used by the gridding program. These data are extracted from a base set of this information which has been prepared for the entire U.S.

SOURCE DATA AVAILABILITY

Currently the source data from Ashville are on hand at Brookhaven National Laboratory, and are accessible through the Battelle-Northwest computer terminal to the CDC 7600 there. Data are available for the entire United States, excluding Alaska, for 1972, 1973 and 1974. Canadian hourly precipitation data will be added to this information soon.

PRESENT STATUS OF PROJECT

Only preliminary tests of the procedure discussed here have yet been performed. The results are being compared with those obtained in Reference 2, and also against hand calculation.

The procedure is expected to be routinely operational by January 1977.

References

1. L. L. Wendell and D. C. Powell, "An Examination of the Effects of Real Time Versus Time-Averaged Precipitation Data on SO_2 and SO_4 Removal in the Regional Assessment Model," Pacific Northwest Laboratory Annual Report for 1975 to the USERDA Division of Biomedical and Environmental Research, Part 3, Atmospheric Sciences, BNWL-2000, PT 3, Battelle, Pacific Northwest Laboratories, 224-229, 1976.

2. L. L. Wendell and C. E. Hane. "Preparation of Hourly Maps of Gridded Precipitation Data for Use in Precipitation Scavenging Calculations," Pacific Northwest Laboratory Annual Report for 1975 to the USERDA Division of Biomedical and Environmental Research, Part 3, Atmospheric Sciences, BNWL-2000, PT 3, Battelle, Pacific Northwest Laboratories, 229-232, 1976.

3. Control Data Corporation, CONTROL DATA,® CYBER 170 Series, CYBER 70 Series, 6000 Series, 7000 Series, Computer Systems, SORT/MERGE Versions 4 and 1 Reference Manual, 1976.

SOME EFFECTS OF ISENTROPIC VERTICAL MOTION SIMULATION IN A REGIONAL SCALE QUASI LAGRANGIAN AIR QUALITY MODEL

W. E. Davis and L. L. Wendell

Isentropic considerations are included in developing a practical way to simulate vertical motion in a multilevel regional scale air quality model. Average potential temperatures of 12 hr observations in four layers are computed at radiosonde stations in the northeastern United States for April 1974. These data are used to produce gridded mean potential temperature fields in each of the layers. The mean potential temperature fields are used with the layer averaged horizontal flow to determine the vertical motion of plume segments. Examples are presented of the changes in model-generated plume patterns that result from inclusion of vertical motions.

INTRODUCTION

In recent years, the suspected regional to long range transport of the combustion products of sulfur-bearing fossil fuels has stimulated the development of assessment models. Such models simulate the interaction of transport, dispersion, chemical transformation and wet and dry removal. Consideration of the complexity of these processes and their interactions has prevented application of time dependent numerical solution techniques to the problem. Part of the transport process, namely the transport and moisture budget, has been modeled;[1] this model predicts three-dimensional velocity fields in frontal storms as well as wet removal by precipitation scavenging. However, the computer time it requires precludes use of this model for assessment. Its value is the insight and guidance provided in developing more practical diagnostic models.

The predominant type of diagnostic model used to study atmospheric transport and dispersion calculates atmospheric trajectories from synoptic meteorological data. Trajectories are generated differently in the various air quality models. Some use winds determined at a specific pressure level,[2] e.g., 850 mb; this is convenient when a large area of ocean is involved and standard level National Meteorological Center analyses are available. Over land areas where radiosonde data are available, some models[3-6] use winds averaged through a layer, e.g., 100-1000 m above the surface. Neither of these approaches considers the vertical component of air motion. Isentropic trajectories which do include the vertical component of air motion have been used in determining pollutant transport for case studies.[7-10]

Isentropic analysis has not been used in long term assessment modeling for two reasons. First the statistical nature of the results seemed to reduce the need for the more accurate individual trajectories calculated using isentropic analysis, especially in view of the more complex and expensive calculation needed. Second, the diabatic effects near the earth's surface threaten the validity of the analyses. Condensation of water vapor also adds complexity and expense to the analysis technique; this condensation and subsequent removal of pollutants by precipitation scavenging have stimulated new interest in more realistic air trajectories in long term assessments.

In the middle latitudes of the northern hemisphere, frontal storms provide effective cleansing of most power plant pollutants.[11,12] The precipitation patterns associated with these storms are quite variable in space and

time. To realistically evaluate the effect of precipitation scavenging, the placement of pollutant-laden air is important, primarily for models using real time precipitation as opposed to models using average precipitation or none at all.

The purpose of this work is to add isentropic considerations to the transport section of an existing regional scale air quality model. These considerations are to be added so they provide a practical method of simulating the isentropic flow which could be used in long-term assessment runs. The method should also be flexible enough to accept modification to handle diabatic effects as their importance becomes clearer through model testing. This testing is to consist of comparisons of the transport results from the isentropic version of the model with the constant layer version as well as results from more conventional isentropic trajectory construction techniques.

MODEL FORMULATION

The version of the air quality model selected was designed to examine simultaneous plume transport in several layers.[13] For this reason, a multilayer averaging technique was devised to provide layer averaged winds, potential temperature, and mixing ratio at each available radiosonde site within the regions of interest. For each map time, the layer averaged values at randomly spaced data locations were interpolated to regularly spaced grid points, using an inverse square of distance for the weighting.[14] These gridded fields for each of the layers were then ready for use in the transport section of the air quality model. The horizontal kinematic advection scheme of the model required no changes. Each sequentially released particle, along the plume centerline, was moved with a wind obtained by a time interpolation between maps and a space interpolation in the grid.

The major addition to the model was a feature which puts each particle in the layer with the most closely matching potential temperatures at each advection step along the trajectory. This feature introduces a stair-step approximation to the vertical motion through "isentropic" considerations. The crudeness of this approximation will depend somewhat on the resolution obtained with the selected thickness of the layers. The mixing ratio is used to test for saturation in cases of upward vertical motion.

The condition of saturation was monitored for two reasons. First, it might be used, along with observed precipitation measurements at the surface, to estimate whether scavenging of pollutants is in-cloud or below-cloud. Second, saturation indicates the release of latent heat, which means vertical motions should be based on equivalent potential temperatures. At present, this is the only diabatic effect accounted for in the model.

Some significant diabatic effects have yet to be examined in this model; most predominant are the effects of radiational heating and cooling, as well as mixing in the lower layers. The magnitude of these effects will vary with the season, cloud cover, wind shear, temperature structure, and humidity. These effects cause concern because they can introduce varying degrees of error in the vertical motion determinations. Work is continuing to establish techniques to account for the diabatic effects determined to be affecting model results significantly. Initially, the only attempt to reduce the impact of the near-surface diabatic effects was to begin the lowest layer 100 m above the surface. This was in keeping with the fact that the concern of the air quality model is with emissions from the tall stacks of power plants.

MODEL TESTING

Initial Specifications and Data

For the initial testing of the model, four layers were selected. These layers were bounded by the following levels above the surface; 100 m, 500 m, 1000 m, 1500 m, and 3000 m. For these tests, all transport was constrained to remain between 100 m and 3000 m. The geographical area in which these tests were conducted was a 1500 km by 2000 km area of the northeast United States. The meteorological data used in the testing was radiosonde data within and surrounding the tested area.

Comparisons with Constant Layer Transport

The air quality model which was modified to include isentropic considerations was designed for multiple sources. This provided a convenient means to compare, within a single run, the transport in a constant layer with transport including isentropic considerations. This was accomplished by defining two sources at the same geographical location and simply constraining the hourly released parcels from one of the sources to move in the lowest layer.

Two sources are compared here: the sources were located near St. Louis, Missouri, and Pittsburgh, Pennsylvania. From these locations, hourly marker particles were released and used to define plume centerlines. At 12-hr intervals, computer plots were generated, showing the positions of the "isentropic" and constant layer plumes from each of the two sources. Saturation of the air associated with the marker particles is indicated on the plots by an asterisk. Sample plots are shown in Figures 1 and 2. Frontal positions and areas of observed precipitation are also shown for the times indicated. Note in Figure 1 that, after the first 12 hr of release, the plumes from St. Louis are nearly the same, whereas the Pittsburgh plumes are exactly superimposed. Superimposed isentropic and constant layer plumes indicate that the marker particles difining the isentropic plumes are either not leaving the first layer or (a less likely possibility) that the winds in the different layers are the same. The dramatic difference in the St. Louis plume positions shown in Figure 2 reflect the vertical movement over the front. We can also observe in Figure 2 both the saturated and unsaturated portions of the St. Louis plume in the observed rain areas. Plots of this type were produced for a total of 45 release periods during the month for compilation and analyses.

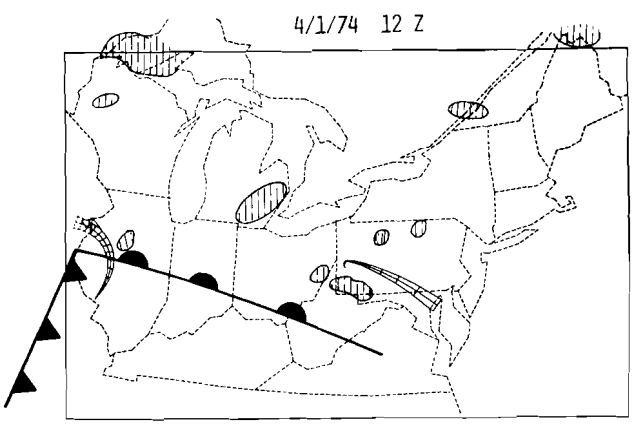

FIGURE 1. Plume Comparison at 12Z April 1, 1974. Plumes are shown after 12 hr of release. (Dashed plumes are constant layer and solid plumes are isentropic. The stippled areas indicate observed precipitation.)

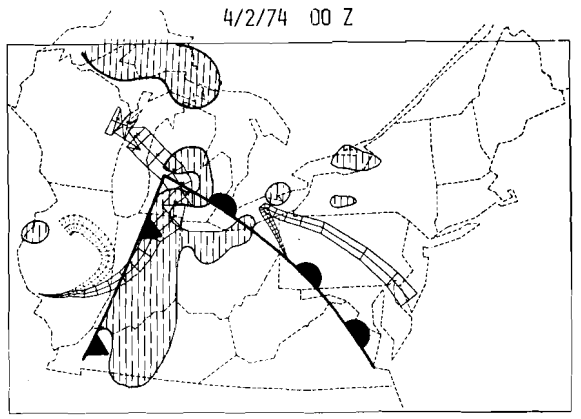

FIGURE 2. Plume Comparison at 00Z April 2, 1974. Plumes are shown after 24 hr of release. (Dashed plumes are constant layer and solid plumes are isentropic. Saturated air parcels denoted by*.)

Analysis of transport differences between constant layer and isentropic consideration consisted of tabulating the separation between the first hour marker particles at 12 and 24 hr. The results are shown in Table 1.

Generally, Table 1 shows that the plumes from the two models behaved similarly when fronts were not encountered. This can be seen from the number of end points which have a separation distance of <100 km (∿63% after 24 hr). On some occasions, rising motions were indicated in the isentropic model when no fronts were present. This was probably due to the lack of an estimate of radiation cooling. Also, since the air parcel was not allowed to sink below the lowest layer, the air parcel in the lowest layer was forced to move with the constant layer flow when radiation heating occurred without modifying the air parcel's potential temperature. These difficulties would be alleviated by compensation in the model for this diabatic effect.

Table 1 also shows the increase over time, of the number of marker particles with end point separation >100 km and of the number of associated air parcels reaching saturation. In approximately 25% of the cases, at 12 hr end point separations were >100 km. At 24 hr 37% of the cases showed end point separations >100 km. This is a 12% increase in 12 hr. For St. Louis and Pittsburgh combined, the total number of cases in which air parcels are saturated increased from 13% at 12 hr to 26% at 24 hr.

TABLE 1. Comparison of Constant Layer to Isentropic Trajectory End Points

1. Distance Separated	St. Louis, MO Number of Trajectories 12 hr	24 hr	Pittsburgh, PA Number of Trajectories 12 hr	24 hr
<100 km	34	23	35	23
100-200 km	5	2	5	1
200-300 km	2	4	5	0
300-400 km	2	2	0	6
>400 km	2	6	0	6
Off Map	0	5	0	5
Dropped due to missing data	0	3	0	4
TOTAL	45	45	45	45
2. Saturated	7	12	5	7

In about 30% of the cases, examined air associated with the marker particles from St. Louis and Pittsburgh were indicated in the model to cross or move along a front during 36 hr of travel time. Seventy percent of these air parcels were saturated after 24 hr.

Analysis of the 45 cases has shown that isentropic considerations in the transport section of the model can cause significant differences in plume positions when they are in the area of a frontal storm. These considerations also provide information with regard to saturation of the air in a plume segment. However, the rather unconventional method of using layer-averaged potential temperatures questions the reliability of the transport. To test the reliability of the method, a comparison was made with transport derived by the more conventional method using flow on isentropic surfaces.

Comparisons Using Isentropic Trajectories

Of the 45 cases analyzed, three cases showing large end point separation between the isentropic and constant layer plumes were selected. For each of these, the initial potential temperature at the source location was used in the construction of flow fields on isentropic surfaces. The flow fields were generated from the same radiosonde information used in the model. Trajectories were computed by hand analyses from these flow fields for comparison with both types of model generated marker particle trajectories. The result was that for the hand analyses versus the isentropic model, the average difference in trajectory end points for the three cases was ∿100 km at 12 hr and ∿250 km at 24 hr. Compare this to the average difference in end points between the hand analyses and constant layer trajectories of ∿275 km at 12 hr and ∿875 km at 24 hr. We see from this comparison that there is some separation between end points of trajectories of the isentropic model and of the hand analyses. However, these differences are considerably less than those between end points of trajectories of the constant layer model and of the hand analyses. From this limited sample, it appears that the model with "isentropic" considerations is providing an acceptable estimate of isentropic flow.

In all three of the cases examined, air parcels associated with the marker particles were saturated after 24 hr of transport. However, in the examination of the hand-analyzed trajectories, only one air parcel was saturated at the end of 24 hr. This indicates that the upper layer (1500 m to 3000 m) is too thick. The use of a layer of this depth causes over-estimation of the vertical movement. This problem can be alleviated by increasing the resolution of the model, through the use of thinner layers, over the same depth.

SUMMARY AND CONCLUSIONS

After modifying the transport phase of the constant layer assessment model to include isentropic approximations and doing some preliminary testing, we find the isentropic method to be feasible. We have shown,

in case studies, that in frontal storms large discrepancies between the isentropic and the constant layer models can occur in plume position estimates and in the subsequent location and occurrence of wet removal, both in-cloud and below-cloud. In a limited comparison, the model including isentropic considerations was shown to reasonably approximate trajectories on isentropic surfaces.

Questions still remain concerning resolution of the layers to more accurately define the saturation of air parcels as well as the inclusion of estimates of diabatic effects. Another vital question yet to be answered is whether the successful inclusion of the isentropic model will be necessary for long-term assessment.

References

1. C. W. Kreitzberg, M. Lutz, and D. J. Perkey, Precipitation Cleansing Computation in a Mesoscale Numerical Weather Prediction Model. To be published in Fate of Pollutants, John Wiley & Sons, Inc., 1976.

2. B. Bolin and C. Persson, Regional Dispersion and Deposition of Atmospheric Pollutants with Particular Application to Sulfur Pollution over Western Europe. Tellus XVII, 3, 281-310, 1975.

3. J. L. Hefter and G. A. Ferber, A Regional Continental Scale Transport, Diffusion and Deposition Model, Part II: Diffusion-Deposition Models. NOAA Tech. memo, ERL ARL-50, 1975.

4. J. Sheih, Application of a Langrangian Statistical Trajectory Model to the Simulation of Sulphur Pollution over North Eastern United States. Appearing in the proceedings of the Third Symposium on Atmospheric Turbulence, Diffusion, and Air Quality, October 1976.

5. Brookhaven National Laboratories, Regional Energy Studies Program. Annual Report, FY 1975, Philip F. Palmedo, Ed., 46-61, 91-106, 1975.

6. L. L. Wendell, D. C. Powell, and R. L. Drake, A Regional Scale Model for Computing Deposition and Ground Level Air Concentration of SO_2 and SO_4 from an Elevated Source. PNL-Annual Report for 1975 to ERDA Div. of Bio. and Envi. Res., Part 3, Atmos. Sciences, BNWL-2000 PT3, UC-11, 218-223, March 1976.

7. E. F. Danielsen, Review of Trajectory Methods, Adv. in Geophysics, 18B, Academic Press, 73-94, 1974.

8. E. R. Reiter and J. D. Mahlman, Heavy Radioactive Fallout over the Southern United States, November 1962. Atmos. Sci. Tech. Paper No. 58, 21-49, Colorado State University, 1964.

9. E. R. Reiter and J. D. Mahlman, Heavy Iodine-131 Fallout over the Midwestern United States, May 1962. Atmos. Sci. Tech. Paper No. 70, USAEC Report COO-1340-2, 1-53, Colorado State University, 1965.

10. H. Rodhe, Some Aspects of the Use of Air Trajectories for the Computation of Large-Scale Dispersion and Fallout Patterns. Adv. in Geophysics, 18B, Academic Press, 1974.

11. M. T. Dana, J. M. Hales, W. G. N. Slinn, and M. A. Wolf, Natural Precipitation Washout of Sulfur Compounds from Plumes. Office of Research and Development, U.S. Environmental Protection Agency, EPA-R3-73-047, June 1973.

12. Precipitation Scavenging, Editors R. J. Engelman and W. G. N. Slinn, U.S.A.E.C. Div. of Tech. Info., CONF-700601, 1970.

13. L. L. Wendell and T. D. Fox, "Examination of the Wind Shear in Regional Scale Flow Layers Derived from Radiosonde Data," Pacific Northwest Laboratories Annual Report for 1975 to the USERDA Division of Biomedical and Environmental Research, Part 3 Atmospheric Sciences, BNWL-2000 PT3, Battelle, Richland, WA, 1976.

14. L. L. Wendell, Mesoscale Wind Fields and Transport Estimates Determined from a Network of Wind Towers. Mon. Wea. Rev., Vol. 100, 565-578, July 1972.

COMPARISON OF TWO CONSTANT LEVEL TRAJECTORY MODELS[a]

W. E. Davis and L. L. Wendell

Trajectories of particles released at 6-hr intervals were calculated using constant layer models developed by Air Resources Laboratory (ARL), Silver Springs, MD, and Battelle, Pacific Northwest Laboratories (PNL), Richland, WA. The laboratories exchanged trajectory sets calculated for common months of data for comparison. A statistical comparison of the separation distances at 3-hr intervals along the trajectories indicated discrepancies of 5 to 10%. This is good agreement considering the difference in trajectory construction techniques. The time-averaged air concentration patterns produced by the models for the 30-day period with similar removal parameters also compared quite favorably.

INTRODUCTION

A comparison of the U.S. scale transport dispersion and removal models of ARL[1] and PNL[2,3] was carried nearly to completion. Both models utilized standard radiosonde data to produce a layer average wind at each measurement site, but used different techniques of trajectory construction and somewhat different techniques in sampling the released material to produce average air concentrations at ground level. The differences in the models have resulted from their different sources. The ARL model evolved from models designed to handle global scale transport, whereas the PNL model is an adaptation of a mesoscale model. The major difference this has caused is in the time and space interpolation processes. The ARL model had to be refined, while the resolution of the PNL model was less than that required by the mesoscale. The purpose of the comparison briefly described below was to determine if the models were producing different results and to provide a basis for the selection of a model for performing the relative diffusion calculations and deposition calculations from five regional sites.

a. This work was sponsored by the Environmental Effects Program--Savannah River LWR.

TRAJECTORY COMPARISON

The PNL model under normal circumstances has a release rate of one particle per hour and uses a 1-hr advection step. A copy of the model was modified to produce punched cards which contained 3-hourly positions along the trajectories of particles released every 6 hr. This was done to match the format of the cards received from ARL. The ARL model has been used to produce 6-hourly trajectories for the month of April 1974.

The fundamental difference in trajectory construction in the two models is in the technique to obtain the wind at each particle position. The ARL model interpolates directly from the randomly spaced wind measurement locations to the particle position at each time step. The PNL model interpolates from the randomly spaced stations to points on a regular rectangular grid. The winds at the particle position are then obtained through a bilinear interpolation in space and a linear time interpolation between maps. This method is less expensive for cases in which many particles are on the grid at one time, but a certain amount of accuracy is sacrificed.

A statistical comparison of the particle separations at successive times along the trajectories is shown in Table 1. For the

TABLE 1. Comparison Between ARL and PNL Trajectories

Time After Release (hr)	No. of Cases	No. of Cases of Greater Distance Traveled[a]	Avg. Separation (Nautical Miles)	Std. Deviation (Nautical Miles)	Avg. Separation/ Distance Traveled
3	111	69	8.82	6.34	0.24
6	111	66	10.20	10.34	0.14
9	111	63	14.89	15.05	0.13
12	111	57	16.52	15.70	0.11
15	111	55	20.43	16.98	0.10
18	110	52	23.33	17.53	0.10
21	106	53	25.80	18.12	0.09
24	97	44	26.29	17.74	0.09
27	88	39	30.94	23.93	0.10
30	78	31	33.18	27.04	0.10
33	72	30	34.47	27.17	0.10
36	65	26	36.86	27.81	0.10
39	61	23	40.38	30.00	0.10
42	58	20	41.61	28.42	0.10
45	57	17	44.06	30.96	0.09
48	52	11	46.68	32.43	0.09
51	47	10	46.25	33.60	0.09
54	44	9	49.64	38.36	0.09
57	41	10	56.63	44.47	0.10
60	38	11	57.52	49.12	0.10
63	36	9	61.79	58.16	0.10
66	35	9	65.65	65.17	0.10
69	33	9	70.44	75.99	0.10
72	32	8	74.34	83.04	0.10
75	29	8	75.57	91.42	0.10
78	29	8	78.45	98.33	0.10
81	26	9	77.32	108.32	0.09
84	25	8	68.99	102.11	0.08
87	24	8	71.54	107.93	0.08
90	21	7	43.43	20.88	0.06
93	20	7	43.19	21.23	0.05
96	19	6	43.37	22.85	0.05
99	19	6	45.65	23.43	0.05
102	17	5	47.64	24.37	0.05
105	15	4	49.86	25.53	0.05
108	15	5	53.02	33.63	0.05
111	14	4	53.99	29.77	0.05
114	14	4	56.84	31.48	0.05
117	12	3	64.22	33.06	0.05
120	12	3	69.37	44.42	0.05

a. This compares total lengths of trajectories and the number indicates how many of the PNL trajectories that were greater in total distance traveled than the ARL trajectories.

quantity "average separation/distance traveled" the discrepancy is about 10% for the first 3 days; then drops to about 5%. The initial error of 24% could be caused by a wind station near the source which would be weighted much more heavily by the ARL model. Since these models are being evaluated for their performance on a regional to U.S. scale, this near source discrepancy is probably not serious. Considering the uncertainty of the trajectories due to layer average assumption, the discrepancies between the trajectories produced by the two models would seem to be insignificant. Examples of these trajectory comparisons are shown in the trajectory plots in Figure 1.

COMPARISON OF AVERAGE CONCENTRATION FIELDS

The major concern in the dose calculations is the reliability of the average concentration fields. The concentration calculations were accomplished with both models running in their design mode using the same meteorological conditions, source rate, dry removal rate, and same average rainfall. The models use a different formulation for the dispersion coefficients and different sampling techniques.

Time average concentration fields were produced by each model for the month of April 1974. In spite of the differences in the models, the resulting patterns were quite similar in shape and magnitude.

VERIFICATION AGAINST MEASURED DATA

Measurements of 12-hourly average concentrations of ^{85}Kr at Indianapolis, Indiana, and Detroit, Michigan, were available by ARL during the month of April 1975. Three-hourly averaged values of the source term were also

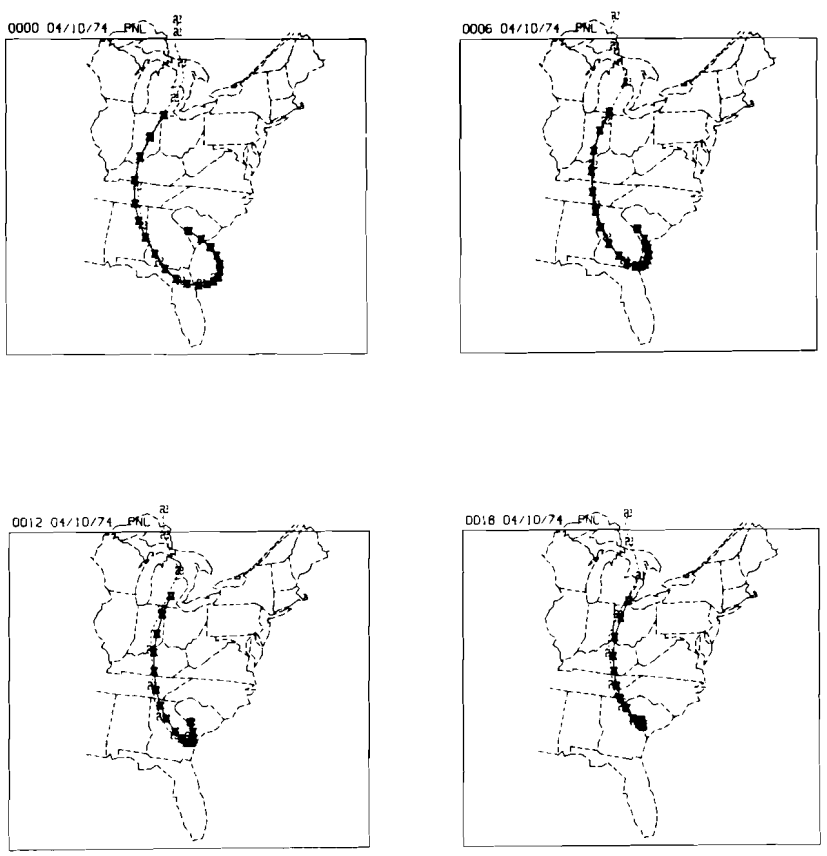

FIGURE 1. Comparison of Trajectories Calculated with Two Different Advection Techniques. The solid lines and symbols were generated with the PNL model. The dashed lines and symbols were generated with the ARL model. The symbols along each trajectory are separated by a 6-hr time interval.

used to try to simulate the 12-hourly average concentrations at the measurement locations. Because of the variability and uncertainty of the source term as well as some meteorological complications due to a frontal system, it would be premature to draw firm conclusions without further investigation of these cases.

CONCLUSIONS AND RECOMMENDATIONS

From the comparison of the PNL and ARL models conducted at PNL, we would conclude that, despite some differences in their structure, they produce very similar results when compared under the same configurations, e.g., layer averaged flow, homogeneous average precipitation conditions, etc. This fact may be comforting; however, it does not prove very much about the accuracy with which the results approximate reality. The comparison with real measurements may be progress in this direction.

Further effort should be expended on comparing the results for the April case with results from a model incorporating isentropic principles as well as the actual time and space distribution of the precipitation over the period. This should help refine the wet deposition estimates as well as suggest methods for including precipitation statistics into the simpler models.

References

1. J. L. Heffter and G. A. Ferber, "A Regional Continental Scale Transport, Diffusion and Deposition Model, Part II: Diffusion - Deposition Models," NOAA Tech. Memo. ERL ARL-50, 1975.

2. L. L. Wendell, "Mesoscale Wind Fields and Transport Estimates Determined From a Network of Wind Powers," Monthly Weather Review, Vol. 1001 No. 2, pp. 565-578, July 1972.

3. L. L. Wendell, D. C. Powell and R. L. Drake, "A Regional Scale Model for Computing Deposition and Ground Level Air Concentrations of SO_2 and SO_4 From an Elevated Source," Pacific Northwest Laboratory Annual Report for 1975 to the USERDA Division of Biomedical and Environmental Research, Part 3, Atmospheric Sciences, BNWL-2000, PT3, UC-11, March 1976.

AN IMPROVED COMPUTER CODE FOR REACTIVE PLUME TRAJECTORY CALCULATIONS

J. M. Hales

A previous model has been improved substantially to provide more detailed estimates of plume transport, reaction and deposition. This new code is expected to be utilized extensively in future MAP3S modeling efforts.

A reactive plume model[1] has been modified and improved for use in MAP3S trajectory modeling efforts. Basically, the model is obtained by performing an integral material balance over a slice of plume, for each of the reactive species, as shown in Figure 1.

$$\frac{d}{dt}\int_0^\infty \int_{-\infty}^\infty c_i dy\, dz\, \delta x$$

= time rate of change of pollutant mass in macroscopic volume element

$$= \int_0^\infty \int_{-\infty}^\infty uc_i dy\, dz \Big|_x$$

$$- \int_0^\infty \int_{-\infty}^\infty uc_i dy\, dz \Big|_{x+\delta x}$$

$$+ \int_0^\infty \int_{-\infty}^\infty G_i(x,y,z)\, dy\, dz\, \delta x \quad , \qquad (1)$$

where

c_i = concentrations of ith plume component

v = the wind speed, and

G_i = the rate of production of the ith component within the volume element by reaction, scavenging and deposition.

Describing scavenging in terms of washout coefficients and dry deposition in terms of deposition velocities, G_i may be written:

$$\int_0^\infty \int_{-\infty}^\infty G_i(x,y,z)\, dy\, dz \Big|_x$$

$$= \int_0^\infty \int_{-\infty}^\infty r_i(x,y,z)\, dy\, dz$$

$$+ \int_0^\infty \int_{-\infty}^\infty - \Lambda_i\, c_i(x,y,z)\, dy\, dz$$

$$+ \int_{-\infty}^\infty V_{d_i}\, c_i(x,y,0)\, dy \quad . \qquad (2)$$

The model utilizes the steady state assumption, and presumes that the shapes of all plumes can be represented by either

1) the bivariate-normal distribution plus a constant background

2) the limited mixing-height distribution plus a constant background.

The model accepts source and meteorological data, and performs numerical integrations of (1) to provide concentrations of plume constituents as a function of downwind position. Most of the parameters in the model can change with position and time. This is made possible by subroutines giving:

- Wind velocities
- Dispersion parameters and mixing heights
- Source strengths

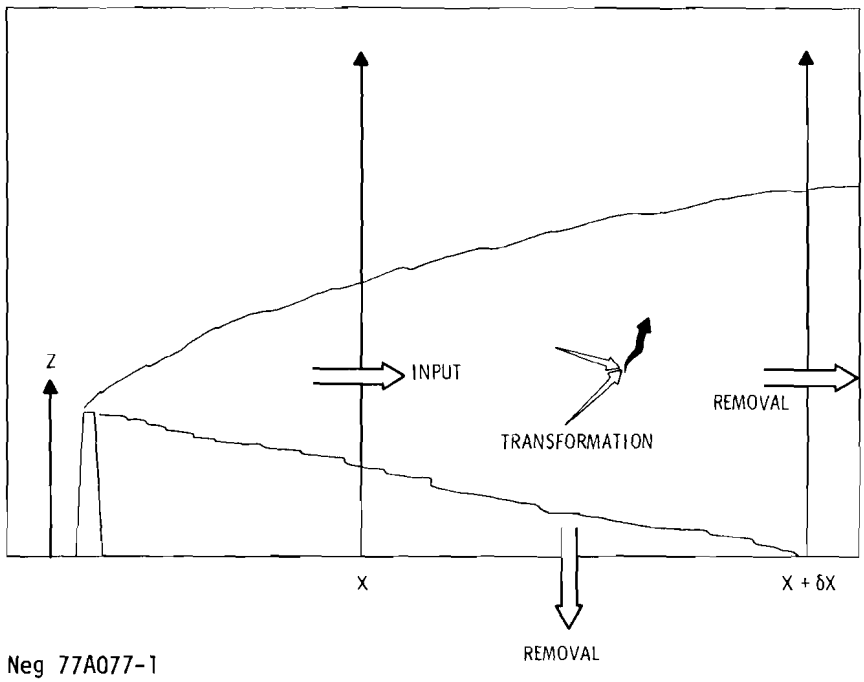

Neg 77A077-1

FIGURE 1. Schematic Illustration of Plume Material Balance

- Scavenging and deposition parameters
- Reaction kinetics.

Reaction kinetics can be as complex as the user desires, within the constraints of computer memory and time. The model is set up to produce concentrations resulting from multiple plumes driven across a region by arbitrary wind fields, if executed by an appropriate calling program.

The original model has been modified to enable more streamlined operation and to perform some of the more sophisticated calculations anticipated for future use. The most important of these are listed as follows:

- The inclusion of stationary states (in the reaction-kinetics sense) has been provided.
- A user may now pick an arbitrary number of components and constrain their concentration behavior to match that of measured substances. This is an important option when the code is used in a diagnostic mode.
- Gas scavenging (reversible washout) calculations are now possible.
- Concentrations of components involving only first-order reactions may now be computed analytically outside of the finite-difference portion of the code.
- Behavior of single plumes now can be calculated without the use of a complex wind-field program. This is accomplished by means of a relatively simple calling program for this purpose.

A result of an example calculation using this code is shown in Figure 2. These results were obtained by executing the program with the Penkett-Cox[2] SO_2 conversion mechanism which was adapted using the reactions

$$NO + O_3 \longrightarrow NO_2 + O_2$$

$$NO_2 \xrightarrow{h\nu} NO + O$$

$$O + O_2 \longrightarrow O_3$$

$$\text{Olefin} + O_3 \longrightarrow \text{Intermediate}$$

$$\text{Intermediate} + SO_2 \longrightarrow SO_4^{=} .$$

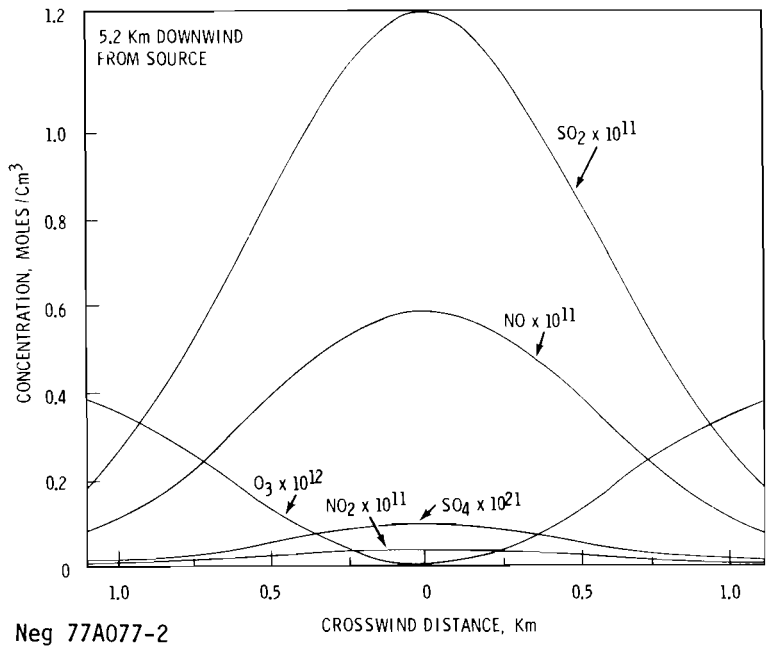

Neg 77A077-2

FIGURE 2. Results of Sample Calculation Using the Code Penket-Cox[2] Conversion Mechanism

Rate expressions associated with these reactions are [cf (2)],

$$r_{NO} = -k_1 [NO] [O_3] + k_2 [NO_2]$$

$$r_{O_3} = k_c [O] - k_1 [NO] [O_3]$$

$$r_{NO_2} = k_1 [NO] [O_3] - k_2 [NO_2]$$

$$r_{olefin} = -155 [olefin] [O_3]$$

$$r_{SO_2} = -\frac{155 [olefin] [O_3] [SO_2]}{[SO_2] + 2.86\times10^{-11}}$$

$$r_{SO_4^=} = -r_{SO_2} ,$$

where r denotes reaction rate in moles/cm^3 sec and [ ] denotes concentration in moles/cm^3.

Source strengths and background concentrations for the various components are listed as follows:

Component	Source Strength moles/sec	Background Concentration parts per billion
NO	30	0
O_3	0	20
NO_2	0	0
SO_2	60	0
Olefin	0	20
$SO_4^=$	0	0

Washout and dry deposition were neglected in this example.

Although this example calculation is not by any means expected to present a valid calculation of SO_2 oxidation kinetics (Cox's and Penhett's mechanism is only one of many that have been proposed), it does give some idea of the model's ability to cope with complex nonlinear systems. In the future we expect to utilize this model extensively in conjunection with historical wind data to compute regional impact of fossil fuel development for the MAP3S program.

References

1. D. C. Powell, J. M. Hales, and T. D. Fox STRAM, An Air Pollution Model Incorporating Nonlinear Chemistry, Variable Trajectories, and Plume Segment Diffusion, Final Report to EPA, in preparation.

2. R. A. Cox and S. A. Penkett, "Aerosol Formation from Sulphur Dioxide in the Presence of Ozone and Hydrocarbons," Trans., Far. Soc. 68, 1735-1753, 1972.

AIR QUALITY SECTOR OF THE ENERGY-RELATED NORTHWEST REGIONAL ASSESSMENT PROGRAM

D. S. Renne and D. L. Elliott

The goal of the Regional Assessment Program at PNL is to assess the environmental and socioeconomic impacts of alternative energy development scenarios in the Pacific Northwest. This report describes the activities of the air quality sector of this program, including modeling efforts, workshops, and future plans.

The air quality sector of the Regional Assessment Program is assessing the impact on air quality, and the deposition of pollutants onto the terrestrial environment, caused by alternative energy development scenarios in the Pacific Northwest. During FY76 we applied a regional scale transport, transformation and removal model to a near term probable coal-related energy development scenario in the Pacific Northwest, assuming generating facilities will emit pollutants at a rate equivalent to the New Source Performance Standards for coal-fired power plants. This effort resulted in a report[1] showing regional ground level air concentrations and surface deposition patterns for this scenario. An example of this output is shown for SO_2 concentrations in Figure 1. This type of effort will continue during FY77 with further application of the regional model to different coal-related scenarios in the west, as a component of the Coal Utilization Assessment, and to energy development scenarios in the northwest as part of PNL's Regional Assessment Program. In addition, we will be applying different types of air quality diffusion models to various development scenarios to assess the "close-in" impacts of alternative developments. These modeling efforts will continue to provide information on the effect regulatory constraints will have on energy development. They will also provide information to other sectors of the Regional Assessment Program, such as the ecosystems effort, for an integrated assessment of alternative energy development scenarios.

During the spring of 1976 PNL hosted a workshop on air quality and meteorological assessments as a part of the Regional Assessment Program.[2] This workshop opened up interlaboratory dialogue on the kinds of models that can be applied to assessments such as these, and on how the labs can combine resources to improve the quality and efficiency of the environmental assessment process. Additional interaction by the workshop participants occurred in subsequent meetings of the air quality working group of the Coal Utilization Assessment. It is intended that interactions such as these will continue at an increasing level of technicality during FY77.

An assessment was made of strippable and underground low sulfur coal reserves in Montana and Wyoming[3] to determine how the New Source Performance Standards for coal-fired power plants promulgated by the Environmental Protection Agency could impact the

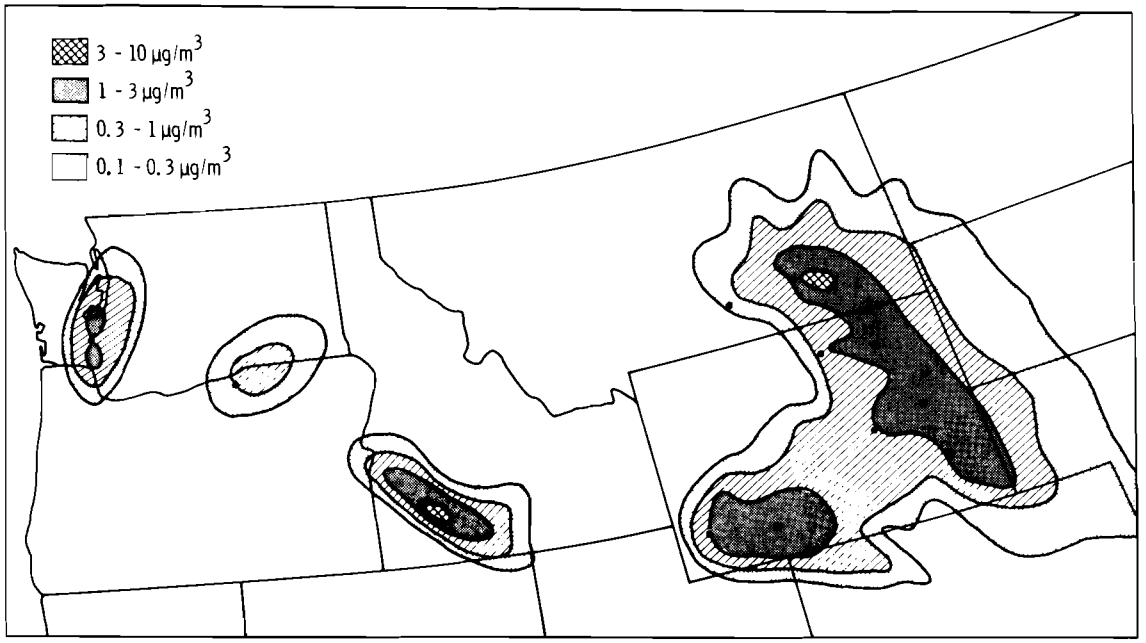

FIGURE 1. Annual Average Ground-Level Air Concentrations of SO_2 from Existing and Proposed Coal-Fired Power Plants in the Northwest Using New Source Performance Standards and a Regional Scale Transport, Transformation and Removal Model

development of these resources. Although the sulfur content of the coal is generally less than 1%, the lower Btu content of the coal requires that a greater amount be burned to achieve the same thermal output as eastern coal. As a result, 43% of the total recoverable resources in the two states would still require sulfur controls when utilized in electric generating facilities.

References

1. D. S. Renne and D. L. Elliott, "Regional Air Quality Assessment for Probable Near-Term Coal-Related Energy Development in the Northwest," BNWL-2084 RAP-9, December 1976.

2. D. S. Renne, Workshop Summary: Regional Studies Program Workshop on Air Quality and Meteorological Assessments, BNWL-2062, June 1976.

3. D. S. Renne, "Assessment of Low Sulfur Coal Resources in Montana and Wyoming," J. Air Pollution Control Association 24(12), December 1976.

A MULTI-SOURCE COMPARISON OF THE EFFECTS OF REAL TIME VERSUS TIME AVERAGED PRECIPITATION DATA ON SO_2 AND SULFATE PARTICULATE REMOVAL IN THE REGIONAL ASSESSMENT MODEL

L. L. Wendell and D. C. Powell

The regional scale atmospheric transport, diffusion and removal model was exercised to produce ground-level air concentration and deposition patterns for SO_2 and sulfate particulate for a 29-day period, with emission estimates from 30 power plant sources in the northeastern United States. The model was run twice with identical parameter specifications and input data; in one run the hourly gridded precipitation was used, as it occurred, for wet removal computations, and in the other run the 29-day average pattern was applied. More than twice the wet removal of SO_2 was observed for the time-averaged precipitation as for the real time precipitation. The SO_2 not removed in the real time precipitation case was available for transformation into sulfate particulate and resulted in higher ground level air concentrations of sulfate particulate by about a factor of 2, as well as more deposited sulfate and significantly more sulfate escaping the computational area.

INTRODUCTION

The regional scale atmospheric transport, diffusion and deposition model under development at PNL for the Multi-state Air Pollution Power Production Study (MAP3S) has been described and tested for a single source near St. Louis, Missouri.[1] Since the ultimate goal of this work is to assess the effect of expanded use of coal as a fuel for power plants in the northeastern United States, the model was developed with a multi-source capability. The model will accept the locations and source strengths for up to 10 sources in any one run. The time integrated concentration fields and deposition amounts may be stored and combined later with the results from other collections of sources. In this way, an assessment can be performed with any number and combination of historical or projected source inventories.

The 18-day single source assessment indicated that the use of hourly precipitation data in the precipitation scavenging calculations removed less than half the SO_2 as was removed using time averaged precipitation data.[1] More SO_2 was available for transformation to sulfate particulate in the latter case. The most striking difference, however, was in the spatial distributions of deposited sulfate.

This report discusses whether any significant differences occur when many sources are considered simultaneously. With the cooperation of the MAP3S project, other Lagrangian type models have been tested using real time precipitation data.[2,3] These models terminated trajectories when they encountered a precipitation rate greater than some specified amount. The PNL model removes material from the plume as a function of the precipitation rate.[1]

DATA DESCRIPTION

The source data for this comparison was obtained from the Federal Power Commission inventory of power plant emissions for 1971.[4] Only power plants which showed non-trivial amounts of SO_2 emissions were selected. Power plants in the same counties were combined to become one power plant source for the county. Eighty-nine utility sources were established with emissions totaling 14,056 kilotons of SO_2. Since the largest 30 sources accounted for 71% of the total emissions, these were selected for the comparison tests. Effective heights for all sources were assumed to be 400 m.

The wind data used for this exercise were derived from 12 hourly radiosonde data for a 29-day period in April 1974. The precipitation data from 777 stations of the NOAA hourly cooperative observing network and about 35 Canadian stations were gridded with a previously described technique for the same period.[1] The transformation and removal parameters for this comparison were specified to be the same as in the single source comparison.

RESULTS

The mass budget for the SO_2 released during the period is summarized in Table 1. The major difference in the results shown in this table and those for the single source at St. Louis, is that much higher percentages of the original SO_2 escaped the computational grid in the form of SO_2 and sulfate particulate for the 30 source release. This occurs because the St. Louis source is the closest of the 30 sources to the upwind boundary of the grid. The material from this source is, on the average, subject to removal mechanisms longer than that from any of the other sources.

As shown in Table 1, the use of average precipitation causes wet removal of over twice as much SO_2 as does the use of real time precipitation. This occurs because the time averaged precipitation, though small in magnitude, is continuously removing material from the plumes. The real time precipitation, however, occurs sporadically and material is removed from a plume only when a plume segment is located in a portion of the grid where precipitation is occurring.

As also seen from Table 1, approximately 13% more of the total released SO_2 is converted to sulfate particulate for the real time case than for the time averaged case. However, only an additional 1% of the total SO_2 released was deposited within the boundaries of the computational grid, while an additional 12% escaped. This probably occurred because both wet and dry removal coefficients for sulfate particulate were an order of magnitude less than for SO_2.

The total budget considerations are only part of the picture. The spatial distributions of the average air concentrations for SO_2 and sulfate particulate are shown in Figure 1 and the deposition patterns are shown in Figure 2. The patterns of ground level sulfate concentrations in the figures are similar, but they show that, over most of the grid, using real time precipitation data results in concentration levels about a factor of 2 greater than those produced from the model run with time averaged precipitation.

Although the difference in the amount of sulfate deposited is small, there is much greater contrast in the deposition patterns. In the real time precipitation case, shown in Figure 2, three local maximum deposition locations may be observed. The most dramatic contrasts between the time averaged and real time precipitation data are seen in upper Michigan, Maine and Northern New Jersey.

TABLE 1. Fate of SO_2 Released for 29 Days from 30 Sources (units % of total SO_2 released)

Transformation Rate $\%hr^{-1}$	Precip. Cond.	Left in air over grid		Deposited on surface of grid		Transported beyond grid	
		SO_2	Sulfate	SO_2	Sulfate	SO_2	Sulfate
5	Dry	2.0	3.1	21.8	5.8	12.6	54.7
5	29-day average	1.2	1.9	53.0	8.1	6.2	29.6
5	Real time	1.6	2.3	35.5	9.3	9.5	41.8

(a)

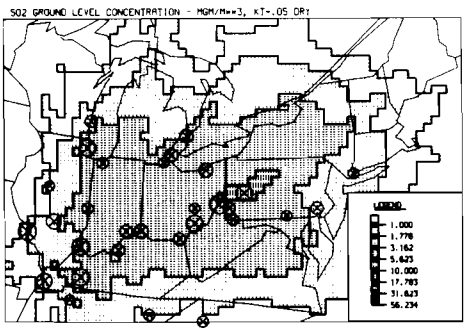

(b)

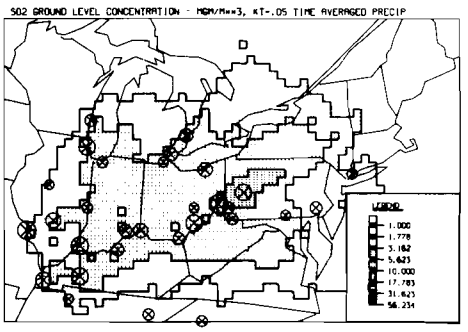

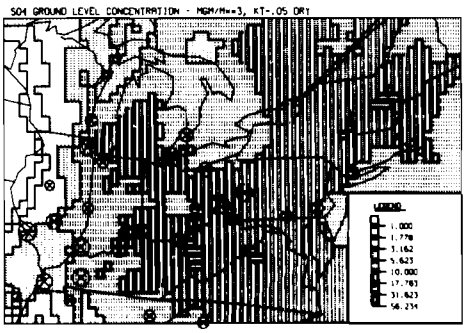

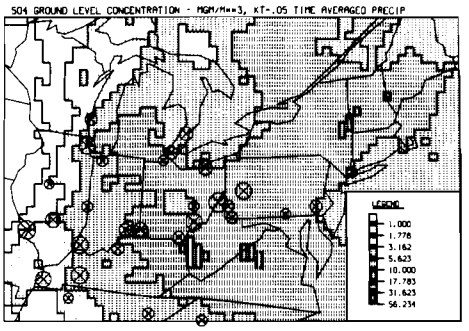

(c)

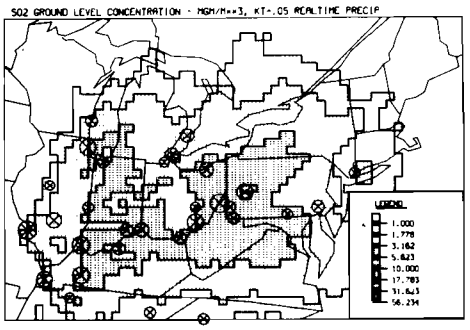

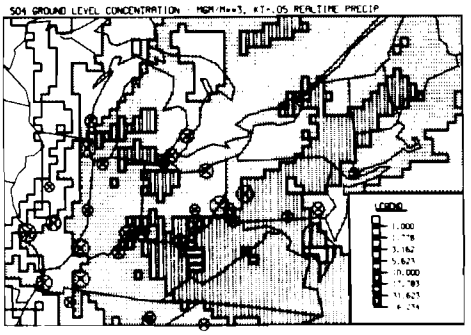

FIGURE 1. Ground Level Air Concentration Patterns ($\mu gm\ m^{-3}$) for SO_2 and Sulfate Particulates Resulting from a 29-Day Period of Releases from 30 Source Locations. Wet removal computations were based on three modes of precipitation representation, a) dry, b) time averaged over the 29 days and c) real time (hourly patterns used in sequence). The circles indicate the relative magnitudes and locations of the sources. The largest circles represent sources emitting SO_2 at a rate of about 600 kilotons yr^{-1}.

(a)

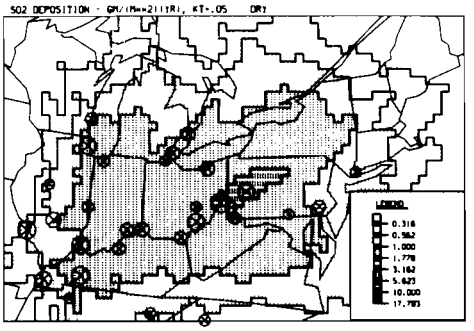

(b)

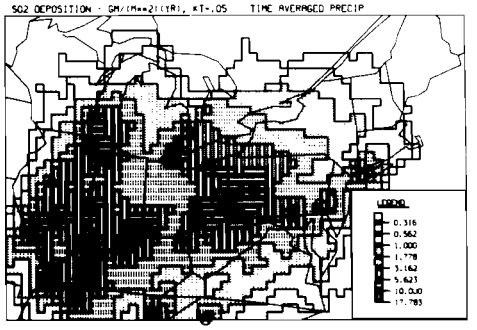

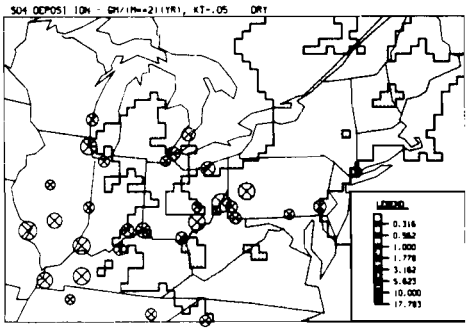

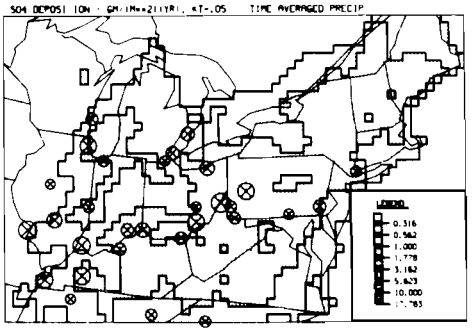

(c)

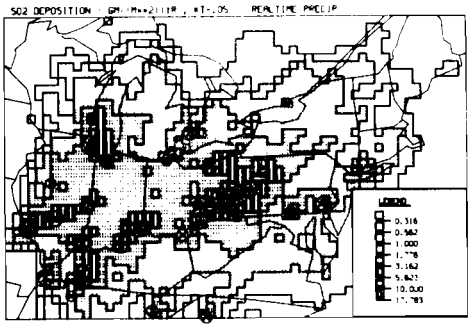

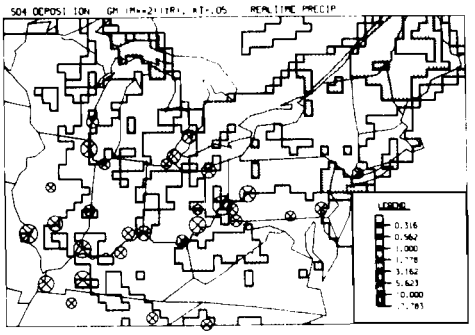

FIGURE 2. Ground Level Deposition Amounts ($\mu gm\ m^{-1} yr^{-2}$) for SO_2 and Sulfate Particulates. For detail see Figure 1.

The differences in amounts of material removed by the two types of precipitation data can be reduced significantly by reducing the removal coefficient. This action will not, however, improve the differences in the deposition patterns. Verification is underway with available concentration measurements and a more complete source inventory. This should more positively indicate the importance of real time precipitation data in various types of assessments.

References

1. L. L. Wendell, D. C. Powell and R. L. Drake, "A Regional Scale Model for Computing Deposition and Ground Level Air Concentrations of SO_2 and Sulfates From Elevated and Ground Sources," Preprint Volume of the Third Symposium on Atmospheric Turbulence, Diffusion and Air Quality, American Meteorolotical Society, Raleigh, NC, October 19-22, 1976.

2. C. M. Sheih, "Application of a Lagrangian Statistical Trajectory Model to the Simulation of Sulfur Pollution Over Northeastern United States," Preprint Volume of the Third Symposium on Atmospheric Turbulence, Diffusion and Air Quality, American Meteorological Society, Raleigh, NC, October 19-22, 1976.

3. R. E. Meyers and R. T. Cederwall, "New Technique to Help Determine the Acid Rain Impact Upon the Ecology of the Eastern United States," Atmospheric Sciences Annual Progress Report for 1974, BNL-50485, 1975.

4. L. L. Wendell and C. E. Hane, "Preparation of Hourly Maps of Gridded Precipitation Data for Use in Precipitation Scavenging Calculation," Pacific Northwest Laboratories, Annual Report for 1975 to the USERDA Division of Biomedical and Environmental Research, Part 3 Atmospheric Sciences, BNWL-2000 PT3, Battelle, Pacific Northwest Laboratories, Richland, WA, March 1976.

PUBLICATIONS AND PRESENTATIONS

PUBLICATIONS AND PRESENTATIONS

DOCUMENTS

Horst, T. W. , The Estimation of Air Concentrations Due to the Suspension of Surface Concentration by the Wind, BNWL-2047, Battelle, Pacific Northwest Laboratories, Richland, WA, March 1976.

Ramsdell, J. V., Impact of a Nuclear Energy Center on Ground Level Fog and Humidity, BNWL-2058, Battelle, Pacific Northwest Laboratories, Richland, WA.

Renné, D. S., and D. C. Elliott, Regional Air Quality Assessment for Probable Near-Term Coal-Related Energy Development in the Northwest, BNWL-2084, RAP-9, Battelle, Pacific Northwest Laboratories, Richland, WA, 1976.

Renné, D. S., Workshop Summary: Regional Studies Program Workshop on Air Quality and Meteorological Assessments, BNWL-2062, Battelle, Pacific Northwest Laboratories, Richland, WA June 1966.

Renné, D. S., and M. A. Wolf, Experimental Studies of Aerial Application Techniques for 2,4-D, BNW-730-2, Final Report to the Pacific Northwest Regional Commission, February 1976.

Schwendiman, L. C., Appraisal of Airborne Radioactive Effluent Sampling Systems -- Comprehensive Analysis Format and In-Place Sampler Validation, BNWL-1921, Battelle, Pacific Northwest Laboratories, Richland, WA, September 1976.

Sehmel, G. A., Airborne ^{238}Pu and ^{239}Pu Associated with the Larger than "Respirable" Resuspended Particles at Rocky Flats During July 1973, BNWL-2119, Battelle, Pacific Northwest Laboratories, Richland, WA, September 1976.

Simpson, C. L., and Staff, Pacific Northwest Laboratory Annual Report for 1975 to the USERDA Division of Biomedical and Environmental Research, Part 3, Atmospheric Sciences, BNWL-2000, Battelle, Pacific Northwest Laboratories, Richland, WA, March 1976.

PUBLICATIONS

Alkezweeny, A. J., and N. S. Laulainen, "Simultaneous Aerosol Size Distributions and Turbidity Measurements Over a Metropolitan Area," Atmospheric Pollution, published in the Proceedings of the 12th International Colloquium, Paris, France, May 5-7, 1976.

Alkezweeny, A. J., "The Growth of Aerosol in an Urban Plume," Atmospheric Pollution, published in the Proceedings of the 12th International Colloquium, Paris, France, May 5-7, 1976.

Dana, M. T., and J. M. Hales, "Statistical Aspects of the Washout of Polydisperse Aerosols," Atmos. Environment, vol. 10, no. 1, pp. 45-50, 1976.

Drake. R. L., "Similarity Solutions for Homogeneous and Nonhomogeneous Aerosol Balance Equations," BNWL-SA-5634, Journal of Colloid and Interface Science, vol. 57, no. 3, December 1976.

Fox, T. D., and J. D. Ludwick, "Lead (Pb) Concentrations Associated with 1000 mb Geostrophic Back Trajectories at Quillayute, Washington," Atmos. Environment, vol. 10, no. 10, pp. 799-803, 1976.

Ludwick, J. D., T. D. Fox and L. L. Wendell, "Ozone and Radionuclide Correlations in Air of Marine Trajectory at Quillayute, WA," Air Pollution Control Association Journal, vol 26, no. 6, pp. 565-569, June 1976.

Orgill M. M., and G. A. Sehmel, "Frequency and Diurnal Variation of Dust Storms in the Contiguous U.S.A.," Atmos. Environment, vol. 10, no. 10, pp. 813-825, 1976.

Orgill, M. M., G. A. Sehmel and M. R. Petersen, "Some Initial Measurements of Airborne DDT over Pacific Northwest Forest," Atmos. Environment, vol. 10, no. 10, pp. 827-833, 1976.

Rancitelli, L. A., J. A. Cooper, and R. W. Perkins, "Multielement Characterization of Atmospheric Aerosols by Instrumental Neutron Activation Analysis and X-Ray Fluorescence Analysis," In: Environmental Quality and Safety, Vol. 5: 152-166, George Thieme Publishers, Stuttgart, Germany, 1976.

Renné, D. S., "Assessing Low Sulfur Coal Resources in Montana and Wyoming," J. of the Air Pollution Control Assoc., vol. 26, no. 12, pp. 1167-1170, December 1976.

Slinn, W. G. N., "Vertical Rise of a Buoyant Plume: Some Elementary Comments on Closure Problems and Dissipative Processes," Atmos. Environment, vol. 10, no. 8, pp. 665-666, 1976.

Slinn, W. G. N., "Formulation and a Solution of the Diffusion - Deposition - Resuspension Problem," Atmos. Environment, vol. 10, no. 9, pp. 763-767, 1976.

Slinn, W. G. N., "Theory of Diffusive Deposition of Particles in a Sphere and in a Cylinder at Small Fourier Numbers," Atmos. Environment, vol. 10, no. 9, p. 790, 1976.

Stoffels, J. J., "A Direct Air-Sampling Inlet for Surface Ionization Mass Spectrometry of Airborne Particles," In: Proceedings of the 24th Annual Conference on Mass Spectrometry and Allied Topics, San Diego, CA, 1976.

Wogman, N. A., "Current Methods for Laboratory Analysis of Environmental Levels of Radioactivity," IEEE Short Course, "Radioactivity in the Environment," November 22, 1975, In: Proceedings IEEE, June 1976.

Wolf, M. A., C. E. Hane and R. L. Drake, "Pacific Northwest Laboratory AENEC Annual Report for FY-1976," Oak Ridge National Laboratory AENEC 1st Annual Technical Progress Report, July, 1976.

PRESENTATIONS

Alkezweeny, A. J., and N. S. Laulainen, "Airborne Measurements of Particle Size Distribution, Light Scattering and Turbidity at Different Altitudes," BNWL-SA-5921, Presented at the Optical Society of America Meeting, NASA Langley Research Center, Williamsburg, VA, December 13-15, 1976.

Alkezweeny, A. J., "SO_2 to Sulfate Transformation in Urban Plume," BNWL-SA-5907, Presented at the 23rd Pacific Northwest Regional Meeting of the American Geophysical Union, Victoria, British Columbia, Canada, September 30 - October 1, 1976.

Alkezweeny, A. J., K. M. Busness, N. S. Laulainen, R. N. Lee, and J. M. Thorp, "Pollutant Transformation in the St. Louis Plume," BNWL-SA-5769, Presented at the 7th Northeast Regional Meeting of the American Chemical Society, Albany, NY, August 8-11, 1976.

Bander, T. J., and D. S. Renné, "A Model for Analyzing the Global Concentrations of Tritium Released from a CTR," BNWL-SA-5768, Presented at the 2nd American Nuclear Society Topical Meeting on the Technology of Controlled Nuclear Fusion, Richland, WA, September 21-23, 1976.

Dana, M. T., "Rain Chemistry in the Vicinity of the Centralia Steam-Electric Plant," BNWL-SA-5927, Presented at the 23rd Pacific Northwest Regional Meeting of the American Geophysical Union, Victoria B.C., Canada, September 30 - October 1, 1976.

Davis, W. E., and L. L. Wendell, "Some Effects of Isentropic Vertical Motion Simulation in a Regional Scale Quasi Lagrangian Air Quality Model," BNWL-SA-5669, Presented at the Third Symposium on Atmospheric Turbulence, Diffusion and Air Quality, Raleigh, NC, October 19-22, 1976.

Drake, R. L., "A Comprehensive Aerosol Growth Model," BNWL-SA-5931, Presented at the Optical Society of America Meeting, NASA Langley Research Center, Williamsburg, VA, December 13-15, 1976.

Brock J., and R. L. Drake, "Coagulation of Aerosols," BNWL-SA-5930, Presented at the 82nd National Meeting of the AICHE, Atlantic City, NJ, August 29 - September 1, 1976.

Drake, R. L., "An Analytical Derivation of a Stable Distribution of Marine Aerosols," BNWL-SA-5732, Presented at the American Meteorological Society 2nd Conference on Ocean-Atmosphere Interactions, Seattle, WA, March 29 - April 2, 1976.

Droppo, J. G., "Dry Removal of Air Pollutants by Vegetation Canopies," BNWL-SA-5973, Presented at the Fourth National Conference on Fire and Forest Meteorology, St. Louis, MO, November 16-18, 1976.

Nickola, P. W., "Measured Differences in Real and Apparent Plume Parameters," BNWL-SA-5653, Presented at the Third Symposium on Atmospheric Turbulence, Diffusion, and Air Quality, Raleigh, NC, October 19-22, 1976.

Powell, D. C., "Unparameterized Variation of Sample Wind Component Spectra and Implications for Diffusion Modeling in the Atmospheric Boundary Layer," BNWL-SA-5656, Presented at the Third Symposium on Atmospheric Turbulence, Diffusion and Air Quality, Raleigh, NC, October 19-22, 1976.

Ramsdell, J. V., "Wind Shear Downwind of Large Surface Roughness Elements," BNWL-SA-5840, Presented at the 7th Conference on Aerospace and Aeronautical Meteorology and Symposium on Remote Sensing from Satellites, Melbourne, FL, November 16-19, 1976.

Renné, D. S., and D. C. Elliott, "Regional Air Quality Assessment for Northwest Energy Scenarios," BNWL-SA-5748, Presented at the 69th Annual Meeting of the Air Pollution Control Association, Portland, OR, June 27 - July 1, 1976.

Renné, D. S., and M. A., Wolf, "Experimental Studies of Herbicide Drift Characteristics," BNWL-SA-5848, Presented at the Fourth National Conference on Fire and Forest Meteorology, St. Louis, MO, November 16-18, 1976.

Schwendiman, L. C., and J. A. Glissmeyer, "An Analysis Format and Evaluation Methods for Effluent Particle Sampling Systems in Nuclear Facilities," BNWL-SA-5713, Presented at the 14th USERDA Air Cleaning Conference, Sun Valley, ID, August 2-4, 1976.

Scott, B. D., and P. V. Hobbs, "A Theoretical Study of the Evoluation of Mixed Phase Cumulus Clouds," BNWL-SA-5880, Presented at the Internation Conference on Cloud Physics, Boulder, CO, July 26-30, 1976.

Sehmel, G. A., "Plutonium and Tracer Particle Resuspension: An Overview of Selected Battelle-Northwest Experiments," BNWL-SA-6022, Presented at the Nevada Applied Ecology Group "Symposium on the Dynamics of Transuranics in Terrestrial and Aquatic Environments," Gatlinburg, TN, October 5, 1976.

Wendell, L. L., D. C. Powell and R. L. Drake, "A Regional Scale Model for Computing Deposition and Ground Level Air Concentration of SO_2 and Sulfates from Elevated and Ground Sources," BNWL-SA-5654, Presented at the Third Symposium on Atmospheric Turbulence, Diffusion, and Air Quality, Raleigh, NC, October 19-22, 1976.

Wendell, L. L., D. C. Powell and R. L. Drake, "A Regional Scale Model for Computing Deposition and Ground Level Air Concentration of SO_2 and SO_4 from Elevated and Ground Sources," BNWL-SA-5654, Presented at the 7th International Technical Meeting on Air Pollution Modeling (NATO/CCMS Air Pollution Pilot Study) Airlie House, VA, September 7-10, 1976.

Slinn, W. G. N., "Wet and Dry Removal Process," BN-SA-617, Presented at Workshop on Tropospheric Transport of Pollutants to the Oceans, Miami, FL, December 8-12, 1976.

ORGANIZATION CHARTS

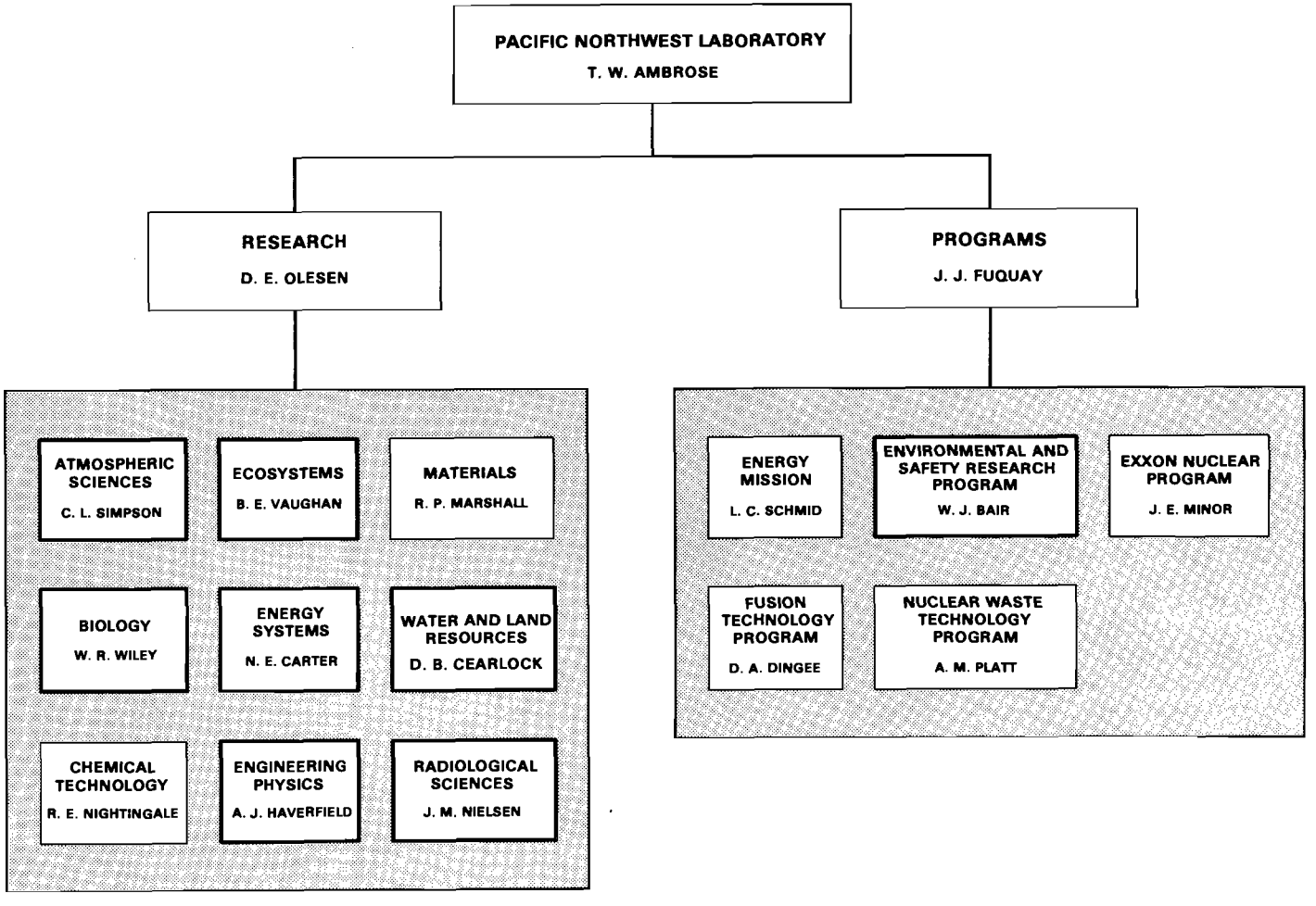
PACIFIC NORTHWEST LABORATORY
T. W. AMBROSE
RESEARCH
D. E. OLESEN
PROGRAMS
J. J. FUQUAY
ATMOSPHERIC SCIENCES
C. L. SIMPSON
ECOSYSTEMS
B. E. VAUGHAN
MATERIALS
R. P. MARSHALL
BIOLOGY
W. R. WILEY
ENERGY SYSTEMS
N. E. CARTER
WATER AND LAND RESOURCES
D. B. CEARLOCK
CHEMICAL TECHNOLOGY
R. E. NIGHTINGALE
ENGINEERING PHYSICS
A. J. HAVERFIELD
RADIOLOGICAL SCIENCES
J. M. NIELSEN
ENERGY MISSION
L. C. SCHMID
ENVIRONMENTAL AND SAFETY RESEARCH PROGRAM
W. J. BAIR
EXXON NUCLEAR PROGRAM
J. E. MINOR
FUSION TECHNOLOGY PROGRAM
D. A. DINGEE
NUCLEAR WASTE TECHNOLOGY PROGRAM
A. M. PLATT

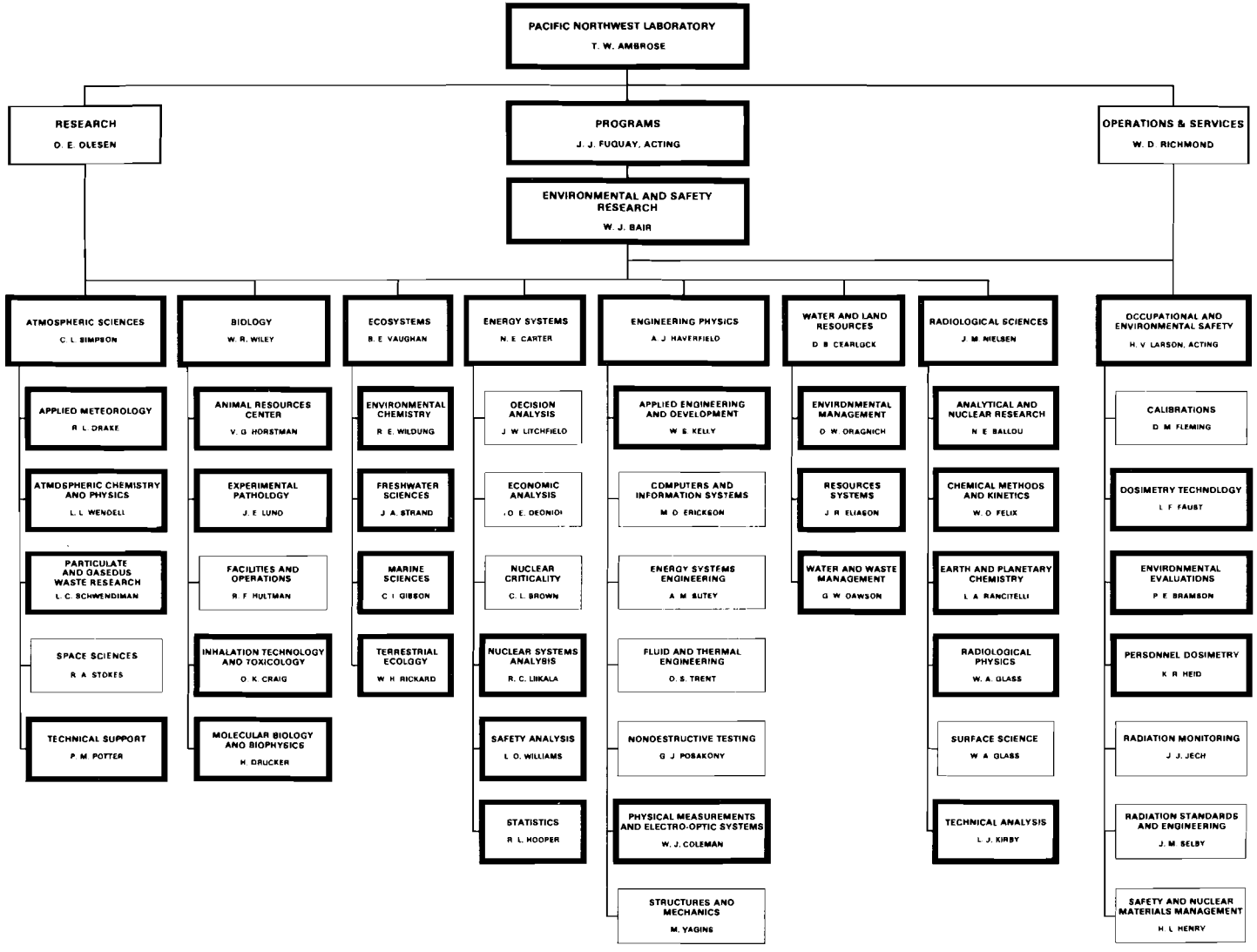
PACIFIC NORTHWEST LABORATORY
T. W. AMBROSE
RESEARCH
D. E. OLESEN
PROGRAMS
J. J. FUQUAY, ACTING
OPERATIONS & SERVICES
W. D. RICHMOND
ENVIRONMENTAL AND SAFETY RESEARCH
W. J. BAIR
ATMOSPHERIC SCIENCES
C. L. SIMPSON
APPLIED METEOROLOGY
R. L. DRAKE
ATMOSPHERIC CHEMISTRY AND PHYSICS
L. L. WENDELL
PARTICULATE AND GASEOUS WASTE RESEARCH
L. C. SCHWENDIMAN
SPACE SCIENCES
R. A. STOKES
TECHNICAL SUPPORT
P. M. POTTER
BIOLOGY
W. R. WILEY
ANIMAL RESOURCES CENTER
V. G. HORSTMAN
EXPERIMENTAL PATHOLOGY
J. E. LUND
FACILITIES AND OPERATIONS
R. F. HULTMAN
INHALATION TECHNOLOGY AND TOXICOLOGY
O. K. CRAIG
MOLECULAR BIOLOGY AND BIOPHYSICS
H. DRUCKER
ECOSYSTEMS
B. E. VAUGHAN
ENVIRONMENTAL CHEMISTRY
R. E. WILDUNG
FRESHWATER SCIENCES
J. A. STRAND
MARINE SCIENCES
C. I. GIBSON
TERRESTRIAL ECOLOGY
W. H. RICKARD
ENERGY SYSTEMS
N. E. CARTER
DECISION ANALYSIS
J. W. LITCHFIELD
ECONOMIC ANALYSIS
D. E. DEONIO
NUCLEAR CRITICALITY
C. L. BROWN
NUCLEAR SYSTEMS ANALYSIS
R. C. LIIKALA
SAFETY ANALYSIS
L. O. WILLIAMS
STATISTICS
R. L. HOOPER
ENGINEERING PHYSICS
A. J. HAVERFIELD
APPLIED ENGINEERING AND DEVELOPMENT
W. S. KELLY
COMPUTERS AND INFORMATION SYSTEMS
M. D. ERICKSON
ENERGY SYSTEMS ENGINEERING
A. M. SUTEY
FLUID AND THERMAL ENGINEERING
O. S. TRENT
NONDESTRUCTIVE TESTING
G. J. POSAKONY
PHYSICAL MEASUREMENTS AND ELECTRO-OPTIC SYSTEMS
W. J. COLEMAN
STRUCTURES AND MECHANICS
M. YAGINS
WATER AND LAND RESOURCES
D. B. CEARLOCK
ENVIRONMENTAL MANAGEMENT
D. W. ORAGNICH
RESOURCES SYSTEMS
J. R. ELIASON
WATER AND WASTE MANAGEMENT
G. W. DAWSON
RADIOLOGICAL SCIENCES
J. M. NIELSEN
ANALYTICAL AND NUCLEAR RESEARCH
N. E. BALLOU
CHEMICAL METHODS AND KINETICS
W. D. FELIX
EARTH AND PLANETARY CHEMISTRY
L. A. RANCITELLI
RADIOLOGICAL PHYSICS
W. A. GLASS
SURFACE SCIENCE
W. A. GLASS
TECHNICAL ANALYSIS
L. J. KIRBY
OCCUPATIONAL AND ENVIRONMENTAL SAFETY
H. V. LARSON, ACTING
CALIBRATIONS
D. M. FLEMING
DOSIMETRY TECHNOLOGY
L. F. FAUST
ENVIRONMENTAL EVALUATIONS
P. E. BRAMSON
PERSONNEL DOSIMETRY
K. R. REID
RADIATION MONITORING
J. J. JECH
RADIATION STANDARDS AND ENGINEERING
J. M. SELBY
SAFETY AND NUCLEAR MATERIALS MANAGEMENT
H. L. HENRY

DISTRIBUTION

DISTRIBUTION

No. of
Copies

OFFSITE

362

A. A. Churm
ERDA Chicago Patent Group
U.S. ERDA
9800 S. Cass Avenue
Argonne, IL 60439

3 T. M. Albert
Division of Biomedical and
Environmental Research
U.S. ERDA
Washington, DC 20545

W. R. Albers
Division of Biomedical and
Environmental Research
U.S. ERDA
Washington, DC 20545

D. S. Ballantine
Division of Biomedical and
Environmental Research
U.S. ERDA
Washington, DC 20545

R. W. Barber
Division of Biomedical and
Environmental Research
U.S. ERDA
Washington, DC 20545

N. F. Barr
Division of Biomedical and
Environmental Research
U.S. ERDA
Washington, DC 20545

R. W. Beadle
Division of Biomedical and
Environmental Research
U.S. ERDA
Washington, DC 20545

M. A. Bell
Division of Biomedical and
Environmental Research
U.S. ERDA
Washington, DC 20545

W. G. Belter
Division of Biomedical and
Environmental Research
U.S. ERDA
Washington, DC 20545

No. of
Copies

W. A. Brobst
Division of Biomedical and
Environmental Research
U.S. ERDA
Washington, DC 20545

W. W. Burr
Division of Biomedical and
Environmental Research
U.S. ERDA
Washington, DC 20545

C. E. Carter
Division of Biomedical and
Environmental Research
U.S. ERDA
Washington, DC 20545

J. A. Coleman
Division of Biomedical and
Environmental Research
U.S. ERDA
Washington, DC 20545

R. D. Cooper
Division of Biomedical and
Environmental Research
U.S. ERDA
Washington, DC 20545

L. J. Deal
Division of Biomedical and
Environmental Research
U.S. ERDA
Washington, DC 20545

C. W. Edington
Division of Biomedical and
Environmental Research
U.S. ERDA
Washington, DC 20545

H. G. Fish
Division of Biomedical and
Environmental Research
U.S. ERDA
Washington, DC 20545

T. J. Gross
Division of Biomedical and
Environmental Research
U.S. ERDA
Washington, DC 20545

No. of
Copies

G. Hagey
Division of Biomedical and
Environmental Research
U.S. ERDA
Washington, DC 20545

H. H. Hollister
Division of Biomedical and
Environmental Research
U.S. ERDA
Washington, DC 20545

H. R. Holt
Division of Biomedical and
Environmental Research
U.S. ERDA
Washington, DC 20545

R. M. Jimeson
Division of Biomedical and
Environmental Research
U.S. ERDA
Washington, DC 20545

J. S. Kirby-Smith
Division of Biomedical and
Environmental Research
U.S. ERDA
Washington, DC 20545

3 W. J. Little, Jr.
Division of Biomedical and
Environmental Research
U.S. ERDA
Washington, DC 20545

2 J. L. Liverman
Division of Biomedical and
Environmental Research
U.S. ERDA
Washington, DC 20545

E. K. Loop
Division of Biomedical and
Environmental Research
U.S. ERDA
Washington, DC 20545

J. N. Maddox
Division of Biomedical and
Environmental Research
U.S. ERDA
Washington, DC 20545

J. R. Maher
Division of Biomedical and
Environmental Research
U.S. ERDA
Washington, DC 20545

No. of
Copies

R. P. Malloch
Division of Biomedical and
Environmental Research
U.S. ERDA
Washington, DC 20545

J. E. Miller
Division of Biomedical and
Environmental Research
U.S. ERDA
Washington, DC 20545

W. E. Mott
Division of Biomedical and
Environmental Research
U.S. ERDA
Washington, DC 20545

J. Nash
Division of Biomedical and
Environmental Research
U.S. ERDA
Washington, DC 20545

C. L. Osterberg
Division of Biomedical and
Environmental Research
U.S. ERDA
Washington, DC 20545

D. E. Patterson
Division of Biomedical and
Environmental Research
U.S. ERDA
Washington, DC 20545

3 W. H. Pennington
Division of Biomedical and
Environmental Research
U.S. ERDA
Washington, DC 20545

D. M. Ross
Division of Biomedical and
Environmental Research
U.S. ERDA
Washington, DC 20545

A. A. Schoen
Division of Biomedical and
Environmental Research
U.S. ERDA
Washington, DC 20545

G. Shippard
Division of Biomedical and
Environmental Research
U.S. ERDA
Washington, DC 20545

No. of
Copies

N. F. Simpson
Division of Biomedical and
Environmental Research
U.S. ERDA
Washington, DC 20545

D. H. Slade
Division of Biomedical and
Environmental Research
U.S. ERDA
Washington, DC 20545

H. P. Smith
Division of Biomedical and
Environmental Research
U.S. ERDA
Washington, DC 20545

J. B. Stromberg
Division of Biomedical and
Environmental Research
U.S. ERDA
Washington, DC 20545

J. Swinebroad
Division of Biomedical and
Environmental Research
U.S. ERDA
Washington, DC 20545

E. J. Vallario
Division of Biomedical and
Environmental Research
U.S. ERDA
Washington, DC 20545

B. W. Wachholz
Division of Biomedical and
Environmental Research
U.S. ERDA
Washington, DC 20545

H. Wasson
Division of Biomedical and
Environmental Research
U.S. ERDA
Washington, DC 20545

W. W. Weyzen
Division of Biomedical and
Environmental Research
U.S. ERDA
Washington, DC 20545

J. C. Whitnah
Division of Biomedical and
Environmental Research
U.S. ERDA
Washington, DC 20545

No. of
Copies

R. W. Wood
Division of Biomedical and
Environmental Research
U.S. ERDA
Washington, DC 20545

C. I. York
Division of Biomedical and
Environmental Research
U.S. ERDA
Washington, DC 20545

F. R. Zintz
Division of Biomedical and
Environmental Research
U.S. ERDA
Washington, DC 20545

Chief, Environmental and
Sanitary Engineering Branch
RRD Division of Reactor
Development and Technology
U.S. ERDA
Washington, DC 20545

233 ERDA Technical Information
Center

W. Singlevich
Air Force Technical
Applications Center/TD-4
Patrick Air Force Base, FL 32925

H. Mueller
Air Resources Laboratory
National Oceanic and
Atmospheric Administration
Research Laboratories
P.O. Box 14985
Las Vegas, NV 89114

L. Machta
Air Resources Laboratory
National Oceanic and
Atmospheric Administration
8060 13th Street
Silver Spring, MD 20910

I. Van der Hoven
Air Resources Laboratory
National Oceanic and
Atmospheric Administration
8060 13th Street
Silver Spring, MD 20910

W. P. Elliott
Air Resources Laboratory
National Oceanic and
Atmospheric Administration
8060 13th Street
Silver Spring, MD 20910

No. of
Copies

L. Hodges
Ames Laboratory, U.S. ERDA
Iowa State University
Physics Bldg., Rm. A530
Ames, IA 50010

P. Frenzen
Argonne National Laboratory
9700 S. Cass Avenue
Argonne, IL 60439

F. Gustafson
Argonne National Laboratory
9700 S. Cass Avenue
Argonne, IL 60439

G. A. Briggs
Atmospheric Turbulence and
Diffusion Laboratory
NOAA, Oak Ridge, TN 37830

F. I. Gifford
Atmospheric Turbulence and
Diffusion Laboratory
NOAA, Oak Ridge, TN 37830

S. R. Hanna
Atmospheric Turbulence and
Diffusion Laboratory
NOAA, Oak Ridge, TN 37830

I. Ophel
Atomic Energy of Canada Limited
Chalk River, Ontario, CANADA

R. V. Osborne
Atomic Energy of Canada Limited
Chalk River, Ontario, CANADA

Librarian, Bldg. 465
Atomic Energy Research
Establishment
Harwell, Oxfordshire
OXIIORB, ENGLAND

A. E. J. Eggleton
Atomic Energy Research
Establishment
Harwell, Oxfordshire
OXIIORB, ENGLAND

D. H. Peirson
Atomic Energy Research
Establishment
Harwell, Oxfordshire
OXIIORB, ENGLAND

No. of
Copies

G. H. Clark
Health Physics Research Section
A.A.E.C. Research Establishment
Private Mailbag, Sutherland
New South Wales 2232
AUSTRALIA

Librarian
Australian AEC
Post Office Coogee
New South Wales 2034
AUSTRALIA

U.C. Mishra
Head, Air Monitoring Section
Bhabha Atomic Research Centre
Bombay-85 AS. INDIA

R. N. Sachdev
Air Monitoring Section
Bhabha Atomic Research Centre
Trombay, Bombay 400-085, INDIA

W. Broecker
Columbia University
Lamong Geological Observatory
Palisades, NY 10964

Capt. D. L. Moffett
Defense Nuclear Agency
HYBLA Valley Bldg.
6801 Telegraph Road
Alexandria, VA 23307

A. V. Dodd
Department of Army
U.S. Army Research Office
Environmental Sciences
Division
Box CM Duke Station
Durham, NC 27706

M. P. Measures
Department of National Health
and Welfare
Radiation Protection Division
Ottawa, CANADA

J. Shapiro
Department of Environmental
Health Sciences
School of Public Health
Harvard University
Boston, MA 02115

L. Jeanmaire
D.P.S. - S.C.S.
B.P. 6, Fontenay-aux-roses
(Seine) FRANCE

No. of
Copies

J. F. Willing
Rockwell International
Rocky Flats Plant
Golden, CO 80401

T. V. Crawford
Environmental Transport
Savannah River Laboratory
E. I. du Pont de Nemours
Aiken, SC 29801

C. D. Kerns
Environmental Transport
Savannah River Laboratory
E. I. du Pont de Nemours
Aiken, SC 29801

D. D. Dominick
Environmental Protection
Agency
Office of Categorical
Programs
Washington, DC 20460

Environmental Protection
Agency/NERC, Meteorology
Laboratory
Research Triangle Park, NC
27711

Harold Barkhau
Air Pollution Technical
Information Center
U.S. Environmental Protection
Agency
Research Triangle Park, NC
27711

W. Cotton
Experimental Meteorology
Laboratory
University of Miami Branch
NOAA P. O. Box 8044
Coral Gables, FL 33124

W. Woodley
Experimental Meteorology
Laboratory
University of Miami Branch
NOAA P. O. Box 8044
Coral Gables, FL 33124

J. W. Winchester
Florida State University
Department of Oceanography
Tallahassee, FL 32306

No. of
Copies

K. Edvarson
Forsvarets Forskningsanstalt
Research Institute of Nation
Defense
Avdelning 4, Stockholm 80
SWEDEN

R. G. Semonin
Illinois State Water Survey
Box 232
Urbana, IL 61801

C. E. Junge
Institut für Chemie
65 Mainz
Saarstrasse 23, Postfach 3060
WEST GERMANY

S. Beilke
Umveltbundesomt-Pilotstation
Frankfurt
6 Frankfurt/Main
Feldbergstrasse 45,
WEST GERMANY

H. W. Georgii
Institut für Meteorolgie und
Geophysik der Johann Wolfgang
Geothe Universitat
600 Frankfurt am Main
Feldbergstrasse 47,
WEST GERMANY

Director, Division of Health,
Safety and Waste Management
International Atomic Energy
Agency
Vienna 1, Kaerntnerring 11,
AUSTRIA

L. Anspaugh
Lawrence Livermore Laboratory
University of California
P. O. Box 808
Livermore, CA 94550

R. E. Heft
Lawrence Livermore Laboratory
University of California
P. O. Box 808
Livermore, CA 94550

J. B. Knox
Lawrence Livermore Laboratory
University of California
P. O. Box 808
Livermore, CA 94550

No. of
Copies

S. Barr
Los Alamos Scientific
Laboratory
University of California
P. O. Box 1663
Los Alamos, NM 87544

J. W. Healy
Los Alamos Scientific
Laboratory
University of California
P.O. Box 1663
Los Alamos, NM 87544

H. W. Kirby
Mound Laboratory
Monsanto Research Corporation
Miamisburg, OH 45345

P. LaFleur
National Bureau of Standards
Nuclear Reactor Laboratory
Gaithersburg, MD 20760

M. Saiki
National Institute of
Radiological Sciences
250, Kurosuna Cho
Chiba-shi, JAPAN

M. Suzuki
National Institute of
Radiological Sciences
250, Kurosuna Cho
Chiba-shi, JAPAN

J. Z. Holland
National Oceanic and
Atmospheric Administration
North Bethesda Office Center
11420 Rockville Heights
Rockville, MD 20852

S. I. Auerbach
Oak Ridge National Laboratory
P. O. Box X
Oak Ridge, TN 37830

G. D. O'Kelley
Oak Ridge National Laboratory
P. O. Box X
Oak Ridge, TN 37830

Kathy Sanders
Oak Ridge National Laboratory
P. O. Box X
Oak Ridge, TN 37830

J. T. Goll
Hydrology-Meteorology Branch
USNRC
Washington, DC 20555

No. of
Copies

D. Lal
Physical Research Laboratory
Navrangpura
Ahmedabad-9, INDIA

P. K. Kuroda
University of Arkansas
Department of Chemistry
Fayetteville, AR 72701

R. C. Srivastava
University of Chicago
Laboratory for Atmospheric
Probing
Geophysical Sciences
5734 S. Ellis Avenue
Chicago, IL 60637

F. I. Badgley
University of Washington
Department of Atmospheric
Sciences
Seattle, WA 98195

J. E. Tillman
University of Washington
Department of Atmospheric
Sciences
Seattle, WA 98195

E. Held
U.S. NRC Directorate
Regulatory Standards
Washington, DC 20545

M. F. Milligan
Los Alamos Scientific Laboratory
M.S. 486
Los Alamos, NM 87544

E. P. Hardy, Jr.
U.S. ERDA Health and Safety
Laboratory
376 Hudson Street
New York, NY 10012

J. H. Harley
U.S. ERDA Health and Safety
Laboratory
376 Hudson Street
New York, NY 10012

P. W. Krey
U.S. ERDA Health and Safety
Laboratory
376 Hudson Street
New York, NY 10012

No. of
Copies

C. W. Sill
U.S. ERDA Idaho Operations
Office
Idaho Falls, ID 83401

C. V. Theis
U.S. Geological Survey
P. O. Box 4369
Albuquerque, NM 87106

B. Baskin
Wayne County Department of
Health
Air Pollution Control Division
1311 E. Jefferson
Detroit, MI 48207

Librarian
World Meteorological
Organization
Geneva, 20
Case Postale No. 5, CH-1211
SWITZERLAND

Paul Michael
Meteorology Group
Brookhaven National Laboratory
Upton, NY 11975

H. W. Hoffman
Oak Ridge National Laboratory
P. O. Box Y
Oak Ridge, TN 37830

E. L. Alpen
Donners Laboratory
Lawrence Berkeley Laboratory
University of California
Berkeley, CA 94720

R. J. Engelmann
Environmental Research
Laboratories
National Oceanic and Atmospheric
Administration
Boulder, CO 80302

J. Davis
Nuclear Regulatory Commission
5650 Nicholson Lane
Rockville, MD 20854

J. D. Macdougall
University of California,
San Diego
P. O. Box 1529
La Jolla, CA 92037

No. of
Copies

J. W. Keizur
Sandia Laboratories
P.O. Box 5800
Albuquerque, NM 87115

W. G. N. Slinn
Atmospheric Sciences Department
Oregon State University
Corvallis, OR 97331

A. N. Dingle
Department of Atmospheric and
Oceanic Science
University of Michigan
Ann Arbor, MI 48104

T. Lyons
School of Environmental &
Life Sciences
Murdock University
Murdock, WESTERN AUSTRALIA 6153

V. V. Shirvaikar
Meteorology Group
Environmental Studies Section
Bhabha Atomic Research Centre
Bombay-85 AS, INDIA

J. K. Munro, Jr.
Oak Ridge National Laboratory
P. O. Box X
Oak Ridge, TN 37830

A. C. Chamberlain
Environmental and Medical
Sciences Division
OX11 ORA
AERA Harwell, Oxfordshire
ENGLAND

J. Durham
U.S. Environmental Protection
Agency
National Environmental Research
Center
Research Triangle Park, NC
27711

J. D. Macdougall
Scripps Institution of Oceanography
Geological Research Division
P.O. Box 1529
La Jolla, CA 92037

B. B. Hicks
Atmospheric Physics Section
Argonne National Laboratory
9700 S. Cass Avenue
Argonne, IL 60439

No. of
Copies

R. S. Paul
Battelle Memorial Institute
Columbus Laboratories
505 King Avenue
Columbus, OH 43201

G. W. Duncan
Battelle Human Affairs Research Centers
4000 N.E. 41st Street
P.O. Box 5395
Seattle, WA 98105

J. E. Rasmussen
Battelle Human Affairs Research Centers
4000 N.E. 41st Street
P.O. Box 5395
Seattle, WA 98105

J. L. Hebert
Battelle Human Affairs Research Centers
4000 N.E. 41st Street
P. O. Box 5395
Seattle, WA 98105

S. M. Nealey
Battelle Human Affairs Research Centers
4000 N.E. 41st Street
P.O. Box 5395
Seattle, WA 98105

ONSITE

9 ERDA Richland Operations Office

P. F. X. Dunigan
N. W. Fraser
P. D. Holsted
J. L. Landon
W. Lei
H. E. Ransom

F. R. Standerfer
J. D. White

3 Rockwell Hanford Operations

D. J. Brown
R. D. Fox
R. E. Isaacson

No. of
Copies

3 Hanford Environmental Health Foundation

B. Breitenstein
P. A. Fuqua
W. D. Norwood

198 Battelle-Northwest

T. W. Ambrose
W. J. Bair (20)
N. E. Ballou
N. E. Carter
D. B. Cearlock
J. P. Corley
G. M. Dalen
R. L. Drake (30)
C. E. Elderkin
J. W. Finnigan
J. C. Fox
J. J. Fuquay
A. G. Gibbs
J. M. Hales
A. J. Haverfield
D. L. Hessel
H. V. Larson
J. D. Ludwick
S. Marks
R. P. Marshall
J. M. Nielsen
R. E. Nightingale
D. E. Olesen
J. F. Park
H. M. Parker
R. W. Perkins
M. R. Peterson
L. A. Rancitelli
W. D. Richmond
L. C. Schwendiman (20)
C. L. Simpson (40)
R. A. Stokes (15)
W. L. Templeton
R. C. Thompson
C. M. Unruh
B. E. Vaughan
E. C. Watson
L. L. Wendell (30)
W. R. Wiley
J. A. Young
Biology Library (2)
Technical Information (5)
Technical Publication (2)